# Resonance Raman Studies of Fe-Ligand Vibrations of Oxygen Binding Heme Proteins and Structure-Function Relationship of Terminal Oxidases

Shun Hirota

Doctor of Philosophy

Department of Functional Molecular Science
School of Mathematical and Physical Science
The Graduate University for Advanced Studies

1994

## Preface

In biological systems, many proteins possess prosthetic groups which are indispensable for their functions. Myoglobin (Mb) and hemoglobin (Hb) are oxygen-storage and -carrier proteins, respectively, whereas terminal oxidases are oxygen reducing proteins. All of these proteins contain a heme as a prosthetic group where oxygen molecules bind, even though they play different roles in biological systems.

Functions of these proteins have been studied for years, but their physicochemical properties have not been fully revealed yet, partially due to the difficulties in application of physicochemical methods to biomolecules. There are some similarities and differences in the physicochemical properties of these heme proteins which are very important for understanding the functions of these proteins. Spectroscopic techniques are very useful to obtain kinetic as well as steady-state information of biomolecules, including heme proteins. Now it is at the stage to study the structure-function relationship of these proteins. Therefore in this thesis, resonance Raman (RR) technique is adopted to examine the three oxygen-binding heme proteins, namely, Mb, Hb, and terminal oxidases.

This thesis consists of two parts, Parts I and II. Part I treats assignment of the Fe-ligand stretching and bending vibrational modes of various diatomic ligand-bound heme proteins. It is important to know the Fe-ligand bond character for understanding the function of these heme proteins. Such information can be obtained by RR spectroscopy, since RR spectroscopy provides information on bond-strength if assignments have been established. For example, the force constant of the ligand bending mode reflects the energy required to bend the Fe-ligand unit in the protein. The ligand-isotope frequency shifts of the Fe-ligand stretching mode reflects its Fe-ligand bent angle. Therefore, the assignments of the ligand stretching and bending modes are studied throughout this part to know the ligand character in ligand-bound heme proteins.

Part II treats the physicochemical properties of terminal oxidases. Terminal oxidases is a group of proteins which serves as the terminal enzyme of the respiratory chain. Most part of oxygen molecules taken into our body are reduced to water by this enzyme. One of the major structural differences of terminal oxidases from Hb and Mb is that they have a heme-

copper binuclear center at the oxygen binding site. Another special character is that the oxidases involve the intramolecular heme to heme electron transfer during the oxygen reduction. To know the structure-function relationship of terminal oxidases, properties of the active site are studied by RR spectroscopy.

**Acknowledgments**

It is a great pleasure to express my deep gratitude to Professor Teizo Kitagawa and Dr. Takashi Ogura for their continual suggestions, discussions, and encouragement throughout the course of this study.

I wish to thank Professor Shinya Yoshikawa and Dr. Kyoko Shinzawa-Itoh for their kind guidance in preparation of cytochrome *c* oxidase from beef heart and for interesting discussions especially on the characters of the enzyme. I also thank people in Yoshikawa's laboratory for their help during my stay in Himeji. I am also indebted to Professor Masako Nagai for her helpful guidance in preparation of isolated chains from human hemoglobin A and for her kind gifts of very pure human hemoglobin A samples. I am also grateful to Dr. Tatsushi Mogi, Mr. Tomoyasu Hirano, and Professor Yasuhiro Anraku for preparation of isolated cytochrome *bo* and cytochrome *bd* from *Escherichia coli*. I am also obliged to Professor Evan H. Appelman for his kind gifts of asymmetrical $^{16}O^{18}O$ gas, and to Dr. Tsuyoshi Egawa and Professor Yuzuru Ishimura for their courtesy of offering purified P-$450_{cam}$. I also thank Professor Paul Stein and Dr. Philip Jewsbury for very useful discussions.

Finally, I express my gratitude to Dr. Yasuhisa Mizutani for helping low temperature measurements and to all the other people who joined Kitagawa's group for fruitful discussions and affectionate encouragement.

## Publication List

1. Superconducting Vibronic Interaction in Model Organic Polymers which Contain Hetero Atoms and Triple Bonds
Tachibana, A.; **Hirota, S.**; Ishikawa, S.; Yamabe, T. *J. Mol. Struct. (Theochem)* **1991**, *235*, 211-226.

2. Time-Resolved Resonance-Raman Elucidation of the Pathway for Dioxygen Reduction by Cytochrome *c* Oxidase
Ogura, T.; Takahashi, S.; **Hirota, S.**; Shinzawa-Itoh, K.; Yoshikawa, S.; Appleman, E. H.; Kitagawa, T. *J. Am. Chem. Soc.* **1993**, *115*, 8527-8536.

3. Vibrational Assignments of the FeCO Unit of CO-Bound Heme Proteins Revisited: Observation of a New CO-Isotope-Sensitive Raman Band Assignable to the FeCO Bending Fundamental
**Hirota, S.**; Ogura, T.; Shinzawa-Itoh, K.; Yoshikawa, S.; Nagai, M.; Kitagawa, T. *J. Phys. Chem.* **1994**, *26*, 6652-6660.

4. Observation of the Fe-$O_2$ and $Fe^{IV}$=O Stretching Raman Bands for Dioxygen Reduction Intermediates of Cytochrome *bo* Isolated from *Escherichia coli*
**Hirota, S.**; Mogi, T.; Ogura, T.; Hirano, T.; Anraku, Y.; Kitagawa, T. *FEBS Lett.* **1994**, *352*, 67-70.

5. Molecular Structure of Redox Metal Centers of the Cytochrome *bo* Complex from *Escherichia coli*
Tsubaki, M.; Mogi, T.; Hori, H.; **Hirota, S.**; Ogura, T.; Kitagawa, T.; Anraku, Y. *J. Biol. Chem.* **1994**, *269*, 30861-30868.

6. Observation of a New Oxygen-Isotope-Sensitive Raman Band for Oxyhemoproteins and Its Implications in Heme Pocket Structures
**Hirota, S.**; Ogura, T.; Appelman, E. H.; Shinzawa-Itoh, K.; Yoshikawa, S.; Kitagawa, T. *J. Am. Chem. Soc.* **1994**, *116*, 10564-10570.

7. Observation of Nonfundamental Fe-$O_2$ and Fe-CO Vibrations and Potential Anharmonicities for Oxy- and Carbonmonoxy-hemoglobin. Evidence Supporting a New Assignment of the Fe-C-O Bending Fundamental
**Hirota, S.**; Ogura, T.; Kitagawa, T. *J. Am. Chem. Soc.* **1995**, *117*, 821-822.

8. A Flash-Photolysis Study of the Reactions of a *caa*$_3$-type Cytochrome *c* Oxidase with Dioxygen and Carbon Monoxide
**Hirota, S.**; Svensson, M.; Sone, N.; Nilsson, T.; Malmström, B. G.; Brzezinski, P., to be submitted.

9. Reduction Mechanism of Respiratory Dioxygen and Its Coupling with Proton Pumping Revealed by Time-Resolved Resonance Raman Spectroscopy
Ogura, T.; **Hirota, S.**; Shinzawa-Itoh, K.; Yoshikawa, S.; Kitagawa, T., to be submitted.

10. Assignments of the Fe-$CN^-$ Stretching and Fe-C-$N^-$ Bending Raman Bands of Cyanide Bound Heme Proteins: Cyanometmyoglobin, Cyanomethemoglobin, and Cyanide-Bound Cytochrome *c* Oxidase
**Hirota, S.**; Ogura, T.; Shinzawa-Itoh, K.; Yoshikawa, S.; Kitagawa, T., to be submitted.

## Contents

# Part I.

# Assignments of the Fe-Ligand Stretching and Bending Raman Bands of Ligand Bound Heme Proteins

# Chapter I-1.

# Introduction

## 1.1 The Aim of Part I

Various ligands bind to the heme irons of various heme proteins. Among these heme proteins, this study focuses on oxygen binding heme proteins. The ligand-bound characters of these heme proteins are essential for their functions. The force constant of the ligand bond provides information on the bending energy of Fe-ligand unit in ligand-bound heme protein. By adopting normal coordinate calculations, the ligand isotope pattern also gives information on the Fe-ligand geometry of the protein. Although these information are very important for the knowledge of the ligand bond character, further investigations have not be achieved. This was because of the difficulty in obtaining an excitation wavelength near the Soret absorption maximum for RR scattering, and the difficulty in measuring different isotope derivatives at similar conditions, so as to make subtraction and find weak but important ligand related vibrational modes.

In this study, an excitation light near 430 nm obtained by a new laser system is used. Also the use of an object lens and careful treatment of the sample made the experimental conditions of different isotopes similar, and significantly increased the S/N ratio of the RR difference spectra. To clarify the assignments, as many ligand isotopes as possible were used for the RR measurements. $^{12}C^{16}O$, $^{13}C^{16}O$, $^{12}C^{18}O$, and $^{13}C^{18}O$ isotopes were used for CO-bound heme proteins, $^{16}O_2$, $^{18}O_2$, and $^{16}O^{18}O$ isotopes were used for $O_2$-bound heme proteins, $^{12}C^{14}N^-$, $^{13}C^{14}N^-$, $^{12}C^{15}N^-$, and $^{13}C^{15}N^-$ isotopes were used for $CN^-$-bound heme proteins, and $^{16}OH^-$, $^{16}OD^-$, $^{18}OH^-$, and $^{18}OD^-$ isotopes were used for $OH^-$-bound heme proteins. The assignment of the ligand related vibrational modes for CO-, $O_2$-, $CN^-$- and $OH^-$-bound heme proteins are reconsidered together with their relation. New information on the ligand character of these ligand bound heme proteins are presented.

## 1.2 Heme Proteins

### Heme Structure

Many proteins have a heme as a prosthetic group which is indispensable for their activities (Figure 1-1a). A heme consists of an aromatic macrocycle and an iron ion. The aromatic macrocycle is called porphyrin, in which four pyrrole rings are linked *via* unsaturated carbon-

carbon bonds (methine bridges), forming a tetrapyrrole ring. The iron is located at the center of the tetrapyrrole ring, and is bound by four pyrrole nitrogens. The iron ion takes normally either a ferrous (+2) or a ferric (+3) oxidation state. This ability of having two oxidation states is one of most important characters for the variety of functions of heme proteins in biosystems.

The heme iron can construct two additional bonds at the axial positions of the heme iron. In hemoglobin (Hb) which is an oxygen transporting protein, myoglobin (Mb) which is an oxygen storage protein, and cytochrome *c* oxidase (CcO) which is the terminal enzyme in the mitochondria respiratory chain, are caught by the surrounding protein at an imidazole nitrogen of a histidine residue through a bond with the heme iron (Figure 1-1b). This histidine is called proximal-histidine. Another histidine exists near the heme iron in the opposite side of the heme for some proteins. This histidine is called distal-histidine and does not coordinate to the heme iron. Oxygen binds to the heme of Hb and Mb without any other reaction. In contrast, the bound oxygen is reduced to water in CcO, consuming four electrons per one oxygen molecule. Physicochemical properties of terminal oxidases will be discussed in details in part II of this thesis. Cytochrome P-450 (P-450) catalyzes monooxygenation of organic substrates, and has a cystein sulfur atom at the axial position of the heme iron. In these proteins, oxygen binds to the heme iron at the distal side of the heme iron, i.e., trans site against the proximal-amide acid site. Various small molecules, such as CO, $CN^-$, NO, could bind to the oxygen binding site and prohibit oxygen binding, while other molecules such as $OH^-$, $F^-$ $N_3^-$ could bind to the ferric heme iron.

**Electronic Character**[1]

Hemes have a very typical optical character which absorbs light intensively in the visible to near-ultraviolet region. A very strong absorption band called the Soret band (B band) appears near 400 nm, and weaker bands called $\alpha$ and $\beta$ bands (Q bands) exist between 500 to 600 nm. The $\alpha$ band corresponds to the lowest $\pi$-$\pi^*$ transition, while the $\beta$ band corresponds to the vibronic envelope ($Q_v$). The two bands of the metalloporphyrins in the visible region split into four bands for free-base porphyrins. This character of free-base porphyrins and

metalloporphyrins could be explained in terms of the lowest $\pi$-$\pi^*$ transition of the cyclic polyene model. Metalloporphyrins have an inner 16-membered conjugation pathway with 18 $\pi$ electrons, whereas free-base porphyrins have 18 $\pi$ electrons on the 18-atom ring since two pyrrole nitrogen are out of conjugation. The highest filled levels and the lowest empty levels are each degenerate and the four possible transitions come in degenerate pairs in the 16-membered ring, whereas the lower two states are not degenerate and splitting of $Q_0^x$ and $Q_0^y$ occurs in the 18-membered ring, but the upper states remain degenerated in both polyenes.

In Hückel LCAO (linear combination of atomic orbitals) calculation, the intensities of the absorption bands could not be explained even though correct energies were predicted. Gouterman successfully included configuration interactions in the description of molecular orbitals of the excited states for porphyrins. In the idealized $D_{4h}$ symmetrical tetrapyrrole ring, the two HOMOs are of $a_{1u}$ and $a_{2u}$ symmetry, which have nearly the same energies. The LUMOs are degenerated having $e_g$ symmetry. The two excited states ($a_{1u}\rightarrow e_g$ and $a_{2u}\rightarrow e_g$) have same symmetry and mix considerably, and thus the transition dipoles add up for the Soret band and cancel each other for the $\alpha$ band, respectively. The $\beta$ band is actually a sum of many different transitions, each of which include one mode of vibrational excitation. This band gains intensity from the Soret transition via vibronic mixing.

### 1.3 Resonance Raman Spectroscopy for Heme Proteins[2]

Resonance Raman (RR) spectroscopy has been utilized for the investigations of various ligand-bound heme proteins for more than two decades. In RR spectroscopy, some selected vibrations among a large number of freedom are enhanced in intensity, and thus it is possible to discuss even on a large protein molecule. Furthermore, RR spectra are suitable for measurements in aqueous solutions since the RR scattering from water is relatively small. For ligand-bound heme proteins, RR spectra can provide the metal-ligand stretching and bending frequencies, which give information about the nature of the ligand bond. These properties of RR spectroscopy have been very effective to study interactions between exogenous ligands and the heme iron for ligand-bound heme proteins in solutions. In this study, all RR spectra are measured at

solution conditions using excitation wavelengths near the Soret maximum and discuss the ligand bond characters.

## 1.4 Ligand Geometry and Ligand Related Vibrational Modes of Ligand-Bound Heme Proteins and Their Model Compounds[3]

### 1.4.1 $O_2$

The dioxygen adducts are the most important derivatives among various derivatives of heme proteins, since they are primarily involved in the functions of the proteins.

#### Ligand Geometry

The Fe-O-O geometry of oxyhemoproteins, which should sensitively affect the $\delta_{FeOO}$ frequency, has not been established unambiguously by X-ray crystallographic analyses: the Fe-O-O angle is reported to be 115° for sperm whale Mb,[4a,b] 153° and 159°, for the α and β subunits of human Hb A, respectively,[5a,b] and 160° for the α subunit of an intermediately ligated $\alpha_{oxy}\beta_{deoxy}$ Hb.[6a] According to recent crystallographic analysis of oxygenated *Scapharca* dimeric Hb,[6b] the Fe-O-O angles are reported to be 135° and 150° for the two subunits. On the other hand, X-ray-absorption near-edge structure (XANES) studies[7] indicate that the Fe-O-O angles are 115° for both dioxygen adducts of hemoglobin ($HbO_2$) and myoglobin ($MbO_2$). This difference might be caused by structural differences between the crystalline state and in solutions, as indicated by an RR study of metMb and deoxyMb,[8] while hydrogen-bonding interaction between the bound $O_2$ and the distal histidine is noted by a neutron diffraction study for crystalline $MbO_2$,[9] and by an RR study for solution $HbO_2$.[10] The Fe-O-O geometries for $HbO_2$, $MbO_2$ and dioxygen adduct of cytochrome *c* oxidase ($CcO{\cdot}O_2$) are discussed in chapter I-2.

#### Vibrational Modes of Heme Proteins

The $\nu_{Fe\text{-}O_2}$ RR band has been identified at 567-572 $cm^{-1}$ for $HbO_2$,[11-13] at 572 $cm^{-1}$ for $MbO_2$,[14] at 571 $cm^{-1}$ for dioxygen adducts of cytochrome P-450 (P-450·$O_2$),[15] at 562 $cm^{-1}$ for oxy-horseradish peroxidase (HRP·$O_2$),[16] at 531 $cm^{-1}$ for lactoperoxidase compound III (LPO·$O_2$),[17] and at 568-571 $cm^{-1}$ for $CcO{\cdot}O_2$.[18-20] Several bands were observed in the oxygen-oxygen stretching ($\nu_{OO}$) region in IR spectroscopy for $HbO_2$ and $MbO_2$, and it was

interpreted in terms of the presence of multiple species.[21] But later, the appearance of several bands in this region was explained from model compounds studies as splitting caused by vibrational coupling of $\nu_{OO}$ with the proximal-histidine internal vibrational modes. The $\nu_{OO}$ band of P-450·$O_2$ was detected with RR spectra at 1140-1141 $cm^{-1}$ with a single peak.[22,23] The iron-oxygen-oxygen bending mode ($\delta_{FeOO}$) is reported at 491 $cm^{-1}$ only for compound III of lactoperoxidase.[17] This will be discussed in chapter I-2.

**Vibrational Modes of Model Compounds**

For model compounds, the complicated pattern of the $\nu_{OO}$ RR band and apparent splitting of the oxygen-isotope-sensitive bands seen in IR spectra of $HbO_2$ have been satisfactorily interpreted in terms of vibrational coupling of bound $O_2$ with a trans ligand without assuming the presence of multiple conformations as written above.[24] The RR bands corresponding to $\nu_{Fe\text{-}O_2}$ and $\delta_{FeOO}$ were reported at 488 and 279 $cm^{-1}$ for (Pc)$FeO_2$ (Pc: phthalocyanine),[25] at 508 and 349 $cm^{-1}$ for (TPP)$FeO_2$ (TPP: tetraphenylporphyrin),[26a] and at 516 and 343 $cm^{-1}$ for (TMP)$FeO_2$ (TMP: tetramesitylporphyrin),[26a] although a single band was observed at 509 $cm^{-1}$ for (OEP)$FeO_2$ (OEP: octaethylporphyrin)[26a,b] and at 568 $cm^{-1}$ for (TpivPP)$FeO_2$ [TpivPP: *meso*-tetra(α,α,α,α-*o*-pivaloylamidophenyl)-porphyrin].[27] These observations suggested that the oxygen-isotope-sensitive RR band of $HbO_2$ around 570 $cm^{-1}$ arose from the $\nu_{Fe\text{-}O_2}$ mode,[23] although there was a suggestion[28] that the behavior of isotopic frequency shifts of this kind[13] could be an indication of the $\delta_{FeOO}$ mode instead of $\nu_{Fe\text{-}O_2}$. The band around 570 $cm^{-1}$ is definitely assigned to the $\nu_{Fe\text{-}O_2}$ mode by the discovery of another $O_2$-isotope-sensitive band assignable to $\delta_{FeOO}$, and the $\nu_{Fe\text{-}O_2}$ and $\delta_{FeOO}$ frequencies were reproduced in normal coordinate calculations as discussed in chapter I-2. The presence of direct correlation between the $\nu_{Fe\text{-}O_2}$ frequencies and the bond-strength of Fe-trans bond has been noted[29] and, moreover, an inverse linear correlation between the $\nu_{OO}$ and $\nu_{Fe\text{-}O_2}$ frequencies has been found. Similar linear correlation between the $\nu_{CO}$ and $\nu_{Fe\text{-}CO}$ frequencies has also been found in CO adducts of heme proteins.[30]

### 1.4.2 CO

The carbon monoxide (CO) adduct of heme has fundamental importance in the studies of heme proteins since it has been extensively used to probe the structural characteristics in their dioxygen binding sites. Moreover, CO adducts of heme proteins attract attention recently, as the endogenously produced CO is likely to be involved in neurotransmission, blood pressure regulation, and hemin catabolism by binding to a heme protein, guanilate cyclase.[31]

**Ligand Geometry**

According to X-ray[32] and neutron[33] diffraction studies of CO-bound sperm whale Mb crystals, the FeCO unit adopts a bent conformation in proteins, and earlier studies[34] inferred that the binding of CO to Mb is selectively inhibited by steric repulsion from the distal histidine (E7-His) that impedes upright binding. It is also reported by picosecond infrared (IR) studies that CO is tilted against the heme plane in CO-bound heme proteins in solution.[35] Recent studies of distal histidine mutants of CO-bound Mb (MbCO) obtained by site-directed mutagenesis showed that the FeCO angles are very similar (156°~171°) among different MbCO mutants, and the angles are independent of the identity of the amino acid residue at the distal histidine position.[36] The FeCO unit of a free porphyrin prefers a linear upright geometry in solutions,[37] and for such a structure the iron-carbon-oxygen bending fundamental mode ($\delta_{FeCO}$), belonging to the E species in $C_{4v}$ symmetry, should be IR active but RR inactive.

**Vibrational Modes**

The iron-carbon stretching mode ($\nu_{Fe\text{-}CO}$), carbon-oxygen stretching mode ($\nu_{CO}$), and $\delta_{FeCO}$ give structural information on the bound CO and the surrounding residues in the heme pocket of CO-bound heme proteins. Caughey and co-workers[38] first pointed out that the $\nu_{CO}$ IR band is a sensitive probe for the distal pocket structure in Hb and Mb. Currently four different CO conformers of mammalian Mb's and Hb's in the ground state are designed $A_i$, in which the subscript specifies frequencies:[38b,39,40] 1965 ($A_0$), 1942 ($A_1$), 1949 ($A_2$), and 1932 ($A_3$) $cm^{-1}$. What is to be stressed is that $A_3$ is a minority species in solution but is a major component in crystal at low temperatures.[39a,40c]

The first direct identification of the iron-carbon bond in CO-bound heme proteins in RR spectroscopy was reported by Tsubaki et al. in 1982.[41] On the basis of CO-isotopic frequency shifts, $\nu_{Fe\text{-}CO}$, $\delta_{FeCO}$ and $\nu_{CO}$ frequencies were assigned to the bands at 507, 578, 1951 $cm^{-1}$ for MbCO, and 512, 577, and 1944 $cm^{-1}$ for CO-bound Hb (HbCO), respectively.[41] Since then, bands around 480-520 $cm^{-1}$ and 550-580 $cm^{-1}$ in other CO-bound heme proteins,[42] including cytochrome *c* peroxidase (CCP),[43] horseradish peroxidase (HRP),[44] cytochrome P-450 (P-450),[45] cytochrome *c* oxidase (CcO),[46] nitric oxide synthase,[47] and model hemes,[48,49] were assigned to the $\nu_{Fe\text{-}CO}$ and $\delta_{FeCO}$ modes, respectively.

The protein-free heme-CO complex with an upright geometry[36,37] gives no RR band between 500-600 $cm^{-1}$, while it yields the $\nu_{Fe\text{-}CO}$ RR band at 495 $cm^{-1}$ in an organic solution.[50,51] In CO-bound model hemes with a $(CH_2)_n$-chain strap over the heme iron which prohibit CO from taking upright geometry, the $\nu_{Fe\text{-}CO}$ RR bands were detected at 500 - 510 $cm^{-1}$ (higher frequencies for shorter straps) and the $\delta_{FeCO}$ RR bands at 570 - 580 $cm^{-1}$ (stronger intensities for shorter straps).[49]

**Normal Coordinate Calculations for a Tetraatomic Model[52]**

By normal coordinate calculations of a tetraatomic LFeCO (L; N-Methylimidazole) unit, it was shown that the higher frequency mode between $\nu_{Fe\text{-}CO}$ and $\delta_{FeCO}$, which becomes mainly $\nu_{Fe\text{-}CO}$ at small Fe-C-O bent angles, exhibits a "zigzag" pattern against the total mass of CO.[52] Therefore, this "zigzag" pattern, which has been used to identify $\delta_{FeCO}$, is not a reliable diagnosis for the assignment of the bending mode for an appreciably bent FeCO geometry.

In normal coordinate calculations, the frequency of the $\nu_{Fe\text{-}CO}$ mode decreases whereas that of $\delta_{FeCO}$ increases as the FeCO unit becomes more bent when the 575 $cm^{-1}$ band was assigned to $\delta_{FeCO}$. This frequency difference between $\nu_{Fe\text{-}CO}$ and $\delta_{FeCO}$ is due to the strong mixing of these two modes.[52] The CO-isotope shifts for $\nu_{Fe\text{-}CO}$ and $\delta_{FeCO}$ were reproduced by normal coordinate calculation for the L-Fe-C-O linear geometry when the 575 $cm^{-1}$ band was assigned to $\delta_{FeCO}$.[52] If a significant bent structure for the FeCO unit (120°-140°) was adopted for the calculation, the $\nu_{Fe\text{-}CO}$ and $\delta_{FeCO}$ frequencies were separated too much compared with the observed frequencies for a wide range of Fe-CO stretching and FeCO bending force constants, and it was not limited by

particular values of these force constants. The only way to reduce this $\nu_{Fe\text{-}CO}/\delta_{FeCO}$ divergence was to introduce large positive stretch–bend interaction force constants; 0.3 mdyn (θ=165°), 0.4 mdyn (θ=150°), and 0.7 mdyn (θ=135°).[52]

**Metal-Ligand Interaction**

There are roughly two types of bonding interactions, σ- and π-bondings, between the ligands and the heme iron, as shown in Figure 1-2.[3] The σ-bonding consists of the interaction of the metal $d_{z^2}$ orbital and the ligand lone-pair orbital. When the ligand is CO (X=C, Y=O in Figure 1-2), this type of interaction becomes significant as CO becomes perpendicular against the heme plane. Another type of the σ-bonding is the interaction of the metal $d_{z^2}$ orbital with the ligand π* orbital. The π-bonding consists of electron donation from the metal $d_{xz}$ and $d_{yz}$ orbitals to the ligand π* orbital. In this case, the increase in electron density of the antibonding π* orbitals of the ligand due to larger donation from the Fe $d_\pi$ orbitals, results in the stronger metal-ligand bond but is accompanied by a weakening of the ligand internal bond. Several groups[53-56] have noted that the $\nu_{Fe\text{-}CO}$ frequencies obtained by RR spectroscopy have a negative linear correlation with the IR $\nu_{CO}$ frequencies for a variety of heme-CO adducts.

**Ligand-Surrounding Protein Interaction**

It has also been proposed that the charge distributions of the surrounding amino acid residues would influence NMR chemical shifts of the heme-bound CO and also the $\nu_{CO}$ frequencies of CO-bound hemoproteins.[57] Recent studies on site specific mutants of MbCO showed that the distal residue-CO ligand interaction is largely electrostatic.[58] These experimental results were well reproduced by molecular dynamics simulations, recently.[59]

### 1.4.3 $CN^-$

Cyanide ($CN^-$) binds to heme proteins in their ferric state, and also binds to the ferrous iron in some proteins such as CcO and LPO.

**Ligand Geometry**

According to X-ray and NMR studies, $CN^-$ is tilted about 15° against the normal of the heme plane without bending significantly in $MbCN^-$.[60,61] This ligand geometry is very similar to those of CO-bound heme proteins.

**$\nu_{Fe\text{-}CN^-}$ and $\delta_{FeCN^-}$ of Heme Proteins**

In the reports up to now, iron-carbon stretching ($\nu_{Fe\text{-}CN^-}$) and iron-carbon-nitrogen bending ($\delta_{FeCN^-}$) frequencies are quite different among various $CN^-$-bound heme proteins. The $\nu_{Fe\text{-}CN^-}$ and $\delta_{FeCN^-}$ modes of $CN^-$ bound heme proteins have been first reported from RR spectroscopy by Yu et al. at 453 $cm^{-1}$ and 412 $cm^{-1}$, respectively, for hemoglobin III of *Chironomus thummi thummi* (CTT III).[62] The $\nu_{Fe\text{-}CN^-}$ mode was detected at 452 $cm^{-1}$ for human cyanometHb ($HbCN^-$),[63] and at 454 $cm^{-1}$ for sperm whale cyanometMb ($MbCN^-$).[64] The bands at 361 and 454 $cm^{-1}$ were assigned to $\nu_{Fe\text{-}CN^-}$ and $\delta_{FeCN^-}$ for cyanoferric myeloperoxidase ($MPO{\cdot}CN^-$), while those at 456 and 404 $cm^{-1}$ were assigned to $\nu_{Fe\text{-}CN^-}$ and $\delta_{FeCN^-}$ for cyanoferric horseradish peroxidase ($HRP{\cdot}CN^-$), respectively.[65] The bands at 360 and 453 $cm^{-1}$ were assigned to $\nu_{Fe\text{-}CN^-}$ and $\delta_{FeCN^-}$ for cyanoferric lactoperoxidase ($LPO{\cdot}CN^-$), respectively.[66] For $LPO{\cdot}CN^-$ there was another clear $CN^-$-isotope-sensitive band at 311 $cm^{-1}$, but this band was unable to explain as either as a $\nu_{Fe\text{-}CN^-}$ nor a $\delta_{FeCN^-}$ since its $CN^-$-isotope shift was only 2 $cm^{-1}$ between $^{12}C^{14}N^-$ and $^{13}C^{15}N^-$ adducts. In all these reports, the bands which showed monotonic frequency decrease as the total mass of $CN^-$ increased were assigned to $\nu_{Fe\text{-}CN^-}$, while the bands which were sensitive to the mass of the carbon atom and not to that of nitrogen were assigned to $\delta_{FeCN^-}$. On the other hand, $\nu_{Fe\text{-}CN^-}$ and $\delta_{FeCN^-}$ for the ferrous state were detected at 511 and 486 $cm^{-1}$, respectively, for $CN^-$ complexes of cytochrome $ba_3$.[67]

However, it is not always correct to assign only from their ligand isotope pattern. For $O_2$- or NO-bound heme proteins in which the ligands are significantly bent, the iron-ligand stretching frequencies depend mainly on the mass of the coordinated atom of the ligand. Thus $\nu_{Fe\text{-}CN^-}$ could express sensitivity only to the mass of the carbon atom of $CN^-$ and not to that of the nitrogen. Systematic discussions will be done in chapter I-6.

**$\nu_{Fe\text{-}CN^-}$ of Model Hemes**

For $CN^-$-bound "strapped hemes", in which the ligand binding site are sterically hindered by a $(CH_2)_n$-chain strap over the heme iron, the $\nu_{Fe\text{-}CN^-}$ frequencies decrease only a little as the strap length decrease; 451 (unhindered), 447 (n=15), 447 (n=14), and 445 $cm^{-1}$ (n=13).[68] For pyridine and pyridine derivatives of Fe(OEP)(pyridine)$CN^-$ (OEP, octaethylporphyrin), $CN^-$ is bound perpendicular against the heme plane,[69] and the $\nu_{Fe\text{-}CN^-}$ frequencies were detected at 442 - 452 $cm^{-1}$, which decreased for complexes with higher pyridine basicities.[70]

**$\nu_{CN^-}$**

The carbon-nitrogen stretching mode ($\nu_{CN^-}$) of $CN^-$-bound heme proteins have been detected with IR spectra at 2122 $cm^{-1}$ for $HbCN^-$, at 2126 $cm^{-1}$ for $MbCN^-$, at 2131 $cm^{-1}$ for HRP·$CN^-$, and at 2152 $cm^{-1}$ for $CN^-$-bound resting (oxidized) CcO ($CcO_{rest}\cdot CN^-$).[71] The $\nu_{Fe\text{-}CN^-}$ frequency for $CN^-$-bound reduced CcO ($CcO_{red}\cdot CN^-$) has been detected at two frequencies, 2045 and 2058 $cm^{-1}$.[71c]

### 1.4.4 NO

Nitric Oxide (NO) binds to both ferric and ferrous states in heme proteins. NO-bound heme proteins are becoming increasingly important, as NO is recently found to be a signal transducing molecule for physiological events, such as blood pressure regulation, immune response, and neutrotransmission.[72]

**Ligand Geometry**

Ferrous nitric oxide Hb takes a bent structure according to X-ray studies, and the Fe-N-O bent angle is reported to be about 145° for both α and β subunits.[73a] NO also bears a bent structure in nitrosylmetalloporphyrins having a ferrous iron state.[73b-e] For all the reported ferrous nitorsylmetalloporphyrins, the Fe-N-O bent angles are also reported to be around 140° - 150° .

**Vibrational Modes of the Ferrous State**

Chottard and Mansuy[74] first detected a NO-isotope-sensitive band at 549 $cm^{-1}$ for $^{14}N^{16}O$-bound ferrous Hb which shifted to 539 $cm^{-1}$ with

$^{15}N^{16}O$, and assigned it to iron-nitrogen stretching mode ($\nu_{Fe\text{-}NO}$). Later, a similar mode at 554 $cm^{-1}$ in NO-bound ferrous Mb was found to be insensible to the terminal oxygen-isotope of the NO ligand, and the band was reassigned to $\delta_{FeNO}$ from its NO-isotope zigzag patern.[75] Similar bands have been detected at ~ 545 $cm^{-1}$ for NO-bound mixed-valence CcO,[76] at 559 $cm^{-1}$ for NO-bound leghemoglobin,[77] and at 558 $cm^{-1}$ for NO-bound sulfite reductase.[78] However, only one ligand-isotope-sensitive mode had been detected in the low frequency region for all these NO-bound ferrous heme proteins.

In 1991, three ligand-isotope-sensitive modes in natural abundance NO-bound ferrous cytochrome $P450_{cam}$ were reported by Hu and Kinkaid[79] at 1591, 554, and 446 $cm^{-1}$. Normal coordinate calculations adopting $\theta$(Fe-N-O) = 150° clearly demonstrated that the 1591, 554, and 446 $cm^{-1}$ bands should be assigned to $\nu_{NO}$, $\nu_{Fe\text{-}NO}$, and $\delta_{FeNO}$, respectively.[79]

**Vibrational Modes of the Ferric State**

Benko and Yu[75] found a NO-isotope-sensitive band at 595, 594, and 604 $cm^{-1}$ in NO-bound ferric Mb, Hb and HRP, respectively. The frequencies of these bands were lower by 4-6 $cm^{-1}$ for the $^{15}N^{16}O$ derivative, and they assigned this band to $\nu_{Fe\text{-}NO}$. They also detected another NO-isotope-sensitive band at 573 and 574 $cm^{-1}$ for NO-bound ferric Mb and HRP, respectively, which downshifted by 19-20 $cm^{-1}$ with $^{15}N^{16}O$ derivative, and thus they assigned this band to the $\delta_{FeNO}$. The $\nu_{Fe\text{-}NO}$ and $\delta_{FeNO}$ bands of NO-bound ferric $P450_{cam}$ in the presence of camphor were detected at 522 and 546 $cm^{-1}$, showing 2 and 13 $cm^{-1}$ downshifts upon $^{15}N^{16}O$ substitution, respectively.[80]

### 1.4.5 $OH^-$

Heme proteins form a hydroxy complex at high pH for ferric states. These derivatives exist in a high- and low-spin equilibrium.

**High- and Low-Spin Equilibrium**

Hydroxy complexes of metMb and metHb have magnetic susceptibilities in between those of high- and low-spin species at room temperature.[81] These derivatives are in thermal spin-state equilibrium. The spin-state equilibrium was investigated by analysis of the visible

spectra,[82] and the temperature dependence of magnetic susceptibility.[81] The population ratio of high-spin to low-spin species in hydroxy derivatives of metMb and metHb are quite different at room temperature, which are 70:30 and 45:55, respectively.[83] The spin-state equilibrium of some metHb derivatives can be induced by addition of allosteric effectors.[84] On the other hand, hydroxy complexes of $Fe^{III}$(TMP) (TMP; *meso*-tetramesityporpyrin) behaves as a typical high-spin, five-coordinate iron (III) compound.[85]

**$\nu_{Fe\text{-}OH}$**

The Fe-OH stretching ($\nu_{Fe\text{-}OH}$) band of hydroxy complexes of heme proteins have been detected at 490 and 495 $cm^{-1}$ for hydroxy-Mb ($MbOH^-$) and -Hb ($HbOH^-$), respectively.[86,87] This band was assigned to the $\nu_{Fe\text{-}OH}$ band of high-spin species since its Raman excitation profile was the same as that for the marker bands of high-spin species.[88] The $\nu_{Fe\text{-}OH}$ band are detected at 450 and 503 $cm^{-1}$ for reaction intermediates of CcO and HRP, respectively.[85,89] The $\nu_{Fe\text{-}OH}$ band has been detected at 565 $cm^{-1}$ for methemerythrin.[90]

The $\nu_{Fe\text{-}OH}$ of the $Fe(TMPPyP)(OH)_{aq}^{4+}$ ( Fe(TMPPyP); [tetrakis-5,10,15,20-(2-N-methylpyridyl)porpyrinato]iron(III) ) complex having a 5-coordinate high-spin $Fe^{III}$ was detected at 541 $cm^{-1}$, while the hydroxy-iron-hydroxy symmetric stretching ($\nu_{sym}(OH)_2$) mode of the $Fe(TMPPyP)(OH)_{2(aq)}^{3+}$ complex having a low-spin 6-coordinate bis hydroxy structure was detected at 443 $cm^{-1}$.[91] But recently, two $\nu_{Fe\text{-}OH}$ bands have been detected at 498 and 447 $cm^{-1}$ for the $Fe(TMPPyP)(OH)_{2(aq)}^{3+}$ complex, and the 447 $cm^{-1}$ band was reassigned to the $\nu_{sym}(OH)_2$ band of the high-spin species while the 498 $cm^{-1}$ band was attributed to the $\nu_{sym}(OH)_2$ band of the low-spin species from their temperature dependencies.[92]

## References


(1) (a) Gouterman, M. In *The Porphyrins*; Dolphin, D., Ed; Academic Press: New York, 1978; Vol. 3, pp. 1-165. (b) Adar, F. In *The Porphyrins*; Dolphin, D., Ed; Academic Press: New York, 1978; Vol. 3, pp. 167-209.

(2) Spiro, T. G., Ed. In *Biological Application of Raman Spectroscopy*; Wiley-Interscience: New York, 1988; Vol. 3

(3) (a) Yu, N. T.; Kerr, E. In *Biological Application of Raman Spectroscopy*; Spiro, T. G., Ed.; Wiley-Interscience: New York, 1988; Vol. 3, pp. 39-95. (b) Yu, N. T. *Methods Enzymol.* **1986**, *130*, 350-409.

(4) (a) Phillips, S. E. V. *Nature*, **1978**, 273, 247-248. (b) Phillips, S. E. V. *J. Mol. Biol.* **1980**, *142*, 531-554.

(5) (a) Shaanan, B. *Nature* **1982**, *296*, 683-684. (b) Shaanan, B. *J. Mol. Biol.* **1983**, *171*, 31-59.

(6) (a) Brzozowski, A.; Derewenda, Z.; Dodson, E.; Dodson, G.; Grabowski, M.; Liddington, R.; Skarzynski, T.; Vallely, D. *Nature* **1984**, *307*, 74-76. (b) Condon, P. J.; Royer Jr., W. E. *J. Biol. Chem.* **1994**, *269*, 25259-25267.

(7) Congiu-Castellano, A.; Bianconi, A.; Dell'Ariccia, M.; Longa, S. D.; Giovannelli, A.; Burattini, E.; Castagnola, M. *Biochem. Biophys. Res. Commun.* **1987**, *147*, 31-38.

(8) Zhu, L.; Sage, J. T.; Champion, P. M. *Biochemistry* **1993**, *32*, 11181-11185.

(9) Phillips, S. E. V.; Schoenborn, B. P. *Nature* **1981**, *292*, 81-82.

(10) Kitagawa, T.; Ondrias, M. R.; Rousseau, D. L.; Ikeda-Saito, M.; Yonetani, T. *Nature* **1982**, *298*, 869-871.

(11) Brunner, H. *Naturwissenschaften* **1974**, *61*, 129.

(12) Nagai, K.; Kitagawa, T.; Morimoto, H. *J. Mol. Biol.* **1980**, *136*, 271-289.

(13) Duff, L. L.; Appelman, E. H.; Shriver, D. F.; Klotz, I. M. *Biochem. Biophys. Res. Commun.* **1979**, *90*, 1098-1103.

(14) Kerr, E. A.; Yu, N.-T.; Bartnicki, D. E.; Mizukami, H. *J. Biol. Chem.* **1985**, *260*, 8360-8365.

(15) Hu, S.; Schneider, A. J.; Kincaid, J. R. *J. Am. Chem. Soc.* **1991**, *113*, 4815-4822.

(16) van Wart, H. E.; Zimmer, J. *J. Biol. Chem.* **1985**, *260*, 8372-8377.

(17) Hu, S.; Kincaid, J. R. *J. Am. Chem. Soc.* **1991**, 113, 7189-7194.

(18) (a) Ogura, T.; Takahashi, S.; Shinzawa-Itoh, K.; Yoshikawa, S.; Kitagawa, T. *J. Am. Chem. Soc.* **1990**, *112*, 5630-5631. (b) Ogura, T.; Takahashi, S.; Shinzawa-Itoh, K.; Yoshikawa, S.; Kitagawa, *T. Bull. Chem. Soc. Jpn.* **1991**, *64*, 2901-2907. (c) Ogura, T.; Takahashi, S.; Hirota, S.; Shinzawa-Itoh, K.; Yoshikawa, S.; Appelman, E. H.; Kitagawa, T. *J. Am. Chem. Soc.* **1993**, *115*, 8527-8536.

(19) Han, S.; Ching, Y.-C.; Rousseau, D. L. *Proc. Natl. Acad. Sci. U.S.A.* **1990**, *87*, 2491-2495.

(20) Varotsis, C.; Woodruff, W. H.; Babcock, G. T. *J. Am. Chem. Soc.* **1989**, *111*, 6439-6440.

(21) Potter, W. T.; Tucker, M. P.; Houtchens, R. A.; Caughey, W. S. *Biochemistry* **1987**, *26*, 4699-4707.

(22) Bangcharoenpaurpong, O; Rizos, A. K.; Champion, P. M.; Jollie, D; Sligar, S. G. *J. Biol. Chem.* **1986**, *261*, 8089-8092.

(23) Egawa, T.; Ogura, T.; Makino, R.; Ishimura, Y.; Kitagawa, T. *J. Biol. Chem.* **1991**, *266*, 10246-10248.

(24) Proniewicz, L. M.; Bruha, A.; Nakamoto, K.; Kyuno, E.; Kincaid, J. R. *J. Am. Chem. Soc.* **1989**, *111*, 7050-7056.

(25) Bajdor, K.; Oshio, H.; Nakamoto, K. *J. Am. Chem. Soc.* **1984**, *106*, 7273-7274.

(26) (a) Proniewicz, L. M.; Paeng, I. R.; Nakamoto, K. *J. Am. Chem. Soc.* **1991**, *113*, 3294-3303. (b) Wagner, W. D.; Paeng, I. R.; Nakamoto, K. *J. Am. Chem. Soc.* **1988**, *110*, 5565-5567.

(27) Burke, J. M.; Kincaid, J. R.; Peters, S.; Gagne, R. R.; Collman, J. P.; Spiro, T. G. *J. Am. Chem. Soc.* **1978**, *100*, 6083-6088.

(28) Benko, B; Yu, N.-T. *Proc. Natl. Acad. Sci. U.S.A.* **1983**, *80*, 7042-7046.

(29) Walters, M. A.; Spiro, T. G., *J. Am. Chem. Soc.* **1980**, *102*, 6857-6858.

(30) Oertling, W. A.; Kean, R. T.; Wever, R.; Babcock, G. T. *Inorg. Chem.* **1990**, *29*, 2633-2645.

(31) (a) Marks, G. S.; Brien, J. F.; Nakatsu, K.; McLaughlin, B. E. *Trends in Pharmacol. Sci.* **1991**, *12*, 185-188. (b) Snyder, S. H.; Brecht, D. S. *Sci. American* **1992**, May 68-77.

(32) Kuriyan, J.; Wilz, S.; Karplus, M.; Petsko, G. A., *J. Mol. Biol.* **1986**, *192*, 133-154.

(33) (a) Cheng, X.; Schoenborn, B. P., *J. Mol. Biol.* **1991**, *220*, 381-399. (b) Cheng, X.; Schoenborn, B. P. *Acta Cryst.* **1990**, *B46*, 195-208. (c) Hanson, J. C.; Schoenborn, B. P. *J. Mol. Biol.* **1981**, *153*, 117-146.

(34) (a) Collman, J. P.; Brauman, J. I.; Iverson, B. L.; Sessler, J. L.; Morris, R. M.; Gibson, Q. H. *J. Am. Chem. Soc.* **1983**, *105*, 3052-3064. (b) Collman, J. P.; Brauman, J. I.; Collins, T. J.; Iverson, B. L.; Lang, G.; Pettman, R. B.; Sessler, J. L.; Walters, M. A. *J. Am. Chem. Soc.* **1983**, *105*, 3038-3052.

(35) (a) Moore, J. N.; Hansen, P. A.; Hochstrasser, R. M.; *Proc. Natl. Acad. Sci. U.S.A.* **1988**, *85*, 5062-5066. (b) Locke, B.; Diller, R.; Hochstrasser, R. M. In *Advances in Spectroscopy*, Clark, R. J. H.; Hester, R. E. Eds.; Wiley & Sons: New York, 1993; Vol. 21B, pp 1-47.

(36) Quillin, M. L.; Arduini, R. M.; Olson, J. S.; Phillips Jr, G. N. *J. Mol. Biol.* **1993**, *234*, 1409-155.

(37) (a) Hoard, J. L. In *Porphyrins and Metalloporphyrins*; Smith, K. M. Ed.; Elsevier: New York, 1975, p 351. (b) Peng, S. M.; Ibers, J. A. *J. Am. Chem. Soc.* **1976**, *98*, 8032-8036.

(38) (a) Alben, J. O. ; Caughey, W. S. *Biochemistry*, **1968**, *7*, 175-183. (b) Caughey, W. S.; Alben, J. O.; McCoy, S.; Boyer, S. H.; Charache, S.; Hathaway, P., *Biochemistry* **1969**, *8*, 59-62.

(39) (a) Makinen, M. W.; Houtchens, R. A.; Caughey, W. S. *Proc. Natl. Acad. Sci. U.S.A.* **1979**, *76*, 6042-6046. (b) Caughey, W. S.; Shimada, H.; Choc H. G.; Tucker, M. P. *Proc. Natl. Acad. Sci. U.S.A.* **1981**, *78*, 2903-2907.

(40) (a) Ansari, A.; Berendzen, J.; Braunstein, D.; Cowen, B. R.; Frauenfelder, H.; Hong, M. K.; Iben, E. T.; Johnson, J. B.; Ormos, P.; Sauke, T. B.; Scholl, R.; Schulte, A.; Steinbach, P. J.; Vittitow, J.; Young, R. D., *Biophys. Chem.* **1987**, *26*, 337-355. (b) Frauenfelder, H.; Park, F.; Young, R. D., *Annu. Rev. Biophys. Chem.* **1988**, *17*, 451-479. (c) Mourant, J. R.; Braunstein, D. P.; Chu, K.; Frauenfelder, H.; Nienhaus, G. U. Ormos, P.; Young, R. D. *Biophys. J.* **1993**, *65*, 1496-1507.

(41) Tsubaki, M.; Srivastava, R. B.; Yu, N. T. *Biochemistry* **1982**, *21*, 1132-1140.

(42) (a) Rousseau, D. L.; Ondrias, M. R.; LaMar, G. N.; Kong, S. B.; Smith, K. M. *J. Biol. Chem.* **1983**, *258*, 1740-1746. (b) Yu, N.-T.; Benko, B.; Kerr, E. A.; Gersonde, K. *Proc. Natl. Acad. Sci. USA* **1984**, *81*, 5106-5110. (c) Uno, T.; Nishimura, Y.; Tsuboi, M.; Makino, R.; Iizuka, T.;

Ishimura, Y. *J. Biol. Chem.* **1987**, *262*, 4549-4556. (d) Nagai, M.; Yoneyame, Y.; Kitagawa, T. *Biochemistry* **1991**, *30*, 6495-6503. (e) Lin, S.-H.; Yu, N.-T.; Tame, J.; Shih, D.; Renaud, J.-P.; Pagnier, J.; Nagai, K. *Biochemistry* **1990**, *29*, 5562-5566. (f) Ramsden, J.; Spiro, T. G. *Biochemistry* **1989**, *28*, 3125-3128. (g) Sakan, Y.; Ogura, T.; Kitagawa, T.; Fraunfelter, F. A.; Mattera, R.; Ikeda-Saito, M. *Biochemisty* **1993**, *32*, 5815-5824. (h) Takahashi, S.; Wang, J.; Rousseau, D. L.; Ishikawa, K.; Yoshida, T.; Takeuchi, N.; Ikeda-Saito, M. *Biochemistry* **1994**, *33*, 5531-5538.

(43) (a) Smulevich, G.; Evangelista-Kirkup, R.; English, A.; Spiro, T. G. *Biochemistry* **1986**, *25*, 4426-4430. (b) Smulevich, G.; Miller, M. A.; Kraut, J.; Spiro, T. G. *Biochemistry* **1991**, *30*, 9546-9558.

(44) Evangelista-Kirkup, R.; Smulevich, G.; Spiro, T. G. *Biochemistry* **1986**, *25*, 4420-4425.

(45) (a) Rousseau, D. L.; Ondrias, M. R.; La Mar, G. N.; Kong, S. B.; Smith, K. M. *J. Biol. Chem.* **1983**, *258*, 1740-1746. (b) Uno, T.; Nishimura, Y.; Makino, R.; Iizuka, T.; Ishimura, Y.; Tsuboi, M. *J. Biol. Chem.* **1985**, *4*, 2023-2026. (c) Tsubaki, M.; Ichikawa, Y. *Biochim. Biophys. Acta.* **1984**, *827*, 268-274. (d) Tsubaki, M.; Hiwatashi, A.; Ichikawa, Y. *Biochemistry* **1986**, *25*, 3563-3569. (e) Wells, A. V.; Li, P.; Champion, P. M.; Martinis, S. A.; Sligar, S. G. *Biochemistry* **1992**, *31*, 4384-4393.

(46) Argade, P. V.; Ching, Y.; Rousseau, D. L. *Nature* **1984**, *225*, 329-331.

(47) Wang, J.; Stuehr, D. J.; Ikeda-Saito, M.; Rousseau, D. L. *J. Biol. Chem.* **1993**, *268*, 22255-22258.

(48) Yu, N.-T.; Kerr, E. A.; Ward, B.; Chang, C. K. *Biochemistry* **1983**, *22*, 4534-4540.

(49) Ray, G. B.; Li, X.-Y.; Ibers, J. A.; Sessler, J. L.; Spiro, T. G. *J. Am. Chem. Soc.* **1994**, *116*, 162-176.

(50) Kerr, E. A.; Mackin, H. C.; Yu, N. T. *Biochemistry* **1983**, *22*, 4373-4379.

(51) Kerr, E. A.; Yu, N. T.; Bartnicki, D. E.; Mizukami, H. *J. Biol. Chem.* **1985**, *260*, 8360-8365.

(52) Li, X.-Y.; Spiro, T. G. *J. Am. Chem. Soc.* **1988**, *110*, 6024-6033.

(53) (a) Tsubaki, M.; Ichikawa, Y. *Biochim. Biophys. Acta* **1985**, *827*, 268-274. (b) Tsubaki, M.; Hiwatashi, A.; Ichikawa, Y. *Biochemistry* **1986**, *25*, 3563-3569.

(54) Uno, T.; Nishimura, Y.; Tsuboi, M.; Makino, R.; Iizuka, T.; Ishimura, Y. *J. Biol. Chem.* **1987**, *262*, 4549-4556.
(55) (a) Li, X. Y.; Spiro, T. G., *J. Am. Chem. Soc.* **1988**, 110, 6024-6033. (b) Smulevich, G.; Miller, M.; Kraut, J.; Spiro, T. G. *Biochemistry* **1991**, *30*, 9546-9558.
(56) Nagai, M.; Yoneyama, Y.; Kitagawa, T., *Biochemistry* **1991**, *30*, 6495-6503.
(57) Augspurger, J. D.; Dykstra, C. E.; Oldfield, E. *J. Am. Chem. Soc.* **1991**, *113*, 2447-2451.
(58) Li, T.; Quillin, M. L.; Phillips., G. N. J.; Olson, J. S. *Biochemistry* **1994**, *33*, 1433-1446.
(59) Jewsbury, P.; Kitagawa, T. *Biophys. J.* **1994**, *67*, 2236-2250.
(60) (a) Deatherage, J. F.; Loe, R. S.; Anderson, C. M.; Moffat, K. *J. Mol. Biol.* **1976**, *104*, 687-796. (b) Steigemann, W.; Weber, E. *J. Mol. Biol.* **1979**, *127*, 309-338.
(61) (a) Rajarathnam, K.; La Mar, G. N.; Chiu, M. L.; Sligar, S. G. *J. Am. chem. Soc.* **1992**, *114*, 9048-9058. (b) Rajarathnam, K.; Qin, J.; La Mar, G. N.; Chiu, M. L.; Sligar, S. G. *Biochemistry* **1993**, *32*, 5670-5680.
(62) Yu, N.-T.; Benko, B.; Kerr, E. A.; Gersonde, K. *Proc. Natl. Acad. Sci. U.S.A.* **1984**, *81*, 5106-5110.
(63) Henry, E. R.; Rousseau, D. L.; Hopfield, J. J.; Noble, R. W.; Simon, S. R. *Biochemistry* **1984**, *24*, 5907-5918.
(64) Sitter, A. J.; Reczek, C. M.; Terner, J. *Biochim. Biophys. Acta.* **1985**, *828*, 229-235.
(65) Lopez-Garriga, J. J.; Anthony, W.; Kean, R. T.; Hoogland, H.; Wever, R.; Babcock, G. T. *Biochemistry* **1990**, *29*, 9387-9395.
(66) (a) Hu, S.; Treat, R. W.; Kincaid, J. R. *Biochemistry* **1993**, *32*, 10125-10130. (b) Al-Mustafa, J.; Kincaid, J. R. *Biochemistry* **1994**, *33*, 2191-2197.
(67) Surerus, K. K.; Ortling, W. A.; Fan, C.; Gurbiel, R. J.; Einarsdottir, O.; Antholine, W. E.; Dyer, R. B.; Hoffman, B. M.; Woodruff, W. H.; Fee, J. A. *Proc. Natl. Acad. Sci. USA* **1992**, *89*, 3195-3199.
(68) Tanaka, T.; Yu, N.-T.; Chang, C. K. *Biophys. J.* **1987**, *52*, 801-805.
(69) Scheidt, W. R.; Lee, Y. J.; Luangdilok, W.; Haller, K. J.; Anzai, K.; Hatano, K. *Inorg. Chem.* **1983**, *22*, 1516-.
(70) Uno, T.; Hatano, K.; Nishimura, Y.; Arata, Y. *Inorg. Chem.* **1988**, *27*, 3215-3219.

(71) (a) Yoshikawa, S.; O'Keeffe, D. H.; Caughey, W. S. *J. Biol. Chem.* **1985**, *260*, 3518-3528. (b) Yoshikawa, S.; Caughey, W. S. *J. Biol. Chem.* **1990**, *265*, 7945-7958. (c) Tsubaki, M.; Yoshikawa. S. *Biochemistry* **1993**, *32*, 164-173.

(72) (a) Traylor, T. G.; Sharma, V. S. *Biochemistry* **1992**, *31*, 2847-2849. (b) Marletta, M. A. *TIBS* **1989**, *14*, 488-492. (c) Ignarro, L. J. *Semin. Hematol.* **1989**, *26*, 63-76. (d) Ignarro, L. J. *Annu. Rev. Pharm. Toxicol.* **1990**, *30*, 535-560. (e) Garthwaite, J. *Treds. Neurosci.* **1991**, *14*, 60-67.

(73) (a) Deatherage, J. F.; Maffat, K. *J. Mol. Biol.* **1979**, *134*, 401-417. (b) Piciulo, P. L.; Rupprecht, G.; Scheidt, W. R. *J. Am. Chem. Soc.* **1974**, *96*, 5293-5295. (c) Scheidt, W. R.; Frisse, M. E. *J. Am. Chem. Soc.* **1975**, *97*, 17-21. (d) Scheidt, W. R.; Piciulo, P. L. *J. Am. Chem. Soc.* **1976**, *98*, 1913-1919. (e) Scheidt, W. R.; Brinegar, A. C.; Ferro, E. B.; Kirner, J. F. *J. Am. Chem. Soc.* **1977**, *99*, 7315-7322.

(74) Chottard, G.; Mansuy, D. *Biochem. Biophys. Res. Commun.* **1977**, *77*, 1333-1338.

(75) Benko, B.; Yu, N.-T. *Proc. Natl. Acad. Sci. USA* **1983**, *80*, 7042-7046.

(76) Rouseau, D. L.; Singh, S.; Ching, Y.-C.; Sassaroli, M. *J. Biol. Chem.* **1988**, *263*, 5681-5685.

(77) Desbois, A.; Lutz, M.; Banerjee, R. *Biochim. Biophys. Acta* **1981**, *671*, 184-192.

(78) Han, S.; Madden, J. F.; Siegel, L. M.; Spiro, T. G. *Biochemistry* **1989**, *28*, 5477-5485.

(79) Hu, S.; Kincaid, J. R. *J. Am. Chem. Soc.* **1991**, *113*, 9760-9766.

(80) Hu, S.; Kincaid, J. R. *J. Am. Chem. Soc.* **1991**, *113*, 2843-2850.

(81) Beetlestone, J.; George, P. *Biochemistry* **1964**, *3*, 707-714.

(82) Smith, D. W.; Williams, R. J. P. *Biochem. J.* **1968**, *110*, 297-301.

(83) (a) George, P.; Beetlestone, J.; Griffith, J. S. *Rev. Mod. Phys.* **1964**, *36*, 441-463. (b) Yonetani, T.; Iizuka, T.; Waterman, M. R. *J. Biol. Chem.* **1971**, *24*, 7683-7689.

(84) (a) Perutz, M. F.; Heidner, E. J.; Ladner, J. E.; Beetlestone, J. G.; Ho, C.; Slade, E. F. *Biochemistry* **1974**, *13*, 2187-2200. (b) Messana, C.; Cerdonio, M.; Shenkin, P.; Noble, R. W.; Fermi, G.; Perutz, R. N.; Perutz, M. F. *Biochemistry* **1978**, *17*, 3652-3663. (c) Perutz, M. F.; Sanders, J. K. M.; Chenery, D. H.; Nobble, R. W.; Pennelly, R. R.; Fung, L. W.-M.; Ho, C.; Giannini, I.; Pörschke, D.; Winkler, H. *Biochemistry* **1978**, *17*, 3640-3652.

(85) Sitter, A. J.; Shifflett, J. R.; Terner, J. *J. Biol. Chem.* **1988**, *263*, 13032-13038.
(86) Cheng, R.-J.; Latos-Grazynski, L.; Balch, A. L. *Inrog. Chem.* **1982**, *21*, 2412-2418.
(87) Desbois, A.; Lutz, M.; Ramaprasad *Biochemisty* **1979**, *18*, 1510-1518.
(88) (a) Asher, S. A.; Vickery, L. E.; Schuster, T. M. *Biochemistry* **1977**, *16*, 5849-5856. (b) Asher, S. A.; Schuster, T. M. *Biochemistry* **1979**, *18*, 5377-5387. (c) Asher, S. A. *Methods in Enzymology* **1981**, *76*, 312-413.
(89) Han, S.; Ching, Y.-C.; Rousseau, D. L. *Nature* **1990**, *348*, 89-90.
(90) Shiemke, A. K.; Loehr, T. M.; Sanders-Loehr, J. *J. Am. Chem. Soc.* **1986**, *108*, 2437-2443.
(91) Reed, R. A.; Rodgers, K. R.; Kushmeider, K.; Spiro, T. G.; Su, Y. O. *Inorg. Chem.* **1990**, *29*, 2881-2883.
(92) Rodgers, K. R.; Reed, R. A.; Spiro, T. G.; Su, Y. O. *New J. Chem.* **1992**, *16*, 533-535.

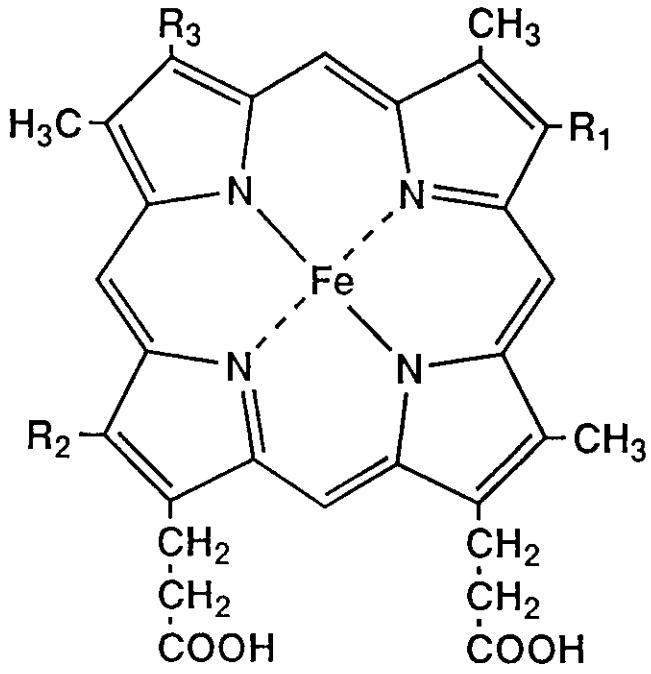


(a) Heme structure

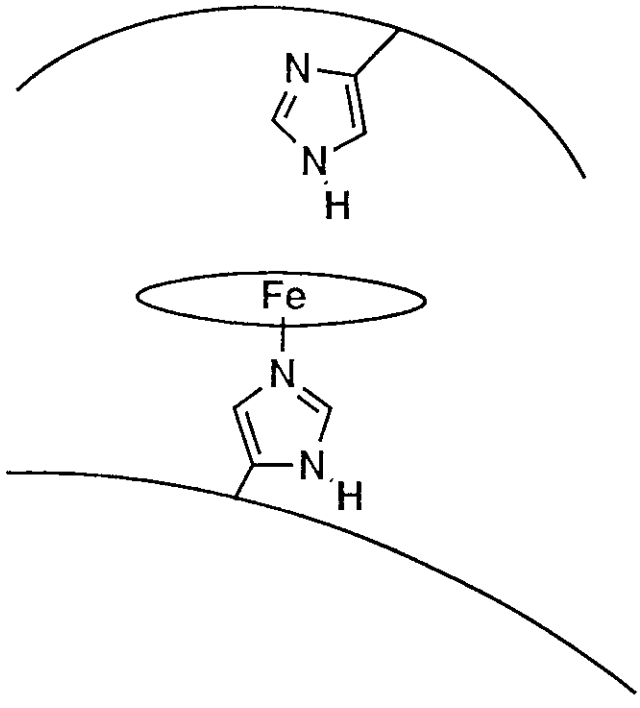


(b) Protein structure around the heme

**Figure 1-1**. Schematic view of a heme.

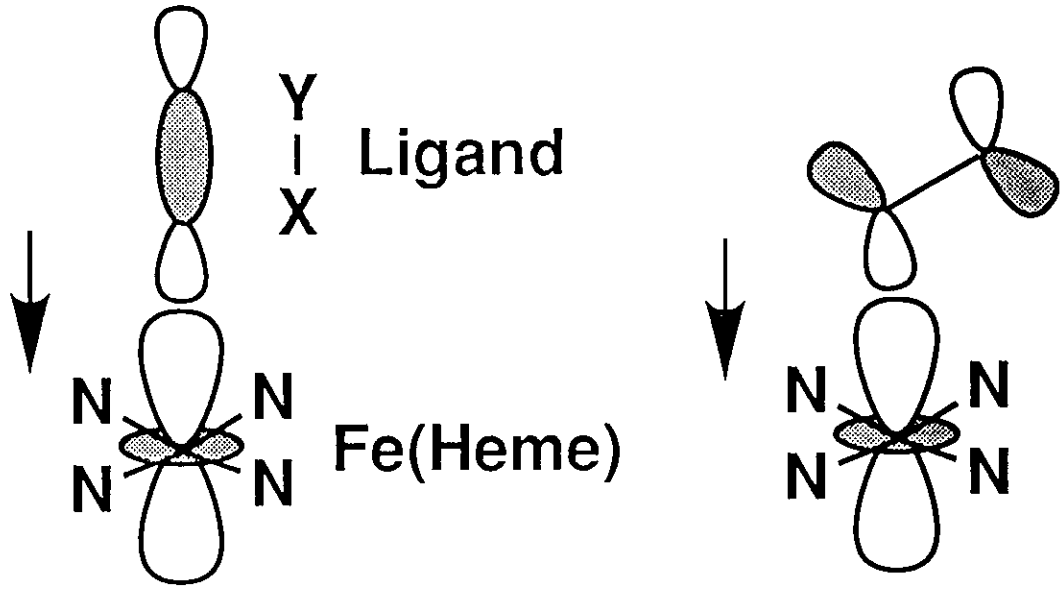


(a) σ-bonding

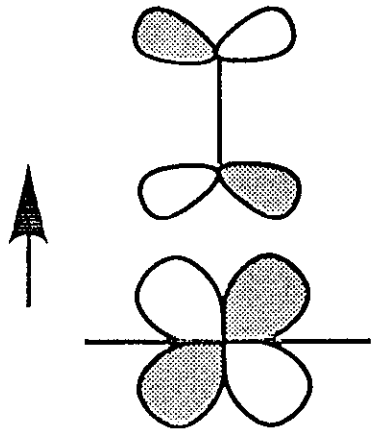

(b) π-bonding

**Figure 1-2.** Schematic view for the ligand-heme interaction, σ- and π-bondings (reproduced from reference 3b).

# Chapter I-2.

# Observation of a New Oxygen-Isotope-Sensitive Raman Band for Oxyhemoproteins and Its Implications in Heme Pocket Structures

## Abstract

A new oxygen-isotope-sensitive Raman band was found for oxyhemoglobin ($HbO_2$) and oxycytochrome *c* oxidase ($CcO{\cdot}O_2$) in the frequency region lower than the Fe-$O_2$ stretching mode ($\nu_{Fe\text{-}O_2}$). This band was located at 425 $cm^{-1}$ for $Hb^{16}O_2$ and shifted to 405 $cm^{-1}$ with $Hb^{18}O_2$ and to ~423 and ~407 $cm^{-1}$ with $Hb^{16}O^{18}O$. The corresponding band appeared at 435 $cm^{-1}$ for $CcO{\cdot}^{16}O_2$ and shifted to 415 $cm^{-1}$ with $CcO{\cdot}^{18}O_2$. Accordingly, this band has been assigned to the Fe-O-O bending mode ($\delta_{FeOO}$). However, the corresponding band could not be identified for oxymyoglobin ($MbO_2$). $\nu_{Fe\text{-}O_2}$ was observed at 568, 567, 544, and 544 $cm^{-1}$ for $Hb^{16}O_2$, $Hb^{16}O^{18}O$, $Hb^{18}O^{16}O$, and $Hb^{18}O_2$, respectively, and the corresponding modes were observed at 571, 569, 547, and 545 $cm^{-1}$ for $MbO_2$ and 571, 567, 548, and 544 $cm^{-1}$ for $CcO{\cdot}O_2$. The $\nu_{Fe\text{-}O_2}$ bandwidths of $HbO_2$ and $MbO_2$ were alike and 1.5 times broader than that of $CcO{\cdot}O_2$, suggesting that the Fe-O-O geometry is more nearly fixed in the latter. Despite the greatly different reactivities of bound $O_2$ in $HbO_2$ and $CcO{\cdot}O_2$, their $\nu_{Fe\text{-}O_2}$ and $\delta_{FeOO}$ frequencies and $O_2$-isotopic frequency shifts were alike, indicating similar Fe-O-O binding geometries. Normal coordinate calculations for an isolated three-atom molecule could reproduce the observed isotopic frequency shifts with the 115° bond angle reported for $MbO_2$, but not with the 155° angle reported for $HbO_2$.

## 2.1 Introduction

Since the Fe-$O_2$ stretching frequency ($\nu_{Fe\text{-}O_2}$) of the dioxygen adducts of heme proteins reflects the strength of the Fe-$O_2$ bond and thus the state of the bound $O_2$, the $\nu_{Fe\text{-}O_2}$ resonance Raman (RR) band has attracted attention in studies of model compounds as well as heme proteins as discussed in chapter I-1.[1] The location of the iron-oxygen-oxygen bending mode ($\delta_{FeOO}$) frequency is also quite important in molecular dynamics studies on $O_2$ adducts of heme proteins, since the Fe-O-O bending force constant, which mainly determines the energy necessary for distortion of the Fe-O-O geometry, should depend upon the experimental $\delta_{FeOO}$ frequency. The RR studies of model compounds suggest possible identification of the $\delta_{FeOO}$ RR band for heme proteins. For example the $\delta_{FeOO}$ band was detected at 279 $cm^{-1}$ in (Pc)$FeO_2$ (Pc: phthalocyaninine),[1a] at 349 $cm^{-1}$ in (TPP)$FeO_2$ (TPP: tetraphenylporphyrin),[2b] and at 343 $cm^{-1}$ in (TMP)$FeO_2$ (TMP: tetramesitylporphyrin).[2b] However, $\delta_{FeOO}$ has only been observed for compound III of lactoperoxidase (at 491 $cm^{-1}$) among various dioxygen bound heme proteins,[3] although the iron-oxygen stretching mode ($\nu_{Fe\text{-}O_2}$) has been detected with several dioxygen bound heme proteins as summarized in chapter I-1.[4-12]

The Fe-ligand geometry of dioxygen derivatives of heme proteins has been discussed in chapter I-1. But there might be structural differences between the crystalline state and in solutions, as has been indicated by RR studies of met Mb and deoxyMb.[13] It is curious to know whether the structure of the FeOO unit has some correlation with reactivities of bound oxygen in solution. Accordingly, in this chapter, RR spectra of two kinds of oxyhemoproteins in solution were investigated, those with unreactive $O_2$ and with $O_2$ to be activated. For the former category the $^{16}O^{18}O$ as well as $^{16}O_2$ and $^{18}O_2$ adducts of Mb and Hb were looked at, whereas for the latter the same dioxygen adducts of CcO were examined.

## 2.2 Experimental Procedures

Raman scattering was excited at 423.0 and 427.0 nm with the laser system depicted in Figure 2-1. The second harmonic of the output of a Ti-sapphire laser (Spectra Physics, Model 3900) pumped by an $Ar^+$ ion laser

(Spectra Physics, Model 2045) was generated with a $KNbO_3$ crystal (VIGRO OPTICS, USA).

The resonance Raman (RR) measurement system is shown in Figure 2-2. The detector was a cooled (- 20 °C) diode array (PAR, 1421HQ) attached to a single polychromator (Ritsu Oyo Kogaku DG-1000). Two interchangeable blazed-holographic gratings (500-nm blaze - 1200 grooves/mm or 900-nm blaze - 1200 grooves/mm) were mounted to the monochromator. The former and latter were used in the first and second order, respectively, and therefore the latter has provided a higher resolution (~0.4 $cm^{-1}$/channel) than the former (~1.0 $cm^{-1}$/channel). The slit width and slit height used were 200 μm and 10 mm, respectively. The exciting laser beam was focused to ~50 μm and its power at the sample point was 4-10 mW. Raman shifts were calibrated with $CCl_4$ and acetone, and the uncertainties of peak positions were 1 $cm^{-1}$.

Measurements for $MbO_2$ and $HbO_2$ were carried out at room temperature with a spinning cell (3500 rpm) to avoid photodissociation of oxygen. Measurements for $CcO{\cdot}O_2$ were carried out at 5 °C with the artificial cardiovascular system for pursuing enzymatic reactions (Figure 1-3).[10c,14] About 75 ml of the sample solution containing 50 μM enzyme, 16.7 μM cytochrome *c*, 100 mM ascorbate, and 50 mM potassium phosphate buffer, pH 7.4 was circulated through a Teflon tube (i.d., 2 mm; o.d., 4 mm) through the peristaltic pump (Cole Parmer, 7553-20). The pushed solution came to Lung 1, which was a highly efficient artificial lung ordinary used for medical purpose (MERA, SILOX-S) and was a 20-cm-long cartridge into which many fine and very thin-skinned silicone tubes were bundled. The membrane of Lung 1 allowed only small molecules to permeate through. The lung was filled with CO, and CO diffused through the silicone wall into the enzyme solution to form a CO adduct. The inside of Lung 2 was filled with $^{16}O_2$, $^{18}O_2$, or $^{16}O^{18}O$ for the formation of reaction intermediates, and $O_2$ molecules penetrated into the solution at this lung. The choices of the $O_2$-isotope paths were controlled by a computer with two-channel synchronous valves driven by compressed $N_2$ gas. This replacement enabled us to observe the individual Raman spectra of intermediates derived from $^{16}O_2$, $^{18}O_2$, and $^{16}O^{18}O$ in turn and repeatedly and to accumulate the quasi-simultaneous spectra in computer memory. The upstream beam was a 590 nm-output of an $Ar^+$ ion laser (Spectra Physics 164) pumped dye laser (Spectra

Physics 375) with Rhodamine 6G. The pump beam of 210 mW was focused to 0.05 x 1 $mm^2$ at a 0.6 x 0.6 mm rectangular type quartz cell by two cylindrical lenses to achieve CO photodissociation, and the photodissociated enzyme reacted with oxygen at once. The downstream beam was a 423.0 nm-output obtained from a $Ar^+$ ion laser (Spectra Physics 2045) pumped dye laser (Spectra Physics 375B) with stilibene-420, and was used to excite Raman scattering. The laser power of this probe beam was 4 mW at the sample point. The flow rate of the sample was 40 ml/min, and the beam distance between the pump and probe beams was 200 μm. Thus the collected Raman scattering of the transient $CcO{\cdot}O_2$ with lifetime of 100 μs was measured. The oxygen remover, also an artificial lung, was used to remove excess oxygen out of the solution and allow the enzyme to return to the fully reduced state by electrons of ascorbate mediated by cytochrome *c*. The sample reservoir was cooled to 5 °C.

Horse Mb (Sigma, type M630) was dissolved in 50 mM Tris-HCl buffer, pH 8.5, and subjected to gel filtration through Sephadex G-25 under $O_2$ after reduction by sodium dithionite. The $MbO_2$ thus obtained was diluted to 90 μM with 50 mM Tris-HCl buffer, pH 8.5. Human adult Hb was prepared according to the method of Geraci et al.,[15] and its concentration was adjusted to 50 μM (heme) with 50 mM Tris-HCl buffer, pH 8.5. Purification of bovine CcO and preparation of its $O_2$ adduct were described elsewhere.[10c,16] $^{16}O^{18}O$ was obtained by the $Ce^{IV}$-oxidation of $H^{16}O^{18}OH$, which was synthesized by reacting $H^{18}OF$ with $H_2{}^{16}O$.[17] The earlier procedure was improved by fluorinating $H^{18}OH$ in acetonitrile to obtain a solution of $H^{18}OF$ stabilized as a complex with CH3CN.[18,19] The mass analysis of $^{16}O^{18}O$ gave $^{16}O^{18}O/^{16}O^{16}O/^{16}O^{17}O/^{17}O^{18}O/^{18}O^{18}O$ = 94:2.2:2.2:0.1:1.4. The $O_2$-isotope adducts of Mb and Hb were obtained from their $^{16}O_2$ adducts by exposure of the sample to $N_2$ gas flow for more than 5 min followed by substitution of $^{18}O_2$ (98.2 atom %, ISOTEC Inc.) or $^{16}O^{18}O$ for $N_2$.

### 2.3 Results

Figure 2-4 shows the RR spectra in the 600-200 $cm^{-1}$ region for the $^{16}O_2$ (A), $^{16}O^{18}O$ (B), $^{18}O_2$ (C) adducts of Hb A obtained with the higher resolution grating and the difference spectrum (D) between the $^{16}O_2$ and

$^{18}O_2$ adducts. The Raman band of $Hb^{16}O_2$ at 568 $cm^{-1}$ is shifted to 544 $cm^{-1}$ with $Hb^{18}O_2$. Although there are porphyrin bands at 586 and 544 $cm^{-1}$, and the isotopic frequency shifts are not self-evident, the difference spectrum gave a clear symmetric differential pattern, and accordingly the $O_2$-isotopic frequency shift is proven, in agreement with the previous assignments.[4,5] In addition to this, we note that there is another difference pattern with a peak at 425 and a trough at 405 $cm^{-1}$. This feature is seen in the raw spectra, in which the relative intensities of the peaks at 423 and 407 $cm^{-1}$ are altered between spectra A and C. The Raman spectrum of $Hb^{16}O^{18}O$ exhibits a pattern intermediate between those of $Hb^{16}O_2$ and $Hb^{18}O_2$. In order to characterize the spectrum of $Hb^{16}O18O$ more definitely, the difference spectra between spectra A-C shown in Figure 2-4 were calculated and are displayed in Figure 2-5.

Spectrum A in Figure 2-5 is an expansion of spectrum D in Figure 2-4, making the difference peaks around 400 $cm^{-1}$ more pronounced. While the ordinate scales in spectra B and C of Figure 2-5 are the same as that of spectrum A, the intensities of the positive peaks near 568 $cm^{-1}$ and the negative peaks at 544 $cm^{-1}$ are about one half of those of spectrum A. This means that half the population of $Hb^{16}O^{18}O$ has the RR spectrum very close to that of $Hb^{16}O_2$, but the other half has that of $Hb^{18}O_2$. In other words, the $\nu_{Fe\text{-}O_2}$ frequency depends primarily on the mass of the oxygen atom directly bound to the Fe ion. However, we note that the position of the positive peak differs slightly among the three spectra: 568 $cm^{-1}$ for A, 569 $cm^{-1}$ for B, and 567 $cm^{-1}$ for C. Such variation is not observed for the negative peaks. Spectrum D, representing spectrum B - (spectrum A + spectrum C)/2 of Figure 2-4, exhibits almost no difference pattern around 570 $cm^{-1}$, indicating that the $Fe^{16}O^{18}O$ stretching frequency is very close to that of $Fe^{16}O^{16}O$ and that the $Fe^{18}O^{16}O$ stretching frequency is close to that of $Fe^{18}O^{18}O$, in agreement with the previous observation by Duff et al.[6] This fact demonstrates the end-on binding of $O_2$ to the heme iron in the solution, although the same feature was previously noted as an indication of the $\delta_{FeOO}$ mode.[20] The difference pattern around 430-400 $cm^{-1}$ is also seen in spectra B and C, but it is weaker than in spectrum A.

Figure 2-6 shows the RR spectra in the 600 to 300 $cm^{-1}$ region of the $^{16}O_2$ (A), $^{16}O^{18}O$ (B), and $^{18}O_2$ (C) adducts of Mb and the difference spectrum (D) between A and C. To get more Raman intensity, the lower resolution grating was used in these measurements. The RR spectrum of

$MbO_2$ in this frequency region is distinct from that of $HbO_2$ shown in Figure 2-4, although the RR spectra of the two species are alike in the frequency region higher than 1200 $cm^{-1}$. In particular, the 503 $cm^{-1}$ band of $MbO_2$ is absent for $HbO_2$, and the 438 $cm^{-1}$ band of $MbO_2$ is shifted to 423 $cm^{-1}$ for $HbO_2$. The latter suggests that geometrical structures of the vinyl side chains of the porphyrin are appreciably different between the two proteins.

The RR band of spectrum A at 571 $cm^{-1}$ is shifted to 545 $cm^{-1}$ in spectrum C. Although the 545 $cm^{-1}$ band appears more intense than the one at 571 $cm^{-1}$, spectrum D displays a symmetric differential pattern, indicating that the 571 $cm^{-1}$ band of $MbO_2$ undergoes a shift by 26 $cm^{-1}$ upon $^{18}O_2$ substitution similar to the shift of the 568 $cm^{-1}$ band of $HbO_2$. The 571 $cm^{-1}$ band is thus assignable to the $\nu_{Fe\text{-}O_2}$ mode. In contrast with the results for $HbO_2$, there is no trace of a differential pattern in the lower frequency region. Since the $\nu_{Fe\text{-}O_2}$ band in the RR spectrum of $Mb^{16}O^{18}O$ is obscured due to the presence of porphyrin bands in the same frequency region, difference spectra were calculated in the same way as for $HbO_2$.

Spectrum A in Figure 2-7 is the same as spectrum D in Figure 2-6. While the ordinate scales in spectra B-D are the same as that of spectrum A, the peaks in spectra B and C are significantly weaker than those in spectrum A. The position of the positive peak shifts from 571 to 573 to 569 $cm^{-1}$ in spectra A-C, while that of the negative peak shifts from 545 to 547 to 544 $cm^{-1}$, suggesting that the peak frequencies of the $\nu_{Fe\text{-}O_2}$ bands of $Mb^{16}O^{18}O$ and $Mb^{18}O^{16}O$ are slightly different from those of $Mb^{16}O_2$ and $Mb^{18}O2$, respectively. In fact, spectrum D, which represents spectrum B - (spectrum A + spectrum C)/2 of Figure 2-6, displays a small double-well pattern.

Figure 2-8 shows the same set of difference spectra observed for $CcO{\cdot}O_2$ excited at 423 nm. The $^{16}O_2/^{18}O_2$ difference spectrum (A) gives a positive peak at 571 $cm^{-1}$ and a negative peak at 545 $cm^{-1}$, similar to the spectrum of $Mb^{16}O_2/Mb^{18}O_2$. In spectra B and C the positive peak shifts to 573 and to 567 cm-1, while the negative peak shifts to 548 and 544 $cm^{-1}$. The shifts are slightly larger than those of $MbO_2$. We stress that spectrum A displays a difference pattern at 435/415 $cm^{-1}$ similar to that in Figure 2-5, although the corresponding peaks are extremely weak in spectra B and C. Difference spectrum D, representing a difference of the

type $CcO{\cdot}^{16}O^{18}O$ - $(CcO{\cdot}^{16}O_2+CcO{\cdot}^{18}O_2)/2$, shows a definite double-well pattern, demonstrating that the $O_2$ binding is of an end-on type.[10c]

## 2.4 Discussion

### The Fe-$O_2$ Stretching Mode

Analysis of the $\nu_{Fe\text{-}O_2}$ RR band of heme proteins has been obscured due to the presence of nearby porphyrin bands. In fact, the raw spectra shown in Figures 2-4 and 2-6 include a few side bands around 550 $cm^{-1}$. However, those side bands can be canceled in the isotope-difference spectra, and thus the oxygen-associated RR bands can be extracted. In order to determine the $\nu_{Fe\text{-}O_2}$ frequency precisely, we carried out simulation calculations of the isotope difference spectra by assuming a Gaussian band shape with an appropriate peak intensity and bandwidth in common to the $Fe^{16}O^{16}O$, $Fe^{16}O^{18}O$, $Fe^{18}O^{16}O$, and $Fe^{18}O^{18}O$ adducts. The results are illustrated in Figure 2-9, where (A), (B), (C), and (D) represent the assumed bands, the experimental difference spectra, the calculated difference spectra, and residuals between the experimental and calculated difference spectra, respectively, in common to the difference combinations of (a) $Mb^{16}O_2$-$Mb^{18}O_2$, (b) $Mb^{16}O_2$-$Mb^{16}O^{18}O$, (c) $Mb^{16}O^{18}O$-$Mb^{18}O_2$, and (d) $Hb^{16}O_2$-$Hb^{18}O_2$. In all four panels, the residuals are reduced to the noise level of the spectra, and therefore the spectral parameters used, including band positions and bandwidths, are considered to characterize the observed bands correctly. For $Hb^{16}O^{18}O$ the two peak positions are so close to those of $Hb^{16}O_2$ and $Hb^{18}O_2$ that the other combinations are similar to $Hb^{16}O_2$-$Hb^{18}O_2$.

The bandwidths thus obtained are 20 $cm^{-1}$ for $MbO_2$, 21 $cm^{-1}$ for $HbO_2$ and 12.9 $cm^{-1}$ for $CcO{\cdot}O_2$. We stress that the $\nu_{Fe\text{-}O_2}$ bandwidths of $MbO_2$ and $HbO_2$ are alike, but distinctly greater than that of $CcO{\cdot}O_2$. This does not depend upon the resolution of the spectrometer, since the higher-resolution grating was used for $HbO_2$ and the lower-resolution one was used for $MbO_2$ and $CcO{\cdot}O_2$. One might think that the large bandwidth for $HbO_2$ is due to an appreciable difference in the $\nu_{Fe\text{-}O_2}$ frequencies of the $\alpha$ and $\beta$ subunits, since according to the x-ray study[21b] the Fe-$O_2$ bond lengths are 1.66 Å for the $\alpha$ and 1.87 Å for the $\beta$ subunits. However, this interpretation seems less likely since the bandwidth of $HbO_2$ is almost the same as that of $MbO_2$. If the $\nu_{Fe\text{-}O_2}$ band is relatively sharp and its

frequency differs slightly between $Fe^{16}O^{16}O$ and $Fe^{16}O^{18}O$ and between $Fe^{18}O^{16}O$ and $Fe^{18}O^{18}O$, the difference spectrum of a $^{16}O^{18}O$-($^{16}O_2$+$^{18}O_2$)/2 type would give rise to two positive and two negative peaks (double-well type). When the band becomes broader at the same frequency separation or when the frequency separations between the $Fe^{16}O^{16}O$ and $Fe^{16}O^{18}O$ and between the $Fe^{18}O^{16}O$ and $Fe^{18}O^{18}O$ adducts become smaller without change in width, the double-well character of the difference spectrum becomes obscure. In fact, this type of difference spectra is less distinct in Figures 2-5 and 2-7 than in Figure 2-8, presumably for these two reasons.

The smaller width of the $\nu_{Fe\text{-}O_2}$ band for $CcO{\cdot}O_2$ would suggest that $O_2$ in $CcO{\cdot}O_2$ has a more tightly fixed geometry at the binding site than do $MbO_2$ and $HbO_2$. However, it is rather unexpected that, except for this difference in mobility, the bound $O_2$ in $CcO{\cdot}O_2$ quite closely resembles that in $HbO_2$ and $MbO_2$, even though there are distinct differences in their reactivities.

**The Fe-O-O Bending Mode**

The present experiments reveal the presence of another oxygen-isotope-sensitive band around 400 $cm^{-1}$ for $HbO_2$ and $CcO{\cdot}O_2$ besides the band around 570 $cm^{-1}$. Since the new isotope-sensitive band overlaps the $C_\beta C_a C_b$ bending mode[22,23] of the 2- and 4-vinyl groups at 407 and 423 $cm^{-1}$, it is hard to observe it in the raw spectrum. Clarification of its presence has required the measurement of two oxygen-isotope adducts under highly controlled conditions. The $^{16}O_2$-$^{18}O_2$ difference peaks were noticed for the first time at 425/405 $cm^{-1}$ for $HbO_2$ and at 435/415 $cm^{-1}$ for $CcO{\cdot}O_2$. These bands were not shifted to intermediate frequencies with $^{16}O^{18}O$, as shown in Figures 2-5 and 2-8. Despite great efforts, the corresponding band could not be recognized for $MbO_2$, even with the higher-resolution grating.

For compound III of lactoperoxidase two pairs of oxygen-isotope-sensitive Raman bands have been observed at 531/513 and 491/482 $cm^{-1}$ for the $^{18}O_2/^{16}O_2$ derivatives.[3] The latter pair was discernible when compound III was obtained from the reaction of compound II with $H_2{}^{16}O_2$ or $H_2{}^{18}O_2$ but not when it was obtained from the reactions of reduced enzyme with $^{16}O_2$ or $^{18}O_2$ and of oxidized enzyme with $H_2{}^{16}O_2$ or $H_2{}^{18}O_2$, while the former pair was observed for all three reactions. The 531/513 $cm^{-1}$ pair was assigned to the Fe-$O_2$ stretching vibration and its unusually

low frequency was attributed to increased delocalization of electrons to $O_2$ which is presumed to interact with the distal arginine. The other pair at 491/482 $cm^{-1}$ was assigned to the $\delta_{FeOO}$ mode. This was the first suggestion for the appearance of $\delta_{FeOO}$ RR band of heme proteins,[2] although it has not been acknowledged widely, partially due to the fact that the corresponding band was not clearly recognized for the Fe-$O_2$ compound derived in a normal way, that is, a reaction of reduced enzyme with dioxygen.

For nitric oxide adducts of ferrous heme proteins, such as MbNO, HbNO, and P-450·NO, the Fe-NO stretching ($\nu_{Fe-NO}$) and Fe-N-O bending ($\delta_{FeNO}$) modes have been observed around 550 and 450 $cm^{-1}$, respectively. The $\nu_{Fe-NO}$ frequencies, which show a zigzag dependence on the increase of the total mass of NO,[24,25] are sensitive to the mass of the atom bound to the iron ion but rather insensitive to the mass of the second atom. The $\nu_{Fe-O_2}$ frequencies of the $O_2$ adducts exhibit the same character as $\nu_{Fe-NO}$ regarding sensitivity to the mass of the atom bound to Fe. The frequencies of the other oxygen-isotope-sensitive bands of $HbO_2$ and $CcO·O_2$ are close to the $\delta_{FeNO}$ frequency. Accordingly, it seems reasonable to assign the new oxygen-isotope-sensitive bands found in this study to $\delta_{FeOO}$. However, the $\delta_{FeOO}$ frequencies of the end-on type Fe-$O_2$ porphyrins are reported around 350 $cm^{-1}$, and their $^{18}O_2$ isotopic frequency shifts are extremely small (~5 $cm^{-1}$) and furthermore, the $\delta_{FeOO}$ frequency of compound III of lactoperoxidase is reported at 491 $cm^{-1}$ and its $^{18}O_2$ isotopic frequency shift is almost the half of the present observation. In order to see how large the isotopic frequency shifts are expected to be for the $\delta_{FeOO}$ mode with end-on geometry, normal coordinate calculations were carried out for an isolated three-atom molecule of FeOO.

**Normal Coordinate Calculations**

In the same way as our previous treatments for the CO adducts,[26,27] the Urey-Bradley force field represented by eq 1 was assumed:

$$2V = K_1(\Delta r_{Fe-O_2})^2 + K_2(\Delta r_{OO})^2 + H(\Delta\theta_{FeOO})^2 + F(\Delta q_{Fe\cdots O})^2 \qquad (1)$$

where $\Delta r_{Fe-O_2}$, $\Delta r_{OO}$, $\Delta\theta_{FeOO}$ and $\Delta q_{Fe\cdots O}$ denote the displacement coordinates for the Fe-$O_2$ bond length, O-O bond length, Fe-O-O bond angle, and Fe···O nonbonding-atoms separation, respectively. The calculated frequencies are compared with the observed frequencies in

TABLE 2-1. The equilibrium bond lengths used for $MbO_2$ were those obtained from the X-ray crystallographic analyses:[28a,b] $r_{Fe\text{-}O_2}$=1.83 Å, $r_{O\text{-}O}$=1.4 Å, and $\theta_{FeOO}$=115°. The force constants used were $K_1$=2.18 mdyn/Å, $K_2$=5.7 mdyn/Å, H=0.58 mdyn·Å, and F=1.28 mdyn/Å. They were adjusted to reproduce the observed frequencies of $MbO_2$. The size of F determines the magnitude of vibrational coupling between the stretching and bending coordinates. F=1.3 mdyn/Å seems to be slightly larger than expected, but if a smaller value were assumed for F, a larger $K_1$ would be needed to reproduce the observed $\nu_{Fe\text{-}O_2}$ frequency. However, this would yield $O_2$-isotopic frequency shifts that were too large. For $HbO_2$ the calculations could not reproduce the observed results satisfactorily, in particular for the $\nu_{Fe\text{-}O_2}$ frequency of the $^{16}O^{18}O$ adduct, so long as the bending angle was assumed to be 155°, which is intermediate between the angles reported for the α and β subunits of $HbO_2$.[21a,b] The best fitted data shown in TABLE 2-1 were obtained with $K_1$=2.52, $K_2$=5.15, and H=0.75, but the fitting level regarding the $O_2$-isotopic frequency shifts was not always satisfactory and was not improved when F was changed from 1.3 to 0.3 mdyn/Å. Since the $\nu_{Fe\text{-}O_2}$ frequencies and their $^{16}O^{18}O$ isotopic frequency shifts for $HbO_2$ are very close to those for $MbO_2$, it is unreasonable to assume different Fe-O-O bend angles between $HbO_2$ and $MbO_2$. This may suggest that the Fe-O-O geometry of $HbO_2$ is altered upon crystallization, as pointed out in the XANES study.[29] Such a structural change upon crystallization is, in fact, reported for Mb, for which some perturbation takes place in the Fe-His bond of the deoxy state,[13] and for which relative populations of different conformers of the CO adducts[30] differ between the crystal and solution states.[31]

**Differences in the Fe-O-O Binding Geometry among Heme Proteins**

The difference spectra of a $^{16}O^{18}O$-($^{18}O_2$+$^{16}O_2$)/2 type were appreciably different among $MbO_2$, $HbO_2$, and $CcO{\cdot}O_2$ (Figures 2-5D, 2-7D, and 2-8D). The difference between $MbO_2$ and $HbO_2$ arises from differences in proximity of the Fe-$^{16}O^{18}O$ frequency to the $Fe^{16}O^{16}O$ one and of the $Fe^{18}O^{16}O$ frequency to the $Fe^{18}O^{18}O$ one, since the widths of the $\nu_{Fe\text{-}O_2}$ bands of $MbO_2$ and $HbO_2$ are alike; the most plausible values for the difference between the Fe-$^{16}O^{18}O$ and Fe-$^{16}O^{16}O$ stretching frequencies are <1, 2, and 4 $cm^{-1}$, respectively, for $HbO_2$, $MbO_2$, and $CcO{\cdot}O_2$. Accordingly, the Fe-O-O valence angle is considered to increase in this

order. It is possible in principle to estimate the difference in angle on the basis of normal coordinate calculations for different geometries without changing the force constants, but we refrain from reporting the values, since the force field and the molecular model used are not sufficiently precise to warrant such a calculation. However, it is evident even from this level of calculation that the new Raman band observed around 425 $cm^{-1}$ is reasonably explained in terms of the $\delta_{FeOO}$ mode, despite the fact that the $^{18}O_2$ isotopic shifts are significantly larger than those of the Fe-porphyrin dioxygen complexes.[2b]

The large difference between the $\delta_{FeOO}$ frequencies of lactoperoxidase and Hb presumably arises from the strong interaction between the terminal oxygen and the distal arginine postulated for lactoperoxidase,[3] since such interaction generally increases the energy required for movements of atoms along the bending coordinate and thus raises the bending frequency. The difference of the $^{18}O_2$ isotopic frequency shifts indicates the difference in the atomic displacement of oxygen atoms during the vibration. Accordingly, the large difference in the $^{18}O_2$ isotopic frequency shifts between lactoperoxidase and Hb means appreciable difference in the Fe-O-O valence angle.

The $\delta_{FeOO}$ RR band was observable for $HbO_2$ but not for $MbO_2$. Similar difference between Hb and Mb is present in the RR spectra of their CO adducts. The assignment of the Fe-C-O bending RR band is currently under debate; the band has been located at a frequency (~570 $cm^{-1}$) higher than that of the Fe-CO stretching ($\nu_{Fe\text{-}CO}$) mode,[32] but a new CO-isotope-sensitive band was found around 350 $cm^{-1}$ for HbCO, CcO·CO, and P-450·CO and was assigned to the $\delta_{FeCO}$ fundamental as discussed in chapter 3.[27] The fact that the new $\delta_{FeCO}$ frequency is lower than the Fe-CO stretching frequency is compatible with the present observation that the $\delta_{FeOO}$ frequency is lower than the Fe-$O_2$ stretching frequency. We note that only for Mb among various heme proteins examined could the $\delta_{FeCO}$ fundamental not be observed. The absence of the bending RR band for the $O_2$ and CO adducts might be characteristic of Mb, although its reason cannot be explained at the present stage. This may suggest that there is a factor controlling the RR intensity of the bending mode in the protein structure of the heme pocket, and that this part of structure is different between Mb and Hb.

## 2.5 Conclusions

We have identified the Fe-O-O bending Raman band for dioxygen complexes of hemoglobin and cytochrome *c* oxidase for the first time. The band was located at 425 $cm^{-1}$ for $Hb^{16}O_2$, shifted to 405 $cm^{-1}$ with $Hb^{18}O_2$, and at 435 $cm^{-1}$ for $CcO{\cdot}^{16}O_2$, shifted to 415 $cm^{-1}$ with $CcO{\cdot}^{18}O_2$. We failed to identify the corresponding band for $MbO_2$. The Fe-$O_2$ stretching Raman band has also been observed for $^{16}O_2$, $^{18}O_2$, and $^{16}O^{18}O$ adducts of Hb, Mb, and CcO. The isotopic frequency shifts suggested that the Fe-O-O angles of these proteins are closer to 115° than to 155°. The band width of $\nu_{Fe\text{-}O_2}$ RR band indicated that the dioxygen in $CcO{\cdot}O_2$ is more tightly fixed than in $HbO_2$ and $MbO_2$.

## References


(1) (a) Yu, N. T.; Kerr, E. In *Biological Application of Raman Spectroscopy*; Spiro, T. G., Ed.; Wiley-Interscience: New York, 1988; Vol. 3, pp. 39-95. (b) Yu, N. T. *Methods Enzymol.* **1986**, *130*, 350-409.

(2) (a) Bajdor, K.; Oshio, H.; Nakamoto, K. *J. Am. Chem. Soc.* **1984**, 106, 7273-7274. (b) Proniewicz, L. M.; Paeng, I. R.; Nakamoto, K. *J. Am. Chem. Soc.* **1991**, *113*, 3294-3303. (b) Wagner, W. D.; Paeng, I. R.; Nakamoto, K. *J. Am. Chem. Soc.* **1988**, *110*, 5565-5567.

(3) Hu, S.; Kincaid, J. R. *J. Am. Chem. Soc.* **1991**, *113*, 7189-7194.

(4) Brunner, H. *Naturwissenschaften*, **1974**, *61*, 129.

(5) Nagai, K.; Kitagawa, T.; Morimoto, H. *J. Mol. Biol.* **1980**, *136*, 271-289.

(6) Duff, L. L.; Appelman, E. H.; Shriver, D. F.; Klotz, I. M. *Biochem. Biophys. Res. Commun.* **1979**, *90*, 1098-1103.

(7) Kerr, E. A.; Yu, N.-T.; Bartnicki, D. E.; Mizukami, H. *J. Biol. Chem.* **1985**, *260*, 8360-8365.

(8) Hu, S.; Schneider, A. J.; Kincaid, J. R. *J. Am. Chem. Soc.* **1991**, *113*, 4815-4822.

(9) Van Wart, H. E.; Zimmer, J. *J. Biol. Chem.* **1985**, *260*, 8372-8377.

(10) (a) Ogura, T.; Takahashi, S.; Shinzawa-Itoh, K.; Yoshikawa, S.; Kitagawa, T. *J. Am. Chem. Soc.* **1990**, *112*, 5630-5631. (b) Ogura, T.; Takahashi, S.; Shinzawa-Itoh, K.; Yoshikawa, S.; Kitagawa, T. *Bull. Chem. Soc. Jpn.* **1991**, *64*, 2901-2907. (c) Ogura, T.; Takahashi, S.; Hirota, S.; Shinzawa-Itoh, K.; Yoshikawa, S.; Appelman, E. H.; Kitagawa, T. *J. Am. Chem. Soc.* **1993**, *115*, 8527-8536.

(11) Han, S.; Ching, Y. C.; Rousseau, D. L. *Proc. Natl. Acad. Sci. U.S.A.* **1990**, *87*, 2491-2495.

(12) Varotsis, C.; Woodruff, W. H.; Babcock, G. T. *J. Am. Chem. Soc.* **1989**, *111*, 6439-6440.

(13) Zhu, L.; Sage, J. T.; Champion, P. M. *Biochemistry* **1993**, *32*, 11181-11185.

(14) Ogura, T.; Yoshikawa, S.; Kitagawa, T. *Biochemistry* **1989**, *28*, 8022-8027.

(15) Geraci, G.; Parkhurst, L. J.; Gibson, Q. H. *J. Biol. Chem.* **1969**, *244*, 4664-4667.

(16) Yoshikawa, S.; Choc, M. G.; O'Toole, M. C.; Caughey, W. S. *J. Biol. Chem.* **1977**, *252*, 5498-5508.
(17) Appelman, E. H.; Thompson, R. C.; Engelkemeir, A. G. *Inorg. Chem.* **1979**, *18*, 909-911.
(18) Rozen, S.; Brand. M. *Angew. Chem. Int. Ed. Engl.* **1986**, *25*, 554-555.
(19) Appelman, E. H.; Dunkelberg, O.; Kol, M. *J. Fluorine Chem.* **1992**, *56*, 199-213.
(20) Benko, B; Yu, N.-T. *Proc. Natl. Acad. Sci. U.S.A.* **1983**, 80, 7042-7046.
(21) (a) Shaanan, B. *Nature* **1982**, *296*, 683-684. (b) Shaanan, B. *J. Mol. Biol.* **1983**, *171*, 31-59.
(22) Lee, H.; Kitagawa, T.; Abe, M.; Pandey, R. K.; Leung, H.-K. Smith, K. M. *J. Mol. Struct.* **1986**, *146*, 329-347.
(23) (a) Hu, S.; Morris, I. K.; Sinch, J. P.; Smith, K. M.; Spiro, T. G. *J. Am. Chem. Soc.* **1993**, *115*, 12446-12458. (b) Choi, S.; Spiro, T. G.; Langry, K. C.; Smith, K. M. *J. Am. Chem. Soc.* **1982**, *104*, 4337-4344.
(24) Tsubaki, M.; Yu, N.-T. *Biochemsitry* **1982**, *21*, 1140-1144.
(25) Hu, S.; Kincaid, J. R. *J. Am. Chem. Soc.* **1991**, *113*, 9760-9766.
(26) Nagai, M.; Yoneyama, Y.; Kitagawa, T. *Biochemistry* **1991**, *30*, 6495-6503.
(27) Hirota, S.; Ogura, T.; Shinzawa-Itoh, K.; Yoshikawa, S.; Nagai, M.; Kitagawa, T. *J. Phys. Chem.* **1994**, *98*, 6652-6660.
(28) (a) Phillips, S. E. V. *Nature*, **1978**, *273*, 247-248. (b) Phillips, S. E. V. *J. Mol. Biol.* **1980**, *142*, 531-554.
(29) Congiu-Castellano, A.; Bianconi, A.; Dell'Ariccia, M.; Longa, S. D.; Giovannelli, A.; Burattini, E.; Castagnola, M. *Biochem. Biophys. Res. Commun.* **1987**, *147*, 31-38.
(30) Mourant, J. R.; Braunstein, D. P.; Chu, K.; Frauenfelder, H.; Nienhaus, G. U.; Ormos, P.; Young, R. D. *Biophys. J.* **1993**, *65*, 1496-1507.
(31) Zhu, L.; Sage, J. T.; Rigos, A. A.; Morikis, D.; Champion, P. M. *J. Mol. Biol.* **1992**, *224*, 207-215.
(32) Ray, G. B.; Li, X. Y.; Ibers, J. A.; Sessler, J. L.; Spiro, T. G. *J. Am. Chem. Soc.* **1994**, *116*, 162-176,
(33) Potter, W. T.; Tucker, M. P.; Houtchens, R. A.; Caughey, W. S. *Biochemistry* **1987**, *26*, 4699-4707.
(34) Proniewicz, L. M.; Bruha, A.; Nakamoto, K.; Kyuno, E.; Kincaid, J. R. *J. Am. Chem. Soc.* **1989**, *111*, 7050-7056.

**TABLE 2-1. Observed Frequencies of $MbO_2$ and $HbO_2$ and Calculated Frequencies of the Isolated FeOO Unit[a]**

| | | $^{16}O_2$ | | $^{18}O^{16}O$ | | $^{16}O^{18}O$ | | $^{18}O_2$ | |
|---|---|---|---|---|---|---|---|---|---|
| | | obs | calc | obs | calc | obs | calc | obs | calc |
| Mb[b] | $\nu_{OO}$ | ~1130[d] | 1133 | | 1102 | | 1100 | | 1068 |
| | $\nu_{Fe\text{-}O2}$ | 571 | 570 | 547 | 547 | 569 | 568 | 545 | 546 |
| | $\delta_{FeOO}$ | (425)[e] | 424 | (~423) | 417 | (~407) | 410 | (405) | 404 |
| Hb[c] | $\nu_{OO}$ | ~1130[d] | 1130 | | 1095 | | 1102 | | 1065 |
| | $\nu_{Fe\text{-}O2}$ | 568 | 568 | 544 | 556 | 567 | 557 | 544 | 546 |
| | $\delta_{FeOO}$ | 425 | 425 | ~407 | 410 | ~423 | 417 | 405 | 402 |

[a] In $cm^{-1}$ unit. [b] Parameters used for calculations are the following: r(Fe-O) = 1.83 Å, r(O-O) = 1.4 Å, $K_1$(Fe-O) = 2.18 mdyn/Å, $K_2$(O-O) = 5.7 mdyn/Å, H(Fe-O-O) = 0.58 mdyn·Å, F(Fe···O) = 1.28 mdyn/Å, θ(Fe-O-O) = 115°. [c] Parameters used for calculations are; r(Fe-O) = 1.83 Å, r(O-O) = 1.4 Å, $K_1$(Fe-O) = 2.52 mdyn/Å, $K_2$(O-O) = 5.15 mdyn/Å, H(Fe-O-O) = 0.75 mdyn·Å, F(Fe···O) = 1.28 mdyn/Å, θ(Fe-O-O) = 155°. [d] The $\nu_{OO}$ frequencies are estimated on the basis of the observed frequencies reported by ref. 33 and the vibronic coupling described by ref. 34. [e] Frequencies observed for $HbO_2$.

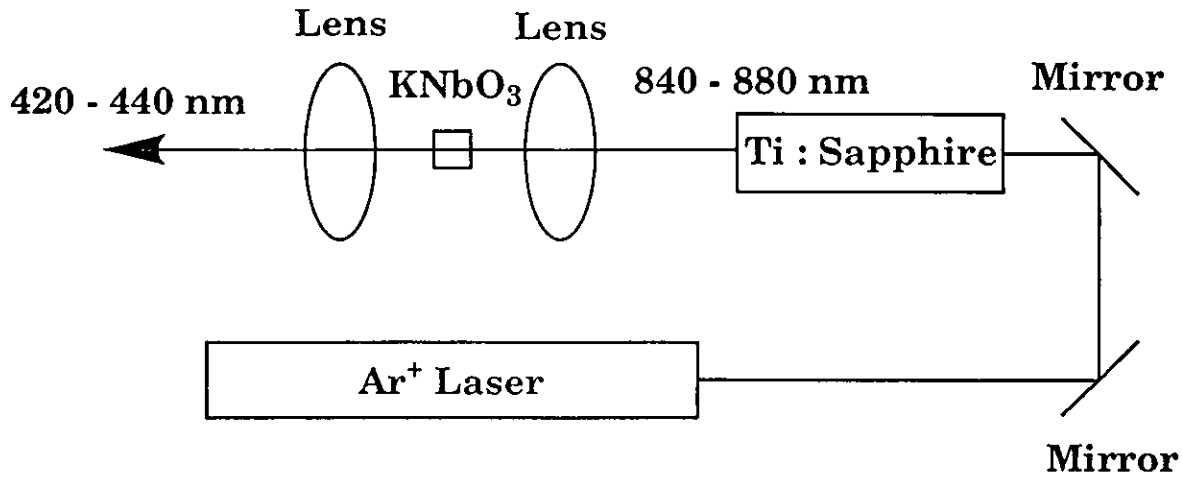


**Figure 2-1.** Schematic view of the 423.0 nm-output laser. The second harmonic of the output of a Ti-sapphire laser pumped by an $Ar^+$ ion laser was generated with a $KNbO_3$ crystal.

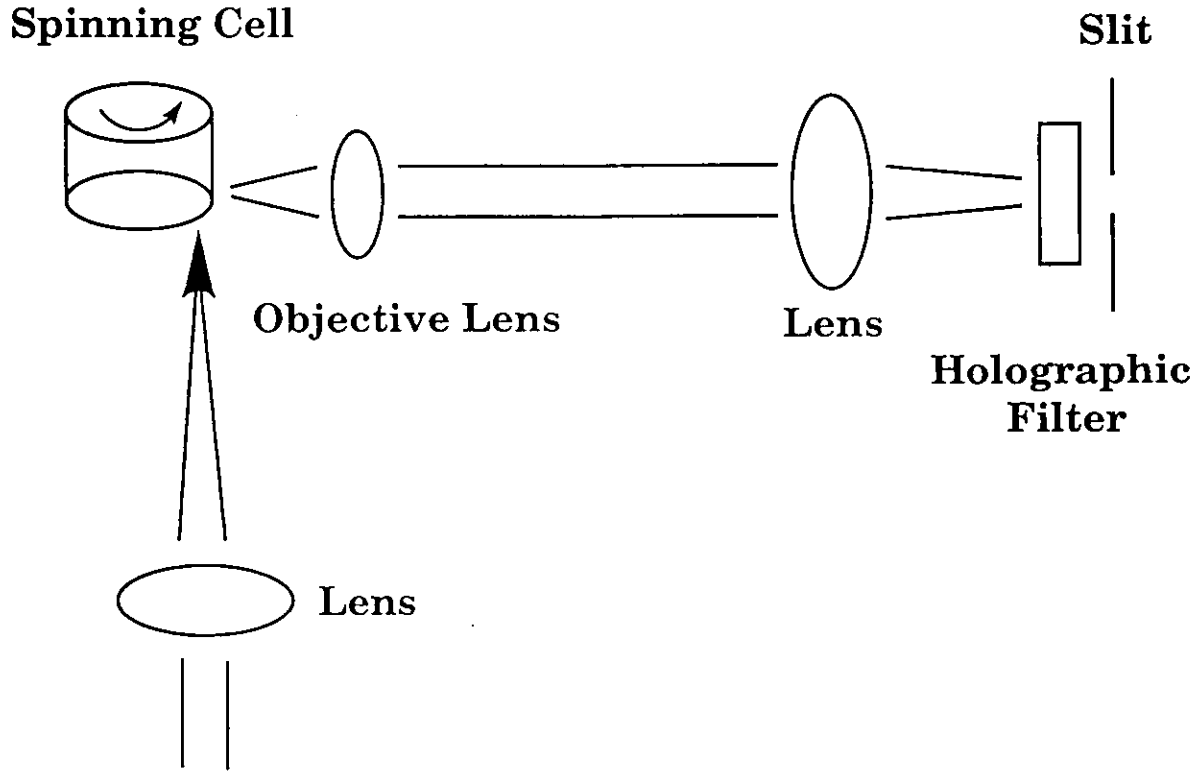


**Figure 2-2.** Schematic view of the detecting device.

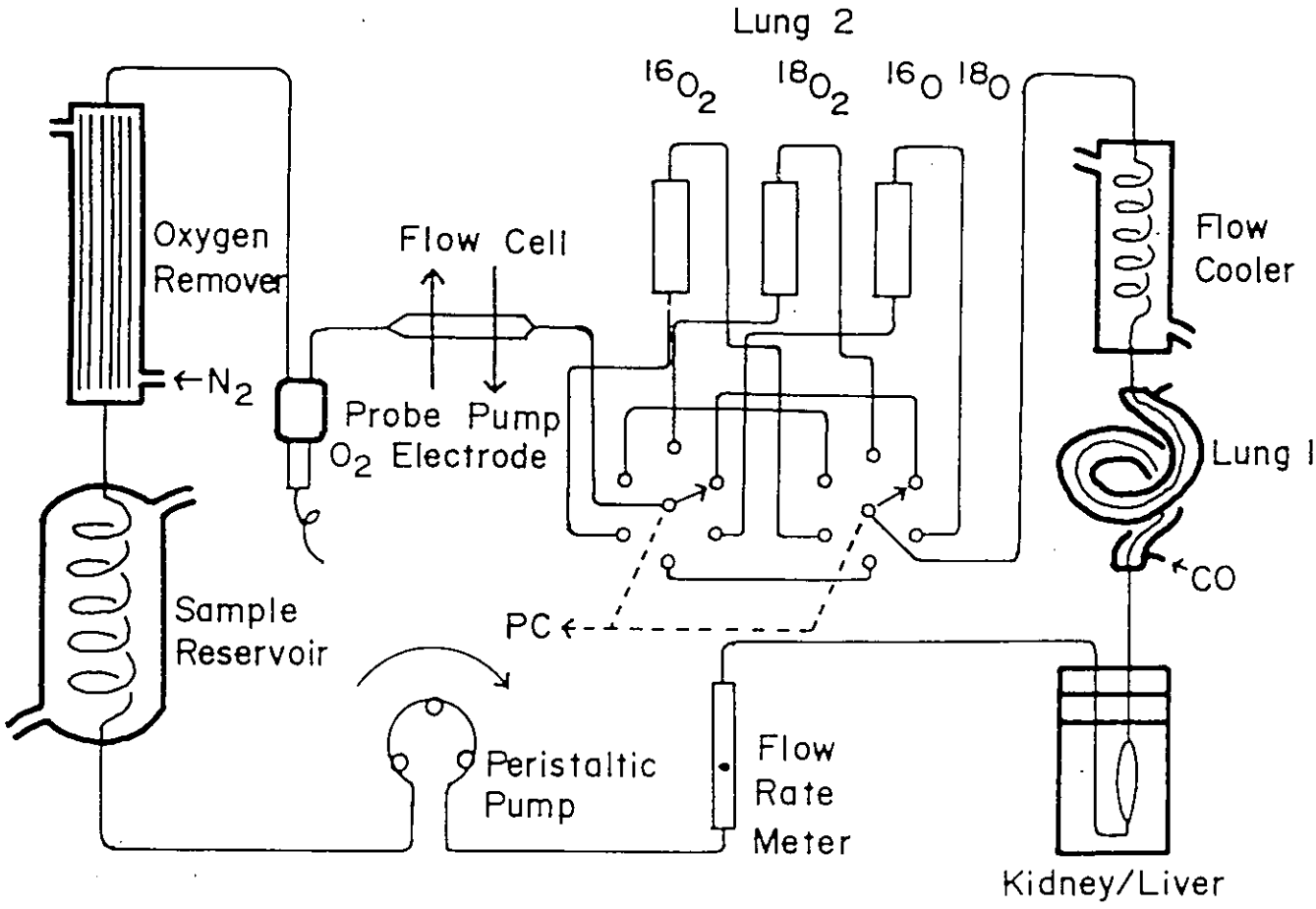


**Figure 2-3.** Schematic view of the artificial cardiovascular system (from ref. 10c).

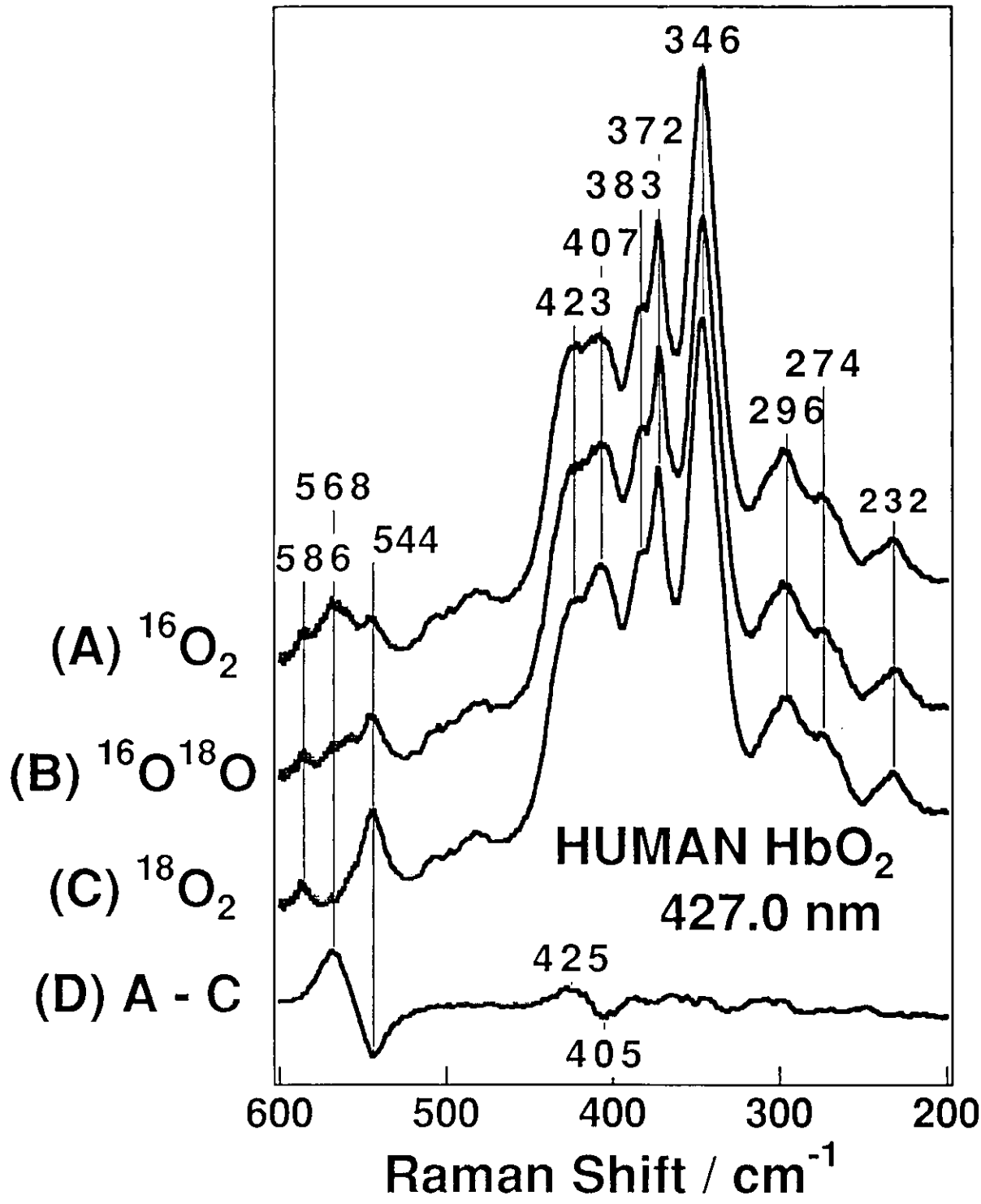


**Figure 2-4.** The RR spectra in the 600 to 200 $cm^{-1}$ region of the $^{16}O_2$ (A), $^{16}O^{18}O$ (B) and $^{18}O_2$ adducts (C) of human Hb, and the difference spectrum (D) between A and C. The ordinate scales of spectra A - C are normalized by the intensity of the porphyrin bands. Experimental conditions: excitation, 427.0 nm, 10 mW at the sample; grating of the monochromator, 900-nm blaze, 1200 grooves/mm, second order; sample, 50 μM (heme) in 50 mM Tris-HCl buffer, pH 8.5.

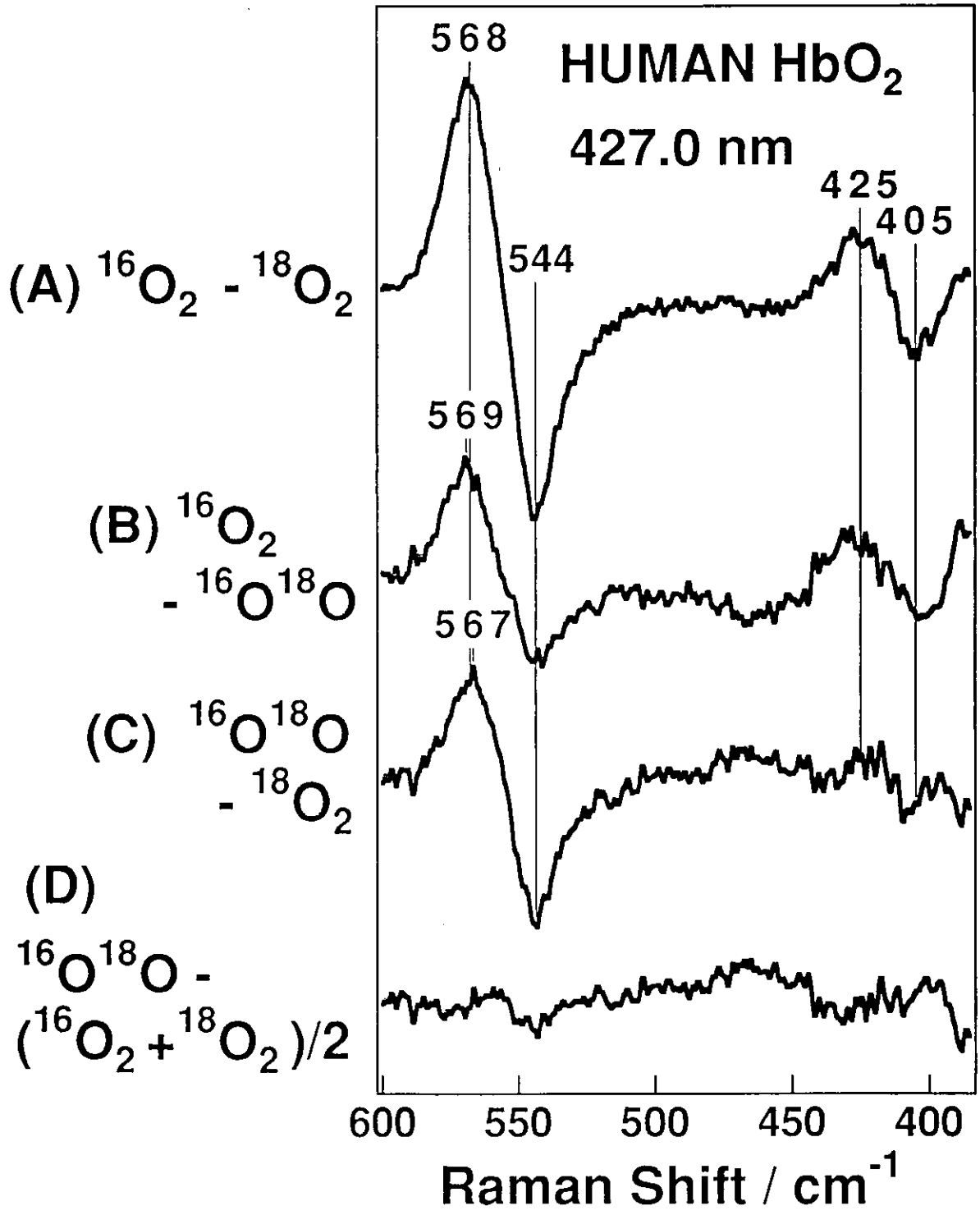


**Figure 2-5.** Differences between the spectra shown in Figure 2-4. (A) $Hb^{16}O_2$ - $Hb^{18}O_2$, (B) $Hb^{16}O_2$ - $Hb^{16}O^{18}O$, (C) $Hb^{16}O^{18}O$ - $Hb^{18}O_2$. (D) $Hb^{16}O^{18}O$ - ($Hb^{16}O_2$ + $Hb^{18}O_2$)/2. The ordinate scales of A through D are the same.

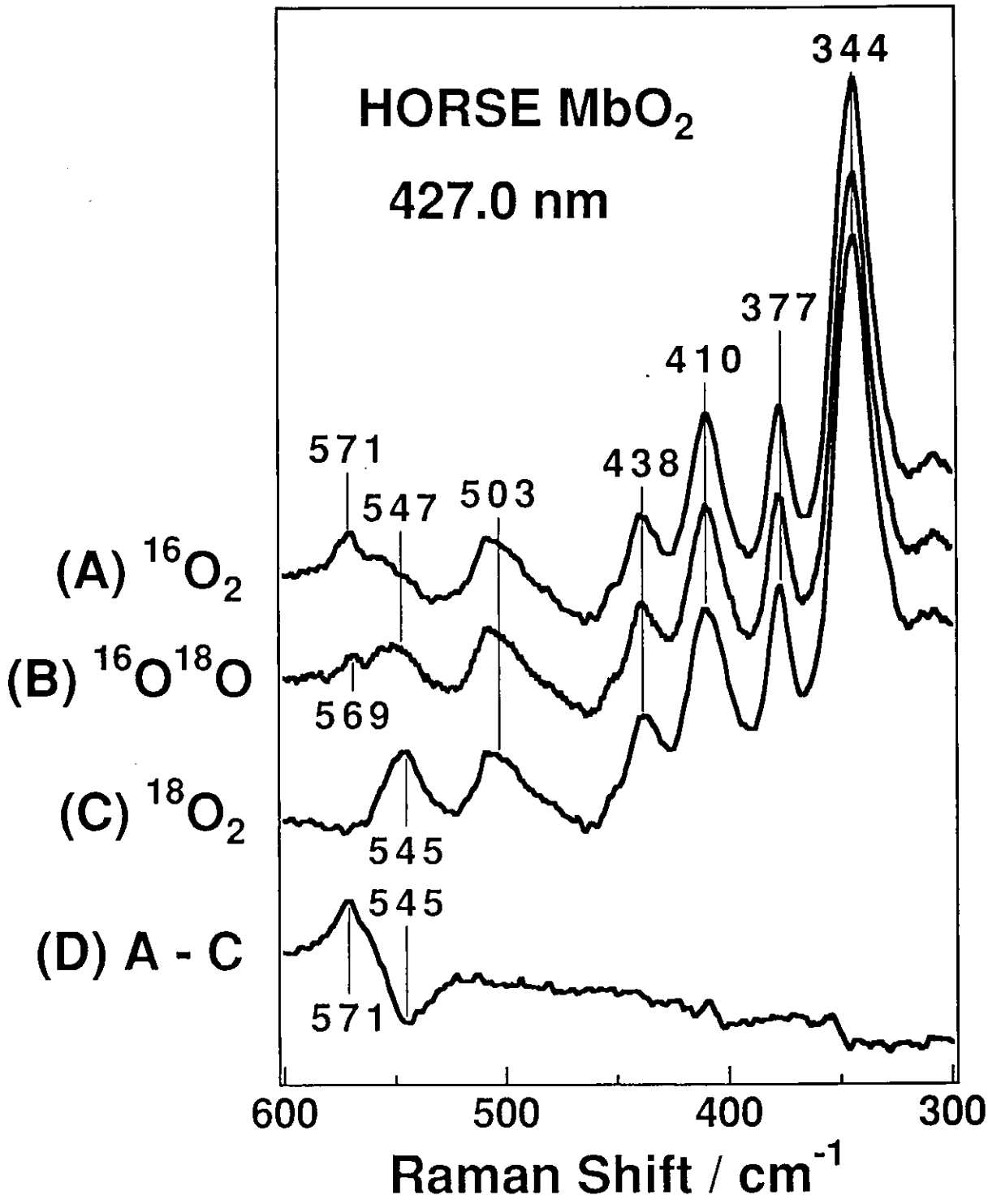


**Figure 2-6.** The RR spectra in the 600 to 300 $cm^{-1}$ region of the $^{16}O_2$ (A), $^{16}O^{18}O$ (B), and $^{18}O_2$ adducts (C) of horse Mb, and the difference spectrum (D) between A and C. The ordinate scales of spectra A through C are normalized by the intensity of the porphyrin bands. Experimental conditions: excitation, 427.0 nm, 5 mW at the sample; grating of the monochromator, 500-nm blaze, 1200 grooves/mm, first order; sample, 90 μM in 50 mM Tris-HCl buffer, pH 8.5.

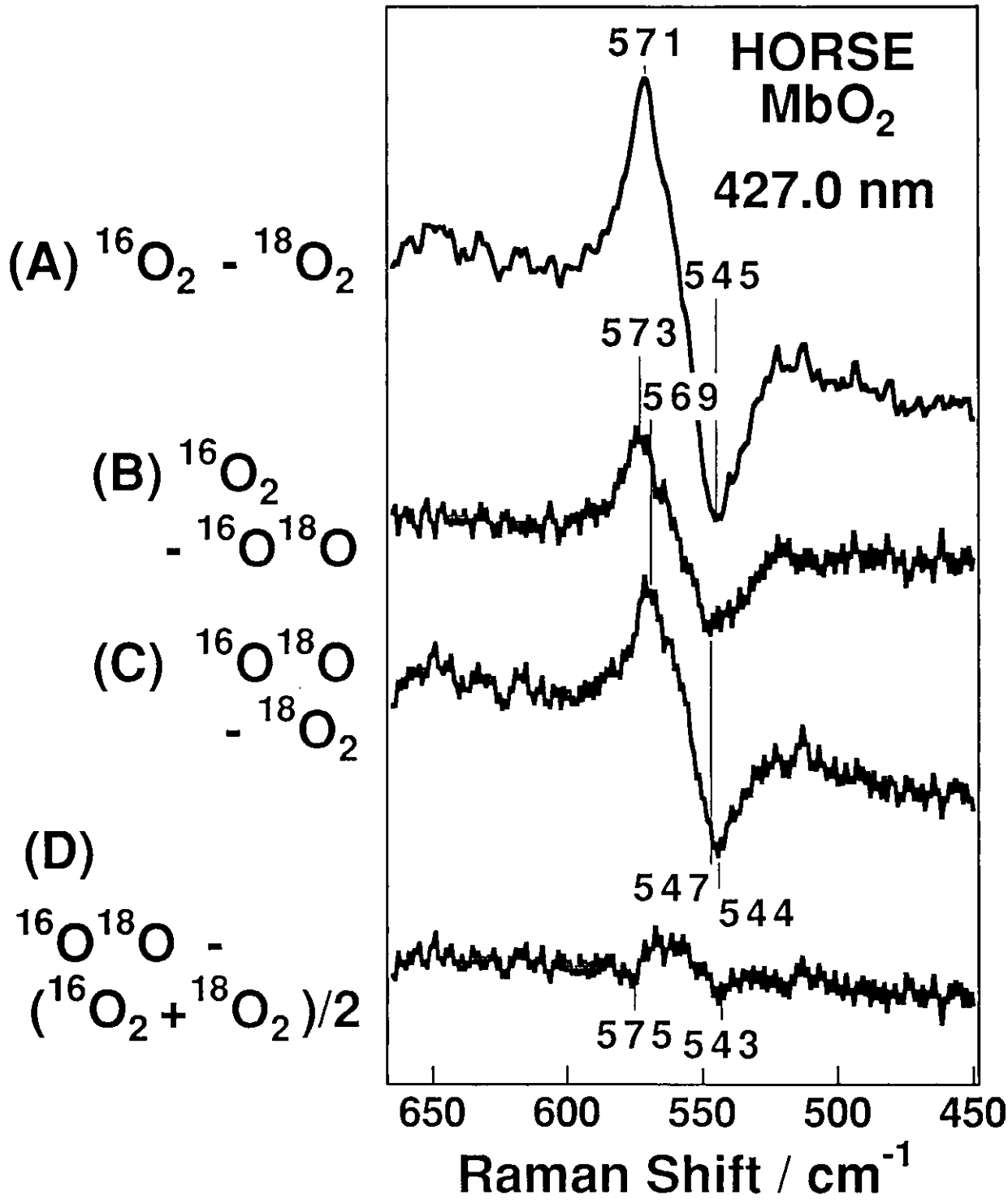


**Figure 2-7.** Differences of the RR spectra shown in Figure 2-6. (A) $Mb^{16}O_2$ - $Mb^{18}O_2$, (B) $Mb^{16}O_2$ - $Mb^{16}O^{18}O$, (C) $Mb^{16}O^{18}O$ - $Mb^{18}O_2$, (D) $Mb^{16}O^{18}O$ - ($Mb^{16}O_2$ + $Mb^{18}O_2$)/2. The ordinate scales of spectra A - D are the same.

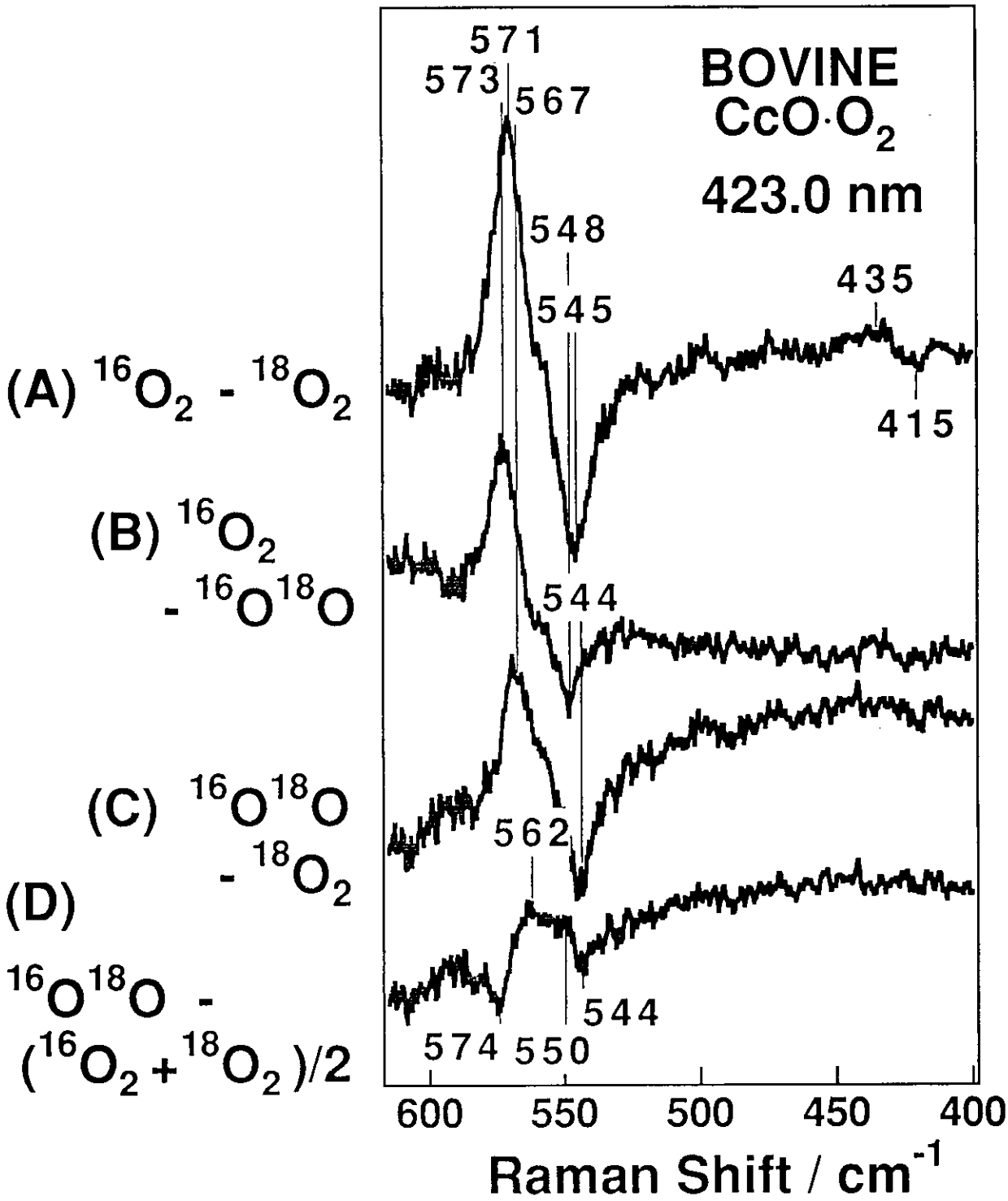


**Figure 2-8.** Differences of the RR spectra of $O_2$-isotope adducts of CcO (A) $CcO.^{16}O_2$ - $CcO.^{18}O_2$, (B) $CcO.^{16}O_2$ - $CcO.^{16}O^{18}O$, (C) $CcO.^{16}O^{18}O$ - $CcO.^{18}O_2$, (D) $CcO.^{16}O^{18}O$ - $(CcO.^{16}O_2 + CcO.^{18}O_2)/2$. Ordinate scales of spectra A through D are the same. Experimental conditions: pump beam, 590 nm, 210 mW at the sample; probe beam, 423.0 nm, 4 mW at the sample; grating of the monochromator, 500-nm blaze, 1200 grooves/mm, first order; delay time after CO photodissociation in the $O_2$ atmosphere, 100 μs.

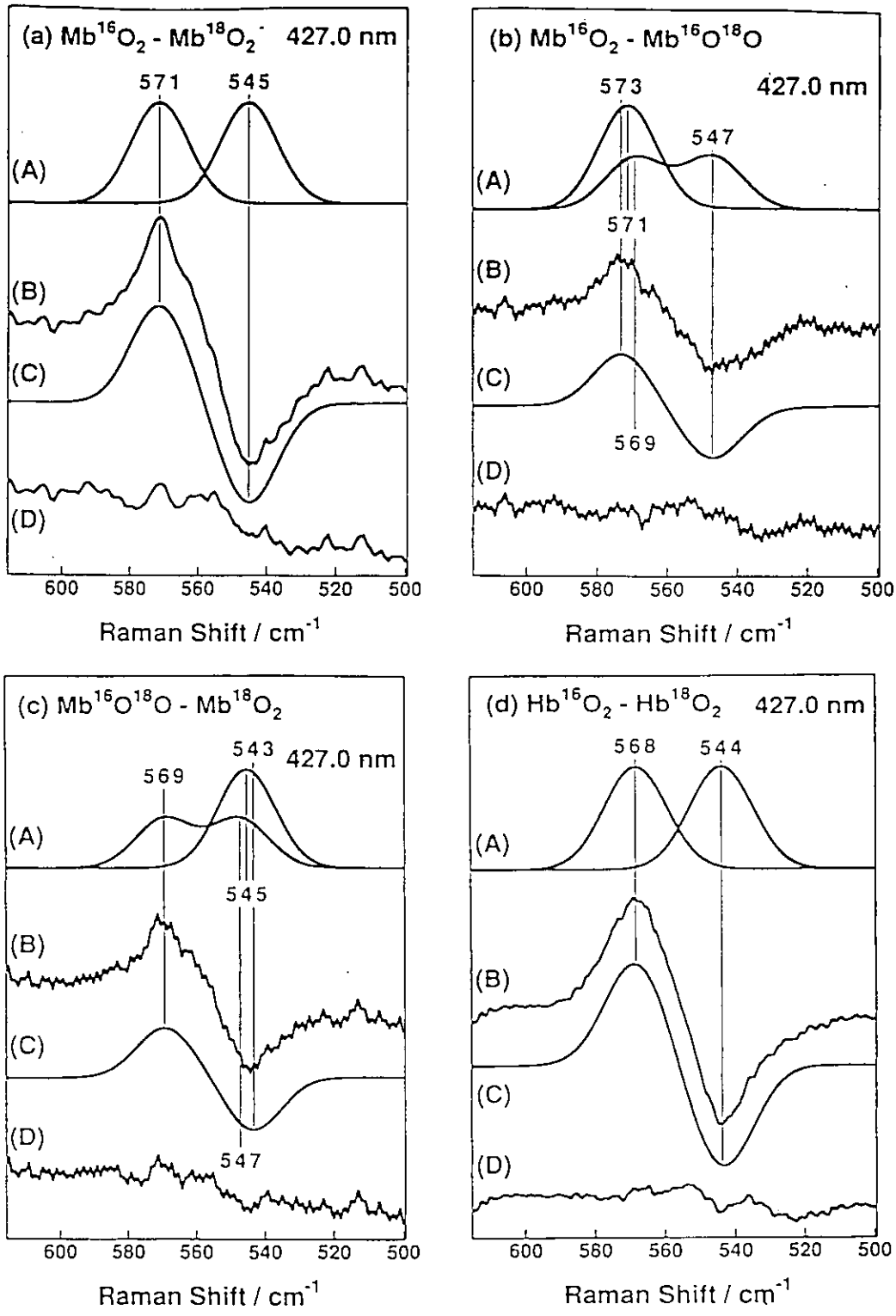


**Figure 2-9.** Simulation of the difference spectra of $MbO_2$ and $HbO_2$. (A) Assumed bands (Gaussian band shape, bandwidth is 20 $cm^{-1}$ for $MbO_2$ and 21 $cm^{-1}$ for $HbO_2$), (B) experimental difference spectra, (C) calculated difference spectra, (D) residuals between the experimental and calculated difference spectra.

# Chapter I-3.

# Vibrational Assignments of the FeCO Unit of CO-Bound Heme Proteins Revisited: Observation of a New CO-Isotope-Sensitive Raman Band Assignable to the FeCO Bending Fundamental

## Abstract

In order to find the FeCO bending ($\delta_{FeCO}$) fundamental, resonance Raman spectra in the 600-200 $cm^{-1}$ region of CO adducts of hemoglobin (Hb), its isolated chains, myoglobin (Mb), cytochrome *c* oxidase (CcO), and cytochrome P-450 (P-450) were reexamined. A new CO-isotope-sensitive band was found around 365 $cm^{-1}$ for all but MbCO. For HbCO this band was located at 367, 355, 363, and 353 $cm^{-1}$ for $^{12}C^{16}O$, $^{13}C^{16}O$, $^{12}C^{18}O$, and $^{13}C^{18}O$ adducts, respectively, and thus exhibited a zigzag pattern against the increase of the total mass of CO, similar to the 575 $cm^{-1}$ band which has been assigned to the $\delta_{FeCO}$ fundamental hitherto. Relative intensity of the ~365 $cm^{-1}$ band to the 575 $cm^{-1}$ band exhibited almost no change upon lowering of temperature from 20 °C to -10 °C, but since temperature dependent frequency shifts were appreciable, the present difference spectra could not determine if the intensity change by 11% expected for a difference combination band of a hot 210 $cm^{-1}$ mode was involved or not. The maximum intensity enhancement of the 365 $cm^{-1}$ band in the excitation profile within the Soret band occurred at longer wavelengths than that of the 575 $cm^{-1}$ band. The frequency differences between the CO-isotope-sensitive band around 575 $cm^{-1}$ and one around 365 $cm^{-1}$ were 208±3, 213±5, and 204±3 $cm^{-1}$ for all CO isotopes of HbCO, CcO·CO, and P-450·CO, respectively. Despite that the Fe-CO and C-O stretching modes exhibited no deuteration shifts, the frequency of the 575 $cm^{-1}$ band was higher in $D_2O$ than in $H_2O$, and this feature was more prominent with MbCO than HbCO. The 575 $cm^{-1}$ band of MbCO was remarkably strong upon excitation at 406.7 nm and this is distinct from other proteins examined. These observations suggest that the ~365 $cm^{-1}$ band arises from the $\delta_{FeCO}$ fundamental and the 575 $cm^{-1}$ band is its combination with a porphyrin vibration or possibly a Fe-C deformation mode. Normal coordinate calculations for the isolated FeCO unit reasonably reproduce the observed isotopic frequency shifts under these assignments.

### 3.1 Introduction

The carbon monoxide (CO) adduct of heme has been extensively used to probe the structural characteristics in their dioxygen binding site. The vibrational frequencies of the FeCO unit obtained by resonance Raman (RR) and infrared (IR) spectroscopy, which include the CO stretching ($\nu_{CO}$) around 1940-1980 $cm^{-1}$, Fe-CO stretching ($\nu_{Fe\text{-}CO}$) around 470-520 $cm^{-1}$, and Fe-C-O bending ($\delta_{FeCO}$) around 550-580 $cm^{-1}$, have served as indicators of interactions between the bound CO and the surrounding residues in the heme pocket.[1] However, the conclusion drawn from the RR and IR studies of CO-bound heme proteins would lose its foundation if the vibrational assignments mentioned above were incorrect. In fact, the assignment of $\delta_{FeCO}$ has not been in full agreement, and there was a suggestion that the 570-580 $cm^{-1}$ band was too high to assign it to the fundamental and was possibly an overtone of $\delta_{FeCO}$.[2]

Recently the $\nu_{Fe\text{-}CO}$ RR band was investigated with various E7-mutants of human Mb generated by site-directed mutagenesis, and it was concluded that the bulkiness of E7-residue and thus its steric hindrance, is not the main determinant of the $\nu_{Fe\text{-}CO}$ frequency.[3] The similar conclusions are obtained for $\nu_{CO}$ of sperm whale Mb mutants[4] and human Hb mutants.[5] On the other hand, a relation between the $\nu_{Fe\text{-}CO}$ frequency and the Fe-C-O bond angle or the tilting angle of the Fe-C bond has been investigated theoretically.[1,6-8] In these treatments a set of potential constants, which can well reproduce the frequencies observed for an equilibrium state, is used without changes of their values to predict the frequencies expected for distorted forms. Unfortunately, one calculation[6] predicts that the $\nu_{Fe\text{-}CO}$ frequency becomes lower as the Fe-C-O bending angle becomes smaller but another[7] predicts the opposite trend. This discrepancy arises from the different assignments of the $\delta_{FeCO}$ RR band. The correct force constant of $\delta_{FeCO}$, which depends on the experimental assignment of the $\delta_{FeCO}$ RR band, is indispensable to evaluate the distortion energy of the FeCO unit.[9]

For further advanced application of RR spectroscopy to structural analysis of heme proteins, correct assignment of the $\delta_{FeCO}$ RR band is necessary. Accordingly, in this chapter, we carefully searched a new CO-isotope-sensitive RR band in a lower frequency region for various heme proteins including Hb, its $\alpha$ and $\beta$ chains, Mb, cytochrome *c* oxidase

(CcO), and cytochrome P-450 (P-450). Here we propose reassignment of the band around 575 $cm^{-1}$ to a combination band and a new band around 365 $cm^{-1}$ to the $\delta_{FeCO}$ fundamental band.

### 3.2 Experimental Procedures

Raman scattering was excited at 406.7 nm by a $Kr^+$ ion laser (Spectra Physics, Model 2016), at 441.6 nm by a He/Cd laser (Kinmon Electrics, Model CD1805B), at 442.5 to 435.0 nm by a dye laser (Spectra Physics, Model 375B) with stilbene-420 pumped by an $Ar^+$ ion laser (Spectra Physics, Model 2045), and at 426.0 to 427.0 nm by the system using a $KNbO_3$ crystal described in chapter I-2 (Figure 2-1).

The Raman scattering was detected by the system similar to that described in Figure 2-2 using a CCD (Astromed, CCD 3200) or a photo diode array (PAR, 1421HQ) attached to a single polychromator (Ritsu Oyo Kogaku, DG-1000). This CCD, which exhibited much less cross-talks between neighboring channels compared with the diode array, was used to observe Raman bands with narrower bandwidths, while the diode array, which apparently exhibited higher sensitivity than CCD, was used to detect weak bands with better S/N ratios. The slit-width of 200 μm and slit-height of 10 mm were used throughout the measurements and the laser power at the sample point was adjusted to be 1-6 mW with a continuous ND filter for the beam diameter of ca. 50 μm. RR spectra were measured at room temperate with a spinning cell (3000 rpm) to avoid photodissociation, except for the experiments for examining temperature dependencies for which the spinning cell was flushed with cold $N_2$ gas and temperature was measured with a thermocouple at the scattering point. Raman shifts were calibrated with $CCl_4$. Uncertainties of peak positions were 1 $cm^{-1}$ for the original spectra but 2 $cm^{-1}$ for difference spectra, unless otherwise stated in figure captions.

Cytochrome *c* oxidase (cytochrome *c*: oxidoreductase, EC 1.9.3.1. CcO) was isolated from bovine heart according to Yoshikawa's method.[10] About 1 mL of the 50 μM CcO solution in 50 mM sodium phosphate buffer, pH 7.2 was transferred to an airtight spinning cell. The CO adduct of CcO (CcO·CO) was formed through repeated evacuation of gas inside the cell (to ca. 0.1 mmHg) followed by incorporation of CO to it (to ca. 1 atm.) by three times. Finally, for complete removal of oxygen, a small amount of

$N_2$-saturated dithionite solution was added so that its final concentration was 10 mM. The CO-isotope adducts of CcO were obtained from the CcO·$^{12}C^{16}O$ sample by evacuating $^{12}C^{16}O$ and incorporating $^{13}C^{16}O$ (ICON, 99 atom % for $^{13}C$), $^{12}C^{18}O$ (Cambridge Isotope Lab, 98 atom % for $^{18}O$) or $^{13}C^{18}O$ (Isotec, 98.6 atom % for $^{13}C$ and 96.8 atom % for $^{18}O$).

Human adult Hb (Hb A), prepared according to the method of Geraci et al.[11] was separated into the constituent α and β chains by the treatment with p-mercuribenzoate[11] followed by fractionation with preparative isoelectrofocussing electrophoresis (pH range 6-9).[12] The α and β chains were obtained by focusing on pI 7.65 and 6.35, respectively. Mercury was removed from the chains by incubating with dithiothreitol.[13] The concentration was adjusted to 50 μM (heme) with 50 mM sodium phosphate buffer, pH 7.2 or with 50 mM Tris-HCl buffer, pH 8.5, while in the experiments for examining temperature dependencies the buffer contained 20% (v/v) glycerol. To replace the solvent $H_2O$ with $D_2O$, 3 mM Hb solution was diluted with $D_2O$ (99.75 %) buffer to the concentration of 50 μM, and CO adducts were formed in the same way as described for CcO.

Horse Mb (Sigma, type M630) was dissolved in 50 mM Tris-HCl buffer, pH 8.5. The concentrated metMb solution was reduced by sodium dithionite and subjected to gel filtration through Sephadex G-25 column. $MbO_2$ thus obtained was diluted to 30 μM with the Tris-HCl buffer, pH 8.5 and transferred to the spinning cell, and CO adducts were formed in the same way as described for CcO. *Pseudomonas putida* P-450 (P-$450_{cam}$) was a kind gift from Drs. T. Egawa and Y. Ishimura of Keio University and its CO adducts (P-$450_{cam}$·CO) were prepared in a way similar to CcO·CO.

### 3.3 Results

The RR spectra in the 600 to 200 $cm^{-1}$ region for $^{12}C^{16}O$ (A) and $^{13}C^{18}O$ (B) adducts of Hb A and their difference spectra (C) excited at 406.7 nm are shown in Figure 3-1. The Raman bands of Hb$^{12}C^{16}O$ at 578 and 505 $cm^{-1}$ are shifted to 558 and 492 $cm^{-1}$, respectively, with Hb$^{13}C^{18}O$ and their difference spectrum clearly demonstrating this. This is in agreement with the spectra reported so far.[1] However, we note that there is a small differential pattern around 365 $cm^{-1}$, which is so small that other investigators have overlooked hitherto. Since there are relatively

strong porphyrin bands around 340-380 $cm^{-1}$, the presence of CO-isotope-sensitive band around 365 $cm^{-1}$ has been difficult to notice in the raw spectra. Furthermore, if the two independent Raman measurements for CO-isotope derivatives include a small amount of shift in the wavenumber axis on account of different dispositions of the spinning cell or fluctuation of the laser beam, differential patterns would appear in the difference spectra particularly at peak positions of the raw spectra. In this study special attention was paid to this problem, and the lack of a differential pattern in the difference spectrum for the plasma lines marked by an asterisk demonstrates the reproducibility of the wavenumber axis. The differential pattern around 365 $cm^{-1}$ is definitely larger than the noise level in Figure 3-1.

Figure 3-2 shows the same pair of RR spectra which were excited at 427.0 nm. This excitation wavelength is closer to the absorption maximum of HbCO (419 nm), but RR spectra excited in such proximity to the absorption maximum have never been reported. The RR bands are generally more intense with 427.0 nm than with 406.7 nm excitation, but we note here that the intensity of the differential pattern at 577 $cm^{-1}$ relative to that at 365 $cm^{-1}$ differs significantly between Figures 3-1 and 3-2. The relative intensity of the 577 $cm^{-1}$ to the 505 $cm^{-1}$ band in the raw spectra is reduced on excitation at longer wavelengths.

Figure 3-3 displays the RR spectra in the 600 to 200 $cm^{-1}$ region of $^{12}C^{16}O$ (A), $^{13}C^{16}O$ (B), $^{12}C^{18}O$ (C), and $^{13}C^{18}O$ (D) adducts of Hb A excited at 426.0 nm. The strong band at 505 $cm^{-1}$ in spectrum A shifts monotonously to lower frequencies with increase of the total mass of CO, that is, to 501 $cm^{-1}$ with $^{13}C^{16}O$, 496 $cm^{-1}$ with $^{12}C^{18}O$, and 492 $cm^{-1}$ with $^{13}C^{18}O$. Therefore, this is assigned to the $\nu_{Fe\text{-}CO}$ mode as believed so far.[1] The presence of a porphyrin band at 587 $cm^{-1}$ often makes it difficult to estimate correctly the intensity of the CO-isotope-sensitive band around 575 $cm^{-1}$. The CO-isotope-sensitive band is located at 576 $cm^{-1}$ in Figure 3-3A, which shifts to 561 $cm^{-1}$ with $^{13}C^{16}O$, to 574 $cm^{-1}$ with $^{12}C^{18}O$, and to 558 $cm^{-1}$ with $^{13}C^{18}O$. These frequencies are in agreement with the reported values.[8a] Since it exhibits a zigzag pattern against the increase of the total mass of CO, it has to date been assigned as $\delta_{FeCO}$.[1] In the frequency region below 500 $cm^{-1}$, it is apparently difficult to see similar CO-isotopic frequency shifts in the raw spectra. In fact, the $C_\beta C_c C_d$ bending bands of the propionic side chain[14] at 385 and 373 $cm^{-1}$ remain

unchanged with the CO-isotopes, but we note that the left wing of a broad band around 355 $cm^{-1}$ is definitely influenced by the CO-isotopes. In order to clarify the changes contained, difference spectra with regard to the $^{12}C^{16}O$ adduct were calculated.

The results are illustrated in Figure 3-4 where positive peaks at 577, 506, and 367 $cm^{-1}$ common to all three spectra are assigned to the $^{12}C^{16}O$ adduct. It is seen that the differential feature around 575 $cm^{-1}$ is appreciable when a carbon atom was replaced by an isotope but is extremely weak when an oxygen atom was replaced by an isotope. We emphasize that there is a CO-isotope-sensitive band around 365 $cm^{-1}$ which exhibits the same character as the 575 $cm^{-1}$ band, i.e. the intensities of the difference peaks are larger for carbon replacement than for oxygen replacement, and their frequencies exhibit a zigzag pattern against the total mass of CO. The difference-peak pattern around 365 $cm^{-1}$ displays slight asymmetry, its trough being shallower and broader than the symmetric case. In order to see if the 365 $cm^{-1}$ band arises from a difference combination of the hot 575 $cm^{-1}$ mode with an unknown mode, temperature dependencies of RR spectra were examined.

Figure 3-5 shows the RR difference spectra in the 600 to 300 $cm^{-1}$ region of $Hb^{12}C^{16}O$ vs. $Hb^{13}C^{18}O$ observed at 20 °C (A) and -10 °C (B). The ordinate scales of the two difference spectra were normalized by a porphyrin band of the individual raw spectra. The presence of 20% glycerol altered little the RR spectrum at 20 °C, but at -10 °C the peak positions were shifted to higher frequencies by 1-3 $cm^{-1}$ for the 575 and 365 $cm^{-1}$ bands while the 505 $cm^{-1}$ band remained unshifted. Although the relative peak intensities of the CO-isotope bands in the difference spectra are almost unaltered upon lowering temperature to -10 °C, the difference peak intensities do not always reflect the correct intensities of raw spectra when frequency shifts are involved. The raw spectra did not allow the estimation of intensity of the 365 $cm^{-1}$ band. Accordingly, we failed to demonstrate the absence of the intensity change of the 365 $cm^{-1}$ band by 11% which is expected for the difference combination of the excited 210 $cm^{-1}$ band.

The difference peak frequencies corresponding to the 575 and 365 $cm^{-1}$ bands for each CO-isotope adduct in Figure 3-4 are summarized in TABLE 3-1. Note that the frequency separation of those two bands appeared to be less sensitive to the mass of CO, i.e. 208±3 $cm^{-1}$, but it is

meaningfully sensitive to the mass of carbon atom of CO. Since this is close to the Fe-histidine stretching ($\nu_{Fe\text{-}His}$) frequency, it was suspected that the 575 $cm^{-1}$ was a combination of $\delta_{FeCO}$ with $\nu_{Fe\text{-}His}$, but this idea will be discarded in the experiments on P-$450_{cam}$ as described later.

Figure 3-6 shows the RR spectra in the 600-300 $cm^{-1}$ region of $^{12}C^{16}O$ (A), $^{13}C^{16}O$ (B), $^{12}C^{18}O$ (C) and $^{13}C^{18}O$ (D) adducts of CcO excited at 426.0 nm. The band at 516 $cm^{-1}$, which was previously assigned to $\nu_{Fe\text{-}CO}$ of cytochrome $a_3$,[15] shifts monotonously with an increase of mass of CO; 512 $cm^{-1}$ ($^{13}C^{16}O$), 506 $cm^{-1}$ ($^{12}C^{18}O$) and 503 $cm^{-1}$ ($^{13}C^{18}O$). The band of the $^{12}C^{16}O$ adduct at 574 $cm^{-1}$, which exhibits the zigzag pattern, i.e. 559 $cm^{-1}$ ($^{13}C^{16}O$), 572 $cm^{-1}$ ($^{12}C18O$), and 556 $cm^{-1}$ ($^{13}C^{18}O$), has to date been assigned to $\delta_{FeCO}$.[15] These frequencies for the $^{12}C^{16}O$ and $^{13}C^{16}O$ adducts are in agreement with the reported values,[15] but the others are new data. There are three porphyrin bands in the region between 330 and 380 $cm^{-1}$ and their apparent peak positions scarcely change with the isotopes of CO, although the band shapes are slightly different.

Differences between the four spectra shown in Figure 3-6 are calculated in Figure 3-7, where the difference spectra with regard to the $^{12}C^{16}O$ adduct (A-C) similar to Figure 3-4A-C and the difference between $^{12}C^{18}O$ -$^{13}C^{18}O$ (D) are displayed. It is evident that there is a differential feature around 360 $cm^{-1}$ in addition to the difference peaks at 575 and 517 $cm^{-1}$, but more than one set of positive and negative peaks are seen in the 360 $cm^{-1}$ region of Figure 3-7A-C.

In order to explore the excitation wavelength dependence of the CO-isotope-sensitive bands, the RR spectra of the $^{12}C^{16}O$ and $^{13}C^{18}O$ adducts of CcO were measured at several wavelengths near the Soret maximum of cytochrome $a_3$·CO. Their difference spectra are illustrated in Figure 3-8, where the peak intensity of the $\nu_{Fe\text{-}CO}$ band at 516 $cm^{-1}$ is adjusted to be common in all the difference spectra. The two sets of positive and negative bands in the region from 380-330 $cm^{-1}$ change in intensity with the excitation wavelength, suggesting that they share intensity via vibrational coupling, but this will be discussed later.

Figure 3-9 shows the RR spectra in the 800-200 $cm^{-1}$ region of $^{12}C^{16}O$ (A), $^{13}C^{16}O$ (B), $^{12}C^{18}O$ (C), and $^{13}C^{18}O$ (D) adducts of P-$450_{cam}$ in the presence of camphor excited at 441.6 nm. The strong band at 484 $cm^{-1}$ in spectrum A, which was previously found at 477 $cm^{-1}$ and assigned to $\nu_{Fe\text{-}CO}$ in ref. 16, shifts to 480 $cm^{-1}$ with $^{13}C^{16}O$, to 475 $cm^{-1}$ with $^{12}C^{18}O$, and to

472 $cm^{-1}$ with $^{13}C^{18}O$. Although the frequency is appreciably lower, the extent of frequency shift of the 484 $cm^{-1}$ band on CO isotopic substitution is the same as those of Hb A (Figure 3-3). The other CO-isotope-sensitive band is seen at 559 $cm^{-1}$ for $^{12}C^{16}O$, 546 $cm^{-1}$ for $^{13}C^{16}O$, 557 $cm^{-1}$ for $^{12}C^{18}O$, ad 544 $cm^{-1}$ for $^{13}C^{18}O$. The similarity in the isotope shifts suggests that the 559 $cm^{-1}$ band of P-450cam.CO arises from the same modes as the 576 $cm^{-1}$ band of HbCO and the 574 $cm^{-1}$ band of CcO·CO. Since there are porphyrin bands at 378 and 353 $cm^{-1}$, it is not clear in Figure 3-9 whether a CO-isotope-sensitive band is present around 350 $cm^{-1}$ or not.

Their difference spectra with regard to the $^{12}C^{16}O$ adduct are shown in Figure 3-10, where the porphyrin band at 674 $cm^{-1}$ has been completely subtracted. For spectrum B the difference pattern of the 560 $cm^{-1}$ band is extremely weak in comparison with that of the $\nu_{Fe\text{-}CO}$ band and similarly the difference feature around 360 $cm^{-1}$ is obscure. However, the presence of the CO-isotope-sensitive band around 365 $cm^{-1}$ is evident in spectrum C. The frequency difference between the 575 and 365 $cm^{-1}$ bands is 201 and 204 $cm^{-1}$ for the $^{12}C^{16}O$ and $^{13}C^{18}O$ adducts, respectively. This value is quite different from the Fe-S(proximal cystein) stretching frequency around 350 $cm^{-1}$.[17] Consequently, it is unreasonable that the 575 $cm^{-1}$ band is a combination of the $\delta_{FeCO}$ mode with the Fe-fifth ligand (trans) stretching mode.

Figure 3-11 shows the RR spectra in the 600 to 200 $cm^{-1}$ region of the $^{12}C^{16}O$ (A) and $^{13}C^{18}O$ (B) adducts of horse Mb excited at 406.7 nm and their difference (C). Similar to other proteins, MbCO exhibits strong CO-isotope sensitive bands around 575 and 510 $cm^{-1}$, although the positive peak around 575 $cm^{-1}$ in spectrum C actually consists of two peaks at 583 and 575 $cm^{-1}$. There is a shoulder at a high frequency side of the 494 $cm^{-1}$ band of the $^{13}C^{18}O$ adduct (spectrum B). Since this spectrum does not show any feature of a band at 575 $cm^{-1}$, contamination by a $^{12}C^{16}O$ adduct is unlikely. This rather means that there is a porphyrin band around 505 $cm^{-1}$ for MbCO and it is overlapped in spectra A and B.

It is quite unexpected that spectrum C exhibits no differential features in the lower frequency region. This was also the case with the CO adduct of sperm whale Mb (data not shown). When excitation wavelength was shifted to longer wavelengths (426.0 nm), the intensity of the 575 $cm^{-1}$ band relative to the $\nu_{Fe\text{-}CO}$ band at 509 $cm^{-1}$ reduced

significantly as shown by spectrum D. Spectrum F in Figure 3-11 illustrates the difference between the RR spectra of the same isotope species as (A) and (B) excited at 426.0 nm. The differential pattern around 575 $cm^{-1}$ is significantly reduced in intensity compared with that of the $\nu_{Fe\text{-}CO}$ band, but again there is no differential feature in the 365 $cm^{-1}$ region.

In order to get an insight into the difference between Hb and Mb, the isolated chains of Hb, which have been postulated as very similar to Mb,[18] were investigated and the results are shown in Figure 3-12, where panels (a) and (b) display the spectra of the α and β chains, respectively. There are appreciable differences between the α and β chains in the raw spectra, but the difference spectra of their $^{12}C^{16}O$ and $^{13}C^{18}O$ adducts shown by spectra C are similar. The intensity of the 575 $cm^{-1}$ feature relative to that of $\nu_{Fe\text{-}CO}$ is much weaker with Hb chains than with Mb (Figure 3-11F). However, contrary to Mb, the isolated chains of Hb A give rise to the differential pattern with a peak at 367-368 $cm^{-1}$ and a trough at 351-353 $cm^{-1}$. In this regard, Hb and Mb are dissimilar.

Figure 3-13 shows the effects of deuteration of globins of Mb (a and b) and Hb (c and d) on the CO-related frequencies. All were excited at 406.7 nm. Here the spectra of $H_2O$ (A) and $D_2O$ (B) solutions and their difference (C) are displayed for the $^{12}C^{16}O$ (a and c) and $^{13}C^{18}O$ (b and d) adducts. It is stressed that the 575 $cm^{-1}$ feature exhibits a high frequency shift in $D_2O$ while the $\nu_{Fe\text{-}CO}$ band is scarcely shifted and that the 575 $cm^{-1}$ band of Mb undergoes more intensity enhancement in $D_2O$. In the case of MbCO, a porphyrin band at 584 $cm^{-1}$ seems to be coupled with the 577 $cm^{-1}$ band in $H_2O$ and it appears as a doublet, whereas this coupling is removed in $D_2O$. This is reflected in the difference spectrum as a negative doublet (C in panel a). When the frequency is shifted by using $^{13}C^{18}O$, the vibrational coupling becomes less important and the band appears as a singlet both in $H_2O$ and $D_2O$, and its frequency is higher in $D_2O$ than in $H_2O$. Since its intensity is increased in $D_2O$, the difference spectrum (C in panel b) does not display a typical differential pattern when the $\nu_{Fe\text{-}CO}$ band is adjusted to disappear. The corresponding bands of HbCO also display shifts to higher frequencies in $D_2O$ (C in c and d), indicating that the vibrational properties of the 575 $cm^{-1}$ bands of HbCO and MbCO are alike. The deuteration shift to higher frequencies cannot be explained by a simple effect of a hydrogen bond between CO and E7-His on the $\delta_{FeCO}$

bending mode, since such a frequency shift would also be expected for the $\nu_{CO}$ and $\nu_{Fe\text{-}CO}$ stretches (except in the special case of a hydrogen near perpendicular to a linear Fe-C-O unit). Such a frequency shift on deuteration is not found for the stretching modes. This difference in behaviors between the 575 $cm^{-1}$ and the stretching bands makes it unlikely that the 575 $cm^{-1}$ band is the fundamental of the FeCO bending mode. However, we were unable to determine if there was a deuteration shift for the 365 $cm^{-1}$ band due to its weakness.

### 3.4 Discussion

**The FeCO Bending Fundamental Mode.**

It became evident from this study that there is a CO-isotope-sensitive band around 365 $cm^{-1}$ in addition to the bands around 575 and 500 $cm^{-1}$ for CcO·CO, P-$450_{cam}$·CO, HbCO and CO adducts of the isolated $\alpha$ and $\beta$ chains of Hb A. Since the assignment of the 500 $cm^{-1}$ band to $\nu_{Fe\text{-}CO}$ is of no doubt, either the 575 or 365 $cm^{-1}$ band should be the $\delta_{FeCO}$ fundamental and the other a nonfundamental mode. Generally, the intensity of the difference combination band becomes significantly weaker when temperature is lowered due to depopulation at an excited level. If the 365 $cm^{-1}$ band were a difference combination of a hot porphyrin mode around 210 $cm^{-1}$ with the 575 $cm^{-1}$ mode, its intensity would be expected to decrease by 11% upon temperature decrease from 20 °C to -10 °C. Since the 365 $cm^{-1}$ band exhibited a small frequency shift upon lowering temperature, it is quite difficult to determine from difference spectra (A) and (B) in Figure 3-5 if this amount of intensity change is involved between 20 and -10 °C or not. This experiment alone cannot determine it, but all the data collected so far suggest that the assignment of this band to the difference combination seems less plausible.

In the excitation profile measurements, the 575 $cm^{-1}$ band has the maximum of intensity enhancement at shorter wavelengths than that of the 365 $cm^{-1}$ band as seen in Figures 3-1, 3-2, 3-8, and 3-11. In RR scattering, the intensities of overtone and combination bands relative to those of fundamental become stronger as the excitation wavelength is brought to shorter wavelengths.[19] Therefore, the excitation profile data favor that the 575 $cm^{-1}$ band is a combination and the 365 $cm^{-1}$ band a fundamental rather than the reversed assignment. Furthermore, the

FeCO bending frequency is lower than the Fe-C stretching frequency for CO adsorbed on an Fe surface.[20] For $O_2$ adducts of Hb and CcO, the Fe-O-O bending RR band was observed around 430 $cm^{-1}$ (chapter 2),[21] which is also significantly lower than the Fe-$O_2$ stretching frequency (570 $cm^{-1}$). These facts also support that the 365 $cm^{-1}$ band rather than the 575 $cm^{-1}$ band is a fundamental of $\delta_{FeCO}$.

The main justification for assigning the 575 $cm^{-1}$ band to a $\delta_{FeCO}$ fundamental was the zigzag pattern of its frequency against the increase of the total mass of CO. The 365 $cm^{-1}$ band exhibits the same feature. As a result, the frequency differences between the 575 and 365 $cm^{-1}$ bands are nearly constant among different CO-isotope adducts of Hb as shown in TABLE 3-1. Furthermore, the absolute values as well as their isotopic frequency shifts of the three bands can be well reproduced by a simple normal coordinate calculations for the isolated FeCO unit. In the same way as chapter 2,[7] the potential function (V) represented by eq 1 was used,

$$2V = K_1(\Delta r_{Fe\text{-}CO})^2 + K_2(\Delta r_{CO})^2 + H(\Delta\theta_{FeCO})^2 + F(\Delta r_{Fe\cdots O})^2 \qquad (1)$$

where $\Delta r_{Fe\text{-}CO}$, $\Delta r_{CO}$, $\Delta\theta_{FeCO}$ and $\Delta r_{Fe\cdots O}$ denote the displacement coordinates for the Fe-CO stretching, C-O stretching, Fe-C-O bending, and Fe···O nonbonding interaction, respectively. For a suitable bending angle as seen for Hb ($\theta$ = 165°), force constants were adjusted so as to reproduce the observed frequencies of HbCO under the assumption that the 365 $cm^{-1}$ band is the fundamental of $\delta_{FeCO}$. The calculated results are compared with the observed values in TABLE 3-2, where the values of force constants are also cited under the table.

The validity of the force constant of H=0.38 mdyn·Å is unknown since there are no *ab initio* calculations available. Spiro and coworkers used H=0.8 mdyn·Å[6,9] and justified the frequency of $\delta_{FeCO}$ higher than $\nu_{Fe\text{-}CO}$ by referring to data on $Mn(CO)_5Br$. However, Jones et al.[22] used 0.45, 0.48 and 0.48 mdyn·Å for the Fe-C-O bending force constant of the valence force field in their normal mode calculations of $Mo(CO)_6$, $Cr(CO)_6$ and $W(CO)_6$, respectively. It is apparent that the electronic state of Fe in Fe-porphyrin is quite different from that of Mn of $Mn(CO)_5Br$ and thus the metal-CO bending force constants could be significantly different. Therefore, the magnitude of the Fe-C-O bending force constant cannot be used as a diagnosis of correct assignment as the present stage. As far as the zigzag pattern of the isotopic frequency shift of CO is concerned, the

present assignment is reasonable, although a more refined force field is required to reproduce the observed frequencies precisely.

### $\delta_{FeCO}$ Band of CcO

The difference spectral patterns in the 365 $cm^{-1}$ region were clear for Hb A and P-$450_{cam}$ but somewhat complicated for CcO, which has heme A as the CO binding site instead of heme B for the former two. In Figure 3-8 there were two positive peaks at 369 and 359 $cm^{-1}$ for the $^{12}C^{16}O$ adduct and two negative peaks at 352 and 332 $cm^{-1}$ for the $^{13}C^{18}O$ adduct, and the trough at 332 $cm^{-1}$ became deeper than that at 352 $cm^{-1}$ as the excitation wavelength became longer. It is evident from Figure 6A that the heme-A·CO has a porphyrin mode at 339 $cm^{-1}$ and this band became more intense when the excitation wavelength was changed from 422.5 to 435.0 nm.

If there is a porphyrin vibration with an intrinsic frequency of $\nu_P$, which interacts with the Fe-ligand mode having an intrinsic frequency of $\nu_L$, the observable frequencies would be $\nu_L^{obs} = \nu_L + \delta$ and $\nu_P^{obs} = \nu_P - \delta$ if $\nu_L > \nu_P$ or $\nu_L^{obs} = \nu_L - \delta$ and $\nu_P^{obs} = \nu_P + \delta$ if $\nu_L < \nu_P$. The size of $\delta$ depends on the magnitude of the interaction and separation between $\nu_L$ and $\nu_P$ modes. For the $^{13}C^{18}O$ adduct of CcO, if we assume that $\nu_P$ = 339 $cm^{-1}$ and $\nu_P^{obs}$ = 332 $cm^{-1}$, it means $\delta$=7 $cm^{-1}$ and therefore $\nu_L^{obs}$ = 353 $cm^{-1}$ would yield $\nu_L$=346 $cm^{-1}$. The values of $\nu_L$ for other CO isotopes can then be estimated from equations mentioned above, and are listed in TABLE 3-3 together with the values of $\nu_P$ and $\delta$ assumed. For the $^{12}C^{18}O/^{13}C^{18}O$ difference spectrum, a single set of $\nu_P^{obs}$ and $\nu_L^{obs}$ is seen in the difference spectrum (D in Figure 3-7) since their counterparts apparently disappear due to subtraction. However, it cannot be reasonably explained why $^{13}C^{16}O$ exhibits no splitting despite of the proximity of $\nu_L$ to $\nu_P$=339 $cm^{-1}$. In addition, for the $^{13}C^{18}O$ adduct, the calculated separation between $\nu_P$ and $\nu_L$ is too large to yield $\delta$=7 $cm^{-1}$. It might imply that $\nu_P$ is an out-of-plane mode buried in the strong in-plane bands in Figure 3-6 or that more than two modes are coupled. Consequently, the estimated $\nu_L$ would contain large errors. Nonetheless, we note that the differences between the observed combination band and the inferred $\nu_L$ fall within 213±5 $cm^{-1}$, which is close to the corresponding values of HbCO shown in TABLE 3-1. If there were no $\delta_{FeCO}$ fundamental in this frequency region, the

vibrational coupling with a porphyrin mode would be so small that no CO-isotope-sensitive RR band would be observed around 350 $cm^{-1}$.

**Assignment of the 575 $cm^{-1}$ Band**

If the bound CO adopts an upright geometry against the porphyrin plane, $\delta_{FeCO}$ is doubly degenerate and is IR active but RR inactive. When CO is slightly deviated from this structure, the degeneracy of $\delta_{FeCO}$ is removed; one is pure bending and the other becomes an internal rotation around the Fe-C bond. In addition, there exists a Fe-C deformation mode which would correspond to the freedom of rotation of the whole FeCO unit for an isolated FeCO molecule and involves the displacement of the carbon atom of CO parallel to the porphyrin plane. This mode would belong to the E species in the putative linear upright geometry ($C_{4v}$) and might be coupled with $\delta_{FeCO}$. Group theoretically, the combination between the split components of the degenerate FeCO bending modes or between the FeCO bending and the Fe-C deformation modes can be a candidate for the 575 $cm^{-1}$ band. The frequency for the internal rotation around the Fe-C bond has never been reported. Although the frequency around 210 $cm^{-1}$ might not be unreasonable as such a mode, it should be accompanied with an isotopic frequency shift for $^{18}O$ substitution. Since the difference (= ~210 $cm^{-1}$) between the 575 and $\delta_{FeCO}$ fundamental shown in TABLE 3-1 scarcely depends on the mass of oxygen, the Fe-C internal rotation mode is less likely as a candidate for a counterpart of the combination to yield the 575 $cm^{-1}$ band. However, since the $^{13}C$ isotope dependence is appreciable for the 210 $cm^{-1}$ mode in TABLE 3-1, the Fe-C deformation mode remains as a candidate for the counterpart.

The corresponding frequency differences between the 575 and 365 $cm^{-1}$ bands for $^{12}C^{16}O$, $^{13}C^{16}O$, and $^{13}C^{18}O$ adducts of P-$450_{cam}$ are 201, 207, and 204 $cm^{-1}$ in Figure 3-10, respectively. Although these values are somewhat smaller than those for Hb, the counterpart which is combined with $\delta_{FeCO}$ to yield the 575 $cm^{-1}$ band would be located around 200-210 $cm^{-1}$. The similarity between P-$450_{cam}$ and Hb rules out an idea of assigning the counterpart of the combination band to a stretching or bending mode of the Fe-fifth ligand.

When the direction of the CO bond is only slightly deviated from the heme normal, the FeCO bending vibration would be accompanied by an in-plane movement of the iron atom and would be coupled with such a

porphyrin mode. The vibrations involving in-plane displacements of iron ion are doubly degenerate (E) under $C_{4v}$ symmetry. Its combination with $\delta_{FeCO}$ under $C_{4v}$ symmetry will include RR active species; E x E = $A_1+A_2+B_1+B_2$. Accordingly, it is group theoretically reasonable that the $\delta_{FeCO}$ fundamental is very weak but the 575 $cm^{-1}$ band has appreciable intensity. However, it is necessary to explain why the particular porphyrin mode is deuteration sensitive. Possible differences in strength of hydrogen bonds between protonated and deuterated proteins may influence some low-frequency porphyrin vibrations. If the effective symmetry is lower than $C_{4v}$, group theoretical consideration is not helpful. It is desirable to specify the counterpart of the combination by observing IR spectra for model compounds.

The deuteration shift of the 575 $cm^{-1}$ band is puzzling. Since this is an upshift, it would not be caused by a simple mass effect. In the case of the $Fe^{IV}$=O heme in compound II of horseradish peroxidase, the $Fe^{IV}$=O stretching frequency was shifted to a higher frequency in $D_2O$ due to weaker deuteron- than hydrogen-bonding to the bound oxygen.[23,24] However, IR measurements of $\nu_{CO}$ on HbCO and CcO·CO noted no detectable effects of protein deuteration on the $\nu_{CO}$ frequency.[25] The $\nu_{Fe-CO}$ frequency is also insensitive to deuteration as demonstrated in Figure 3-13. It is unlikely that a putative hydrogen bonding to CO causes a frequency shift only for the Fe-C-O bending but not for the Fe-CO and C-O stretching except for a less likely structure in which the hydrogen bond to the oxygen atom is perpendicular to the C-O bond. Therefore, the deuteration shift data are also unfavorable to assign the 575 $cm^{-1}$ band to the $\delta_{FeCO}$ fundamental. If the counterpart of $\delta_{FeCO}$ in the combination mode were slightly altered by protein-deuteration, the 575 $cm^{-1}$ band would also be so.

Hb and Mb are oxygen carrier proteins having evolutionary a common origin of genes. Both have a histidine-coordinated protoheme and another histidine near the ligand-binding site called the distal histidine. The oxygen binding affinities of the isolated α and β chains of Hb A are close to that of Mb.[18] The angle between the CO axis and the heme normal, determined by the picosecond IR spectroscopy, is 18° for HbCO and 20° (main component, $\nu_{CO}$=1940 $cm^{-1}$) for sperm whale MbCO.[26] These facts have led one to think that the surrounding structures around the ligand binding site of Hb and Mb are alike.

However, the results shown in Figures 3-11, 3-12, 3-13 revealed distinct differences between the CO adducts of Hb and Mb. Although the vibrational characters are little altered between Hb and Mb, the very strong intensity of the 575 $cm^{-1}$ band, its larger upshift in $D_2O$, and the absence of the 365 $cm^{-1}$ band are characteristic of Mb. Such differences are also seen in $O_2$ adducts for which the Fe-O-O bending RR band is observable for $HbO_2$ but not for $MbO_2$.[21] The origin of these differences remains to be explored. This would clarify the band origin of the 575 $cm^{-1}$ band.

## References


(1) (a) Yu, N. T.; Kerr, E. In *Biological Application of Raman Spectroscopy*; Spiro, T. G., Ed.; Wiley-Interscience: New York, 1988; Vol. 3, pp. 39-95. (b) Yu, N. T. *Methods Enzymol.* **1986**, *130*, 350-409.

(2) Tsuboi, M. *Indian J. Pure Appl. Phys.* **1988**, *26*, 188-191.

(3) Sakan, Y.; Ogura, T.; Kitagawa, T.; Fraunfelter, F. A.; Mattera, R.; Ikeda-Saito, M. *Biochemistry* **1993**, *32*, 5815-5824.

(4) Li, T.; Quillin, M. L.; Phillips, G. N. Jr.; Olson, J. S.; *Biochemistry* **1994**, *33*, 1433-1446.

(5) Nagai, K. Luisi, B.; Shih, D.; Miyazaki, G.; Imai, K.; Poyart, C.; DeYoung, C.; Kwiatkowsky, L.; Noble, R. W.; Lin, S. -H.; Yu, N.-T. *Nature (London)* **1987**, *329*, 858-860.

(6) Li, X. Y.; Spiro, T. G., *J. Am. Chem. Soc.* **1988**, *110*, 6024-6033.

(7) Nagai, M.; Yoneyama, Y.; Kitagawa, T. *Biochemistry* **1991**, *30*, 6495-6503.

(8) (a) Tsubaki, M.; Srivastava, R. B.; Yu, N. T. *Biochemistry* **1982**, *21*, 1132-1140. (b) Yu, N. T.; Kerr, E. A.; Ward, B.; Chang, C. K. *Biochemistry* **1983**, *22*, 4534-4540.

(9) Ray, G. B.; Li, X. Y.; Ibers, J. A.; Sessler, J. L.; Spiro, T. G. *J. Am. Chem Soc.* **1994**, *116*, 162-176.

(10) Yoshikawa, S.; Choc, M. G.; O'Toore, M. C.; Caughey, W. S. *J. Biol. Chem.* **1977**, *252*, 5498-5508.

(11) Geraci, G.; Parkhurst, L. J.; Gibson, Q. H. *J. Biol. Chem.* **1969**, *244*, 4664-4667.

(12) Nagai, M.; Yubisui, T.; Yoneyama, Y. *J. Biol. Chem.* **1980**, *255*, 4599-4602.

(13) Ikeda-Saito, M.; Inubushi, T.; Yonetani, T. *Methods Enzymol.* **1981**, 76, 113-121.

(14) Hu, S.; Morris, I. K.; Singh, J. P.; Smith, K. M.; Spiro, T. G. *J. Am. Chem. Soc.* **1993**, *115*, 12446-12458.

(15) Argade, P. V.; Ching, Y.-C; Rousseau, D. L. *Science* **1984**, *225*, 329-331.

(16) Tsubaki, M.; Ichikawa, Y. *Biochim. Biopys. Acta* **1985**, *827*, 268-274.

(17) Champion, P. M.; Stallard, B. R.; Wagner, G. C.; Gunsalus, I. C. *J. Am. Chem. Soc.* **1982**, *104*, 5469-5470.

(18) Imai, K. In *Allosteric Effects in Haemoglobin*; Cambridge University Press: Cambridge, UK, 1982; p 166.
(19) Friedman, J. M.; Hochstrasser, R. M. *J. Am. Chem. Soc.* **1976**, *98*, 4043-4048.
(20) Kroeker, R. M.; Hansma, P. K.; Kaska, W. C. *J. Chem. Phys.* **1980**, *72*, 4845-4852.
(21) Hirota, S.; Ogura, T.; Appelman, E. H.; Kitagawa, T.; Shizawa-Itoh, K.; Yoshikawa, S. *J. Am. Soc. Chem.*, in press.
(22) Jones, L. H.; McDowell, R. S.; Goldblatt, M. *Inorg. Chem.* **1969**, *8*, 2349-2363.
(23) Hashimoto, S.; Tatsuno, T.; Kitagawa, T. *Proc. Natl. Acad. Sci. U.S.A.* **1986**, *83*, 2417-2421.
(24) Sitter, A. J.; Reczek, C. M.; Terner, J. *J. Biol. Chem.* **1985**, *260*, 7515-7522.
(25) Caughey, W. S. In *Methods for Determining a Metal Environments in Proteins: Structure and Function of Metalloproteins*; Darnall, D. W., Willkins, R. G. Eds.; Elsevier/North-Holland: New York, 1980; pp 95-115.
(26) (a) Moore, J. N.; Hansen, P. A.; Hochstrasser, R. M. *Proc. Natl. Acad. Sci. U.S.A.* **1988**, *85*, 5062-5066. (b) Locke, B.; Diller, R.; Hochstrasser, R. M. In *Advances in Spectroscopy;* Clark, R. J. H., Hester, R. E. Eds.; Wiley & Sons: New York, 1993; Vol. 21B, pp 1-47,.

**TABLE 3-1. Peaks in the Difference Spectra for the $\delta_{FeCO}$ and Combination Modes and the Frequency Differences of These Peaks for Each CO-Isotope Adduct of Hb[a]**

| | $\delta_{FeCO}$[b] | Combination | Difference |
|---|---|---|---|
| $^{12}C^{16}O$ | 367 | 577 | 210 |
| $^{13}C^{16}O$ | 355 | 561 | 206 |
| $^{12}C^{18}O$ | 360 | 571 | 211 |
| $^{13}C^{18}O$ | 353 | 558 | 205 |

[a] Average frequencies (in $cm^{-1}$ unit) in several measurements. [b] The peak positions for the 355, 360 and 353 $cm^{-1}$ bands have the standard deviation of 3 $cm^{-1}$, but others have that of 2 $cm^{-1}$.

**TABLE 3-2. Calculated Frequencies for the Isolated FeCO Unit and Observed Frequencies of HbCO[a,b]**

| | $^{12}C^{16}O$ | | $^{13}C^{16}O$ | | $^{12}C^{18}O$ | | $^{13}C^{18}O$ | |
|---|---|---|---|---|---|---|---|---|
| | obs | calc | obs | calc | obs | calc | obs | calc |
| $\nu_{CO}$ | 1952 | 1952 | 1907 | 1907 | 1906 | 1908 | 1862 | 1861 |
| $\nu_{Fe\text{-}CO}$ | 505 | 506 | 501 | 499 | 496 | 496 | 492 | 489 |
| $\delta_{Fe\text{-}C\text{-}O}$ | 367 | 366 | 355 | 356 | 363[c] | 360 | 353 | 350 |

[a] In $cm^{-1}$ unit. [b] Parameters used for calculations are r(Fe-C) = 1.8 Å, r(C-O) = 1.2 Å, $K_1$(Fe-C) = 2.05 mdyn/Å, $K_2$(C-O) = 14.62 mdyn/Å, H(Fe-C-O) = 0.38 mdyn·Å, F(Fe···O) = 0.7 mdyn/Å, θ(Fe-C-O) = 165°. [c] Since the frequency of the negative peak corresponding to the 574 $cm^{-1}$ band is read lower by 3 $cm^{-1}$ in Figure 3-4B than that in Figure 3-3C, the reading for the 365 $cm^{-1}$ band in the difference spectrum (Figure 3-4B) was deduced to be higher than the true frequency by 3 $cm^{-1}$, and therefore the frequency is estimated to be 363 $cm^{-1}$.

**TABLE 3-3. Observed Frequencies and Estimated Intrinsic Fe-C-O Bending Fundamental Frequencies for CO-Isotope Adducts of Cytochrome *c* Oxidase[a]**

| | Observed[b] | | | Estimated[c] | | | |
|---|---|---|---|---|---|---|---|
| | Combination | $\nu_P^{obs}$ | $\nu_L^{obs}$ | $\nu_P$ | $\nu_L$ | $\delta$ | Difference[d] |
| $^{12}C^{16}O$ | 574 | 356 | 368 | ~358 | 366 | 2 | 208 |
| $^{13}C^{16}O$ | 559 | | 343 | | (343) | 0 | 216 |
| $^{12}C^{18}O$ | 572 | 360 | 352 | ~358 | 354 | 2 | 218 |
| $^{13}C^{18}O$ | 556 | 353 | 332 | ~339 | 346 | 7 | 210 |

[a] In $cm^{-1}$ unit. [b] Frequencies are read from the difference spectra shown in Figure 3-7. [c] $\nu_P$ are assumed and $\nu_L$ are deduced according to eq 1, $\nu_L^{obs}$, and $\delta$. [d] Difference between the combination mode and $\nu_L$.

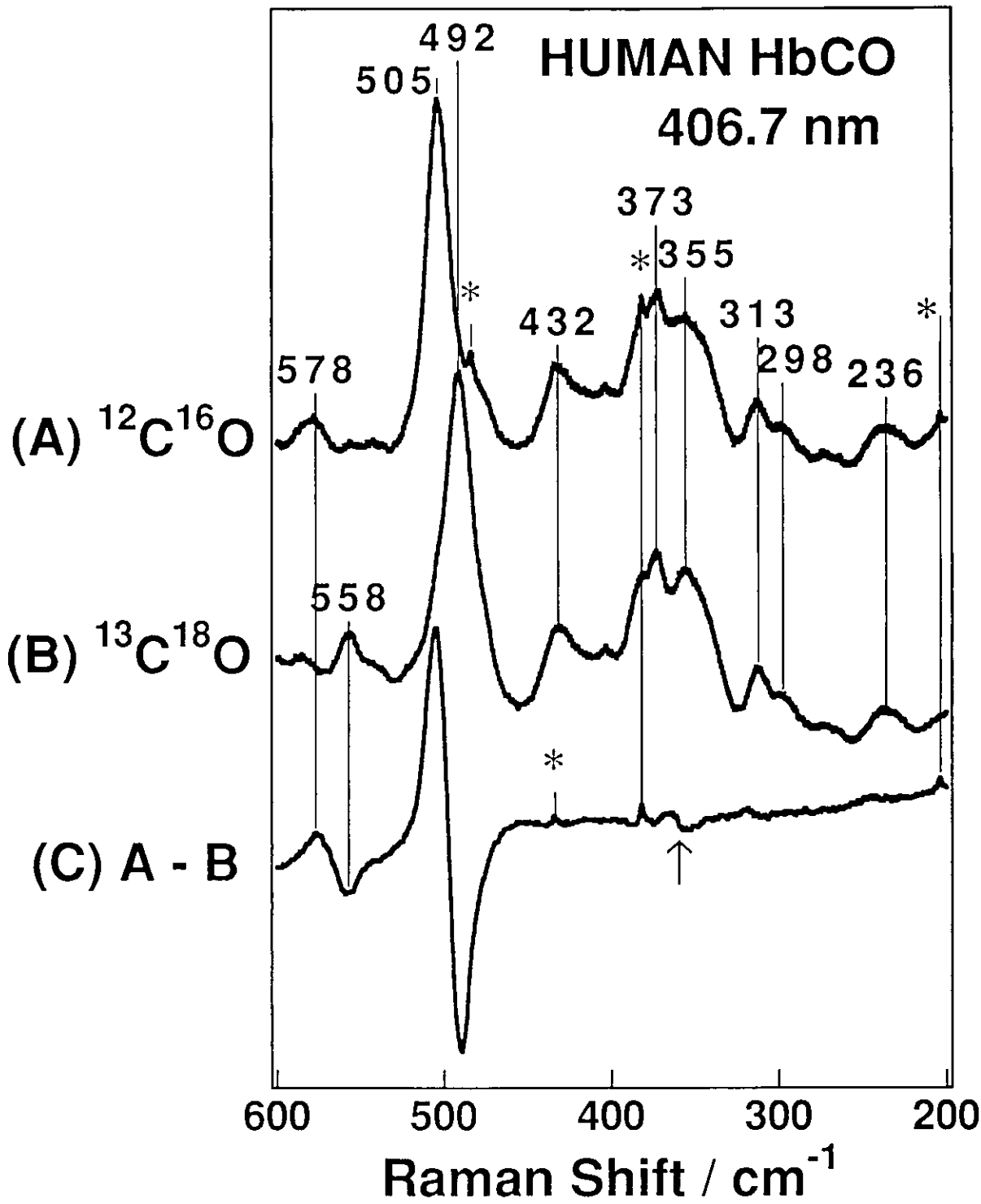


**Figure 3-1.** RR spectra in the 600 to 200 $cm^{-1}$ region of the $^{12}C^{16}O$ (A) and $^{13}C^{18}O$ (B) adducts of Hb A and their difference (C). The ordinate scales in spectra A and B are normalized with the intensity of porphyrin bands. Peaks marked by an asterisk denote the plasma lines from a $Kr^+$ ion laser. Experimental conditions; excitation: 406.7 nm, 6 mW at the sample; detector, diode array; sample, 50 μM (heme) in 50 mM sodium phosphate buffer, pH 7.2. An arrow for spectrum C indicates the difference pattern around 365 $cm^{-1}$.

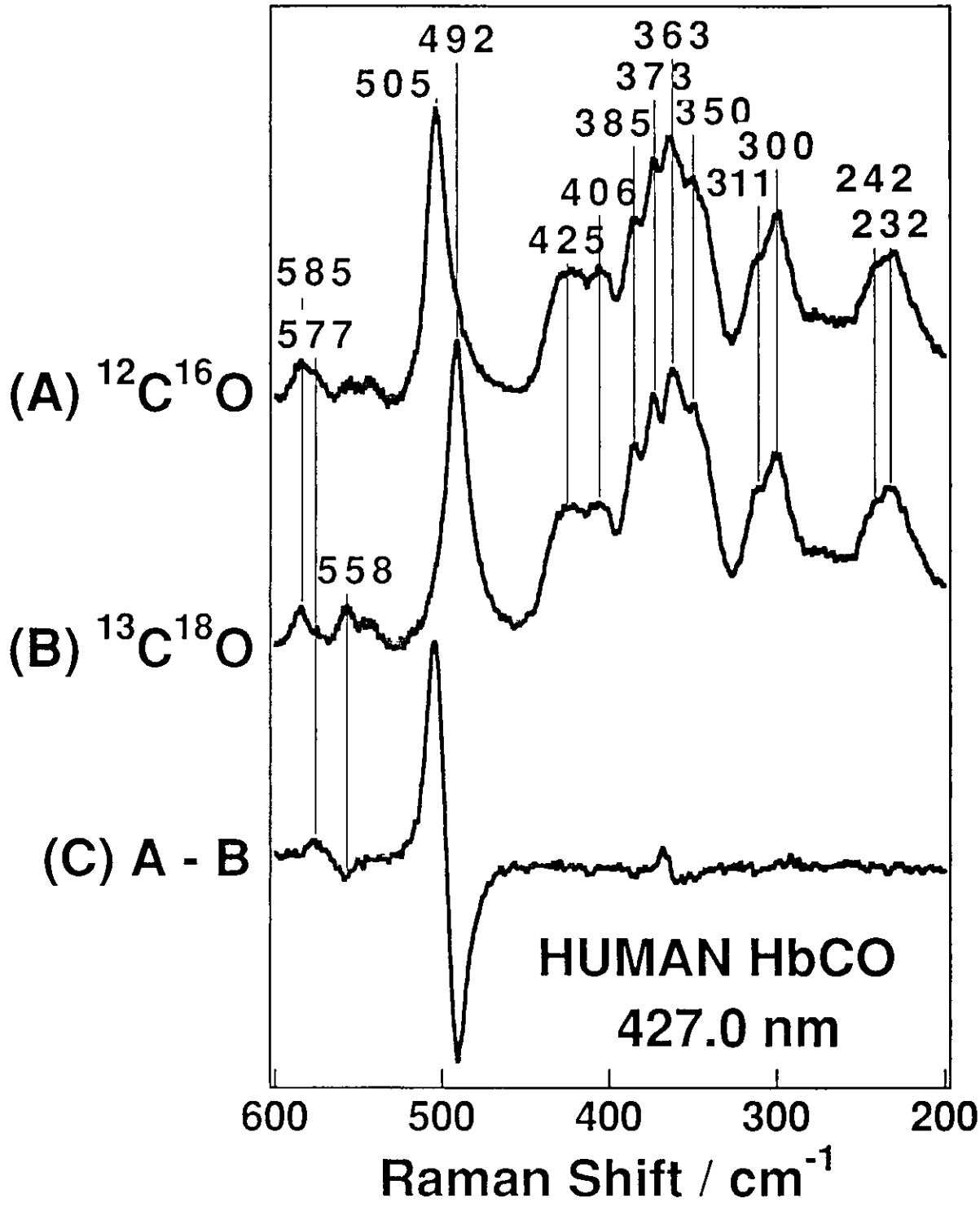


**Figure 3-2.** RR spectra in the 600 to 200 $cm^{-1}$ region of the $^{12}C^{16}O$ (A) and $^{13}C^{18}O$ (B) adducts of Hb A and their difference (C). The ordinate scales are treated in the same way as that in Figure 3-1. Experimental conditions: excitation, 427.0 nm obtained with a Ti-sapphire laser, 4 mW at the sample; detector, diode array; sample, the same as that for Figure 3-1.

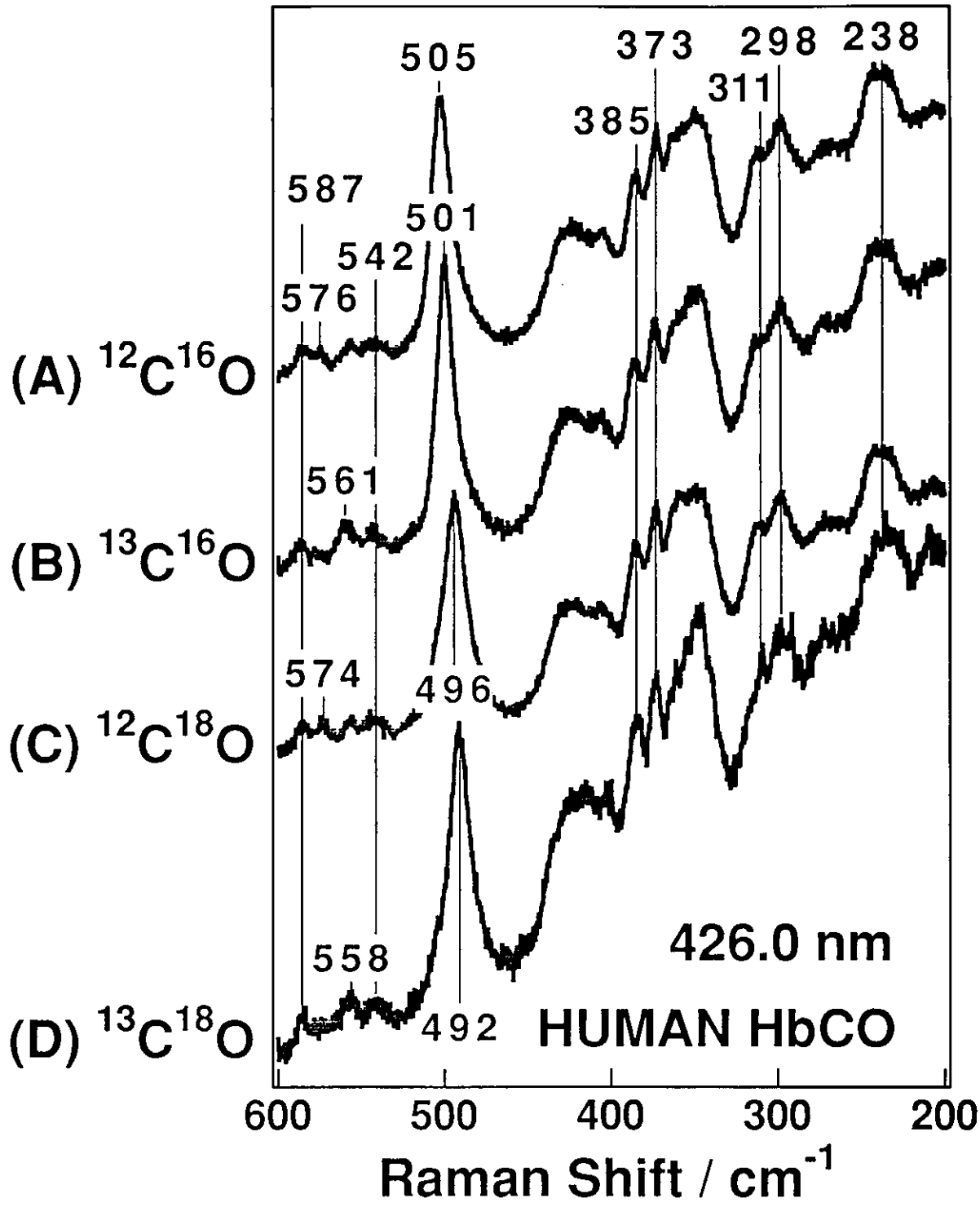


**Figure 3-3.** Comparison of RR spectra of the four CO-isotope adducts of Hb A in the 600 to 200 $cm^{-1}$ region. The ordinate scales are normalized with the intensity of porphyrin bands. Experimental conditions: excitation, 426.0 nm obtained with a Ti-sapphire laser, 5 mW at the sample; sample, 50 μM (heme) in 50 mM Tris-HCl buffer, pH 8.5.

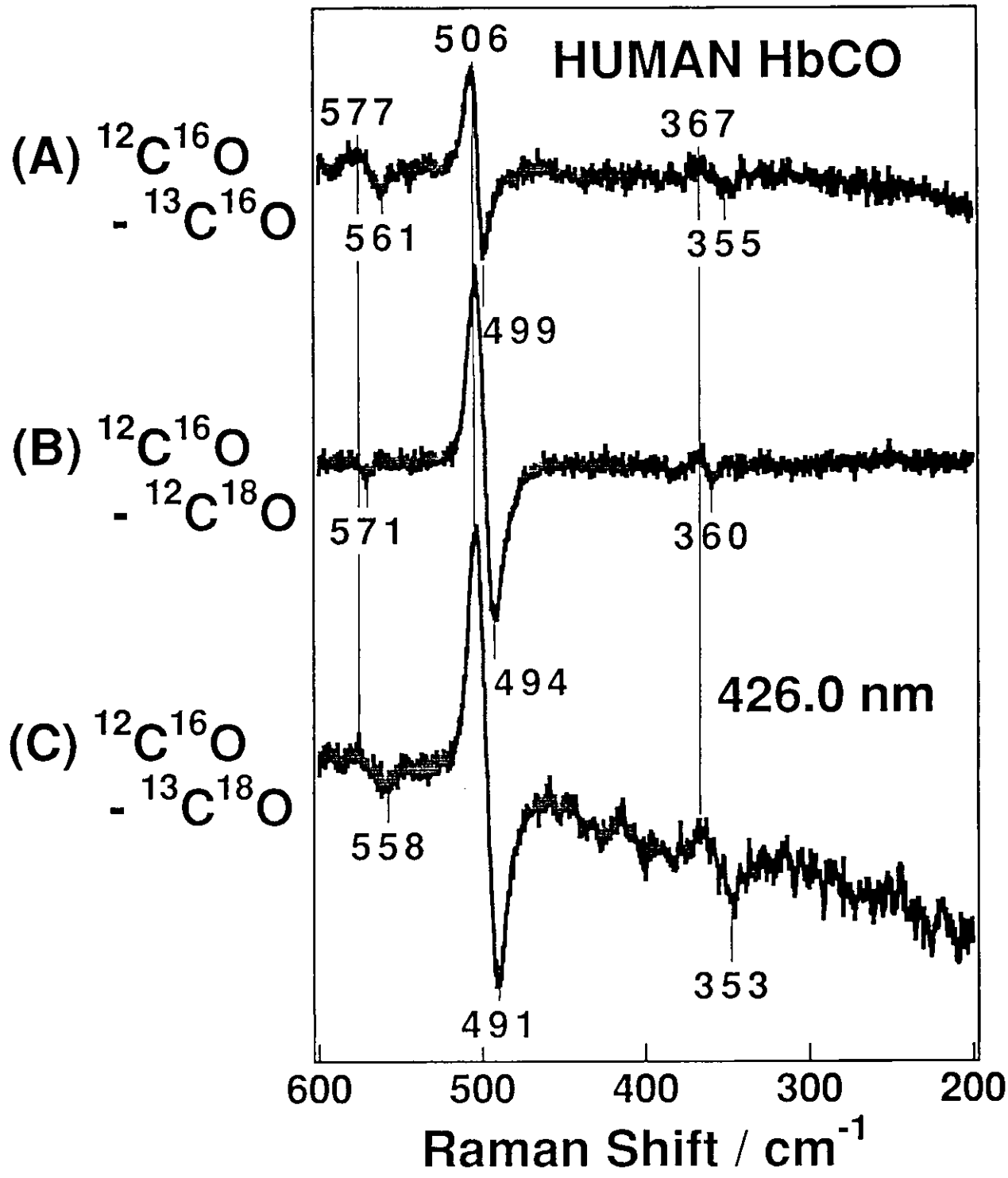


**Figure 3-4.** Differences between the RR spectra shown in Figure 3-3. The differences with regard to the $^{12}C^{16}O$ adduct are displayed. The difference combinations are specified at the left of each spectrum. The peak positions are an average of several measurements, and their standard deviations are at most 3 $cm^{-1}$.

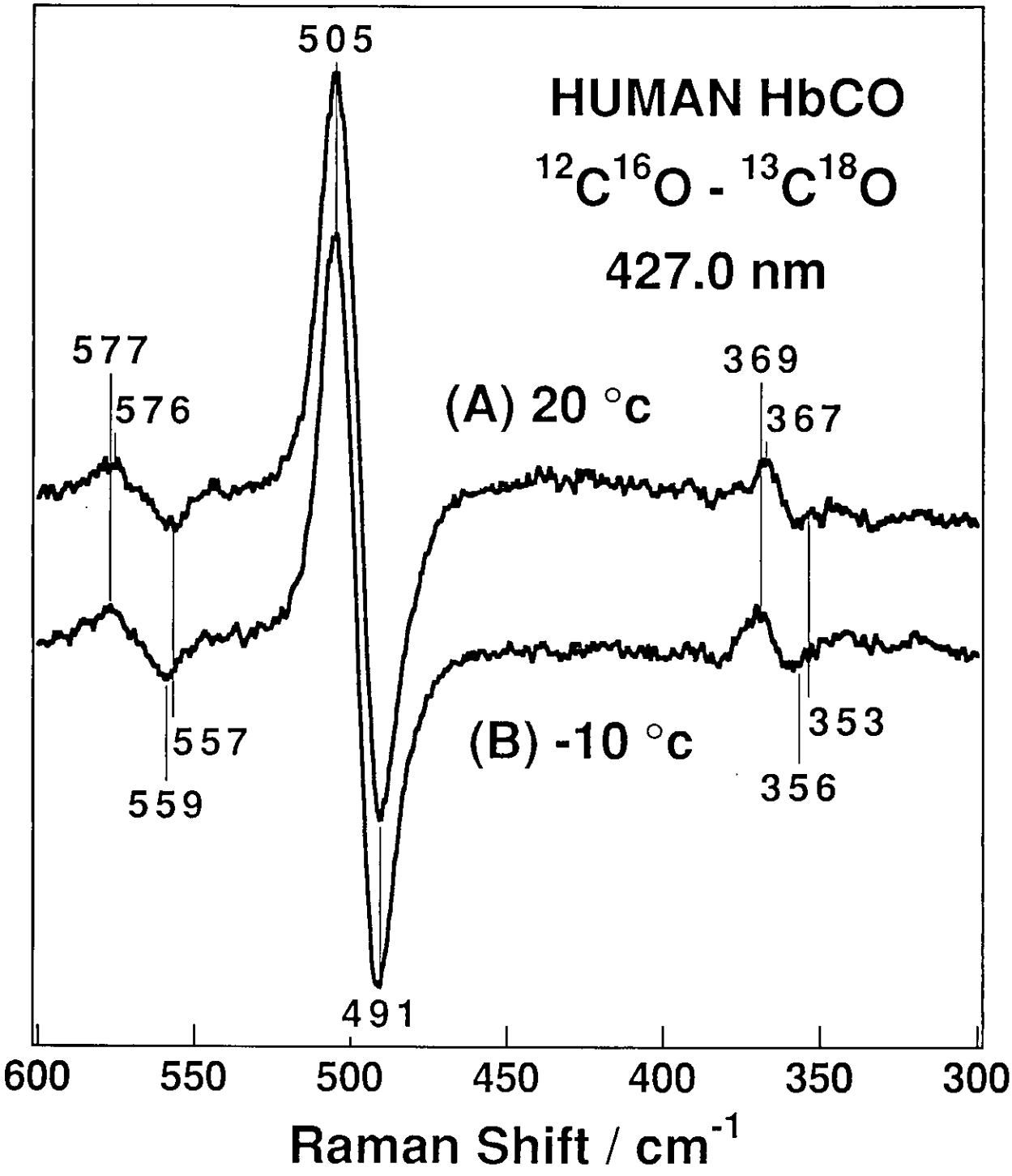


**Figure 3-5.** The $Hb^{12}C^{16}O$ versus $Hb^{13}C^{18}O$ RR difference spectra in the 600 to 300 $cm^{-1}$ region at 20 (A) and -10 °C (B). The ordinate scales of the difference spectra are normalized by the intensity of porphyrin bands in individual raw spectra. Experimental conditions: excitation, 427.0 nm obtained with a Ti-sapphire laser, 1.5 mW at the sample; detector, diode array; sample, 75 μM (heme) in 50 mM sodium phosphate buffer containing 20% glycerol, pH 7.2.

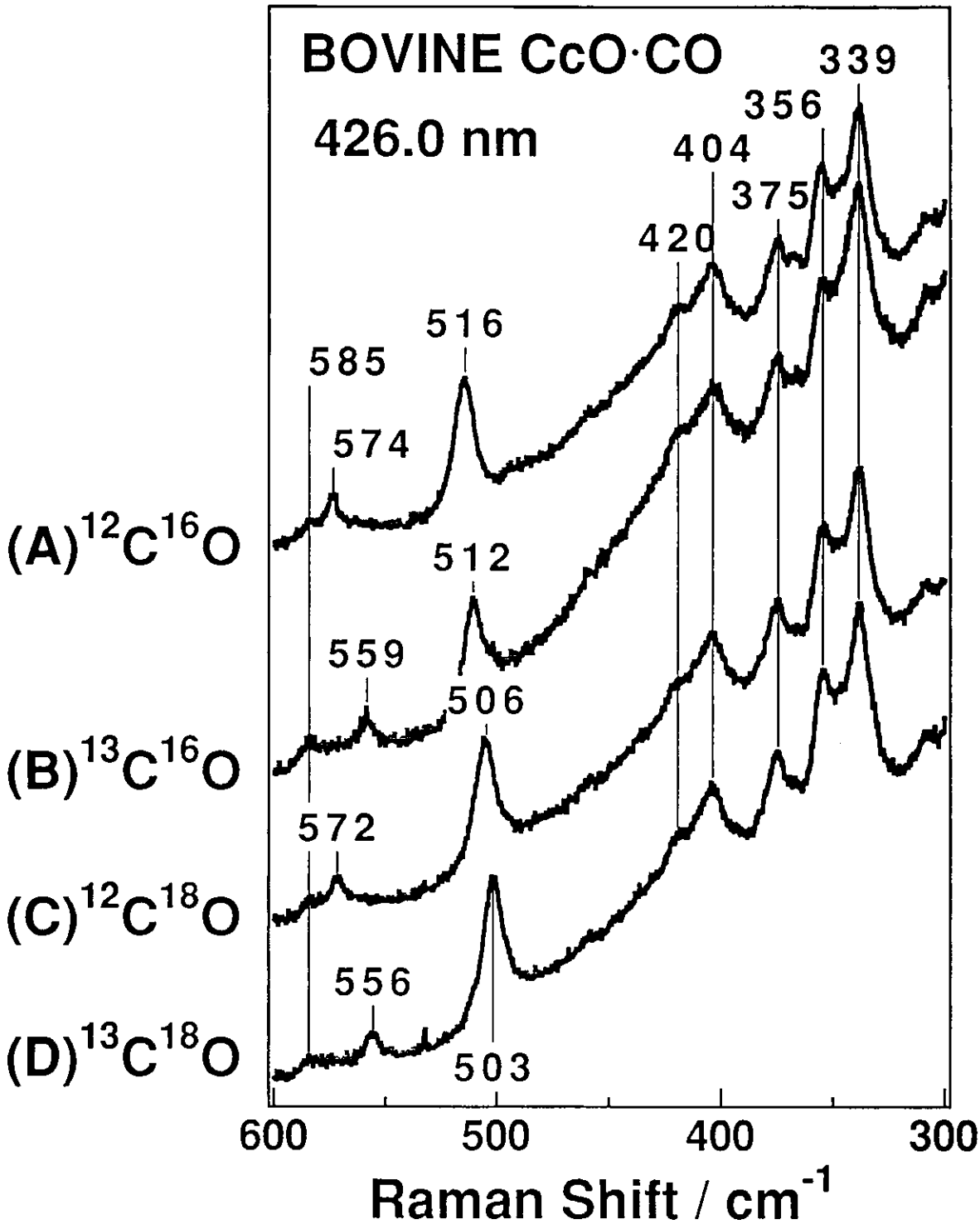


**Figure 3-6.** RR spectra of CcO·CO in the 600 to 300 $cm^{-1}$ region for the $^{12}C^{16}O$ (A), $^{13}C^{16}O$ (B), $^{12}C^{18}O$ (C) and $^{13}C^{18}O$ (D) adducts. The ordinate scales of the four spectra are normalized by the intensity of porphyrin bands. Experimental conditions are the same as those for Figure 3-3 except that the laser used was a dye laser and that the sample condition was 50 μM (heme) in 50 mM sodium phosphate buffer, pH 7.2.

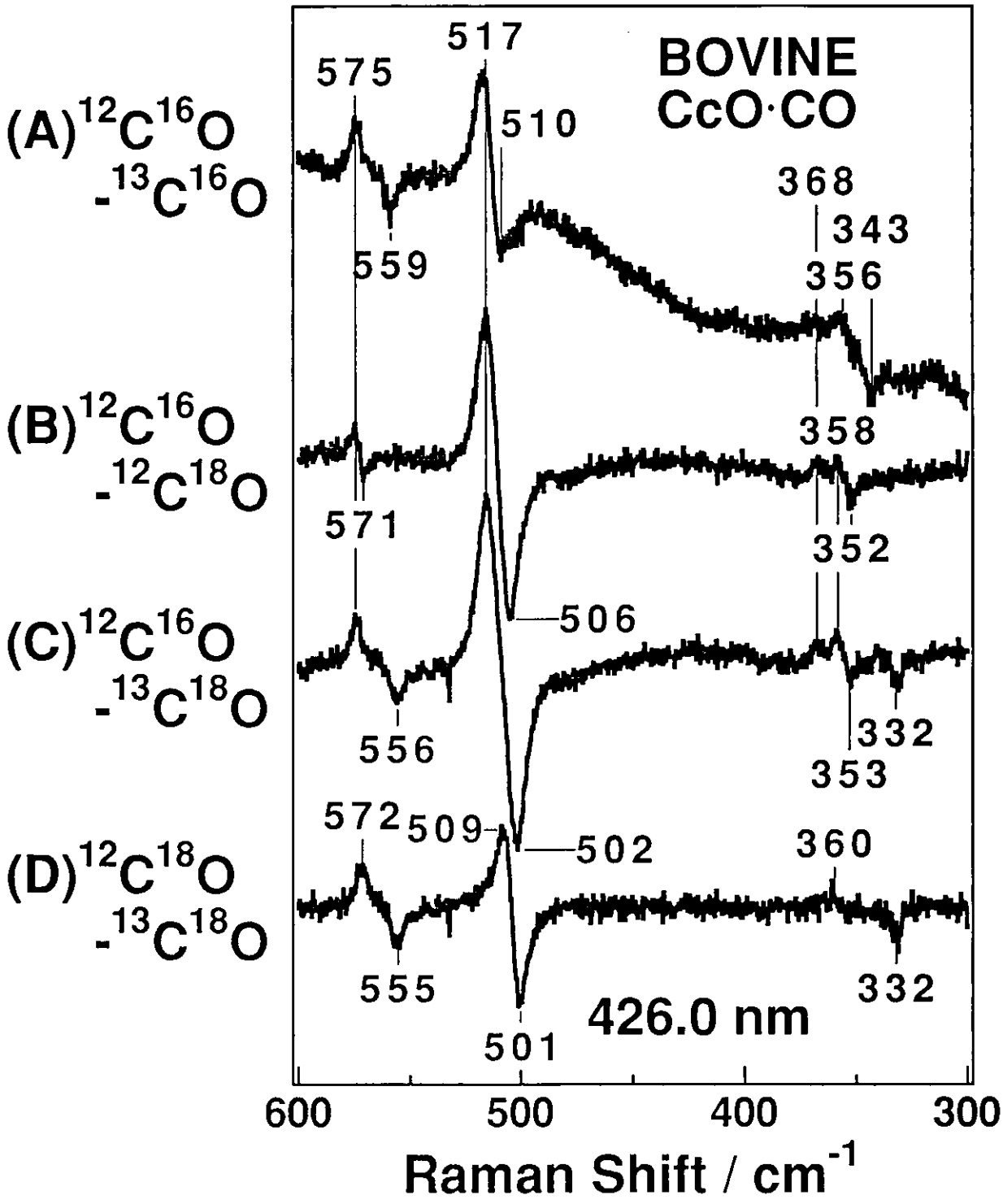


**Figure 3-7.** Differences between the RR spectra of CcO·CO shown in Figure 3-6. Differences with regard to the $^{12}C^{16}O$ adduct are shown in spectra A - C while the difference between the $^{12}C^{18}O$ and $^{13}C^{18}O$ adducts is shown in spectrum D. The difference combinations are specified at the left of each spectrum.

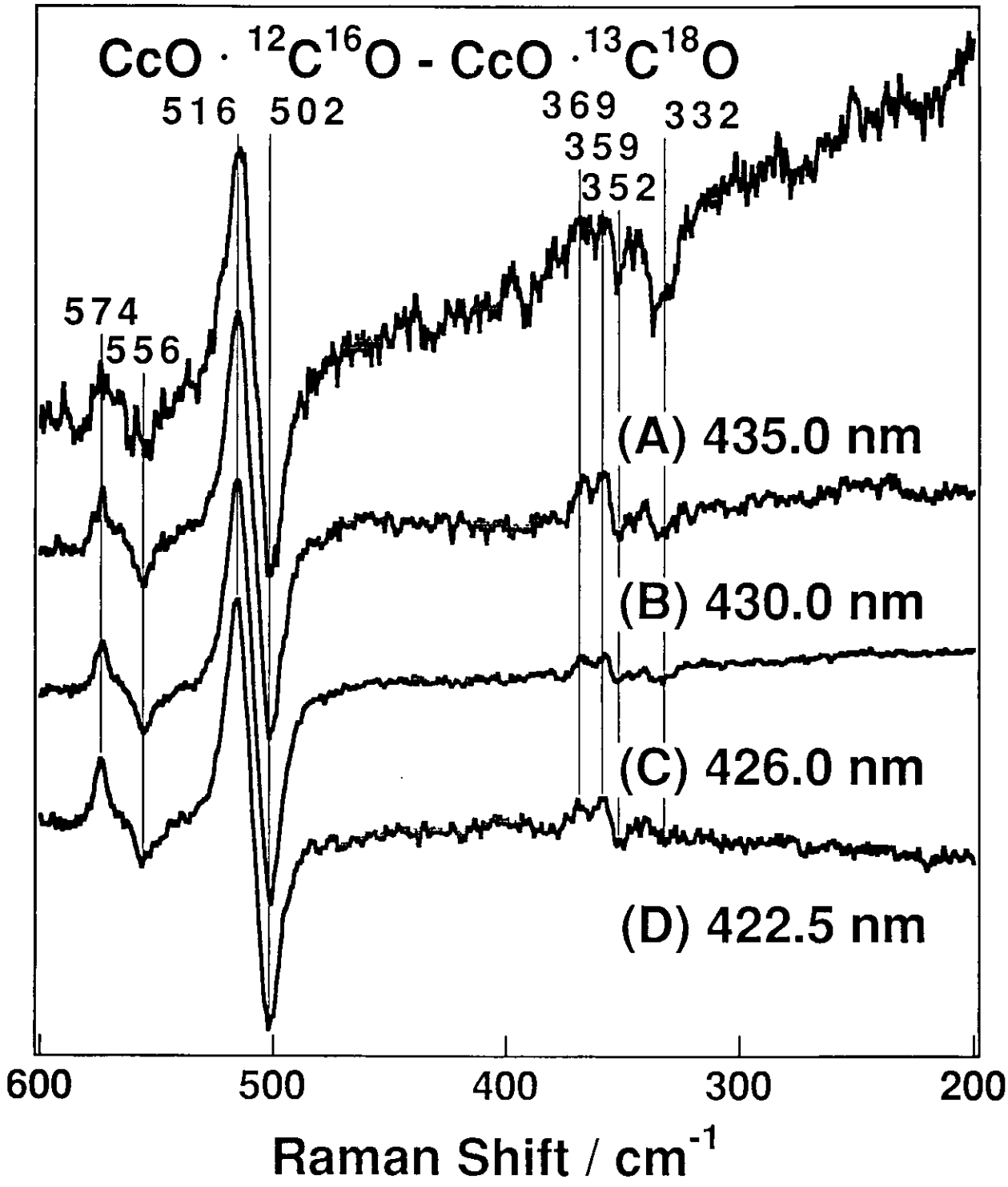


**Figure 3-8.** The excitation wavelength dependence of the difference spectra between $CcO \cdot {}^{12}C^{16}O$ and $CcO \cdot {}^{13}C^{18}O$. Difference calculations were carried out in the same way as those for Figure 3-4. Experimental conditions: laser, 1 mW for (A-C) and 5 mW for (D) generated with a dye laser; detector, diode array; sample, 50 μM (heme) in 50 mM sodium phosphate buffer, pH 7.2.

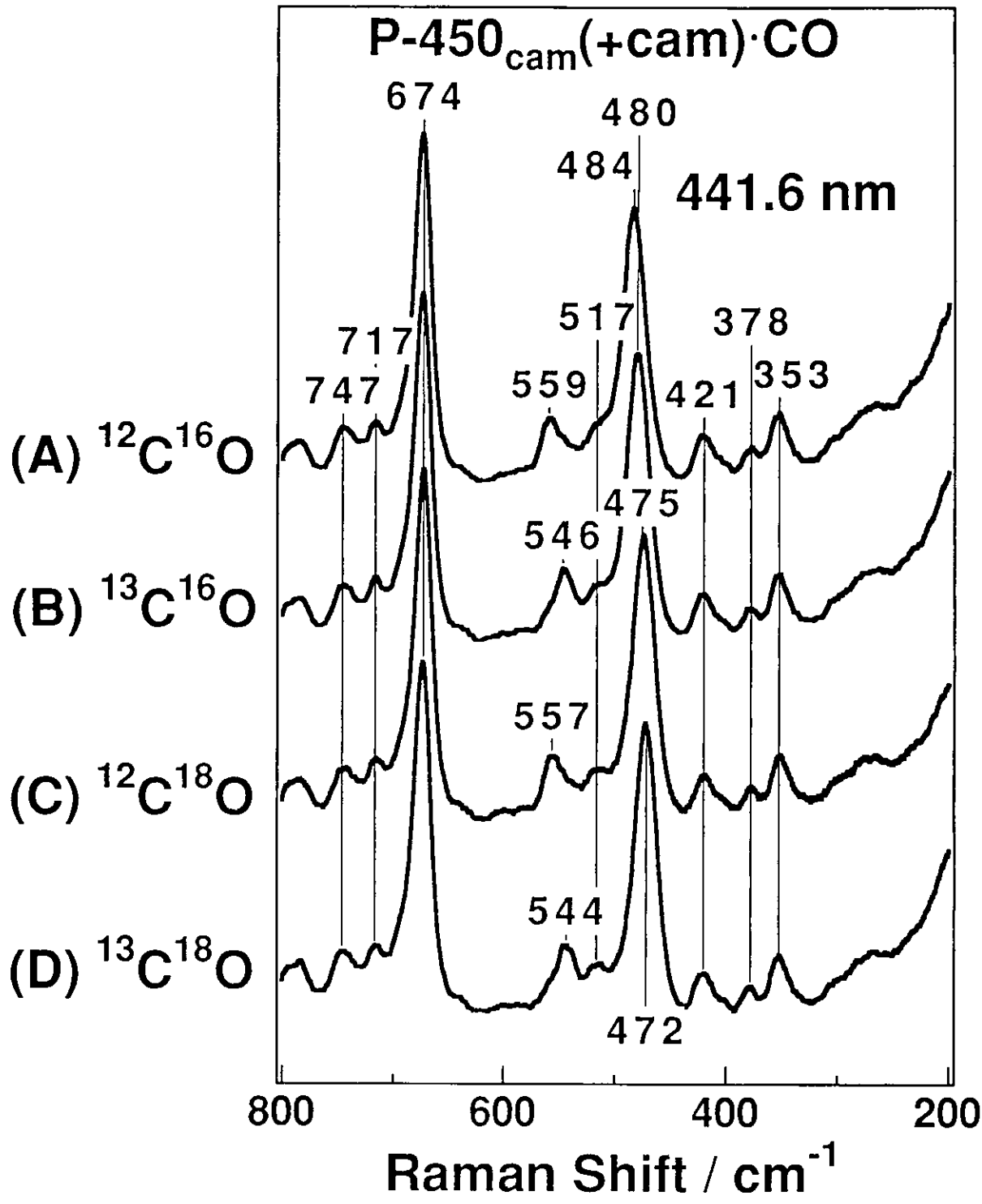


**Figure 3-9.** The RR spectra in the 800 to 200 $cm^{-1}$ region of P-$450_{cam}$·CO in the presence of 1 mM camphor . (A) $^{12}C^{16}O$, (B) $^{13}C^{16}O$, (C) $^{12}C^{18}O$, (D) $^{13}C^{18}O$. The ordinate scales of four spectra are normalized with the intensity of porphyrin bands. Experimental conditions: excitation, 441.6 nm, 5 mW at the sample; sample, 40 μM in 50 mM sodium phosphate buffer, pH 7.2.

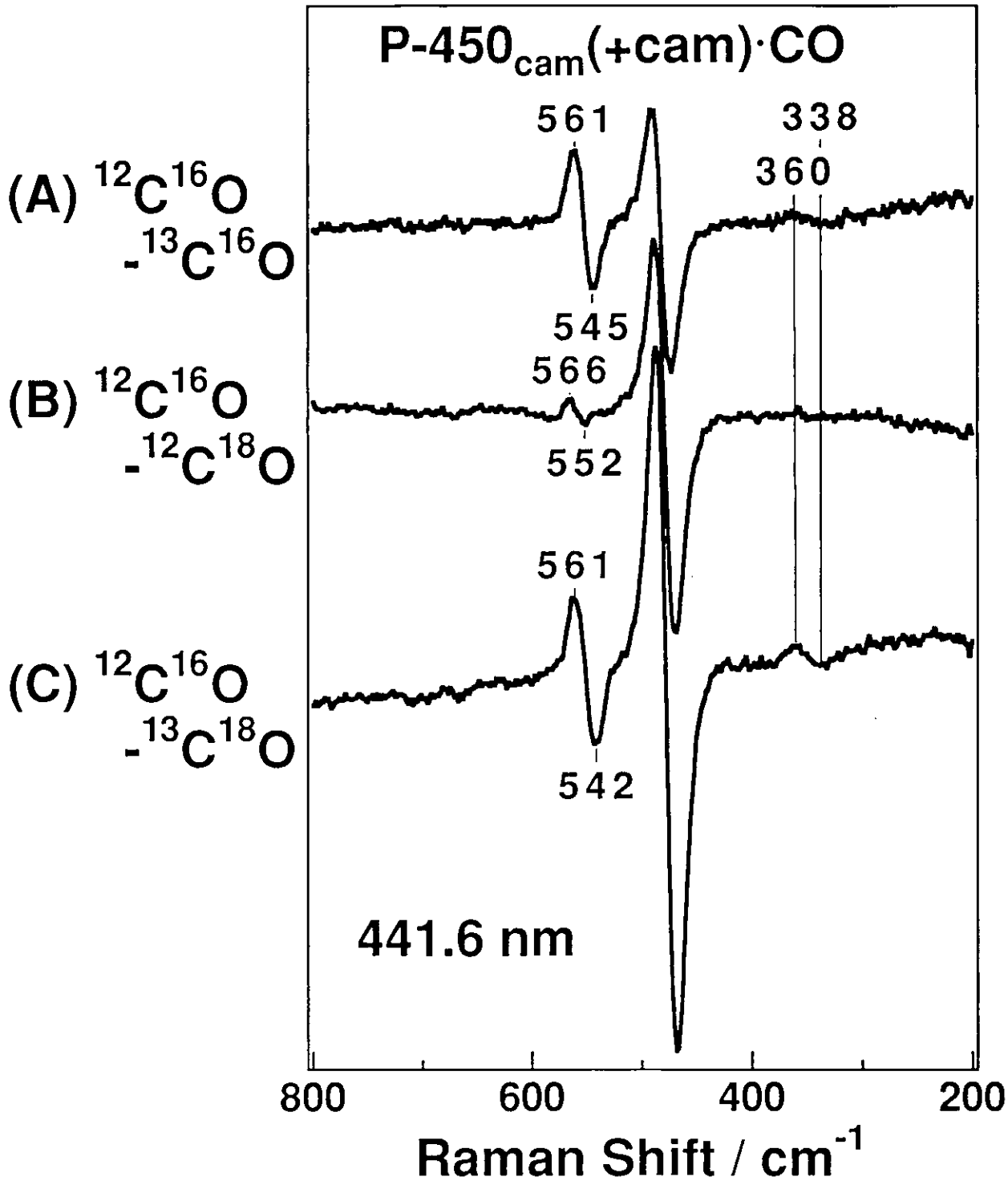


**Figure 3-10.** Differences between the RR spectra shown in Figure 3-9. Difference with regard to the $^{12}C^{16}O$ adduct as specified at the left are displayed.

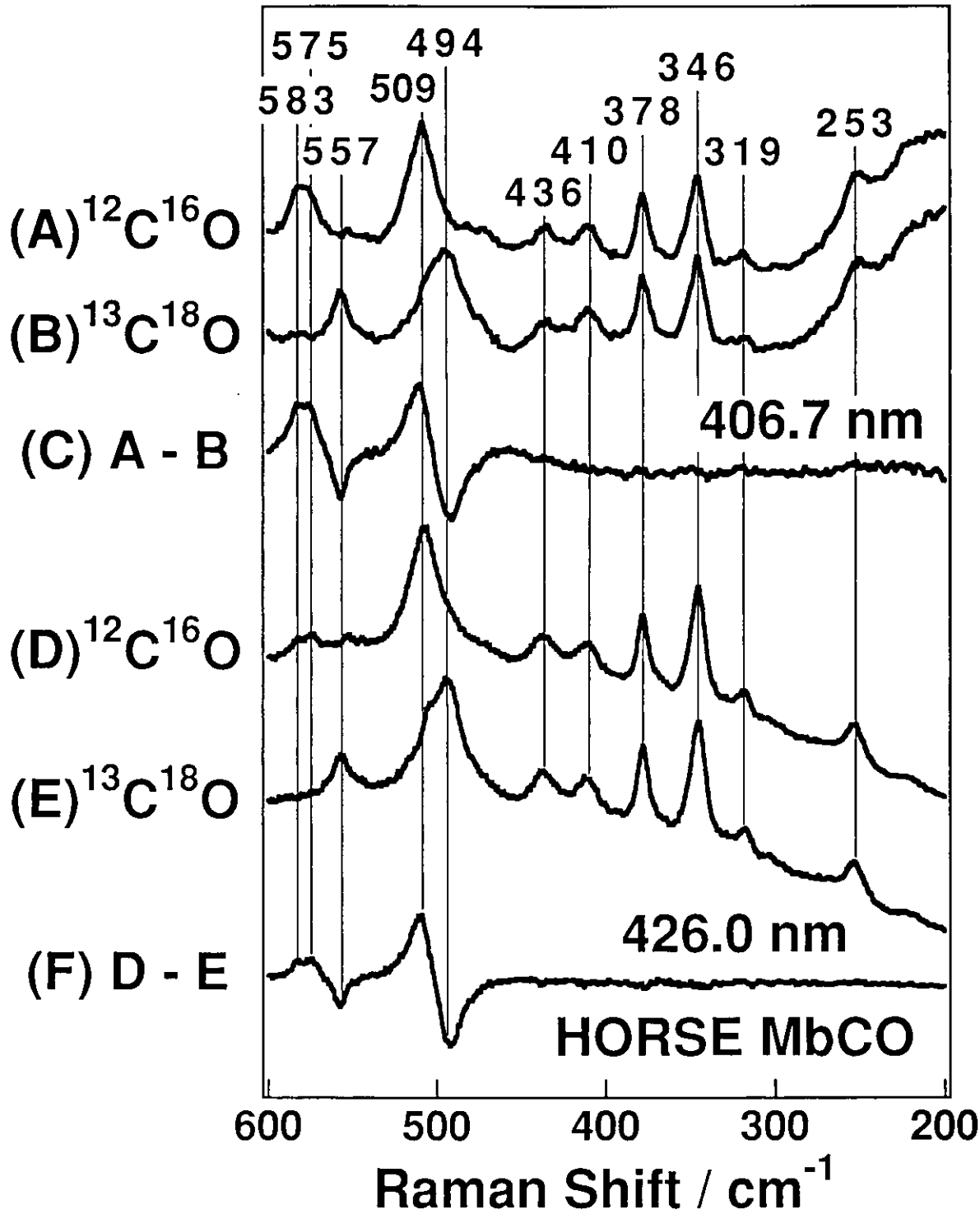


**Figure 3-11.** RR spectra of $^{12}C^{16}O$ and $^{13}C^{18}O$ adducts of horse Mb and their difference spectra. The ordinate scales of the four spectra are normalized with the intensity of porphyrin bands. Traces C and F indicate the difference; spectrum C = spectrum A - spectrum B and spectrum F = spectrum D - spectrum E. Experimental conditions: excitation, 406.7 nm and 5 mW (at the sample) for (A) and (B), and 426.0 nm obtained with a dye laser and 1 mW (at the sample) for (D) and (E); detector, diode array; sample, 30 μM in 50 mM Tris-HCl buffer, pH 8.5.

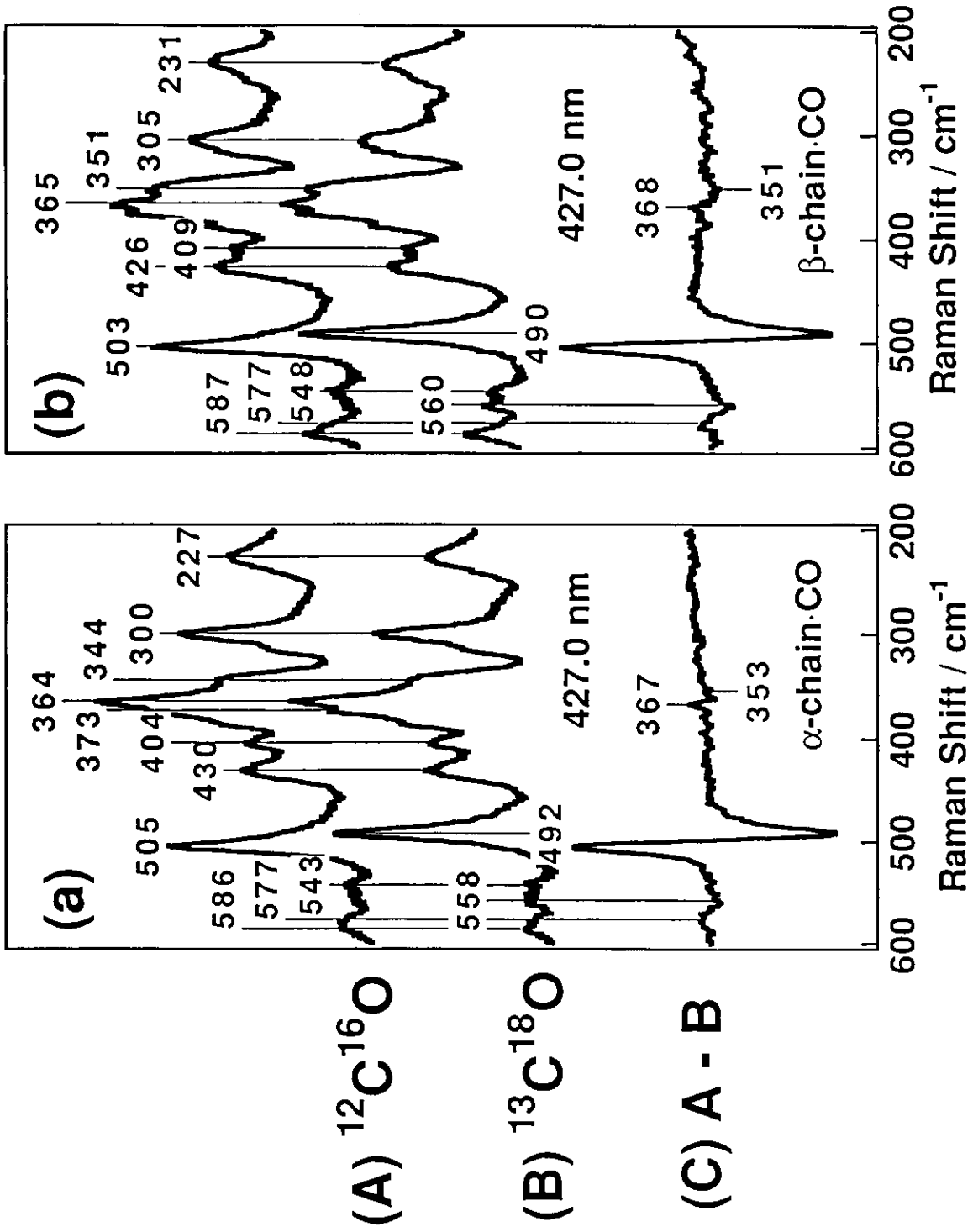


**Figure 3-12.** RR spectra in the 600 to 200 $cm^{-1}$ region of the $^{12}C^{16}O$ and $^{13}C^{18}O$ adducts of the α- and β-chains of HbA . Panels a and b show the results for the α- and β-chains, respectively, and traces A and B denote the spectra of the $^{12}C^{16}O$ and $^{13}C^{18}O$ adducts, respectively. Traces C indicate the difference between spectra A and B. The ordinate scales are normalized with porphyrin bands. Experimental conditions: excitation, 427.0 nm obtained with a Ti-sapphire laser, 3 mW at the sample; detector, diode array; sample 50 μM in 50 mM Tris-HCl buffer, pH 8.5.

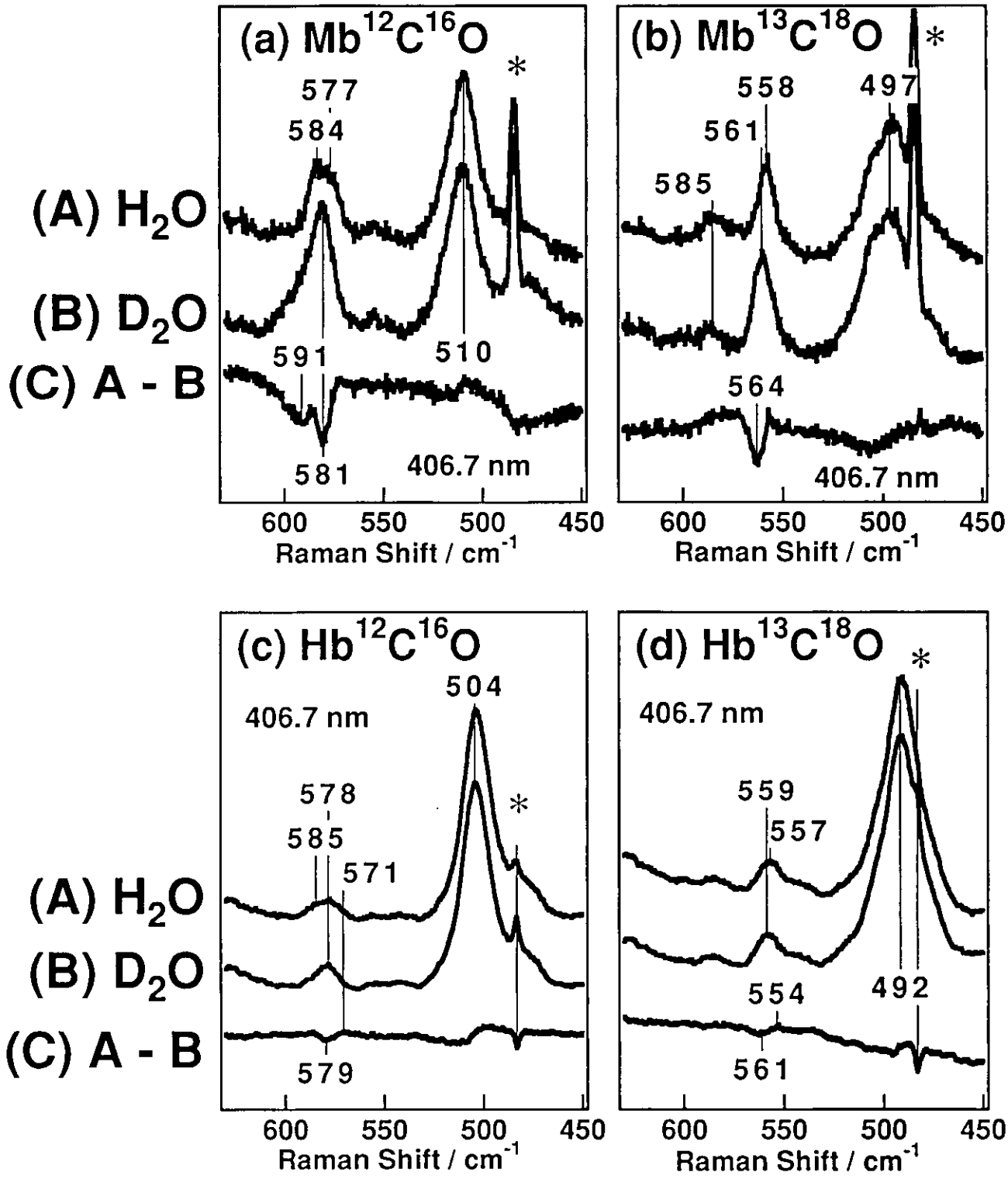


**Figure 3-13.** RR spectral differences between the $H_2O$ and $D_2O$ solutions of CO adducts of Mb and Hb. (A) and (B) represent the spectra observed for the $H_2O$ and $D_2O$ solutions, respectively and (C) shows their difference; (a) $Mb^{12}C^{16}O$, (b) $Mb^{13}C^{18}O$, (c) $Hb^{12}C^{16}O$, (d) $Hb^{13}C^{18}O$. Experimental conditions: excitation, 406.7 nm, 5 mW at the sample; detector: CCD for (a) and (b) and diode array for (c) and (d); sample, 30 μM for MbCO and 50 μM for HbCO both in 50 mM sodium phosphate buffer, pH 7.2.

# Chapter I-4.

# Extended Studies on Vibrational Assignments of the FeCO Unit of CO-Bound Heme Proteins: Observation of Resonance Raman Spectra for CO-Bound Cytochrome *bo* Labeled with $^{54}Fe$ and $^{15}N$ Isotopes

## Abstract

Based on extensive resonance Raman studies on CO-bound heme proteins including cytochrome *c* oxidase, we have proposed in chapter I-3 that the CO-isotope-sensitive band around 365 $cm^{-1}$ is attributed to the $\delta_{FeCO}$ fundamental mode while the 575 $cm^{-1}$ band is reassignable to a combination mode of the $\delta_{FeCO}$ fundamental and a porphyrin or a Fe-C distortion mode. Studies on Fe isotopes now became essential for verification of the proposal.

In this study, we examined the resonance Raman spectra of CO-isotope adducts of cytochrome *bo* complexes (cyt.*bo*) biosynthetically labeled with $^{54}Fe$, $^{56}Fe$, and $^{15}N$. The C, O, Fe, and N isotopes showed frequency shifts for the $\nu_{Fe\text{-}CO}$ band of CO-bound cyt.*bo* by 4.5, 9.5, 3.5, and 1 $cm^{-1}$, and for the 575 $cm^{-1}$ band of it by 16, 2.5, 1.5 and 0 $cm^{-1}$, respectively. Difference peaks were also observed around 365 $cm^{-1}$ for the CO-isotope difference spectra. Normal-coordinate calculations for the isolated FeCO unit well reproduced the observed Fe isotopic shifts for the $\nu_{Fe\text{-}CO}$ and $\delta_{FeCO}$ bands when we assigned the 365 $cm^{-1}$ band to the $\delta_{FeCO}$ fundamental, while it was unable to reproduce them when we assign the 575 $cm^{-1}$ band to the $\delta_{FeCO}$ fundamental, because of their strong vibrational mixing. However, if the 575 $cm^{-1}$ band is a combination mode, the counterpart other from the $\delta_{FeCO}$ is not an $E_u$ porphyrin mode, since the 575 $cm^{-1}$ band was not shifted with $^{15}N$ substitution.

## 4.1 Introduction

In chapter I-3, a new CO-isotope-sensitive band is reported around 365 $cm^{-1}$ for CO adducts of Hb, its isolated chains, cytochrome *c* oxidase (CcO), and cytochrome P-450 (P-450). For HbCO, this band was located at 367, 353, 363, and 351 $cm^{-1}$ for $^{12}C^{16}O$, $^{13}C^{16}O$, $^{12}C^{18}O$, and $^{13}C^{18}O$ adducts, respectively.[1] This band exhibited a "zigzag" pattern against the increase of the total mass of CO, similar to the 575 $cm^{-1}$ band which had been assigned to the $\delta_{FeCO}$ fundamental.[2] In chapter I-3, it is proposed that the ~ 365 and 575 $cm^{-1}$ bands arise from the $\delta_{FeCO}$ fundamental and its combination with a porphyrin mode or a Fe-C deformation mode of the FeCO unit, respectively. As discussed in the following chapter, an overtone mode for the 365 $cm^{-1}$ band and a combination mode of $\nu_{Fe-CO}$ and the 365 $cm^{-1}$ band were observed in HbCO and MbCO, while an overtone mode of the 575 $cm^{-1}$ band was undetectable.[3] These results strongly supports our proposal in chapter I-3.

Cytochrome *bo* complex (cyt.*bo*) is a terminal oxidase in the respiratory chain of *Escherichia coli* (*E. coli*) predominantly expressed under high oxygen tension. It contains two hemes, one five-coordinated heme O and one six coordinated heme B. In this protein CO binds to the heme O iron, and the $\nu_{Fe-CO}$ frequency of this complex has been detected around 520 $cm^{-1}$.[4-6] The $^{54}Fe$- and $^{15}N$-isotope-labeled cyt.*bo* that have the same structure as the non-labeled complex can be prepared by growing *E. coli* cells in $^{54}Fe$- or $^{15}N$-enriched mediums and then purifying cyt.*bo* from the cells.

To explore the nature of the $\nu_{Fe-CO}$, $\delta_{FeCO}$, and 575 $cm^{-1}$ bands, RR spectra of the CO adducts of these $^{54}Fe$- and $^{15}N$-isotope labeled cyt.*bo* were measured. The Fe isotope frequency shifts in the $\nu_{Fe-CO}$ and 575 $cm^{-1}$ bands of CO-bound cyt.*bo* were 3.5 and 1.5 $cm^{-1}$ in average, respectively.

## 4.2 Experimental Procedures

Raman scattering was excited at 406.7 nm by a $Kr^+$ ion laser (Spectra Physics, Model 2016) and detected with a cooled (-20°C) diode array (PAR, 1421HQ) attached to a single polychromator (Ritsu Oyo Kogaku, DG-1000). The slit width of 200 μm (spectral slit width of 4 $cm^{-1}$) and slit-height of 10 mm were used. The laser power and width at the sample point were 6 to 7 mW and ca. 50 μm, respectively. All

measurements were carried out at room temperature with a spinning cell (3500 rpm) to avoid photodissociation of CO. Raman shifts were calibrated with $CCl_4$ and acetone as standards. Uncertainties of the Raman bands were ±1 $cm^{-1}$.

$^{54}Fe$ (99.85 atom %) and $^{56}Fe$ (99.7 atom %) were obtained from ICON Services Inc. (Summit, New Jersey) as metal and were dissolved in hydrochloric acid to make 50 mg/ml solution. [$^{15}N$]-$(NH_4)_2SO_4$ (99.6 atom %) was purchased from Shoko Co., Ltd. (Tokyo, Japan). Cyt.*bo* was purified from a merodiploid strain of the cyt.*bo* operon, GO103/pMFO2 (*cyo*$^+$ *Δcyd*-Km$^r$/*cyo*$^+$ Ap$^r$), as described elsewhere.[7] For labeling with stable iron isotopes, *E. coli* cells were grown aerobically in 10 L of a rich medium supplemented with 5 μg/mL $^{54}Fe$ or $^{56}Fe$, 25 μg/mL $CuSO_45H_2O$, 10 mg/mL glycerol, 50 μg/mL L-tryptophan, and 25 μg/mL ampicillin sodium salt. For labeling with $^{15}N$, cells were grown aerobically in 8 L of minimal sodium medium A,[8] supplemented with 2.5 μg/mL [$^{15}N$]-$(NH_4)_2SO_4$, 20 mg/mL glycerol, 25 μg/mL ampicillin sodium salt, 25 μg/mL kanamaycin sulfate, and 1 μg/mL thiamine Cyt.bo isolated by anion-exchange HPLC was washed 3 times with 50 mM Tris-HCl (pH7.4) containing 0.1 % sucrose monolaurate, and was concentrated to about 250 μM by utrafiltration.[7]

Cyt.*bo* was dissolved in 50 mM Tris-HCl buffer, pH7.2, with 0.1 % sucrose monolaurate. CO-bound cyt.*bo* (cyt.*bo*·CO) was formed by the same way as described in chapter I-3 for obtaining the CO adduct of CcO.[1] CO isotope adducts of cyt.*bo* were obtained as the same way as cyt.*bo*·CO, followed by incorporating $N_2$ gas into the cell for two times and finally incorporating $^{13}C^{16}O$ (ICON, 99 atom % for $^{13}C$), $^{12}C^{18}O$ (Cambridge Isotope Lab, 98 atom % for $^{18}O$), or $^{13}C^{18}O$ (Isotec, 98.6 atom % for $^{13}C$ and 96.8 atom % for $^{18}O$).

### 4.3 Results

The RR spectra for the 700 to 300 $cm^{-1}$ region of $^{12}C^{16}O$ (A), $^{13}C^{16}O$ (B), $^{12}C^{18}O$ (C), and $^{13}C^{18}O$ (D) adducts of $^{56}Fe$ cyt.*bo* excited at 406.7 nm are shown in Figure 4-1. The Raman band at 521 $cm^{-1}$ of $^{12}C^{16}O$-bound $^{56}Fe$ cyt.*bo* (A) is shifted to 516, 511, and 507 $cm^{-1}$ for $^{13}C^{16}O$ (B), $^{12}C^{18}O$ (C), and $^{13}C^{18}O$ (D) adducts, respectively. This band shifted monotonously to

lower frequencies according to the total mass of CO, and was consistent with the previous assignment to the $\nu_{Fe\text{-}CO}$ mode.[4]

The CO-isotope-sensitive band located at 574 $cm^{-1}$ is shifted to 557, 571, and 555 $cm^{-1}$ with $^{13}C^{16}O$ (B), $^{12}C^{18}O$ (C), and $^{13}C^{18}O$ (D) adducts, respectively. This band had similar frequencies as the 575 $cm^{-1}$ band in other CO-bound heme proteins.[2,9-14] Since these bands in all CO-bound heme proteins exhibited a "zigzag" pattern against the increase of the total mass of CO, it had been assigned to the $\delta_{FeCO}$ mode.[2,9-14] But we found a new CO-isotope-sensitive band around 365 $cm^{-1}$ and assigned this new band to the $\delta_{FeCO}$ fundamental and reassigned the band around 575 $cm^{-1}$ to a combination mode as discussed above.[1]

A shoulder band at 362 $cm^{-1}$ in $^{12}C^{16}O$-bound cyt.*bo* (A) disappeared in other CO-isotope-bound cyt.*bo* (B-D). This frequency was very close to the frequencies of the new CO-isotope sensitive band we observed for other CO-bound heme proteins. Accordingly, we calculated the difference spectra between each CO-isotope spectrum of Figure 4-1 against the $^{13}C^{18}O$-bound spectrum (Figure 4-1D), and the results are shown in Figure 4-2: (A) $^{12}C^{18}O$ adduct - $^{13}C^{18}O$ adduct, (B) $^{13}C^{16}O$ adduct - $^{13}C^{18}O$ adduct, (C) $^{12}C^{16}O$ adduct - $^{13}C^{18}O$ adduct. Large difference peaks around 510 $cm^{-1}$ are attributed to the $\nu_{Fe\text{-}CO}$ mode, and small difference peaks around 570 $cm^{-1}$ are due to so-called 575 $cm^{-1}$ band. There also appeared difference peaks around 365 $cm^{-1}$ where we detected the $\delta_{FeCO}$ mode in other CO-bound heme proteins. However, the difference peaks around 365 $cm^{-1}$ did not show clear CO-isotope shifts and the difference patterns differed among different CO-isotope pairs.

Figure 4-3 shows the RR spectra for the 700 to 300 $cm^{-1}$ region of CO-bound $^{54}Fe$-labeled cyt.*bo* excited at 406.7 nm: (A) cyt.*bo*·$^{54}Fe^{12}C^{16}O$, (B) cyt.*bo*·$^{54}Fe^{13}C^{16}O$, (C) cyt.*bo*·$^{54}Fe^{12}C^{18}O$, and (D) cyt.*bo*·$^{54}Fe^{13}C^{18}O$. The RR band at 521 $cm^{-1}$ of $^{12}C^{16}O$-bound $^{56}Fe$ cyt.*bo* (Figure 4-1A) is shifted to 525 $cm^{-1}$ for $^{12}C^{16}O$-bound $^{54}Fe$-labeled cyt.*bo* (A). Similarly, the $\nu_{Fe\text{-}CO}$ bands at 516, 511, and 507 $cm^{-1}$ for $^{13}C^{16}O$-, $^{12}C^{18}O$-, and $^{13}C^{18}O$-bound $^{56}Fe$ cyt.*bo* (Figure 4-1A-C), are shifted to 519, 514, and 511 $cm^{-1}$ in $^{13}C^{16}O$-, $^{12}C^{18}O$-, and $^{13}C^{18}O$-bound $^{54}Fe$ labeled cyt.*bo* (B-D), respectively. The $\nu_{Fe\text{-}CO}$ frequencies in each CO isotope bound $^{54}Fe$-labeled cyt.*bo* shifted higher by 3~4 $cm^{-1}$ from those of the same CO-isotope-bound $^{56}Fe$ cyt.*bo*.

The CO-isotope-sensitive band located at 574 $cm^{-1}$ in $^{12}C^{16}O$-bound $^{56}Fe$ cyt.*bo* (Figure 1A) is also shifted to 575 $cm^{-1}$ in $^{12}C^{16}O$-bound $^{54}Fe$-

labeled cyt.*bo* (A). The same band at 557, 571, and 555 $cm^{-1}$ in $^{13}C^{16}O$-, $^{12}C^{18}O$-, and $^{13}C^{18}O$-bound $^{56}Fe$ cyt.*bo* (Figure 4-1B-D) is also shifted to higher frequencies by 1~2 $cm^{-1}$ ( 559, 572, and 557 $cm^{-1}$ with $^{13}C^{16}O$-, $^{12}C^{18}O$-, and $^{13}C^{18}O$-bound $^{54}Fe$-labeled cyt.*bo* (B-D), respectively ), although the 680 $cm^{-1}$ porphyrin band did not shift more than 0.5 $cm^{-1}$.

The differences between the RR spectra shown in Figure 4-3 are shown in Figure 4-4. The difference peaks around 570 $cm^{-1}$ shifted to higher frequencies by 1~2 $cm^{-1}$ from the difference peaks in the corresponding difference spectra for CO-bound $^{56}Fe$ cyt.*bo* (Figure 4-2). The difference peaks around 365 $cm^{-1}$ were also observed in these difference spectra.

Figure 4-5 shows the RR spectra for the 700 to 300 $cm^{-1}$ region of $^{12}C^{16}O$- (A) and $^{13}C^{18}O$- (B) bound $^{15}N$-labeled cyt.*bo* excited at 406.7 nm, their difference spectra (C), and the corresponding CO-isotope difference spectra of $^{14}N$ cyt.*bo* (D). Each porphyrin band is shifted to a lower frequency by 2~4 $cm^{-1}$ than that of the CO adduct $^{14}N$ cyt.*bo*. The $\nu_{Fe\text{-}CO}$ frequencies were observed at 520 and 506 $cm^{-1}$ for $^{12}C^{16}O$- (A) and $^{13}C^{18}O$- (B) bound $^{15}N$-isotope-labeled cyt.*bo*, respectively. These frequencies were lower by 1 $cm^{-1}$ than those for the corresponding CO-isotope-bound $^{14}N$ cyt.*bo*. The weak broad bands around 495 and 480 $cm^{-1}$ for $^{12}C^{16}O$- and $^{13}C^{18}O$-bound $^{15}N$-isotope-labeled cyt.*bo* (Figure 4-5A-B), respectively, represent the $\nu_{Fe\text{-}CO}$ band of the $Cu_B$-deleted proteins, since the $\nu_{Fe\text{-}CO}$ of the $Cu_B$-deleted cyt.*bo* prepared by mutagenesis is observed at these frequencies.[6] Upon $^{15}N$ substitution of pyrrole nitrogens, the band at 574 $cm^{-1}$ did not shift in the resolution of 1 $cm^{-1}$, but the difference pattern around 365 $cm^{-1}$ changed drastically. This indicates that the 574 $cm^{-1}$ band is not accompanied with nitrogen, but the 365 $cm^{-1}$ mode is so.

## 4.4 Discussion

### $\nu_{Fe\text{-}CO}$ Band

The frequencies for the $\nu_{Fe\text{-}CO}$ and 575 $cm^{-1}$ bands for each CO and iron isotopes are listed in TABLE 4-1. The average frequency shifts for the $\nu_{Fe\text{-}CO}$ and $\delta_{FeCO}$ bands between the iron, carbon, oxygen, and nitrogen isotopes are listed in TABLE 4-2. The $\nu_{Fe\text{-}CO}$ is shifted to higher frequency by 3.5 $cm^{-1}$ in average by changing $^{56}Fe$ to $^{54}Fe$. This value is close to the iron isotope shift estimated by a simple diatomic harmonic oscillator

approximation for an iron atom and a CO molecule. This indicates that this band contains mostly the Fe-CO stretching character and thus little $\delta_{FeCO}$ character. If the 574 $cm^{-1}$ band was assigned to the $\delta_{FeCO}$ fundamental mode, vibrational mixing would occur drastically between $\nu_{Fe\text{-}CO}$ and $\delta_{FeCO}$ for a bent FeCO geometry,[15] and the $\nu_{Fe\text{-}CO}$ band would not show such a large isotope shift upon $^{54}$Fe-labeled cyt.*bo*.

**Difference Pattern around 365 $cm^{-1}$**

Difference peaks were observed around 365 $cm^{-1}$ in all the CO-isotope difference spectra calculated (Figures 4-2, 4-4, 4-5), but the difference pattern is complicated. In both $^{56}$Fe and $^{54}$Fe-labeled cyt.*bo*, the shoulder at 362 $cm^{-1}$ in $^{12}C^{16}O$ adducts disappeared in other CO-isotope adducts. This frequency was very close to the frequencies of the CO-isotope-sensitive bands, which we assigned to the $\delta_{FeCO}$ mode (see chapter I-3). The difference pattern around 365 $cm^{-1}$ changed among different CO-isotope pairs, but all the difference spectra had a peak at 362 $cm^{-1}$ and a trough at 353 $cm^{-1}$ in Figures 4-2 and 4-4. The peaks around 365 $cm^{-1}$ in the difference spectra between $^{12}C^{16}O$- and $^{13}C^{18}O$-bound cyt.*bo* changed drastically between $^{14}$N and $^{15}$N (Figure 4-5). The $\delta_{FeCO}$ fundamental mode in CO-bound cyt.*bo* could couple with porphyrin modes. Such phenomena was seen in CO-bound cytochrome *c* oxidase (see chapter I-3). The way of vibrational mixing in CO-bound cyt.*bo* seems to change more when the mass of N is changed than the cases in which those of CO or Fe are changed. At least one of the modes which causes the difference patterns around 365 $cm^{-1}$ should be sensitive to the mass of nitrogen and is possibly a porphyrin mode.

**575 $cm^{-1}$ Band**

The band at 575 $cm^{-1}$ shifted by 1.5 $cm^{-1}$ in average upon the change of iron isotopes, while it is shifted only by 2.5 $cm^{-1}$ in average upon the change of oxygen isotopes. As the iron is fixed by the pyrrole rings and the mass of iron is about three times larger than that of oxygen, the shifts by iron isotopes should be smaller than those by oxygen isotopes. Nonetheless, the observed behavior of the 575 $cm^{-1}$ band is not so.

We performed normal coordinate calculations in the same way as in the previous chapters.[1,16] The potential function (V) represented by eq 1 was used,

$$2V = K_1(\Delta r_{Fe\text{-}CO})^2 + K_2(\Delta r_{CO})^2 + H(\Delta\delta_{FeCO})^2 + F(\Delta r_{Fe\cdots O})^2 \quad (1)$$

where $\Delta r_{Fe\text{-}CO}$, $\Delta r_{CO}$, $\Delta\delta_{FeCO}$, and $\Delta r_{Fe\cdots O}$ denote the displacement coordinates for the Fe-CO stretching, C-O stretching, Fe-C-O bending and Fe···O nonbonding distance, respectively. The bond length r(Fe-C) = 1.8 Å, r(C-O) = 1.2 Å, and the bending angle δ=165° were used.

The $\delta_{FeCO}$ mode was first estimated at 575 $cm^{-1}$ as done by other groups, and force constants of $K_1$ = 2.12 mdyn/Å, $K_2$ = 14.62 mdyn/Å, H = 0.81 mdyn·Å, and F = 1.27 mdyn/Å were used.[15] The frequencies of 521 and 574 $cm^{-1}$ could not be reproduced without using a value of F higher than 1.0. If we used a smaller value for it the two frequencies would split apart. The calculated frequencies are listed in TABLE 4-3. The $^{54}Fe$ frequency shifts were 1.5 and 2.2 $cm^{-1}$ for the $\nu_{Fe\text{-}CO}$ and 575 $cm^{-1}$ bands, respectively, and the $\nu_{Fe\text{-}CO}$ and $\delta_{FeCO}$ modes were mixed significantly ( ~ 40 % in terms of the potential energy distribution in this calculation. ). Therefore the observed $^{54}Fe$ isotope frequency shift of 3.5 $cm^{-1}$ for the $\nu_{Fe\text{-}CO}$ band which was very close to that for a simple Fe-CO harmonic oscillator approximation, was unable to be reproduced. This calculation shows a difficulty to assign the 575 $cm^{-1}$ band to the $\delta_{FeCO}$ fundamental, and it seems more likely to assign the band to a combination mode as we proposed.

To estimate the $\delta_{FeCO}$ mode at 362 $cm^{-1}$ we used force constants of $K_1$ = 2.24 mdyn/Å, $K_2$ = 14.68 mdyn/Å, H = 0.37 mdyn·Å, and F = 0.68 mdyn/Å. The $\nu_{Fe\text{-}CO}$ mode was localized and the frequency shift for this band against $^{54}Fe$ isotope was 3.0 $cm^{-1}$, which was much closer to the experimental value than the value obtained from estimating the $\delta_{FeCO}$ band at 574 $cm^{-1}$. The frequency shift of $\delta_{FeCO}$ for $^{54}Fe$ isotopes was 0.4 $cm^{-1}$, which was much smaller than the experimental frequency shift for the 575 $cm^{-1}$ band. If the 575 $cm^{-1}$ band is a combination mode of the $\delta_{FeCO}$ fundamental mode and a porphyrin mode or a Fe-C deformation mode, the counterpart mode other from the $\delta_{FeCO}$ mode should be sensitive to the mass of the iron.

The 575 $cm^{-1}$ band did not shift in the resolution of 1 $cm^{-1}$ between the corresponding CO-isotope-bound $^{15}N$-labeled cyt.*bo* and $^{14}N$ cyt.*bo* spectra. If the 575 $cm^{-1}$ band is a combination band, the counterpart of $\delta_{FeCO}$ should not be a nitrogen sensitive mode and is not related to the proximal histidine mode or an $E_u$ porphyrin mode.

## References


(1) Hirota, S.; Ogura, T.; Shinzawa-Itoh, K.; Yoshikawa, S.; Nagai, M.; Kitagawa, T., J. Phys. Chem. **1994**, *98*, 6652-6660.

(2) (a) Yu, N. T.; Kerr, E. In *Biological Application of Raman Spectroscopy*; Spiro, T. G., Ed.; Wiley-Interscience: New York, 1988; Vol. 3, pp. 39-95. (b) Yu, N. T. *Methods Enzymol.* **1986**, *130*, 350-409.

(3) Hirota, S.; Ogura, T.; Kitagawa, T., *J. Am. Chem. Soc.*, **1995**, *117*, 821-822.

(4) Uno, T.; Nishimura, Y.; Tsuboi, M.; Kita, K.; Anraku, Y. *J. Biol. Chem.* **1985**, *260*, 6755-6760.

(5) Wang, J.; Ching, Y.-C.; Rousseau, D. L.; Hill, J. J.; Rumbley, J.; Gennis, R. B. *J. Am. Chem. Soc.* **1993**, *115*, 3390-3391.

(6) Uno, T.; Mogi, T.; Tsubaki, M.; Nishimura, Y.; Anraku, Y. *J. Biol. Chem.* **1994**, *269*, 11912-11920.

(7) Tsubaki, M.; Mogi, T.; Anraku, Y.; Hori, H. *Biochemistry* **1993**, *32*, 6065-6072.

(8) Davis, B. D.; Mingioli, E. S. *J. Bacteriol.* **1959**, *60*, 17-28.

(9) Tsubaki, M.; Srivastava, R. B.; Yu, N.-T. *Biochemistry* **1982**, *21*, 1132-1140.

(10) Smulevich, G.; Evangelista-Kirkup, R.; English, A.; Spiro, T. G. *Biochemistry* **1986**, *25*, 4426-4430.

(11) Evangelista-Kirkup, R.; Smulevich, G.; Spiro, T. G. *Biochemistry* **1986**, *25*, 4420-4425.

(12) (a) Rousseau, D. L.; Ondrias, M. R.; La Mar, G. N.; Kong, S. B.; Smith, K. M. *J. Biol. Chem.* **1983**, *258*, 1740-1746. (b) Uno, T.; Nishimura, Y.; Makino, R.; Iizuka, T.; Ishimura, Y.; Tsuboi, M. *J. Biol. Chem.* **1985**, *4*, 2023-2026. (c) Tsubaki, M.; Ichikawa, Y. *Biochim. Biophys. Acta.* **1984**, *827*, 268-274. (d) Tsubaki, M.; Hiwatashi, A.; Ichikawa, Y. *Biochemistry* **1986**, *25*, 3563-3569. (e) Wells, A. V.; Li, P.; Champion, P. M.; Martinis, S. A.; Sligar, S. G. *Biochemistry* **1992**, *31*, 4384-4393.

(13) Argade, P. V.; Ching, Y.; Rousseau, D. L. *Nature* **1984**, *225*, 329-331.

(14) (a) Yu, N.-T.; Benko, B.; Kerr, E. A.; Gersonde, K. *Proc. Natl. Acad. Sci. USA* **1984**, *81*, 5106-5110. (b) Uno, T.; Nishimura, Y.; Tsuboi, M.; Makino, R.; Iizuka, T.; Ishimura, Y. *J. Biol. Chem.* **1987**, *262*, 4549-4556. (c) Nagai, M.; Yoneyame, Y.; Kitagawa, T. *Biochemistry* **1991**, *30*, 6495-6503. (d) Lin, S.-H.; Yu, N.-T.; Tame, J.; Shih, D.; Renaud, J.-P.;

Pagnier, J.; Nagai, K. *Biochemistry* **1990**, *29*, 5562-5566. (e) Ramsden, J.; Spiro, T. G. *Biochemistry* **1989**, *28*, 3125-3128. (f) Sakan, Y.; Ogura, T.; Kitagawa, T.; Fraunfelter, F. A.; Mattera, R.; Ikeda-Saito, M. *Biochemisty* **1993**, *32*, 5815-5824.

(15) Li, X.-Y.; Spiro, T. G. *J. Am. Chem. Soc.* **1988**, *110*, 6024-6033.

(16) Nagai, M.; Yoneyame, Y.; Kitagawa, T. *Biochemistry* **1991**, *30*, 6495-6503.

**TABLE 4-1. Observed $\nu_{Fe\text{-}CO}$ and 575 $cm^{-1}$ Band Frequencies in Each Iron, Carbon and Oxygen Isotope[a]**

| | $\nu_{Fe\text{-}CO}$ | | 575 $cm^{-1}$ band | |
|---|---|---|---|---|
| | $^{54}Fe$ | $^{56}Fe$ | $^{54}Fe$ | $^{56}Fe$ |
| $^{12}C^{16}O$ | 525 | 521 | 575 | 574 |
| $^{13}C^{16}O$ | 519 | 516 | 559 | 557 |
| $^{12}C^{18}O$ | 514 | 511 | 572 | 571 |
| $^{13}C^{18}O$ | 511 | 507 | 557 | 555 |

[a] In $cm^{-1}$ unit.

**TABLE 4-2. Average Frequency Differences of the $\nu_{Fe\text{-}CO}$ and 575 $cm^{-1}$ Band between Iron, Carbon, Oxygen and Nitrogen Isotopes[a]**

| | $^{54}Fe \rightarrow ^{56}Fe$ | $^{12}C \rightarrow ^{13}C$ | $^{16}O \rightarrow ^{18}O$ | $^{14}N \rightarrow ^{15}N$ |
|---|---|---|---|---|
| $\nu_{Fe\text{-}CO}$ | 3.5 | 4.5 | 9.5 | 1 |
| 575 $cm^{-1}$ band | 1.5 | 16 | 2.5 | 0 |

[a] In $cm^{-1}$ unit.

**TABLE 4-3. Observed Frequencies of cyt.*bo*·CO and Calculated Frequencies of the Isolated FeCO Unit[a]**

| | obs | | | calc[b] | | | calc[c] | | |
|---|---|---|---|---|---|---|---|---|---|
| | $\nu_{CO}$ | $\nu_{Fe-CO}$ | | $\nu_{CO}$ | $\nu_{Fe-CO}$ | $\delta_{FeCO}$ | $\nu_{CO}$ | $\nu_{Fe-CO}$ | $\delta_{FeCO}$ |
| $^{12}C^{16}O$ | 1959.7[d] | 521 | 574 | 1959.4 | 521.2 | 574.4 | 1959.5 | 520.9 | 360.9 |
| $^{13}C^{16}O$ | | 516 | 557 | 1914.4 | 510.8 | 562.5 | 1913.7 | 513.9 | 351.3 |
| $^{12}C^{18}O$ | | 511 | 571 | 1914.7 | 510.1 | 566.2 | 1915.9 | 510.1 | 355.4 |
| $^{13}C^{18}O$ | | 507 | 555 | 1868.3 | 500.6 | 554.0 | 1868.8 | 503.5 | 345.8 |
| $^{54}Fe$ | | 525 | 575 | 1959.4 | 522.7 | 576.6 | 1959.5 | 523.9 | 361.3 |

[a] In $cm^{-1}$ unit. [b] Parameters used for calculations are the following: r(Fe-O) = 1.8 Å, r(C-O) = 1.2 Å, $K_1$(Fe-C) = 2.12 mdyn/Å, $K_2$(C-O) = 14.62 mdyn/Å, H(Fe-C-O) = 0.81 mdyn·Å, F(Fe...O) = 1.27 mdyn/Å, θ(Fe-C-O) = 165°. [c] Parameters used for calculations are the following: r(Fe-O) = 1.8 Å, r(C-O) = 1.2 Å, $K_1$(Fe-C) = 2.24 mdyn/Å, $K_2$(C-O) = 14.68 mdyn/Å, H(Fe-C-O) = 0.37 mdyn·Å, F(Fe···O) = 0.68 mdyn/Å, θ(Fe-C-O) = 165°. [d] Reference 6.

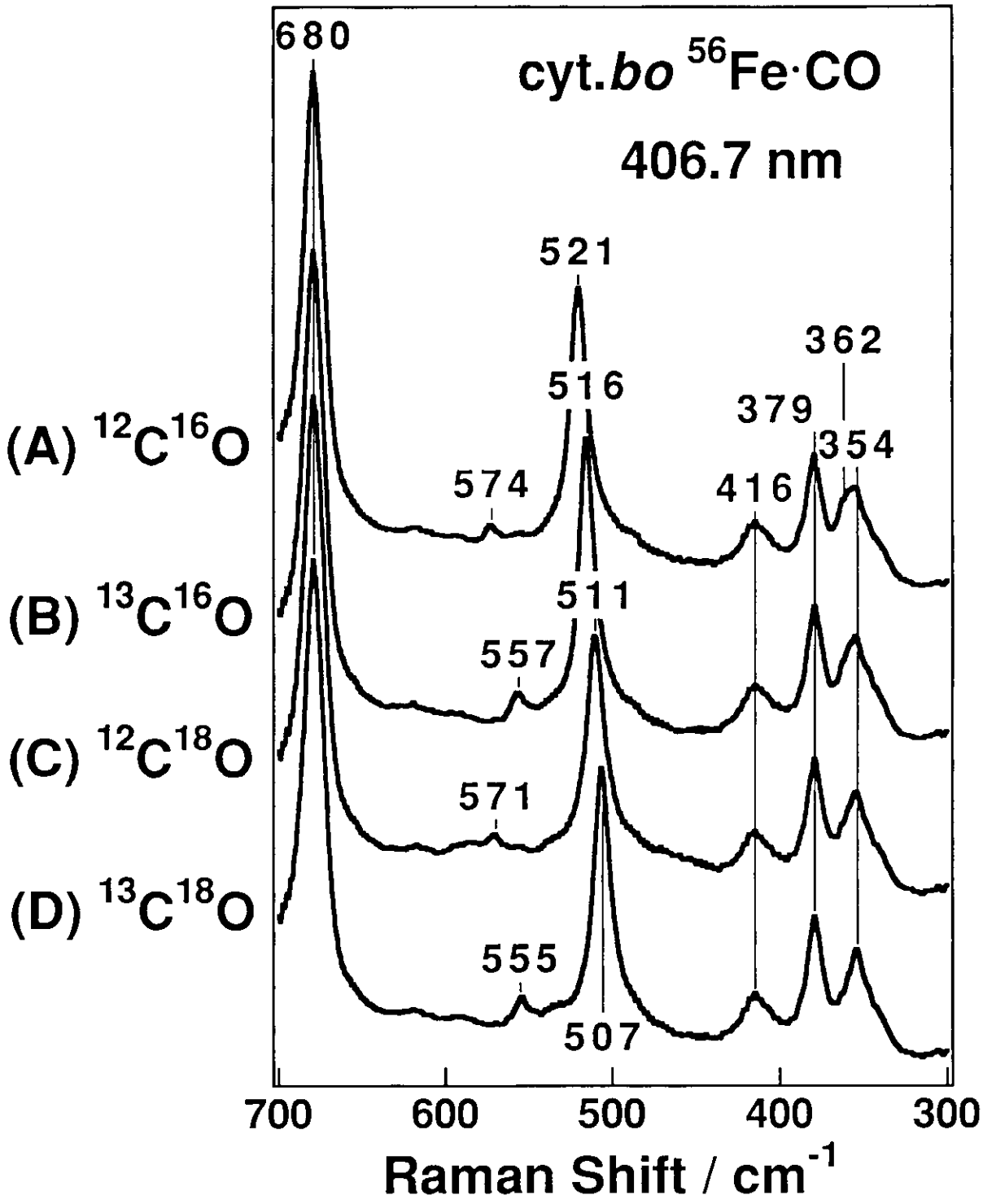


**Figure 4-1.** RR spectra in the 700 to 300 $cm^{-1}$ region for $^{12}C^{16}O$ (A), $^{13}C^{16}O$ (B), $^{12}C^{18}O$ (C), and $^{13}C^{18}O$ (D) adducts of $^{56}Fe$ cyt.*bo*. The ordinate scales are normalized by the intensity of porphyrin bands. Experimental conditions: excitation, 406.7 nm with 6 mW at the sample; sample, 50μM (heme) in 50 mM Tris-HCl buffer, pH7.2, with 0.1 % sucrose monolaurate.

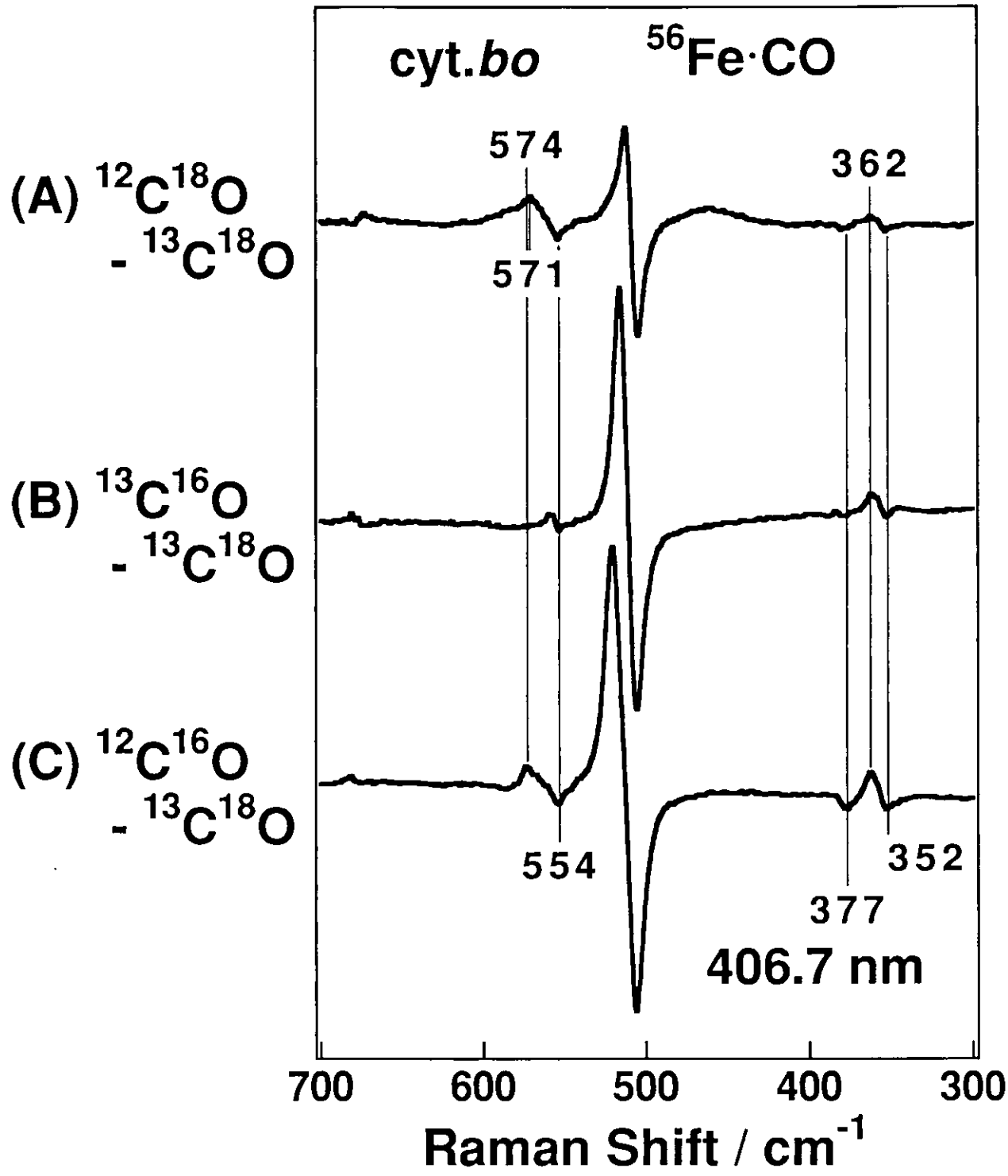


**Figure 4-2.** Differences of the RR spectra shown in Figure 4-1. Three pairs of differences are shown: (A) cyt.*bo*·$^{12}C^{18}O$ - cyt.*bo*·$^{13}C^{18}O$, (B) cyt.*bo*·$^{13}C^{16}O$ - cyt.*bo*·$^{13}C^{18}O$, (C) cyt.*bo*·$^{12}C^{16}O$ - cyt.*bo*·$^{13}C^{18}O$.

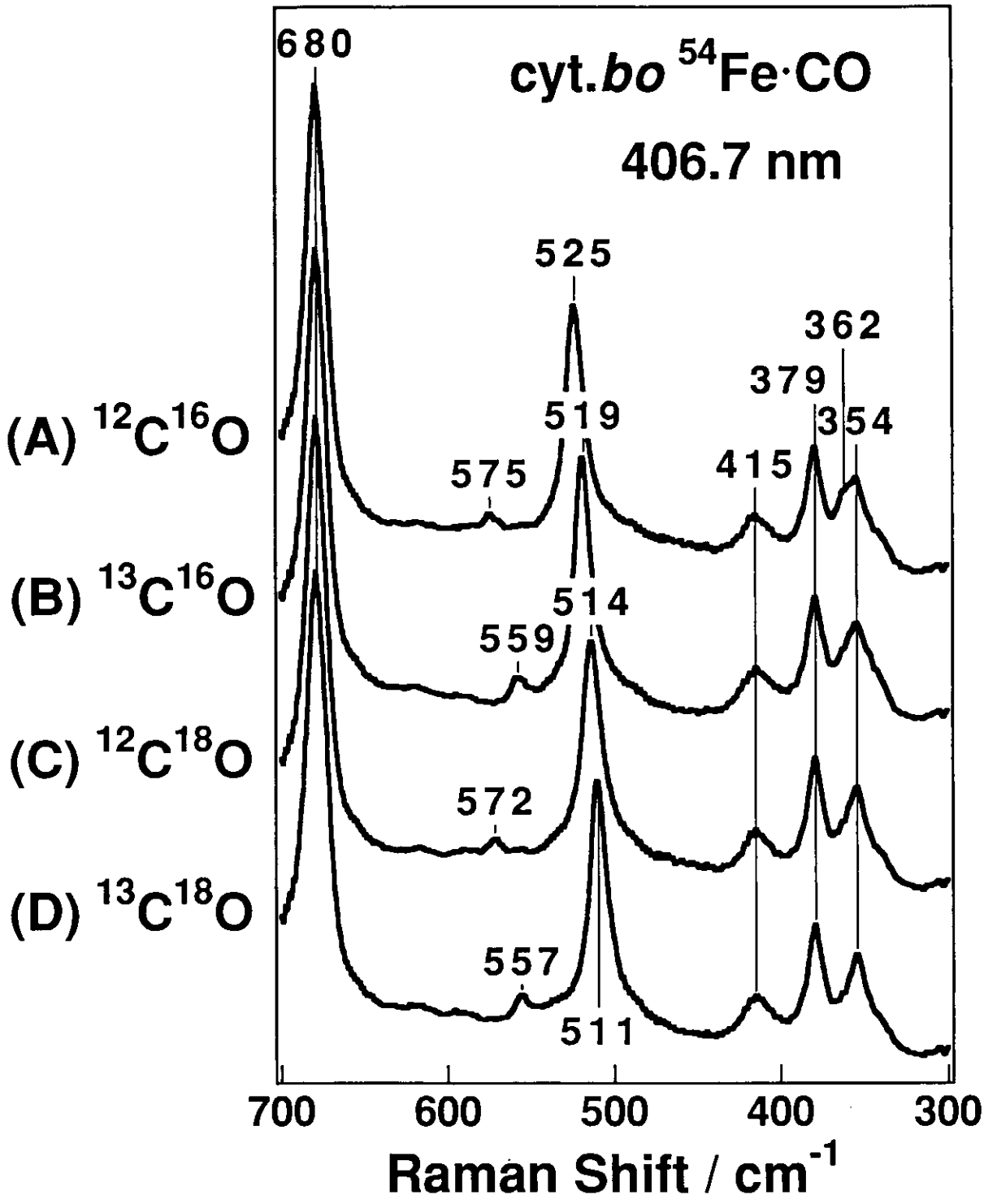


**Figure 4-3.** RR spectra in the 700 to 300 $cm^{-1}$ region for $^{12}C^{16}O$ (A), $^{13}C^{16}O$ (B), $^{12}C^{18}O$ (C), and $^{13}C^{18}O$ (D) adducts of $^{54}Fe$-labeled cyt.*bo*. The ordinate scales are normalized by the intensity of porphyrin bands. Experimental conditions are the same as those for Figure 4-1.

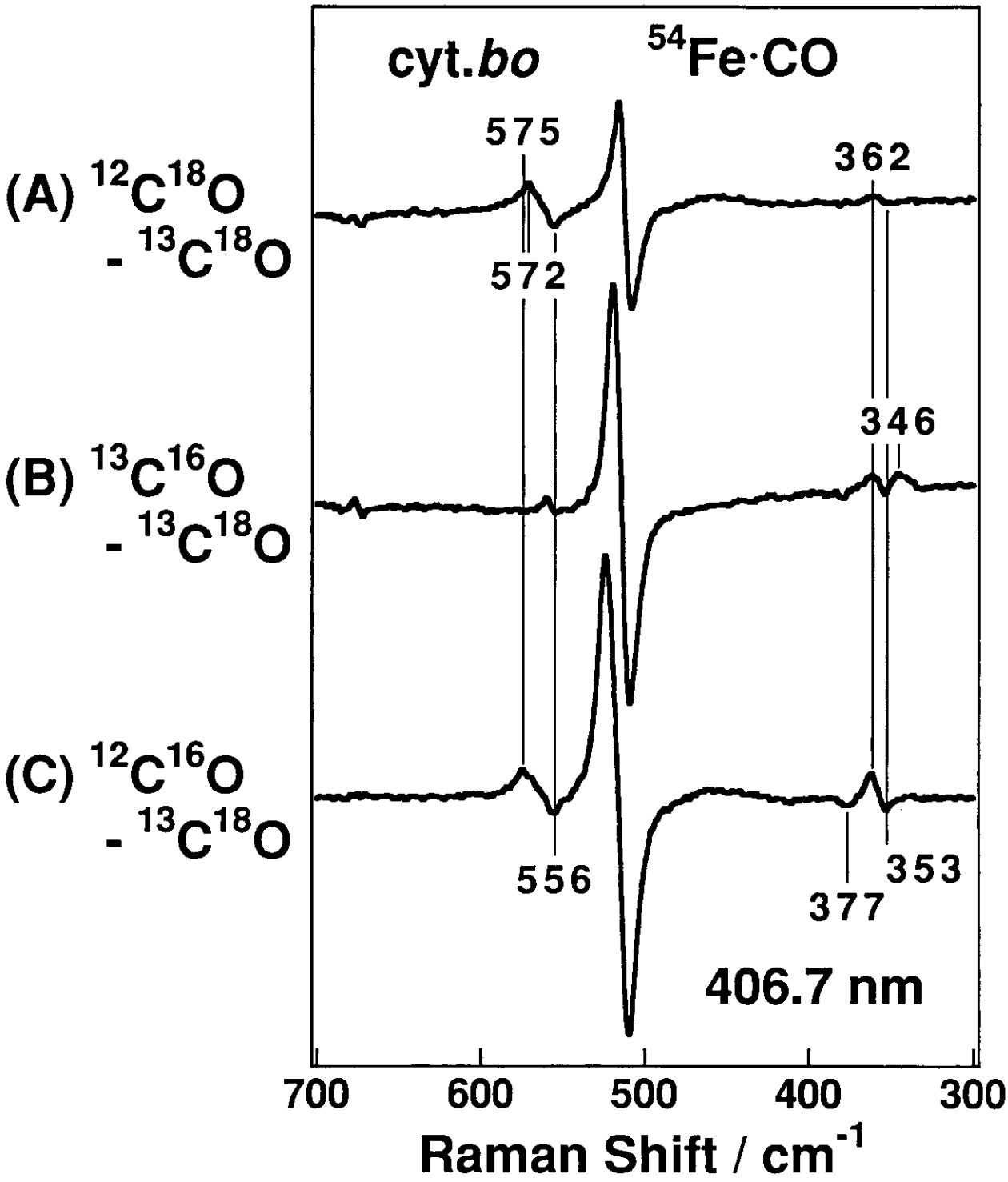


**Figure 4-4.** Differences of the RR spectra shown in Figure 4-3. Difference calculations were carried out in the way as in Figure 4-2, and are specified at the left side.

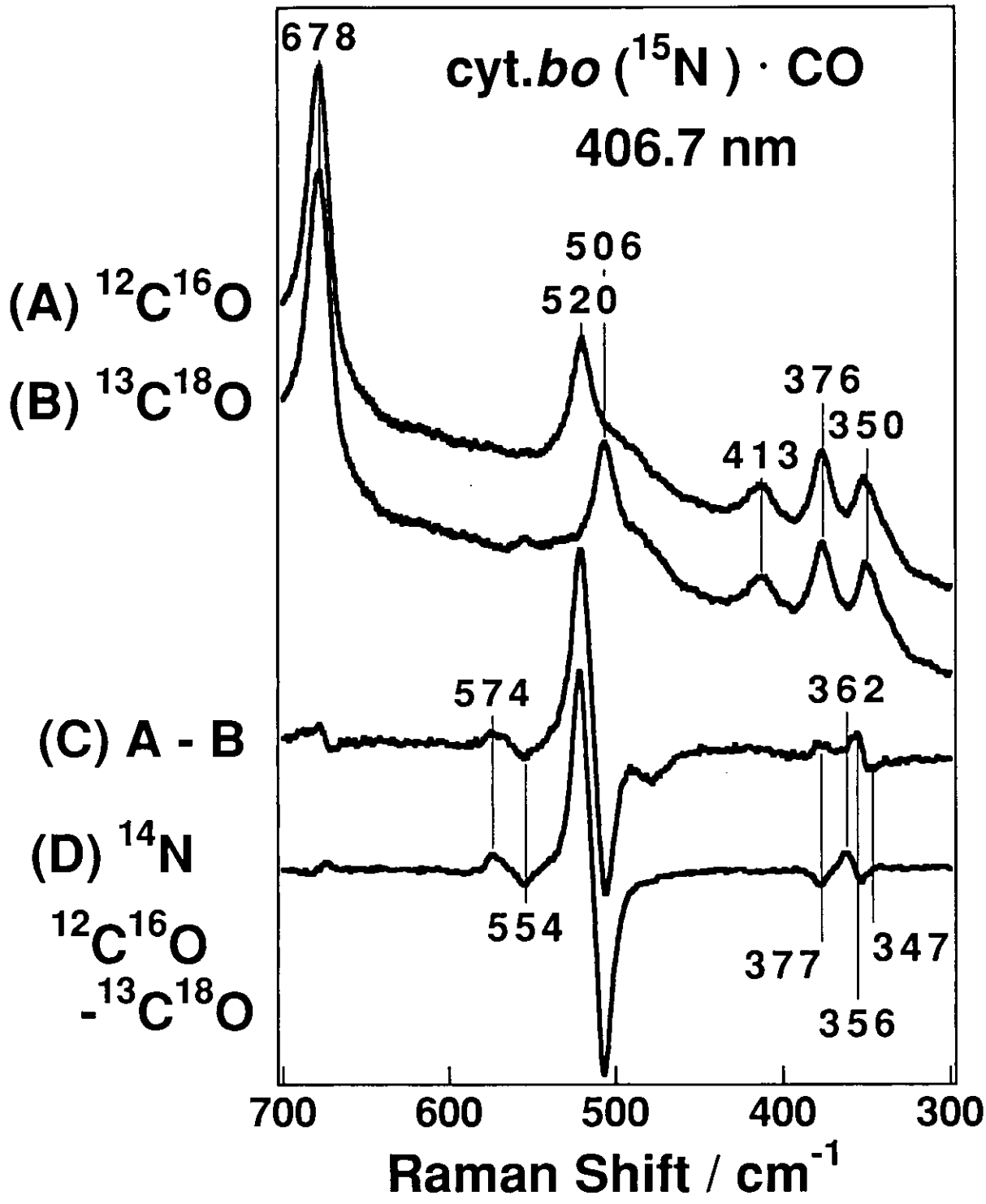


**Figure 4-5.** RR spectra in the 700 to 300 $cm^{-1}$ region for $^{12}C^{16}O$ (A) and $^{13}C^{16}O$ (B) adducts of $^{15}N$-labeled cyt.*bo* and their difference spectrum (C), and the difference spectrum between $^{12}C^{16}O$ and $^{13}C^{16}O$ adducts of $^{14}N$ cyt.*bo*. The ordinate scales are normalized by the intensity of porphyrin bands. Experimental conditions: excitation, 406.7 nm with 7 mW at the sample; sample, the same as those for Figure 4-1.

# Chapter I-5.

# Observation of Nonfundamental Fe-$O_2$ and Fe-CO Vibrations and Potential Anharmonicities for Oxy- and Carbonmonoxy-hemoglobin and myoglobin: Evidence Supporting a New Assignment of the Fe-C-O Bending Fundamental

## Abstract

The overtone and combination Raman bands of the Fe-ligand vibrations of heme proteins were investigated for the first time. The combination of the Fe-O-O bending ($\delta_{FeOO}$) with the Fe-$O_2$ stretching ($\nu_{Fe-O_2}$) of oxyhemoglobin ($HbO_2$) was found at 996 $cm^{-1}$ for $^{16}O_2$ adduct (953 $cm^{-1}$ for $^{18}O_2$) and the overtone of $\nu_{Fe-O_2}$ at 1136 $cm^{-1}$ for $^{16}O_2$ (1088 $cm^{-1}$ for $^{18}O_2$). For the latter, the corresponding band for $^{16}O^{18}O$ adduct did not appear at an intermediate frequency and therefore, a possibility for assigning it to the O-O stretching was ruled out. Similar overtone and combination bands were found in $MbO_2$ at 1140/1061 and 998/954 $cm^{-1}$. For carbonmonoxyHb (HbCO), CO-isotope-sensitive bands were found at 738, 859-890, 1002, 1183 and 1257 $cm^{-1}$ for $^{12}C^{16}O$ (718, 836, 971, 1161, and 1238 $cm^{-1}$ for $^{13}C^{18}O$). The 738/718, 1002/971, and 859-890/836 $cm^{-1}$ pairs for $^{12}C^{16}O/^{13}C^{18}O$ are reasonably interpreted as the overtones of the Fe-CO bending ($\delta_{FeCO}$), Fe-CO stretching ($\nu_{Fe-CO}$), and their combination ($\nu_{Fe-CO}+\delta_{FeCO}$), respectively, when the difference peaks at 369/355 $cm^{-1}$ was assigned to $\delta_{FeCO}$ fundamental. On the contrary, when the 577/558 $cm^{-1}$ pair was assigned to the $\delta_{FeCO}$ fundamental, nonfundamental band was not recognized at the corresponding frequencies. The difference peaks 1183/1161 $cm^{-1}$ are assigned to the combination of $\nu_7$ with $\nu_{Fe-CO}$, in agreement with the recent report by Wang et al. The 1257/1238 $cm^{-1}$ pair may be assigned to the combination of $\nu_{15}$ or $\nu_{16}$ with $\nu_{Fe-CO}$. Similar overtone and combination bands were detected in MbCO at 732/712, 857/837, 1017/975, and 1188/1167 $cm^{-1}$ ($^{12}C^{16}O/^{13}C^{18}O$). These observations strongly support the new assignment of $\delta_{FeCO}$ fundamental proposed in chapter I-3. The anharmonic constant for the Fe-CO stretching potential in HbCO was calculated to be 0.010, but that for Fe-$O_2$ in $HbO_2$ was much smaller (<0.001).

## 5.1 Introduction

The Fe-ligand interaction is a matter of fundamental concern in the chemistry of heme proteins, and resonance Raman (RR) spectroscopy has provided basic information on Fe-ligand vibrations for a variety of heme proteins and ligands.[1] The Fe-$O_2$ stretching mode ($\nu_{Fe\text{-}O_2}$) was found at ~570 $cm^{-1}$ for oxyhemoglobin ($HbO_2$),[2-4] oxymyoglobin ($MbO_2$),[4,5] oxy-cytochrome *c* oxidase ($CcO{\cdot}O_2$),[6] at 530~560 $cm^{-1}$ for oxyperoxidases,[7] and at ~540 $cm^{-1}$ for oxycytochromes P-450.[8] Vibrational coupling between the O-O stretching and other modes causes splitting of the $O_2$-isotope-sensitive band and/or the observed frequency to be shifted from its intrinsic one.[9] The Fe-O-O bending ($\delta_{FeOO}$) RR band has been recently identified at ~430 $cm^{-1}$ for $HbO_2$ and $CcO{\cdot}O_2$,[4] and at ~490 $cm^{-1}$ for oxylactoperoxidase.[7b]

The Fe-CO stretching ($\nu_{Fe\text{-}CO}$) and Fe-C-O bending ($\delta_{FeCO}$) modes were first assigned to the RR bands around 510 and 570 $cm^{-1}$, respectively,[10] but the latter assignment has not achieved full agreement.[11] A new CO-isotope-sensitive band assignable to $\delta_{FeCO}$ was found at ~360 $cm^{-1}$ for various heme proteins (chapter I-3).[12] Observation of nonfundamental bands would not only solve the assignment controversy but also provide new information on anharmonicities of potential functions, which are quite important for molecular dynamics calculations for the ligand. Accordingly, we have carefully examined the RR spectra of $HbO_2$, $MbO_2$, HbCO, and MbCO, and report several nonfundamental Fe-ligand modes for the first time.

## 5.2 Methods and Materials

Raman scattering was excited at 413.1 nm with a $Kr^+$ ion laser (Spectra Physics 2016) and detected with a single polychromator (Ritsu Oyo Kogaku, DG-1000) equipped with a cooled diode array (PAR 1421HQ). Samples were contained in a spinning cell (3500 rpm) and the measurements were carried out at room temperature. Exposure time for one measurement was 320 s and ten measurements were carried out for each sample. Slitwidth and slitheight were 200 μm and 10 mm, respectively. The ordinate scale of spectra of different isotopes are normalized by using intensity of porphyrin bands. Raman shifts were calibrated with ethanol and acetone as secondary standard.

Uncertainties of peak frequencies are 1 $cm^{-1}$ for raw spectra and 2 $cm^{-1}$ for difference spectra.

Human adult Hb (HbA) was prepared according to the method of Geraci et al.[13] and its concentration was adjusted to 50 μM (heme) with 50 mM Na-phosphate buffer pH 7.2. $^{16}O^{18}O$ was prepared as described in chapter I-2. $Hb^{16}O^{18}O$ and $Hb^{18}O_2$ were obtained by substituting the gas inside the cell first with $N_2$, followed by substitution with $^{16}O^{18}O$ or $^{18}O_2$ (ICON, 99.5 atom%). $Hb^{16}O_2$ was obtained by exposing $Hb^{18}O_2$ and/or $Hb^{16}O^{18}O$ to $^{16}O_2$ for 5 min.

Horse Mb (Sigma, type M630) was dissolved in 50 mM Tris-HCl buffer, pH 8.0. Sperm whale Mb mutants, H64A (histidine64 mutated to alanine) and L29F (leucine mutated to phenylalanine), were kind gifts from Prof. Olson of Rice University. Minimum amount of dithionite was added to the sample to reduce the sample, followed by gel filtration through Sephadex G-25 to remove dithionite. $Mb^{16}O_2$ and $Mb^{18}O_2$ were obtained similarly as $Hb^{16}O_2$ and $Hb^{18}O_2$, respectively.

The $^{12}C^{16}O$- and $^{13}C^{18}O$- (ICON, 99 atom% for $^{13}C$ and 98 atom% for $^{18}O$) adducts of Hb and Mb were obtained as described in chapter I-3.[12]

**5.3 Results**

Figure 5-1 shows the RR spectra in the 1300-350 $cm^{-1}$ region for $Hb^{16}O_2$ (A) and $Hb^{18}O_2$ (B) excited at 413.1 nm and their difference (C). Trace D shows two Gaussian bands with peak positions at 1136 and 1088 $cm^{-1}$ having the bandwidth of 86 $cm^{-1}$, and their difference spectrum is depicted by a broken line in trace C. Ten measured spectra were almost similar, but the spectra shown here are those from one measurement. When partial oxidation occurred during the measurement, it was noticed easily from the noise levels and such spectra were discarded. In the raw spectra, the peak intensity of the 544 $cm^{-1}$ band in B [largely $\nu(Fe\text{-}^{18}O_2)$] appeared stronger than that of the 568 $cm^{-1}$ band in A [$\nu(Fe\text{-}^{16}O_2)$] due to the presence of a porphyrin mode at ~540 $cm^{-1}$, but the difference spectrum (Figure 5-1C) yielded the expected symmetric derivative pattern. The difference peak at 428/404 $cm^{-1}$ was recently assigned to $\delta_{FeOO}$ (chapter I-2).[4] We stress here that there are additional difference patterns at 1150/1071 and 996/953 $cm^{-1}$.

Figure 5-2 displays the difference spectrum between $^{16}O_2$ and $^{16}O^{18}O$ adducts of HbA. A difference peak appeared at 1146/1075 $cm^{-1}$, and its peak position did not differ significantly from 1150/1071 $cm^{-1}$ obtained form the $Hb^{16}O_2$ - $Hb^{18}O_2$ difference spectrum (Figure 5-1C).

Figure 5-3 shows the RR spectra in the 1300-350 $cm^{-1}$ region for $Mb^{16}O_2$ (A) and $Mb^{18}O_2$ (B) excited at 413.1 nm and their difference (C). Partial oxidation occurred more easily than the $HbO_2$ case, but it was noticed easily from the noise levels, and such spectra were discarded. Similar to $HbO_2$, the 543 $cm^{-1}$ band in B [largely $\nu(Fe\text{-}^{18}O_2)$] had stronger intensity than that of the 570 $cm^{-1}$ band in A [$\nu(Fe\text{-}^{16}O_2)$] due to the presence of a porphyrin mode at ~540 $cm^{-1}$, but the difference spectrum (Figure 5-3C) showed an expected symmetric derivative pattern. A difference peak that was detected in $HbO_2$ around 428/404 $cm^{-1}$ was undetectable as reported in chapter I-2.[4] Similar to the difference spectrum of $Hb^{16}O_2$ - $Hb^{18}O_2$ (Figure 5-1C), additional difference patterns appeared at 1140/1061 and 998/954 $cm^{-1}$ in the $Mb^{16}O_2$ - $Mb^{18}O_2$ difference spectrum (Figure 5-3C).

Figure 5-4 shows the RR spectra in the 1300-300 $cm^{-1}$ region of $Hb^{12}C^{16}O$ (A) and $Hb^{13}C^{18}O$ (B) excited at 413.1 nm and their difference (C). Spectrum D is an expansion of spectrum C by a factor of 10. Spectra A and B are the sums of five measurements with the exposure time of 320 s. This set of measurements were carried out twice for different samples and the results were completely reproduced. The most intense difference peak at 505/492 $cm^{-1}$ in spectrum C has been assigned to $\nu_{Fe\text{-}CO}$.[10-12] The difference peaks at 577/558 $cm^{-1}$ have been assigned to $\delta_{FeCO}$,[10,11a,d] but those at 369/355 $cm^{-1}$ are now reassigned to $\delta_{FeCO}$ by a new proposal in chapter I-3.[12] Here we want to point out the presence of additional difference peaks at 738/718, 859-890/836, 1002/971, 1183/1161, and 1257/1238 $cm^{-1}$ as illustrated by spectrum D.

Figure 5-5 displays the RR spectra in the 1300-300 $cm^{-1}$ of $Mb^{12}C^{16}O$ (A) and $Mb^{13}C^{18}O$ (B) excited at 413.1 nm and their difference (C). The 509/496 and 578/558 $cm^{-1}$ bands have been assigned to $\nu_{Fe\text{-}CO}$ and $\delta_{FeCO}$, respectively.[10-12] There was no isotope difference pattern around 360 $cm^{-1}$ that was seen in HbCO and other CO-bound heme proteins.[12] We want to stress the presence of additional difference peaks at 732/712, 857/837, 1017/975, and 1188/1167 $cm^{-1}$ as illustrated by spectrum C. From group theory, the overtone mode of $\delta_{FeCO}$ would RR sensitive. If the 578/558 $cm^{-1}$

bands are assigned to the Fe-C-O bending band, it is expected expect to observe a strong overtone of this mode around 1160/1110 $cm^{-1}$. However, there is no strong overtone bands of the 578 $cm^{-1}$ band around 1160/1110 $cm^{-1}$, even though the 578/558 $cm^{-1}$ increased in its intensity relative to the $\nu_{Fe\text{-}CO}$ (505/496 $cm^{-1}$) band compared to HbCO.

The RR spectra of $^{12}C^{16}O$ (A) and $^{13}C^{18}O$ (B) adducts of sperm whale Mb mutant H64A(histidine64 mutated to alanine) (Mb(H64A)$^{12}C^{16}O$, Mb(H64A)$^{13}C^{18}O$) excited at 413.1 nm are shown in Figure 5-6 with their difference (C). The 492/480 and 573/554 $cm^{-1}$ bands have been assigned to $\nu_{Fe\text{-}CO}$ and $\delta_{FeCO}$, respectively.[10-12] It is not clear whether a difference pattern exists around 360 $cm^{-1}$ or not.[12] Additional difference peaks appeared at 850/825, 989/944, and 1175/1153 $cm^{-1}$ as illustrated by spectrum C.

Figure 5-7 shows the RR spectra of $^{12}C^{16}O$ (A) and $^{13}C^{18}O$ (B) adducts of sperm whale Mb mutant L29F (leucine29 mutated to phenylalanine) (Mb(L29F)$^{12}C^{16}O$, Mb(L29F)$^{13}C^{18}O$) excited at 413.1 nm and their difference (C). The 518/506 and 581/561 $cm^{-1}$ bands have been assigned to $\nu_{Fe\text{-}CO}$ and $\delta_{FeCO}$ bands, respectively.[10-12] The existence of a difference pattern around 360 $cm^{-1}$ was not clear in this case,[12] and the additional difference peaks at 1034/1001 and 1198/1181 $cm^{-1}$ were observed in the difference spectrum C.

## 5.4 Discussion

### $HbO_2$ and $MbO_2$

The 996/953 $cm^{-1}$ difference peak of $Hb^{16}O_2/Hb^{18}O_2$ is easily interpreted as the stretching+bending combination (568+428/544+404), while the 1150/1071 $cm^{-1}$ difference peak needs some discussion. The O-O stretching ($\nu_{OO}$) IR bands of $HbO_2$ are reported at 1155 and 1106 $cm^{-1}$ (1094 and 1065 $cm^{-1}$ for $^{18}O_2$),[14] but their frequencies are clearly different from the present observation. When Gaussian bands with bandwidth of 86 $cm^{-1}$ were assumed at 1136 and 1088 $cm^{-1}$ as shown by trace D, their difference spectrum well reproduced the observed spectrum as drawn by a broken line in trace C.

If the band was associated with $\nu_{OO}$, the band would shift to the center frequency of $Hb^{16}O_2$ and $Hb^{18}O_2$, i.e., to ~ 1110 $cm^{-1}$, and cause the difference peak in $Hb^{16}O_2$ - $Hb^{16}O^{18}O$ to shift to significantly higher

frequencies. But the difference between $Hb^{16}O_2$ - $Hb^{16}O^{18}O$ gave difference peaks at 1146 and 1075 $cm^{-1}$ (Figure 5-2), close to 1150/1071 $cm^{-1}$ (Figure 5-1), indicating that the band is not associated with $\nu_{OO}$. Consequently, it is reasonable to assign the 1150/1071 $cm^{-1}$ peaks to an overtone of $\nu_{Fe\text{-}O_2}$. Although its peak intensity appears to be only 18% of the fundamental, its area intensity is one half that of the fundamental due to its large bandwidth. The large bandwidth might be due to the vibrational interaction with $\nu_{OO}$. It is noted that the large overlapping between the $2\nu(Fe\text{-}^{16}O_2)$ and $2\nu(Fe\text{-}^{18}O_2)$ bands locates the difference peaks at significantly outside of the true positions (by 14~17 $cm^{-1}$). The broad bandwidth character of the overtone band of $\nu_{Fe\text{-}O_2}$ was also seen in $MbO_2$ (Figure 5-3).

**HbCO and MbCO**

In HbCO, the two positive peaks at 859 and 890 $cm^{-1}$ presumably resulted from vibrational coupling and the unperturbed frequency would be ~875 $cm^{-1}$, since the sum of their intensities appears to be equal to the intensity of the negative peak at 836 $cm^{-1}$. The 1002/971 $cm^{-1}$ difference pattern was well reproduced when difference was calculated for two Gaussian bands at 1000 and 972 $cm^{-1}$ with the widths of 30 $cm^{-1}$. The 1002/971 and 738/718 $cm^{-1}$ peaks in HbCO are assignable to overtones of $\nu_{Fe\text{-}CO}$ (2x505/2x492) and $\delta_{FeCO}$ (2x369/2x355). The 859-890/836 $cm^{-1}$ pair can be interpreted in terms of combination of $\nu_{Fe\text{-}CO}$ and $\delta_{FeCO}$ (505+369/492+355).

A difference pair was also observed at 1017/975 $cm^{-1}$ for MbCO. This pair shifted to the same direction as the $\nu_{Fe\text{-}CO}$ shifted by twice more in frequency compared to $\nu_{Fe\text{-}CO}$ in Mb(H64A)CO (989/944 $cm^{-1}$) and Mb(L29F)CO (1034/1001 $cm^{-1}$). These results strongly supports the assignment of this band to overtones of $\nu_{Fe\text{-}CO}$ ($2\nu_{Fe\text{-}CO}$). This assignment is in agreement with Wang et al.[15] who recently reported on $2\nu_{Fe\text{-}CO}$ for Mb and CcO and discussed the anharmonicities of the Fe-CO stretching modes of a large number of proteins.

One may argue that the 738/718 $cm^{-1}$ difference pattern in HbCO might be interpreted as a combination of $\nu_{Fe\text{-}CO}$ and the $\nu_{Fe\text{-}His}$ mode. This difference pattern is shifted to lower frequency by 6 $cm^{-1}$ (732/712 $cm^{-1}$) in MbCO, although the $\nu_{Fe\text{-}CO}$ frequency is shifted to higher frequency by 4 $cm^{-1}$. If this band was a combination of $\nu_{Fe\text{-}CO}$ and $\nu_{Fe\text{-}His}$, the

frequency of $\nu_{Fe\text{-}His}$ in HbCO should be 9 $cm^{-1}$ higher than that in MbCO. Since the $\nu_{Fe\text{-}His}$ frequency of deoxyMb is higher by 5 $cm^{-1}$ than that of deoxy Hb A, this proposal seems unlikely. Therefore, it is more reasonable to assign the 738/718 $cm^{-1}$ peaks to overtones of $\delta_{FeCO}$, although the corresponding Raman band cannot be identified with Mb and its mutants.[12]

The difference peak at 1183/1161 $cm^{-1}$ in HbCO correspond to the difference peaks at 1188/1167 $cm^{-1}$ in MbCO, 1175/1153 $cm^{-1}$ in Mb(H64A)CO, and 1198/1181 $cm^{-1}$ in Mb(L29F)CO. These difference peaks are shifted by similar amounts to the frequency shifts of $\nu_{Fe\text{-}CO}$. The differences between these frequencies and the $\nu_{Fe\text{-}CO}$ frequencies are all close to 676 $cm^{-1}$, the $\nu_7$ frequency. Therefore this band is assigned to $\nu_7+\nu_{Fe\text{-}CO}$ combination (676+505/676+492). These assignments are also in agreement with the recent observation of $\nu_7+\nu_{Fe\text{-}CO}$ bands for Mb and CcO by Wang et al.[15] From the frequencies,[16] the weak difference peak at 1257/1238 $cm^{-1}$ in HbCO could be assigned to a $\nu_{15}+\nu_{Fe\text{-}CO}$ or $\nu_{16}+\nu_{Fe\text{-}CO}$ combination (752+505/752+492).

**Anharmonicity**

When an anharmonic term proportional to $-\Delta r^3$ is incorporated as a perturbation to a harmonic potential, the energy level corresponding to a quantum number, v, is represented with the anharmonic constant, x, as

$E_v = h\nu_e(v+1/2) - h\nu_e x(v+1/2)^2$.

Under this approximation, the frequency for the $v \rightarrow v+1$ transition is $\nu = \nu_0 - v\Delta\nu$, $\nu_0 = \nu_e - 2\nu_e x$, $\Delta\nu = 2\nu_e x$, and the thermal average of frequency observable at T K is $\langle\nu\rangle \approx \nu_0 - 2\Delta\nu/[\exp(h\nu_0/kT)-1]$. Since the expected frequencies for the fundamental and overtone in the presence of anharmonicity are $\nu_e(1-2x)$ and $2\nu_e(1-3x)$, respectively, the anharmonic constant (x) for $\nu_{Fe\text{-}CO}$ is calculated to be 0.010. This suggests that the corresponding frequency at T=0 K is $\nu_0$=507 $cm^{-1}$ and $\Delta\nu$=10 $cm^{-1}$. The same calculations for $\nu_{Fe\text{-}O_2}$ yielded $x<0.001$. Therefore, anharmonicity for the Fe-CO potential in HbCO is much larger than that of the $Fe\text{-}O_2$ potential in $HbO_2$.[15]

The anharmonicity for the Fe-CO potential in MbCO is calculated to be 0.008, and those in Mb(H64A)CO and Mb(L29F)CO are both 0.006. The strength of the anharmonicities did not differ significantly among CO complexes of different Mb mutants, although their $\nu_{Fe\text{-}CO}$ frequencies

differed. The anharmonicity for CO-bound cytochrome *c* oxidase (CcO·CO) was reported to be larger than those for other CO-bound proteins and the anharmonicities seem to depend on the protein, but the anharmonicities did not differ so much among CO-bound Mb mutants. The strong anharmonicity of CO bound CcO·CO should be characteristic of this protein, and this could be caused by the existence of the Cu ion close to the heme Fe in CcO.[15]

## References


(1) Yu, N.-T. *Methods Enzymol.* **1986**, 130, 350-409. b) Yu, N. T.; Kerr, E. In *Biological Application of Raman Spectroscopy*; Spiro, T. G., Ed.; Wiley-Interscience: New York, 1988; Vol. 3, pp. 39-95.

(2) Brunner, H. *Naturwissenschaften* **1974**, *61*, 129.

(3) Nagai, K.; Kitagawa, T.; Morimoto, H. J. *Mol. Biol.* **1980**, *136*, 271-289.

(4) Hirota, S.; Ogura, T.; Appelman, E. V.; Shinzawa-Itoh, K.; Yoshikawa, S.; Kitagawa, T. *J. Am. Chem. Soc.*, **1994**, *116*, 10564-10570.

(5) Kerr, E. A.; Yu, N.-T.; Bartnicki, D. E.; Mizukami, H. *J. Biol. Chem.* **1985**, *260*, 8360-8365.

(6) (a) Ogura, T.; Takahashi, S.; Shinzawa-Itoh, K.; Yoshikawa, S.; Kitagawa, T. *J. Am. Chem. Soc.* **1990**, *112*, 5630-5631. (b) Han, S.; Ching, Y.-C.; Rousseau, D. L. *Proc. Natl. Acad. Sci. U.S.A.* **1990**, *87*, 2491-2495. (c) Varotsis, C.; Woodruff, W. H.; Babcock, G. T. *J. Am. Chem. Soc.* **1989**, *111*, 6439-6440.

(7) (a) Van Wart, H. E. V.; Zimmer, J. *J. Biol. Chem.* **1985**, *260*, 8372-8377. (b) Hu, S.; Kincaid, J. R. *J. Am. Chem. Soc.* **1991**, *113*, 7189-7194.

(8) (a) Bangcharoenpaurpong, O.; Rizos, A. K.; Champion, P. M.; Jollie, D.; Sligar, S. G. *J. Biol. Chem.* **1986**, *261*, 8089-8092. (b) Hu, S.; Schneider, A. J.; Kincaid, J. R. *J. Am. Chem. Soc.* **1991**, *113*, 4815-4822. (c) Egawa, T.; Ogura, T.; Makino, R.; Ishimura, Y.; Kitagawa, T. *J. Biol. Chem.* **1991**, *266*, 10246-10248.

(9) Proniewicz, L. M.; Bruha, A.; Nakamoto, K.; Kyuno, E.; Kincaid, J. R. *J. Am. Chem. Soc.* **1989**, *111*, 7050-7056.

(10) Tsubaki, M.; Srivastava, R. B.; Yu, N.-T. *Biochemistry* **1982**, *21*, 1132-1140.

(11) (a) Li, X. Y.; Spiro, T. G. *J. Am. Chem. Soc.* **1988**, *110*, 6024-6033. (b) Tsuboi, M. Indian *J. Pure Appl. Phys.* **1988**, *26*, 188-191. (c) Nagai, M.; Yoneyama, Y.; Kitagawa, T. *Biochemistry* **1991**, *30*, 6495-6503. (d) Ray, G. B.; Li, X. Y. Ibers, J. A.; Sessler, J. L.; Spiro, T. G. *J. Am. Chem. Soc.* **1994**, *116*, 162-176.

(12) Hirota, S.; Ogura, T.; Shinzawa-Itoh, K.; Yoshikawa, S.; Nagai, M.; Kitagawa, T. *J. Phys. Chem.* **1994**, *98*, 6652-6660.

(13) Geraci, G.; Parkhurst, L. J.; Gibson, Q. H. *J. Biol. Chem.* **1969**, *244*, 4664-4667.

(14) Potter, W. T.; Tucker, M. P.; Houtchens, R. A.; Caughey, W. S. *Biochemistry* **1987**, *26*, 4699-4707.
(15) Wang, J.; Takahashi, S.; Rousseau, D. L. *Proc. IVXth Intnl. Conf. Raman Spectrosc.*; Yu, N.-T., Li, X. Y., Eds.; Wiley-Sons: Chichester, 1994, pp 118-119.
(16) (a) Kitagawa, T.; Abe, M.; Ogoshi, H. *J. Chem. Phys.* **1978**, *69*, 4516-4525. (b) Hu, S.; Morris, I. K.; Singh, J. P.; Smith, K. M.; Spiro, T. G. *J. Am. Chem. Soc.* **1993**, *115*, 12446-12458.

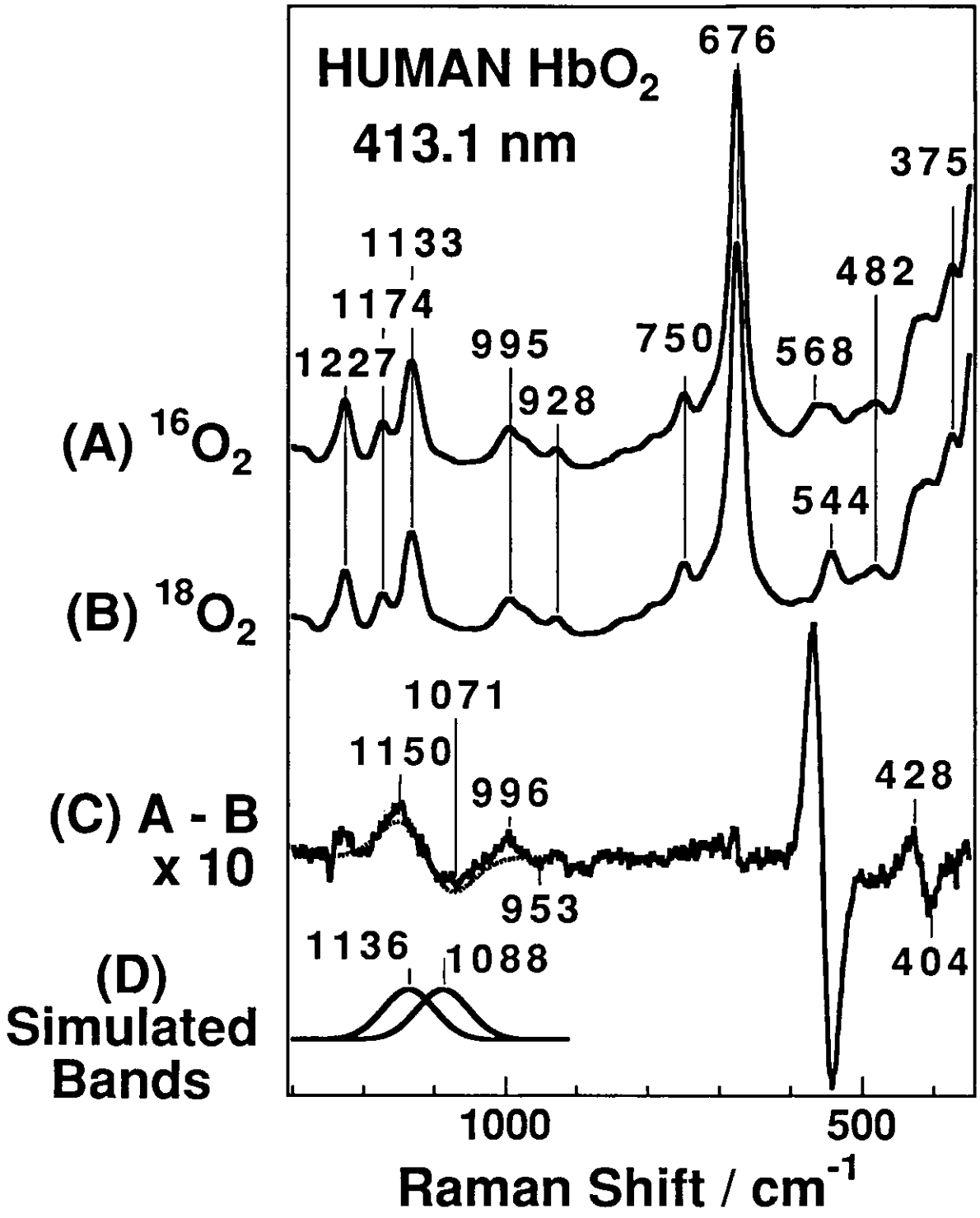


**Figure 5-1.** RR spectra in the 1300 to 350 $cm^{-1}$ region for $^{16}O_2$- (A) and $^{18}O_2$-adducts (B) of HbA and their difference spectrum (C) expanded by a factor of 10. Trace D shows two Gaussian bands with the bandwidth of 86 $cm^{-1}$ and their difference depicted by a broken line in trace C. Spectra were observed with the following conditions: slit width, 200 μm; slit height, 10 mm; laser, 413.1 nm, 5 mW at the sample; laser beam, 50 μm at the sample; sample, 50 μM (heme) in 50 mM phosphate buffer, pH 7.2.

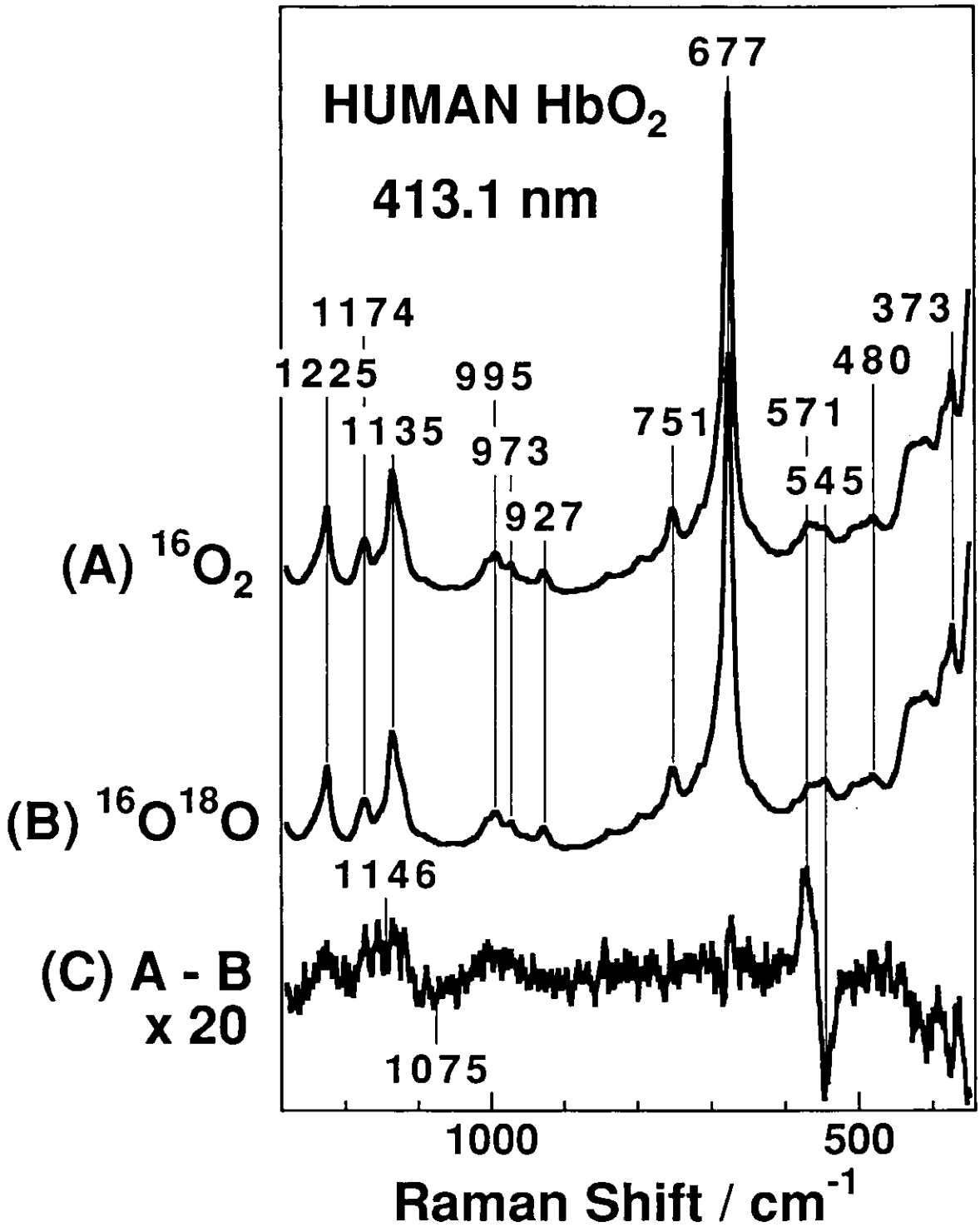


**Figure 5-2.** RR spectra in the 1300 to 350 $cm^{-1}$ region for $^{16}O_2$- (A) and $^{16}O^{18}O$-adducts (B) of human HbA and their difference spectrum (C) expanded by a factor of 20.

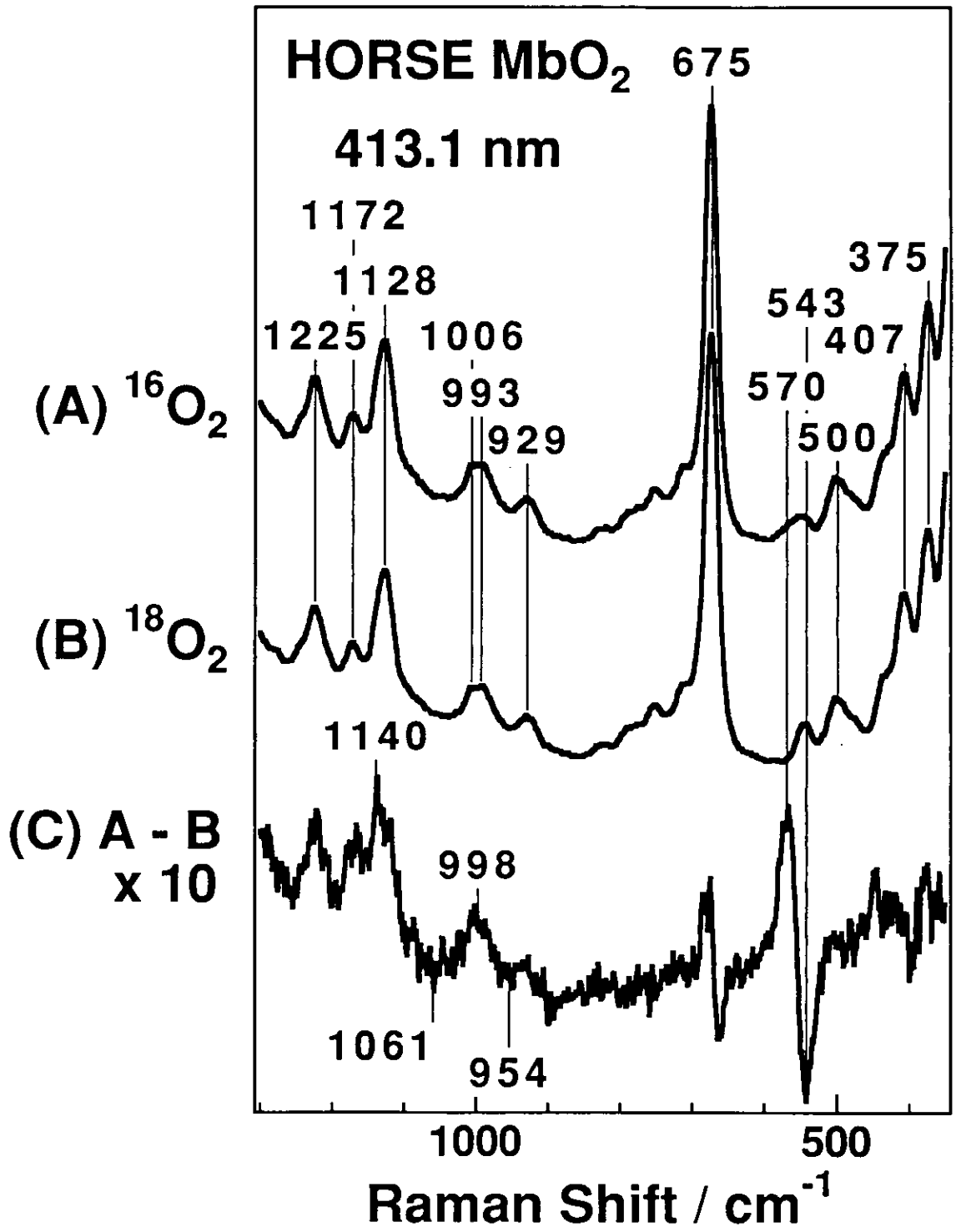


**Figure 5-3.** RR spectra in the 1300 to 350 $cm^{-1}$ region for $^{16}O_2$- (A) and $^{18}O_2$-adducts (B) of horse Mb and their difference spectrum (C) expanded by a factor of 10.

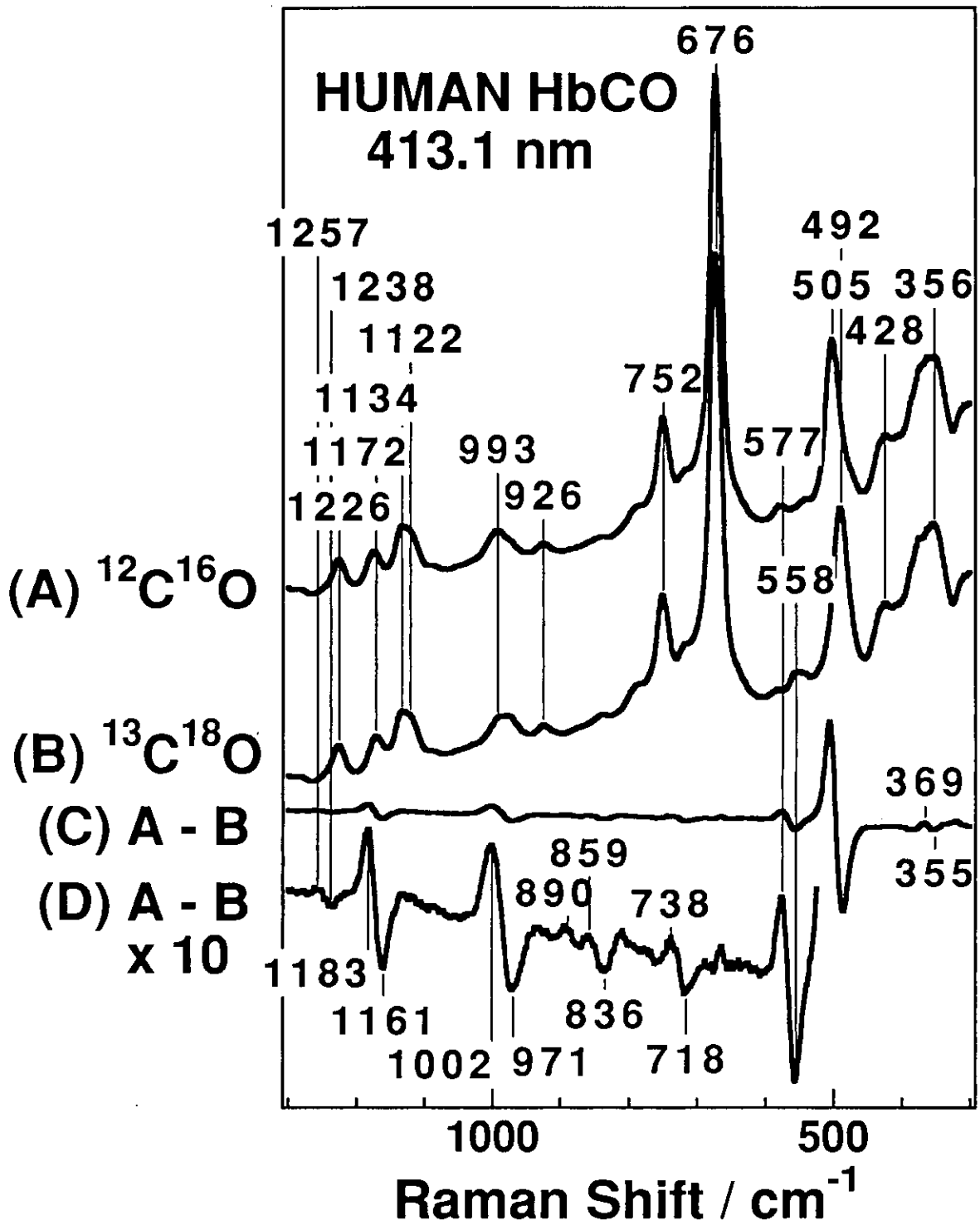


**Figure 5-4.** RR spectra in the 1300 to 300 $cm^{-1}$ region for $^{12}C^{16}O$- (A) and $^{13}C^{18}O$-adducts (B) of human HbA and their difference (C). Trace D depicts the ordinate scale expansion of trace C by a factor of 10. Experimental conditions are the same as those in Figure 5-1 except for the laser power, which is 3 mW at the sample.

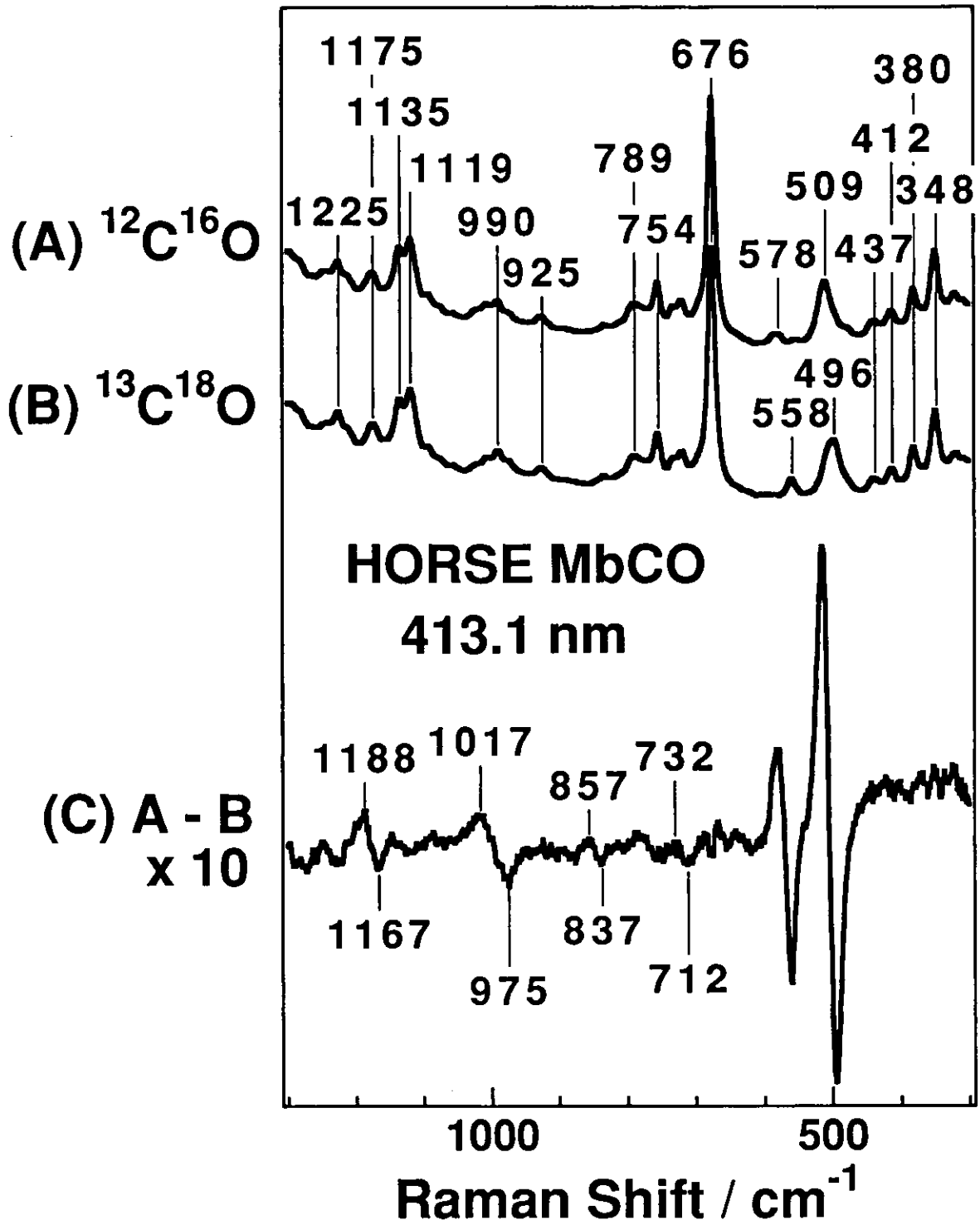


**Figure 5-5.** RR spectra in the 1300 to 300 $cm^{-1}$ region for $^{12}C^{16}O$- (A) and $^{13}C^{18}O$-adducts (B) of horse Mb and their difference (C) expanded by a factor of 10. Experimental conditions are the same as those in Figure 5-1.

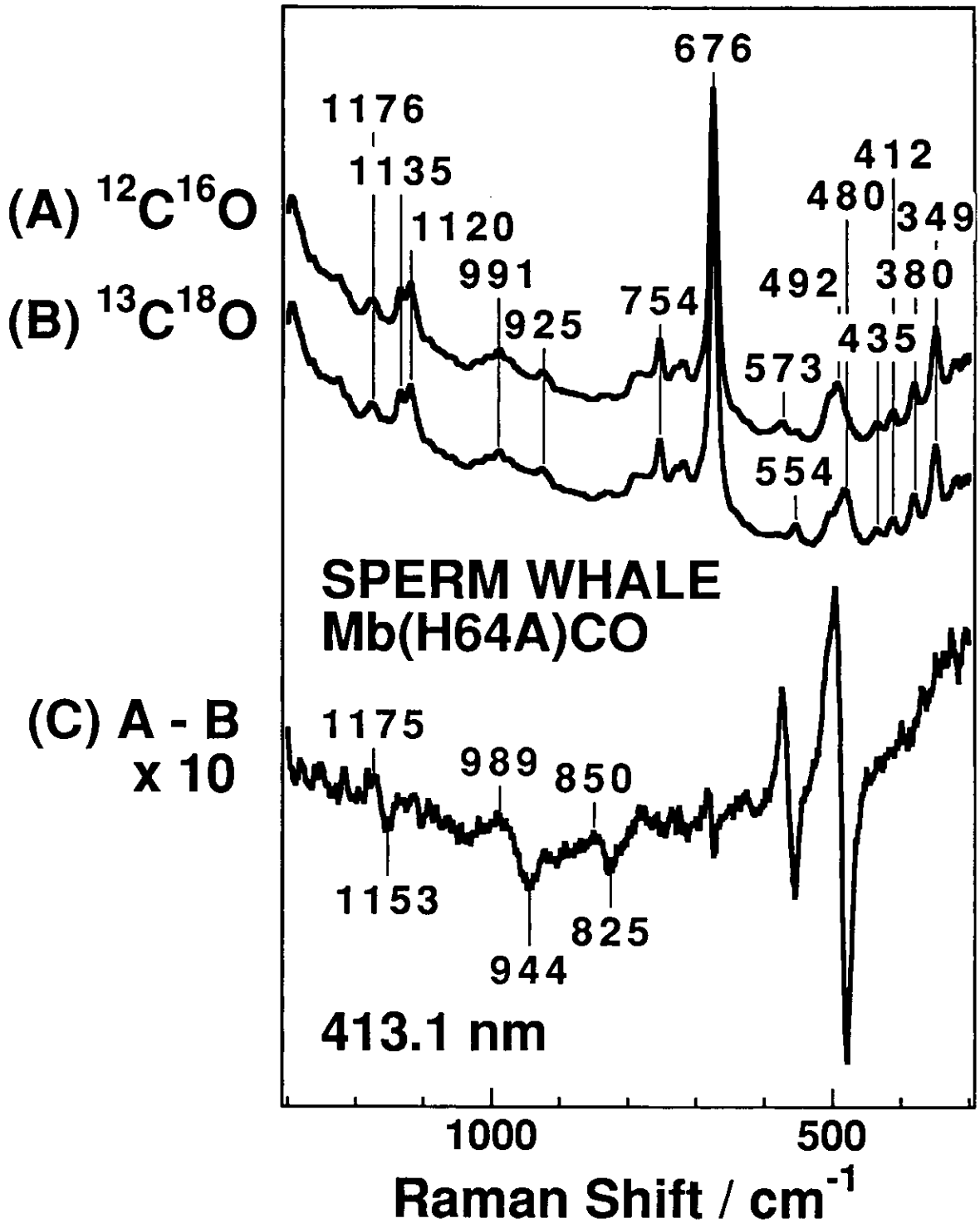


**Figure 5-6.** RR spectra in the 1300 to 300 $cm^{-1}$ region for $^{12}C^{16}O$- (A) and $^{13}C^{18}O$-adducts (B) of sperm whale Mb H64A mutant and their difference (C) expanded by a factor of 10. Experimental conditions are the same as those in Figure 5-1.

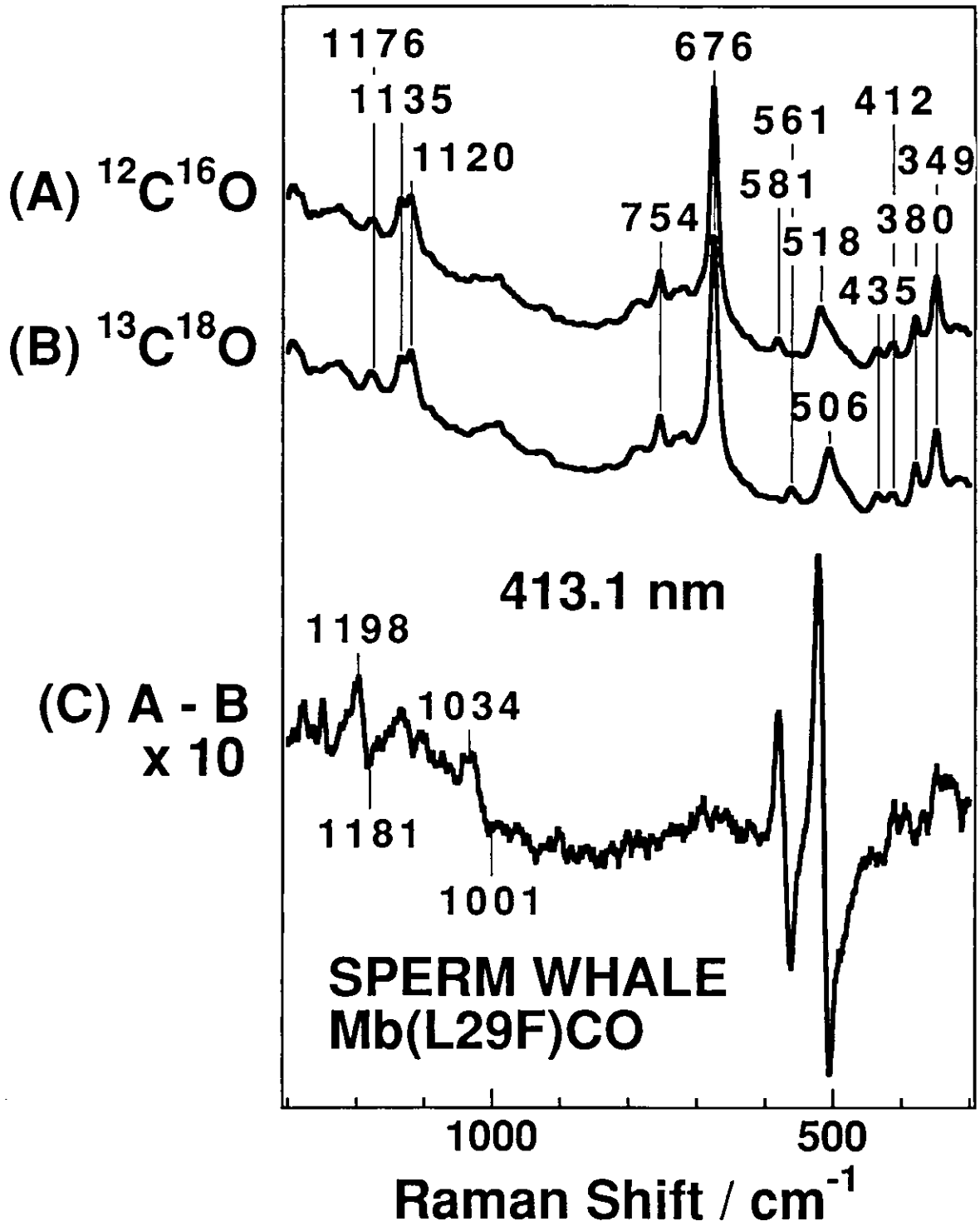


**Figure 5-7.** RR spectra in the 1300 to 300 $cm^{-1}$ region for $^{12}C^{16}O$- (A) and $^{13}C^{18}O$-adducts (B) of sperm whale Mb L29F mutant and their difference (C) expanded by a factor of 10. Experimental conditions are the same as those in Figure 5-1.

# Chapter I-6.

# Assignments of the Fe-$CN^-$ Stretching and Fe-C-$N^-$ Bending Raman Bands of Cyanide Bound Heme Proteins; Cyanometmyoglobin, Cyanomethemoglobin, and Cyanide-Bound Cytochrome *c* Oxidase

## Abstract

The RR spectra were observed for $CN^-$ and its isotope-bound heme proteins including Hb, Mb, and CcO, and the $CN^-$-isotope-sensitive bands were investigated systematically. All proteins gave the isotope-sensitive bands around 450-480 and 340-440 $cm^{-1}$ regions. CyanometHb ($HbCN^-$) gave an isotope-sensitive band at 452, 448, 447, and 443 $cm^{-1}$ for $^{12}C^{14}N^-$, $^{13}C^{14}N^-$, $^{12}C^{15}N^-$, and $^{13}C^{15}N^-$. CyanometMb ($MbCN^-$) gave them at similar frequencies, but $CN^-$-bound resting CcO($CcO_{rest}{\cdot}CN^-$) gave them at distinctly higher frequencies; 478 $cm^{-1}$ ($^{12}C^{14}N^-$), 473 $cm^{-1}$ ($^{13}C^{14}N^-$), 473 $cm^{-1}$ ($^{12}C^{15}N^-$), and 468 $cm^{-1}$ ($^{13}C^{15}N^-$). They are shifted slightly to lower frequencies in the $CN^-$-bound reduced CcO ($CcO_{red}{\cdot}CN^-$); 475 $cm^{-1}$ ($^{12}C^{14}N^-$), 472 $cm^{-1}$ ($^{13}C^{14}N^-$), 472 $cm^{-1}$ ($^{12}C^{15}N^-$), and 465 $cm^{-1}$ ($^{13}C^{15}N^-$). The monotonous feature of the frequency changes against the increase of total mass of $CN^-$ suggest that these bands arise from the Fe-$CN^-$ stretching mode ($\nu_{Fe\text{-}CN^-}$). The higher frequency of $\nu_{Fe\text{-}CN^-}$ for CcO than those for $MbCN^-$ and $HbCN^-$ suggests that the $CN^-$ binding site of CcO has a special environment presumably due to the presence of the $Cu_B$ ion. Besides this main band, several weak $CN^-$-isotope-sensitive bands were observed below 440 $cm^{-1}$, but the pattern of the isotope-difference spectra were specific to each protein. These low frequency difference peaks were significantly weaker in intensity for $^{15}N$ isotopes compared with $^{13}C$ isotopes in common. This suggests that the $FeCN^-$ bending mode ($\delta_{FeCN^-}$) is present around ~380 $cm^{-1}$ and this mode is coupled with more than two porphyrin vibrations which differ among Hb, Mb, and CcO. The $CN^-$ stretching ($\nu_{CN^-}$) Raman band was detected for the first time at 2127 cm-1 for $MbCN^-$. This frequency was close to that of the IR observation reported.

## 6.1 Introduction

As summarized in chapter I-1, quite different frequencies among different $CN^-$-bound heme proteins have been assigned to the $\nu_{Fe\text{-}CN^-}$ and $\delta_{FeCN^-}$. The iron-carbon stretching mode ($\nu_{Fe\text{-}CN^-}$) and iron-carbon-nitrogen bending mode ($\delta_{FeCN^-}$) of $CN^-$-bound heme proteins have been first reported in RR spectroscopy at 453 $cm^{-1}$ and 412 $cm^{-1}$, respectively, by Yu et al. for hemoglobin III isolated from *Chironomus thummi thummi* (CTT III).[1] The $\nu_{Fe\text{-}CN^-}$ mode for human cyanometHb ($HbCN^-$) and sperm whale cyanometMb ($MbCN^-$) were detected at 452 $cm^{-1}$.[2,3] The 361 and 454 $cm^{-1}$ bands were assigned to the $\nu_{Fe\text{-}CN^-}$ and $\delta_{FeCN^-}$ for cyanoferric myeloperoxidase ($MPO{\cdot}CN^-$), while the 456 and 404 $cm^{-1}$ bands were assigned to $\nu_{Fe\text{-}CN^-}$ and $\delta_{FeCN^-}$ for cyanoferric horseradish peroxidase ($HRP{\cdot}CN^-$), respectively,[4] and the 360 and 453 $cm^{-1}$ bands were assigned to $\nu_{Fe\text{-}CN^-}$ and $\delta_{FeCN^-}$ for cyanoferric lactoperoxidase ($LPO{\cdot}CN^-$), respectively.[5] For $LPO{\cdot}CN^-$ there was another clear $CN^-$-isotope-sensitive band at 311 $cm^{-1}$ which was unable to be explained as either $\nu_{Fe\text{-}CN^-}$ nor $\delta_{FeCN^-}$ since its isotope shift was only 2 $cm^{-1}$ between $^{12}C^{14}N^-$ and $^{13}C^{15}N^-$ adducts. In all these reports, the $\nu_{Fe\text{-}CN^-}$ band was confirmed by a monotonic frequency decrease character as the total mass of $CN^-$ increased, while the $\delta_{FeCN^-}$ band were decided by the higher sensitivity to the mass of the carbon atom than that of the nitrogen atom.

But it is strange to have so different frequencies for the same mode among different proteins. For example, iron-carbon stretching mode ($\nu_{Fe\text{-}CO}$), iron-carbon-oxygen bending mode ($\delta_{FeCO}$), and another CO-isotope sensitive mode appear around 480 - 520 $cm^{-1}$, 365 $cm^{-1}$, and 560 - 580 $cm^{-1}$, respectively, in various CO-bound heme proteins.[6,7] Dioxygen ($O_2$) bound heme proteins also have very similar frequencies for the iron-oxygen stretching mode ($\nu_{Fe\text{-}O_2}$) and iron-oxygen-oxygen bending mode ($\delta_{FeOO}$), respectively.[8,9] Furthermore, it is very dangerous to assign the mode only from its ligand isotope shift pattern. Since the FeOO unit in $O_2$ bound heme proteins are significantly bent,[10] $\nu_{Fe\text{-}O_2}$ is sensitive to the mass of the oxygen atom which is bound to the heme iron but not to the terminal oxygen atom.[11] Also in NO-bound heme proteins, the iron-nitrogen stretching modes ($\nu_{Fe\text{-}NO}$) are sensitive to the nitrogen atom but not to the oxygen atom.[12]

For "strapped hemes", in which the ligand binding site is sterically hindered by a $(CH_2)_n$-chain strap over the heme iron at the $CN^-$ binding

site, the $\nu_{Fe\text{-}CN^-}$ bands are observed at very close frequencies, 451 (unhindered), 447 (n=15), 447 (n=14), and 445 $cm^{-1}$ (n=13).[13] The $\nu_{Fe\text{-}CN^-}$ frequency was detected at 449 $cm^{-1}$ for Fe(OEP)(pyridine)$CN^-$ (OEP, octaethylporphyrin), and at 442 - 452 $cm^{-1}$ for all pyridine derivatives of Fe(OEP)(pyridine)$CN^-$, varying according to the pyridine basicity.[14]

$CN^-$-bound resting cytochrome *c* oxidase (CcO·$CN^-$) is of great interest since it may give a μ-peroxy intermediate in the reaction with oxygen. For the case of the ferrous iron, $\nu_{Fe\text{-}CN^-}$ and $\delta_{FeCN^-}$ were observed at 511 and 486 $cm^{-1}$, respectively, for $CN^-$ complexes of cytochrome $ba_3$.[15]

The carbon-nitrogen stretching mode ($\nu_{CN^-}$) of $CN^-$-bound heme proteins have been detected by infrared (IR) spectra for several proteins,[16] but not yet by RR spectra for any $CN^-$ adduct heme proteins.

Assignments of the ligand related modes are essential to discuss their $FeCN^-$ geometry. Accordingly, we measured the RR spectra for low frequency regions for cyanometMb ($MbCN^-$), $HbCN^-$, and CcO·$CN^-$, and in the high frequency region for $MbCN^-$ using an excitation wavelength near the Soret peak. Here we discuss systematically three $CN^-$-isotope-sensitive modes detected in RR spectra for $CN^-$-bound heme proteins.

### 6.2 Experimental Procedures

Raman scattering was excited at 441.6 nm by a He/Cd laser (Kinmon Electrics, Model CD1805B), and at 426.0 to 427.0 nm by an $Ar^+$ ion laser (Spectra Physics, Model 2045) pumped dye laser (Spectra Physics, Model 375B) with stilbene 420 or by the laser system with a $KNbO_3$ crystal (VIGRO OPTICS, USA) described in chapter I-2. Raman scattering was detected with a CCD (Astromed CCD, 3200) or a cooled (-20 °C) intensified photodiode array (Princeton Applied Research, 1421HQ) attached to a single polychrometer (Ritsu Oyo Kogaku, DG-1000). The spectrometer had two interchangeable-blazed holographic gratings; a 500 nm blazed - 1200 grooves/mm grating was used in the first order geometry and a 900 nm blazed - 1200 grooves/mm one was used in the second order. The 900nm blazed - 1200 grooves/mm grating gives higher resolution (~0.4 $cm^{-1}$/channel), while the 500 nm blazed -1200 grooves/mm grating (~1.0 $cm^{-1}$/channel) gives better S/N ratio. The slitwidth and slitheight were 200 μm and 10 mm, respectively, for all measurements. The excitation laser beam was focused to the sample to about 50 μm, and the laser power was

adjusted to 5 - 10 mW (at the sample). A spinning cell was used for measurements in the low frequency region and was rotated at 3000 rpm to avoid photodissociation of $CN^-$. A 0.6 x 0.6 mm flow cell was used for measurements in the high frequency region, and the flow rate was adjusted to 40 ml/min. All measurements were carried out at room temperature. Raman shifts were calibrated by $CCl_4$ for the low frequency region and by indene and cyanomethane for the high frequency region. The accuracy of the peak positions of the Raman bands were ±1 $cm^{-1}$.

Horse myoglobin (Sigma, type M630) was dissolved in minimum amount of 50 mM Tris-HCl buffer, pH 8.0. Gel filtration through Sephadex G-25 was performed after completely oxidizing remaining deoxy Mb by adding a slight amount of potassium ferricyanide solution. The sample was diluted to 50 μM with 50 mM Tris-HCl buffer, pH 8.0. The $CN^-$ complex were formed by adding 100 mM KCN / 0.05N NaOH, ~pH 8.0, to the sample solution obtaining the final concentration of KCN to ~1 mM. $CN^-$-isotope complexes were formed in the same way using $K^{13}CN$ (ICON, $^{13}C$ 99 atom %), $KC^{15}N$ (ICON, $^{15}N$ 99 atom %), and $K^{13}C^{15}N$ (ICON, $^{13}C$ 99 atom % and $^{15}N$ 99 atom %).

Human adult Hb (HbA) was prepared according to the method of Geraci et al[17] and $CN^-$ complexes were obtained in the same way as that for $MbCN^-$.

Cytochrome *c* oxidase (cytochrome *c*: oxidoreductase, EC 1.9.3.1.) was isolated from bovine heart according to Yoshikawa's method.[18] Samples were dissolved in 50 mM sodium phosphate buffer, pH 7.2. $CN^-$-bound resting CcO ($CcO_{rest}{\cdot}CN^-$) was obtained by adding a little amount of 100 mM KCN / 0.5N NaOH, ~pH8.0, in the same way as for Mb and Hb, and leaving it for more than 3 hours before measurements. $CN^-$-bound reduced CcO ($CcO_{red}{\cdot}CN^-$) was obtained by repeating three times the evacuation of gas inside the cell to ca. 0.1 mmHg followed by incorporation of $N_2$ gas into it to ca. 1 atm. Reduction of remaining oxygen was performed by adding $N_2$ saturated dithionite solution so that the final concentration of dithionite became 10 mM. Finally we added a little amount of ~1 M KCN / 0.05N NaOH, pH ~8.0, solution to the sample to obtain the final concentration of KCN of ~10 mM. The formation of $CN^-$ adducts were checked by the disappearance of the iron-histidine stretching band at 214 $cm^{-1}$.[19]

## 6.3 Results

Figure 6-1 shows the RR spectra in the region from 550 to 200 $cm^{-1}$ of $^{12}C^{14}N^-$ (A), $^{13}C^{14}N^-$ (B), $^{12}C^{15}N^-$ (C), and $^{13}C^{15}N^-$ (D) adducts of ferric horse Mb excited at 426.0 nm. The band located at 452 $cm^{-1}$ for $Mb^{12}C^{14}N^-$ (A) shifted to 448 $cm^{-1}$ for $Mb^{13}C^{14}N^-$ (B) , to 447 $cm^{-1}$ for $Mb^{12}C^{15}N^-$ (C) , and to 443 $cm^{-1}$ for $Mb^{13}C^{15}N^-$ (D). This band is shifted to lower frequencies with the increase of the total mass of $CN^-$, and has been assigned to $\nu_{Fe\text{-}CN^-}$.[3] These $\nu_{Fe\text{-}CN^-}$ frequencies are very close to the $\nu_{Fe\text{-}CN^-}$ frequencies reported for $HbCN^-$ and cyanomet CTT III.[1,2] For some other cyanoferric heme proteins, $\delta_{FeCN^-}$ is reported to show a "zigzag" pattern in the RR spectra, that is, its frequency changes in the order of $^{12}C^{14}N^- \rightarrow {}^{13}C^{14}N^- \rightarrow {}^{12}C^{15}N^- \rightarrow {}^{13}C^{15}N^-$ adducts. However, there is no clear RR band which shows a "zigzag" pattern in Figure 6-1.

The difference spectra of the RR spectra shown in Figure 6-1 are shown in Figure 6-2. The difference peaks around 450 $cm^{-1}$ are most pronounced when the difference of the total mass of $CN^-$ is the largest, i.e., between $Mb^{12}C^{14}N^-$ and $Mb^{13}C^{15}N^-$ (C). These difference peaks are due to the $\nu_{Fe\text{-}CN^-}$ band. We note an interesting character in this figure, that is, there exists many extra difference peaks in a wide frequency range, 300 - 450 $cm^{-1}$. These difference peaks are enhanced when the mass of the carbon atom is changed between the $CN^-$ adducts (Figures 6-2A and 6-2C), while these peaks have weaker intensity when only the mass of the nitrogen atom is changed (Figures 6-2B and 6-2D). The bandwidth of the 342 $cm^{-1}$ band seems to change upon different $CN^-$-isotope bound forms, and this bandwidth change causes an up peak at 344 $cm^{-1}$ and down peaks at 338 and 349 $cm^{-1}$ (Figures 6-2A and 6-2C). The band at 374 $cm^{-1}$ seems to shift slightly to lower frequencies upon carbon isotopes to the bound $CN^-$ causing difference peaks at 386-377/371 $cm^{-1}$ (Figures 6-2A and 6-2C). The porphyrin band at 442 $cm^{-1}$ also seems to be altered upon carbon isotopes of the bound $CN^-$, causing a down peak at 438 $cm^{-1}$ in the $CN^-$-isotope difference spectra (Figure 6-2A and 6-2C).

Figure 6-3 shows the RR spectra in the region from 550 to 200 $cm^{-1}$ for $^{12}C^{14}N^-$ (A), $^{13}C^{14}N^-$ (B), $^{12}C^{15}N^-$ (C), and $^{13}C^{15}N^-$ (D) adducts of ferric human HbA excited at 426.0 nm. The band at 452 $cm^{-1}$ for $Hb^{12}C^{14}N^-$ (A) shifted to lower frequencies according to the increase of the total mass of $CN^-$; 448 $cm^{-1}$ ($Hb^{13}C^{14}N^-$, B), 447 $cm^{-1}$ ($Hb^{12}C^{15}N^-$, C), and 443 $cm^{-1}$ ($Hb^{13}C^{15}N^-$, D). This band represents the $\nu_{Fe\text{-}CN^-}$ mode, and is in

agreement with the results reported.[2] No other clear $CN^-$-isotope-sensitive band was detected in this figure except for the left shoulder of the strong band at 345 $cm^{-1}$, which seemed to be definitely influenced by $CN^-$-isotopes.

The difference corresponding to Figure 6-2 were calculated for the spectra shown in Figure 6-3 to clarify the changes in the band around 350 $cm^{-1}$, and the results are shown Figure 6-4. Apart from the difference peaks around 450 $cm^{-1}$ which represents the $\nu_{Fe\text{-}CN^-}$ mode, many difference peaks appeared when the mass of the carbon atom was changed (Figures 6-4A and 6-4C), while it reduced in intensity when that of nitrogen was changed (Figures 6-4B and 6-4D), similar to the case for $MbCN^-$ (Figure 6-2). A band around 380 $cm^{-1}$ which is not clear in the raw spectra (Figure 6-3) seems to have a broader bandwidth when the $^{12}C$ of the bound $CN^-$ is changed to $^{13}C$, which causes an up peak at 380 $cm^{-1}$ and down peaks at 374 and 392 $cm^{-1}$ (Figures 6-4A and 6-4C). On the other hand, the band at 350 $cm^{-1}$ seems to have a narrower bandwidth for $^{13}C$ isotopes of $CN^-$ than for $^{12}C$ isotopes of it, causing up peaks at 346 and 357 $cm^{-1}$ and a down peak at 350 $cm^{-1}$ (Figures 6-4A and 6-4C). The band at 309 $cm^{-1}$ also seems to be slightly changed by $CN^-$-isotopes causing an up peak at 312 $cm^{-1}$ in the difference spectra (Figure 6-4A and 6-4C).

Figure 6-5 shows the polarized RR spectra in the region from 600 to 200 $cm^{-1}$ of parallel (//) and perpendicular ($\perp$) polarized components for $Mb^{12}C^{14}N^-$ (A) and $Mb^{13}C^{15}N^-$ (B) excited at 427.0 nm, and their difference spectra (C), where panels (a) and (b) depict the parallel and perpendicular components of the spectra, respectively. The intensity ratios of bands of perpendicular to parallel components were all ca. 0.25, and therefore they are regarded as polarized bands. Both difference spectra (C) and (F) showed difference peaks around 330 - 390 $cm^{-1}$, and the intensity ratio of the difference peaks of the perpendicular and to the parallel components were ca. 0.25.

Figure 6-6 shows the RR spectra in the region from 600 to 300 $cm^{-1}$ for $^{12}C^{14}N^-$ (A), $^{13}C^{14}N^-$ (B), $^{12}C^{15}N^-$ (C), and $^{13}C^{15}N^-$ (D) adducts of resting CcO ($CcO_{rest}{\cdot}CN^-$) excited at 427.0 nm, and their difference spectra $CcO_{rest}{\cdot}^{12}C^{14}N^-$ - $CcO_{rest}{\cdot}^{13}C^{14}N^-$ (E), $CcO_{rest}{\cdot}^{12}C^{14}N^-$ - $CcO_{rest}{\cdot}^{12}C^{15}N^-$ (F), and $CcO_{rest}{\cdot}^{12}C^{14}N^-$ - $CcO_{rest}{\cdot}^{13}C^{15}N^-$ (G). The presence of $CN^-$-isotope-sensitive bands is not clear in the raw spectra, but it becomes clear in the difference spectra, having the largest difference peak and shift

value in the difference spectra between $^{12}C^{14}N^-$ and $^{13}C^{15}N^-$ adducts (G), while the band at 498 $cm^{-1}$ was completely canceled in all of the difference spectra (E-G). The band at 478 $cm^{-1}$ for $CcO_{rest}\cdot^{12}C^{14}N^-$ (A) shifted to lower frequencies according to the increase of the total mass of $CN^-$; 473 $cm^{-1}$ ($CcO_{rest}\cdot^{13}C^{14}N^-$, B), 473 $cm^{-1}$ ($CcO_{rest}\cdot^{12}C^{15}N^-$, C), and 468 $cm^{-1}$ ($CcO_{rest}\cdot^{13}C^{15}N^-$, D). Therefore, this band is assigned to $\nu_{Fe\text{-}CN^-}$. We note that the $\nu_{Fe\text{-}CN^-}$ frequency at 478 $cm^{-1}$ was higher than those for $MbCN^-$ and $HbCN^-$ which had $\nu_{Fe\text{-}CN^-}$ frequencies around 452 $cm^{-1}$ (Figures 6-1 and 6-2).

The RR spectra in the region from 600 to 200 $cm^{-1}$ for $^{12}C^{14}N^-$ (A), $^{13}C^{14}N^-$ (B), $^{12}C^{15}N^-$ (C), and $^{13}C^{15}N^-$ (D) adducts of reduced CcO ($CcO_{red}\cdot CN^-$) excited at 441.6 nm are shown in Figure 6-7. The band at 475 $cm^{-1}$ shifted to lower frequencies according to the increase of the total mass of $CN^-$; 472 $cm^{-1}$ ($CcO_{red}\cdot^{13}C^{14}N^-$, B), 472 $cm^{-1}$ ($CcO_{red}\cdot^{12}C^{15}N^-$, C), and 465 $cm^{-1}$ ($CcO_{red}\cdot^{13}C^{15}N^-$, D), and we assign it to the $\nu_{Fe\text{-}CN^-}$ mode. The difference spectrum between A and D is shown in the inset, in which the band at 583 $cm^{-1}$ is canceled completely, but the presence of the difference peaks around 485 - 456 $cm^{-1}$ is clear although it is very broad.

Figure 6-8 presents the RR spectra of the $MbCN^-$ in the higher frequency region excited at 427.0 nm. There was no clear $CN^-$-isotope-sensitive band in the raw spectra of $Mb^{12}C^{14}N^-$ (A) and $Mb^{12}C^{15}N^-$ (B), but in their difference spectrum C, there appeared a positive peak at 2127 $cm^{-1}$ and a negative peak at 2097 $cm^{-1}$. These frequencies were in good agreement with the $\nu_{CN^-}$ frequencies of $Mb^{12}C^{14}N^-$ and $Mb^{12}C^{15}N^-$ reported from IR spectra.[16a]

## 6.4 Discussion

### $\nu_{Fe\text{-}CN^-}$ Mode of $MbCN^-$ and $HbCN^-$

The $\nu_{Fe\text{-}CN^-}$ frequencies of $MbCN^-$ and $HbCN^-$ were observed around 452 $cm^{-1}$ (Figures 6-1 and 6-3) which were lower than the iron-carbon stretching ($\nu_{Fe\text{-}CO}$) frequencies of CO-bound Mb and CO-bound Hb (HbCO). These results are comparable with the results of model compounds.[20] The $\nu_{Fe\text{-}CN^-}$ frequencies of $MbCN^-$ and $HbCN^-$ were very close to that of cyanomet CTT III, while the $\nu_{Fe\text{-}CO}$ frequencies of their CO adducts differ; 512 $cm^{-1}$ for MbCO, 507 $cm^{-1}$ for HbCO, and 500 $cm^{-1}$ for CO-bound CTT III.[1,6a,21] This suggests that environments at the binding

sites of $CN^-$ in $MbCN^-$ and $HbCN^-$ are virtually identical, while those of their CO adducts slightly differ; CO being more bent in MbCO than in HbCO as according to X-ray and time resolved IR studies.[22,23]

### $\delta_{FeCN^-}$ Mode of $MbCN^-$ and $HbCN^-$

As the $CN^-$ binding geometry is very close to that of CO, the behavior of $\delta_{FeCN^-}$ against the $CN^-$-isotope substitution will be similar to the case of $\delta_{FeCO}$ in CO-bound heme proteins. It means that the $\delta_{FeCN^-}$ frequency should be sensitive to the mass of the middle carbon atom. The $\delta_{FeCN^-}$ RR band could not be seen clearly in the raw spectra of $MbCN^-$ and $HbCN^-$ (Figures 6-1 and 6-3). However, many difference peaks appeared in the difference spectra when the mass of carbon atom of $CN^-$ was different, but the difference were extremely weaker when the mass of nitrogen was changed (Figures 6-2 and 6-4). It is reported[2] that there is a coupling between the $\delta_{Fe\text{-}CN^-}$ mode and the porphyrin mode at 377 $cm^{-1}$, but we detected more difference peaks at a wider region. The results were similar for $CcO_{rest}{\cdot}CN^-$ (data not shown). The wide frequency region where difference peaks appeared was around 300 to 440 $cm^{-1}$, and was close to the $\delta_{FeOO}$, $\delta_{FeCO}$, and $\delta_{FeNO}$ frequencies of $O_2$-, CO-, and NO-bound ferrous heme proteins observed around 430, 370, and 450 $cm^{-1}$, respectively.[9b,12,21] Therefore the difference peaks observed around 300-440 $cm^{-1}$ should be attributed to modes involving $\delta_{FeCN^-}$. The presence of more than a single difference peak indicates that $\delta_{FeCN^-}$ couples with several porphyrin modes. Such phenomenon was not seen for MbCO, HbCO and any other CO or $O_2$ complexes, and should arise from the structural characteristic.

The modes which couple with $\delta_{FeCN^-}$ should be those which give polarized bands, as the ratio of the intensities of the difference peaks in the perpendicular to parallel polarization components were ca. 0.25. The bands of $MbCN^-$ at 342, 374 and 409 $cm^{-1}$(Figure 6-1) are assignable to the $\nu_8$ skeletal vibration, the bending vibration of the propionic acid, and the bending vibration of the vinyl group of the porphyrin, respectively.[24] These modes are the candidates to couple with $\delta_{FeCN^-}$. The point to be stressed here is that the porphyrin modes to be coupled with $\delta_{FeCN^-}$ are not unique.

### $\nu_{Fe\text{-}CN^-}$ and $\delta_{FeCN^-}$ Assignments of Cyanoferric Heme Proteins

The $\nu_{Fe\text{-}CN^-}$ $\delta_{Fe\text{-}CN^-}$, and $\nu_{CN^-}$ frequencies of $MbCN^-$, $HbCN^-$, and $CcO_{rest}\cdot CN^-$ obtained in this study together with the results of other cyanoferric heme proteins reported so far are summarized in TABLE 6-1. Each heme protein has a $CN^-$-isotope sensitive band around 452 $cm^{-1}$, even though the assignments are different for each report. The $\nu_{Fe\text{-}CN^-}$ band of $MbCN^-$ and $HbCN^-$ is shifted by 9 $cm^{-1}$ between $^{13}C^{15}N^-$ and $^{12}C^{14}N^-$ adducts (Figure 6-1 and Figure 6-3). The $CN^-$-isotope shift of 4 $cm^{-1}$ for the assigned $\nu_{Fe\text{-}CN^-}$ band of $MPO\cdot{}^{13}C^{15}N^-$ against $MPO\cdot{}^{12}C^{14}N^-$ was too small, compared with the expected value from its frequency (7 $cm^{-1}$). Three $CN^-$-isotope sensitive bands were observed at 453, 360, and 311 $cm^{-1}$ for $LPO\cdot CN^-$, and the 360 and 453 $cm^{-1}$ bands were assigned to $\nu_{Fe\text{-}CN^-}$ and $\delta_{FeCN^-}$, respectively.[5] The two $CN^-$-isotope-sensitive bands detected at 311 and 360 $cm^{-1}$ both represented a monotonous pattern against the change of the mass of $CN^-$, but their frequency shift seems too small to assign them to $\nu_{Fe\text{-}CN^-}$ (2 ~ 4 $cm^{-1}$), although the 360 $cm^{-1}$ band was assigned to $\nu_{Fe\text{-}CN^-}$.[5] This character having many $CN^-$-isotope-sensitive bands around 300-440 $cm^{-1}$ was the same as what we obtained here for $MbCN^-$ and $HbCN^-$. The $FeCN^-$ unit of oxidized $LPO\cdot CN^-$ could adopt a bent structure, and $\nu_{Fe\text{-}CN^-}$ must be sensitive primarily to the mass of the carbon atom which is bound to the iron but not to that of the nitrogen atom.[9] Therefore for $LPO\cdot CN^-$, it is more reasonable to re-interpret that the 453 $cm^{-1}$ band arises from $\nu_{Fe\text{-}CN^-}$, while 310 and 360 $cm^{-1}$ bands are coupled modes of $\delta_{FeCN^-}$ with porphyrin modes. This strong coupling with porphyrin modes might mislead the authors[5] to assign those bands to $\nu_{Fe\text{-}CN^-}$. We systematically assign the 452 $cm^{-1}$ band to $\nu_{Fe\text{-}CN^-}$ and suggest that $\delta_{FeCN^-}$ is present around ~380 $cm^{-1}$ which couples with more than two porphyrin vibrations for various $CN^-$-bound heme proteins.

### $\nu_{Fe\text{-}CN^-}$ Mode of $CN^-$ Bound Resting CcO

The $\nu_{Fe\text{-}CN^-}$ frequency for $CcO_{rest}\cdot CN^-$ was detected at 478 $cm^{-1}$. This $\nu_{Fe\text{-}CN^-}$ frequency was higher than those for other cyanoferric heme proteins which have the $\nu_{Fe\text{-}CN^-}$ frequency around 452 $cm^{-1}$. The $\nu_{CN^-}$ frequency observed by IR spectroscopy also had a higher frequency than those for other cyanoferric heme proteins.[16] This character was the same with the CO-bound CcO, whose $\nu_{Fe\text{-}CO}$ frequency was higher than that expected from the linear correlation between $\nu_{Fe\text{-}CO}$ and $\nu_{CO}$ of histidine-

coordinated heme proteins.[6g,25] This might be caused by the $Cu_B$ which is located close to the ligand with a distance of 3.75 Å from the heme iron (Figure 6-9).[26] When $Cu_B$ is removed from the protein of cytochrome *bo* complexes by mutagenesis, the iron-histidine stretching frequency shifts slightly to a higher frequency,[27] but the $\nu_{Fe\text{-}CO}$ shifts to a lower frequency. Therefore $Cu_B$ is more likely to cause an upshift in the Fe-ligand stretching frequencies for CO and $CN^-$-bound forms.[28] The electrons in the d orbital of $Cu_B$ might increase the $\sigma$ bonding between Fe and CO, and cause $\nu_{Fe\text{-}CO}$ to have higher frequency than expected. The similar thing must be happening in $CcO_{red}{\cdot}CN^-$ also (Figure 6-9).

The iron-ligand stretching and ligand internal frequencies for CO-, $CN^-$-, and $O_2$-bound Mb, Hb, and CcO are listed in TABLE 6-2. Both ligand stretching and ligand internal frequencies for $CcO_{rest}{\cdot}CN^-$ and $CcO{\cdot}CO$ are higher than those of the corresponding ligand-bound Mb and Hb. But the $O_2$-bound Mb, Hb and CcO have similar $\nu_{Fe\text{-}O_2}$ frequencies around 570 $cm^{-1}$. The $O_2$ ligand is bound more bent against the heme plane than CO or $CN^-$ ligands in Mb and Hb. $CcO{\cdot}O_2$ is also thought to be bent significantly as shown in Figure 6-9, similar to $MbO_2$ and $HbO_2$ inferred from similar $\nu_{Fe\text{-}O_2}$ frequencies and their $^{18}O_2$ isotope shifts.[9b] As the $Cu_B$ ion has smaller effect to the ligand stretching frequencies, it seems that $O_2$ is bent significantly away from the $Cu_B$ ion.

### $\nu_{Fe\text{-}CN^-}$ Mode of $CN^-$ Bound Reduced CcO

The $\nu_{Fe\text{-}CN^-}$ band of $CcO_{red}{\cdot}CN^-$ exhibited a broad bandwidth. For this molecule, two $\nu_{CN^-}$ modes are detected at 2045 and 2058 $cm^{-1}$ in the IR spectra,[11c] and are interpreted in terms of the presence of two conformers. This might cause the broadening of the $\nu_{Fe\text{-}CN^-}$ band. Even so, the bandwidth seems too large. Other $CN^-$-isotope-sensitive bands at 2093 and 2037 $cm^{-1}$ in the IR spectra are assigned to $\nu_{CN^-}$ of the Cu-$CN^-$ species, but one of them could be a $\nu_{CN^-}$ of the Fe-$CN^-$ species, and this species could cause the broadness.

The $\nu_{Fe\text{-}CN^-}$ and $\nu_{CN^-}$ frequencies of $MbCN^-$, $CcO_{rest}{\cdot}CN^-$, and $CcO_{red}{\cdot}CN^-$ are summarized in Figure 6-10. In $CcO_{red}{\cdot}CN^-$ the $CN^-$ is not bound as HCN, since the $\nu_{CN^-}$ band shows no $D_2O$ shift and the $CN^-$-isotope-frequency shifts of $\nu_{CN^-}$ matches with the shifts calculated with a simple harmonic oscillator model for $CN^-$.[16b,29] The $\nu_{Fe\text{-}CN^-}$ frequencies scarcely differ between $CcO_{red}{\cdot}CN^-$ and $CcO_{rest}{\cdot}CN^-$, while the $\nu_{CN^-}$

frequency is lower for the former. This may be caused by the fact that the extra d orbital electron of $Fe^{2+}$ compared with $Fe^{3+}$ serves as an effective $\pi^*$ electron of the C-N bond,[25] without effecting the Fe-C bond significantly.

### $\nu_{CN^-}$ Mode

We detected the $\nu_{CN^-}$ mode for $MbCN^-$. This was the first report to detect the $\nu_{CN^-}$ mode in the RR spectra for cyanomet heme proteins although it was weak. If the Fe-$CN^-$ bond is completely ionic, the $\nu_{CN^-}$ RR band could not be detected. This indicates that the heme iron-cyanide bond contains some covalent factor.

## References


(1) Yu, N.-T.; Benko, B.; Kerr, E. A.; Gersonde, K. *Proc. Natl. Acad. Sci. U.S.A.* **1984**, *81*, 5106-5110.

(2) Henry, E. R.; Rousseau, D. L.; Hopfield, J. J.; Noble, R. W.; Simon, S. R. *Biochemistry* **1984**, *24*, 5907-5918.

(3) Sitter, A. J.; Reczek, C. M.; Terner, J. *Biochim. Biophys. Acta.* **1985**, *828*, 229-235.

(4) Lopez-Garriga, J. J.; Anthony, W.; Kean, R. T.; Hoogland, H.; Wever, R.; Babcock, G. T. *Biochemistry* **1990**, *29*, 9387-9395.

(5) (a) Hu, S.; Treat, R. W.; Kincaid, J. R. *Biochemistry* **1993**, *32*, 10125-10130. (b) Al-Mustafa, J.; Kincaid, J. R. *Biochemistry* **1994**, *33*, 2191-2197.

(6) (a) Tsubaki, M.; Srivastava, R. B.; Yu, N.-T. *Biochemistry* **1982**, *21*, 1132-1140. (b) Uno, T.; Nishimura, Y.; Tsuboi, M.; Makino, R.; Iizuka, T.; Ishimura, Y. *J. Biol. Chem.* **1987**, *262*, 4549-4556. (c) Smulevich, G.; Evangelista-Kirkup, R.; English, A.; Spiro, T. G. *Biochemistry* **1986**, *25*, 4426-4430. (d) Evangelista-Kirkup, R.; Smulevich, G.; Spiro, T. G. *Biochemistry* **1986**, *25*, 4420-4425. (e) Rousseau, D. L.; Ondrias, M. R.; La Mar, G. N.; Kong, S. B.; Smith, K. M. *J. Biol. Chem.* **1983**, *258*, 1740-1746. (f) Nagai, M.; Yoneyame, Y.; Kitagawa, T. *Biochemistry* **1991**, *30*, 6495-6503. (g) Argade, P. V.; Ching, Y.; Rousseau, D. L. *Nature* **1984**, *225*, 329-331.

(7) (a) Hu, S.; Kincaid, J. R. *J. Am. Chem. Soc.* **1991**, *113*, 9760-9766. (b) Hu, S.; Kincaid, J. R. *J. Biol. Chem* **1993**, *268*, 6189-6193.

(8) (a) Brunner, H. *Naturwissenschaften* **1974**, *69*, 129. (b) van Wart, H. E.; Zimmer, J. *J. Biol. Chem.* **1985**, *260*, 8372-8377. (c) Kerr, E. A.; Yu, N.-T.; Bartnicki, D. E.; Mizukami, H. *J. Biol. Chem.* **1985**, 8360-8365. (d) Ogura, T.; Takahashi, S.; Shinzawa-Itoh, K.; Yoshikawa, S.; Kitagawa, T. *J. Am. Chem. Soc.* **1990**, *112*, 5630-5631. (e) Han, S.; Ching, Y.-c.; Roussian, D. L. *Biochemistry* **1990**, *29*, 1380-1384. (f) Varotsis, C.; Woodruff, W. H.; Babcock, G. T. *J. Am. Chem. Soc.* **1989**, *111*, 6439-6440. (g) Hu, S.; Schneider, A. J.; Kincaid, J. R. *J. Am. Chem. Soc.* **1991**, *113*, 4815-4822.

(9) (a) Ogura, T.; Takahashi, S.; Hirota, S.; Shinzawa-Itoh, K.; Yoshikawa, S.; Appleman, E. H.; Kitagawa, T. *J. Am. Chem. Soc.* **1993**, *115*, 8527-8536. (b) Hirota, S.; Ogura, T.; Appelman, E. H.; Shinzawa-Itoh, K.; Yoshikawa, S.; Kitagawa, T. *J. Am. Chem. Soc.* **1994**, *116*, 10564-10570.

(10) Phillips, S. E. V. *Nature* **1978**, *273*, 247-248. (b) Phillips, S. E. V. *J. Mol. Biol.* **1980**, *142*, 531-554. (c) Shaanan, B. *Nature* **1982**, *296*, 683-684. (d) Shaanan, B. *J. Mol. Biol.* **1983**, *171*, 31-59.

(11) Tsubaki, M.; Yu, N.-T. *Biochemistry* **1982**, *21*, 1140-1144.

(12) (a) Hu, S.; Kincaid, J. R. *J. Am. Chem. Soc.* **1991**, *113*, 9760-9766. (b) Hu, S.; Kincaid, J. R. **1993**, *268*, 6189-6193.

(13) Tanaka, T.; Yu, N.-T.; Chang, C. K. *Biophys. J.* **1987**, *52*, 801-805.

(14) Uno, T.; Hatano, K.; Nishimura, Y.; Arata, Y. *Inorg. Chem.* **1988**, *27*, 3215-3219.

(15) Surerus, K. K.; Ortling, W. A.; Fan, C.; Gurbiel, R. J.; Einarsdottir, O.; Antholine, W. E.; Dyer, R. B.; Hoffman, B. M.; Woodruff, W. H.; Fee, J. A. *Proc. Natl. Acad. Sci. USA* **1992**, *89*, 3195-3199.

(16) (a) Yoshikawa, S.; O'Keeffe, D. H.; Caughey, W. S. *J. Biol. Chem.* **1985**, *260*, 3518-3528. (b) Yoshikawa, S.; Caughey, W. S. *J. Biol. Chem.* **1990**, *265*, 7945-7958. (c) Tsubaki, M.; Yoshikawa. S. *Biochemistry* **1993**, *32*, 164-173.

(17) Geraci, G.; Parkhurst, L. J.; Gibson, Q. H. *J. Biol. Chem.* **1969**, *244*, 4664-4667.

(18) Yoshikawa, S.; Choc, M. G.; O'Toole, M. C.; Caughey, W. S. *J. Biol. Chem.* **1977**, *252*, 5498-5508.

(19) Ogura, T.; Yoshikawa, S.; Kitagawa, T. *Biochemistry* **1985**, *24*, 7746-7752.

(20) Nakamoto, K. in *Infrared and Raman Spectra of Inorganic and Coordination Compounds*, 4th ed.; Wiley-Interscience: New York, **1986**.

(21) Hirota, S.; Ogura, T.; Shinzawa-Itoh, K.; Yoshikawa, S.; Nagai, M.; Kitagawa, T. *J. Phys. Chem.* **1994**, 98, 6652-6660.

(22) (a) Phillips, S. E. V. *Nature* **1978**, *273*, 247-248. (b) Phillips, S. E. V. *J. Mo. Biol.* **1980**, *142*, 531-554.

(23) (a) Moore, J. N.; Hansen, P. A.; Hochstrasser, R. M. *Proc. Natl. Acad. Sci. USA* **1988**, *85*, 5062-5066. (b) Locke, B., Diller. R., & Hochstrasser, R. M. in *Advances in Spectroscopy* ; Clark, R. J. H. & Hester, R. E. Eds.; Wiley Johns & Sons: New York, **1993**, vol. 21, pp 1-47. (c) Ivanov, D.; Sage, J. T.; Keim, M.; Powell, J. R.; asher, S. A.; Champion, P. M. *J. Am. Chem. Soc.* **1994**, *116*, 4139-4140.

(24) Hu, S.; Morris, I. K.; Singh, J. P.; Smith, K. M.; Spiro, T. G. *J. Am. Chem. Soc.* **1993**, *115*, 12446-12458.

(25) Einarsdottir, O.; Choc, M. G.; Weldon, S.; Caughey, W. S. *J. Biol. Chem* **1988**, *263*, 13641-13654.
(26) Powers, L.; Chance, B.; Ching, Y.; Angiolillo, P. *Biophysical J.* **1981**, *34*,
(27) Tsubaki, M.; Mogi, T.; Hori, H.; Hirota, S.; Ogura, T.; Kitagawa, T.; Anraku, Y. *J. Biol. Chem.* **1994**, *269*, 30861-30868.
(28) Uno, T.; Mogi, T.; Tsubaki, M.; Nishimura, Y.; Anraku, Y. *J. Biol. Chem.* **1994**, *269*, 11912-11920.
(29) Caughey, W. S.; Dong, A.; Sampath, V.; Yoshikawa, S.; Zhao, X.-J. *J. Bioenerg. Biomem.* **1993**, *25*, 81-91.
(30) Han, S.; Madden, J. F.; Siegel, L. M.; Spiro, T. G. *Biochemistry* **1989**, *28*, 5477-5485.
(31) (a) Alben, J. O.; Caughey, W. S. *Biochemistry* **1968**, *7*, 175-183. (b) Caughey, W. S.; Shimada, H.; Choc, M. G.; Trucker, M. P. *Proc. Natl. Acad. Sci. U.S.A.* **1981**, *76*, 2903-2907.

**TABLE 6-1.** $\nu_{Fe\text{-}CN}$, $\delta_{FeCN}$, and $\nu_{CN}$ **Frequencies for Cyanoferric Heme Proteins**[a]

| | $^{12}C^{14}N$ | $^{13}C^{14}N$ | $^{12}C^{15}N$ | $^{13}C^{15}N$ | mode[f] | $^{12}C^{14}N$ | $^{13}C^{14}N$ | $^{12}C^{15}N$ | $^{13}C^{15}N$ | mode[f] | $\nu_{CN}$[g] |
|---|---|---|---|---|---|---|---|---|---|---|---|
| CCTIII Hb[b] | 452 | | | | $\nu_{Fe\text{-}CN}$ | 412 | | | | $\delta_{FeCN}$ | |
| HRP[c] | 456 | 452 | 453 | 448 | $\nu_{Fe\text{-}CN}$ | 405 | 397 | 405 | 397 | $\delta_{FeCN}$ | 2131 |
| MPO[c] | 453 | 448 | 453 | 448 | $\delta_{FeCN}$ | 361 | 359 | 359 | 356 | $\nu_{Fe\text{-}CN}$ | |
| LPO[d] | 453 | 448 | 452 | 445 | $\delta_{FeCN}$ | 360 | 358 | 357 | 356 | $\nu_{Fe\text{-}CN}$ | |
| (pH=7.0) | | | | | | (311) | (310) | (310) | (309) | | |
| LPO[d] | 452 | 446 | 451 | 444 | $\delta_{FeCN}$ | 355 | 353 | 353 | 352 | $\nu_{Fe\text{-}CN}$ | |
| (pH=10.5) | | | | | | (311) | (310) | (310) | (309) | | |
| SiRHP[e] | 451 | 445 | 449 | 443 | $\nu_{Fe\text{-}CN}$ | 390 | 376 | 388 | 374 | $\delta_{FeCN}$ | |
| | 451 | 434 | 449 | 434 | $\delta_{FeCN}$ | 352 | 350 | 348 | 346 | $\nu_{Fe\text{-}CN}$ | |
| Mb | 452 | 448 | 447 | 443 | $\nu_{Fe\text{-}CN}$ | couples with porphyrin modes around 300-440 | | | | $\delta_{FeCN}$ | 2126 |
| Hb | 452 | 448 | 447 | 443 | $\nu_{Fe\text{-}CN}$ | couples with porphyrin modes around 310-440 | | | | $\delta_{FeCN}$ | 2122 |
| CcO($aa_3$) | 478 | 473 | 473 | 468 | $\nu_{Fe\text{-}CN}$ | couples with porphyrin modes around 340-440 | | | | $\delta_{FeCN}$ | 2152 |

[a] In $cm^{-1}$ unit. [b] Reference 1. [c] Reference 4. [d] Reference 5. [e] Siroheme protein, reference 30.

[f] Assignment reported. [g] Reference 16.

**TABLE 6-2. $\nu_{Fe\text{-}XY}$ and $\nu_{XY}$ Frequencies for Ligand Bound Heme Proteins (Fe-X-Y)[a]**

| | Fe(II) · C O | | Fe(III) · C N$^-$ | | Fe(II) · $O_2$ |
|---|---|---|---|---|---|
| | $\nu_{Fe\text{-}CO}$[b] | $\nu_{CO}$ | $\nu_{Fe\text{-}CN}$[f] | $\nu_{CN}$ | $\nu_{Fe\text{-}O_2}$[i] |
| Hb | 505 | 1951[c] | 452 | 2122[g] | 568 |
| Mb | 509 | 1944[d] | 452 | 2126[g] | 571 |
| CcO | 516 | 1963.5[e] | 478 | 2152[h] | 571 |

[a] In $cm^{-1}$ unit. [b] Reference 21. [c] Reference 31a. [d] Reference 31b. [e] Reference 25. [f] This work. [g] Reference 16a. [h] Reference 16c. [i] Reference 9.

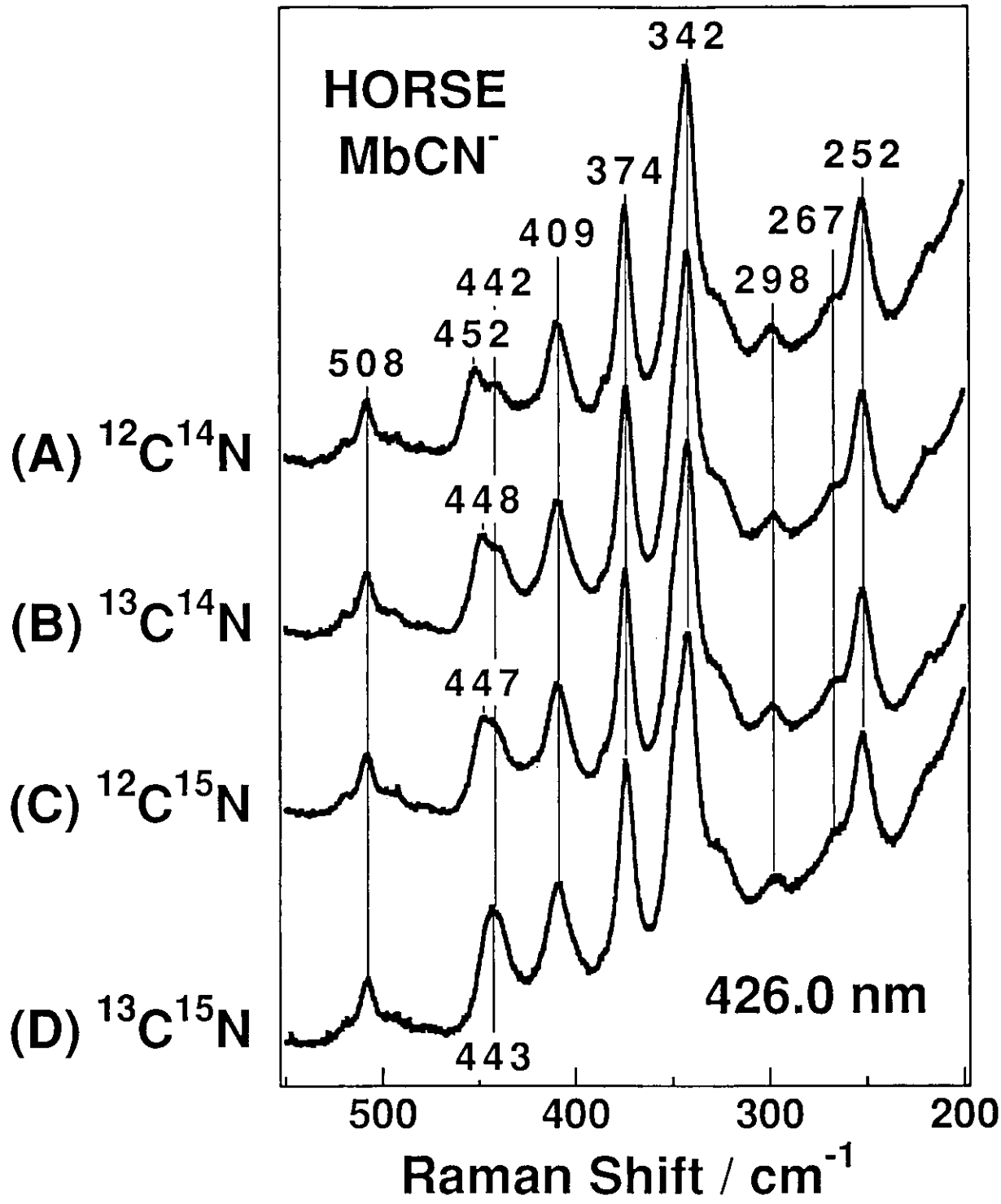


**Figure 6-1.** RR spectra in the 550 to 200 $cm^{-1}$ region for $^{12}C^{14}N^-$ (A), $^{13}C^{14}N^-$ (B), $^{12}C^{15}N^-$ (C), and $^{13}C^{15}N^-$ (D) adducts of ferric horse Mb. The ordinate scales of the bands in each spectrum are normalized by the intensity of porphyrin bands. Experimental conditions: excitation, 426.0 nm obtained with a dye laser and 5 mW (at the sample); detector, CCD; grating, 900 nm - 1200 grooves/mm; sample, 50μM (heme) in 50 mM Tris-HCl buffer, pH8.0, with ~1 mM KCN.

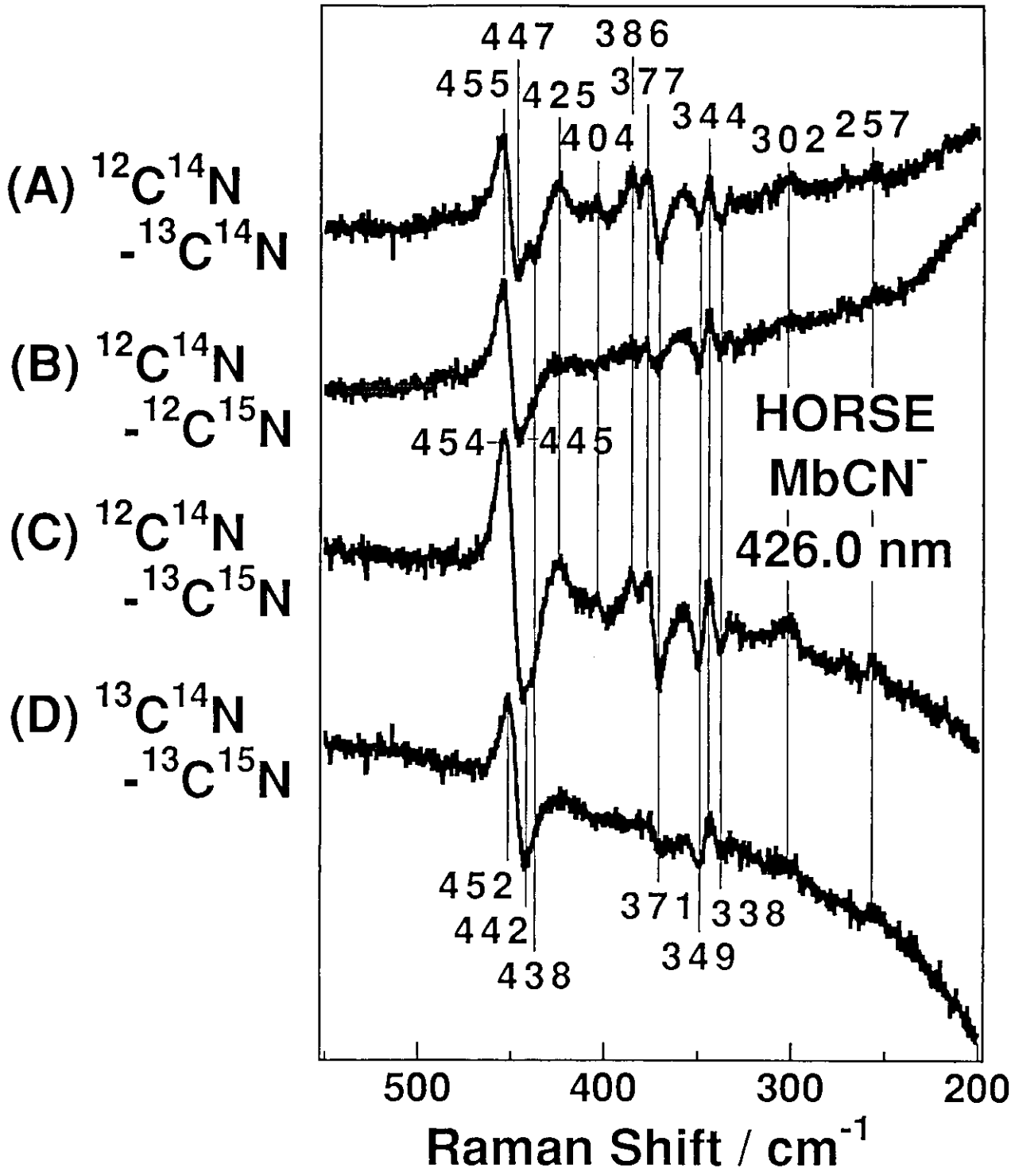


**Figure 6-2.** RR difference spectra of $MbCN^-$. Four pairs of differences, $Mb^{12}C^{14}N^-$ - $Mb^{13}C^{14}N^-$ (A), $Mb^{12}C^{14}N^-$ - $Mb^{12}C^{15}N^-$ (B), $Mb^{12}C^{14}N^-$ - $Mb^{13}C^{15}N^-$ (C), and $Mb^{13}C^{14}N^-$ - $Mb^{13}C^{15}N^-$ (D) are shown.

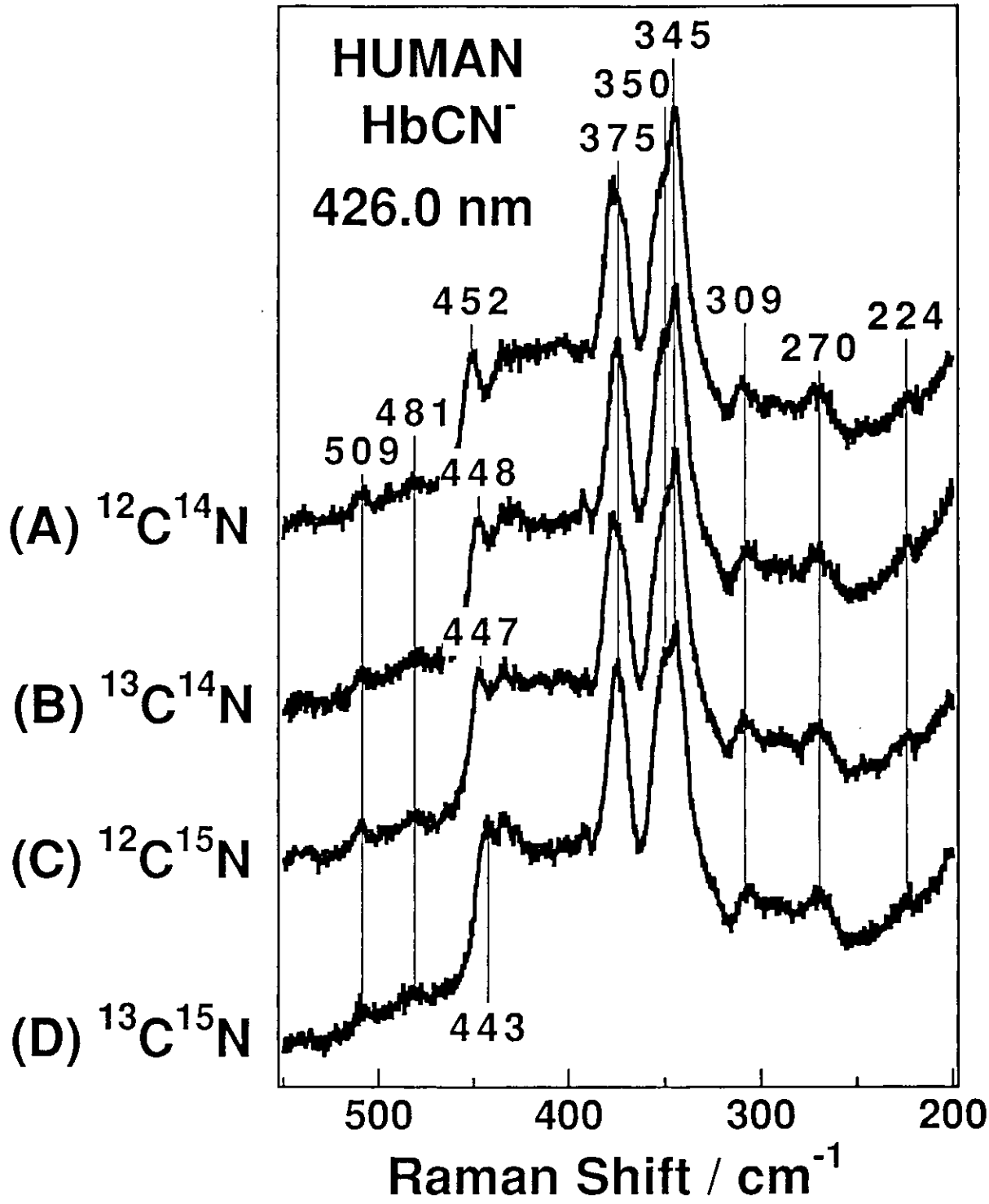


**Figure 6-3.** RR spectra in the 550 to 200 - $cm^{-1}$ region for $^{12}C^{14}N^-$ (A), $^{13}C^{14}N^-$ (B), $^{12}C^{15}N^-$ (C), and $^{13}C^{15}N^-$ (D) adducts of ferric human HbA. The ordinate scales of the bands in each spectrum are normalized by the intensity of porphyrin bands. Experimental conditions were the same as those for Figure 6-1.

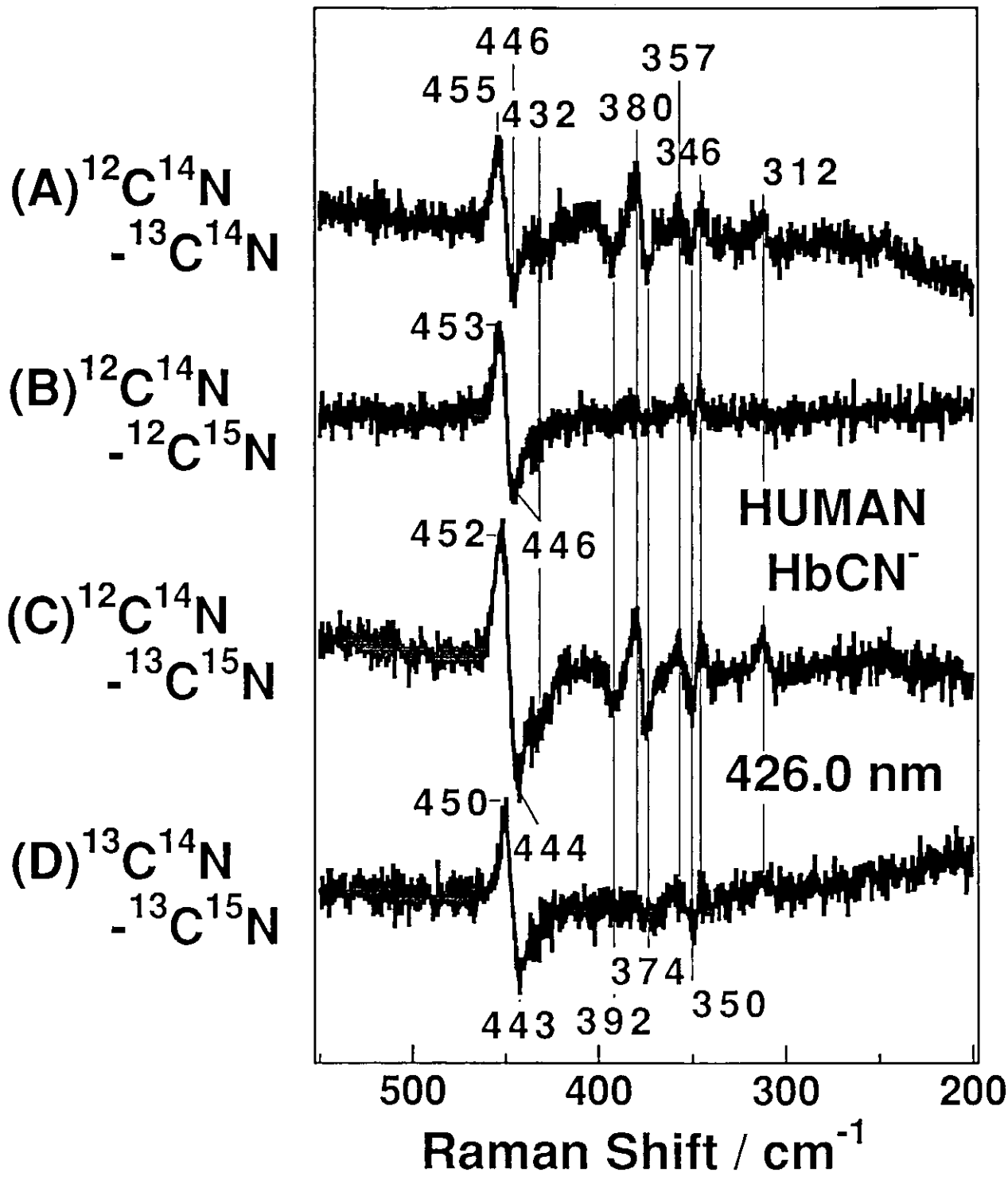


**Figure 6-4.** RR difference spectra of $HbCN^-$. Difference calculations were carried out in the way as in Figure 6-2. The difference are specified in the left side.

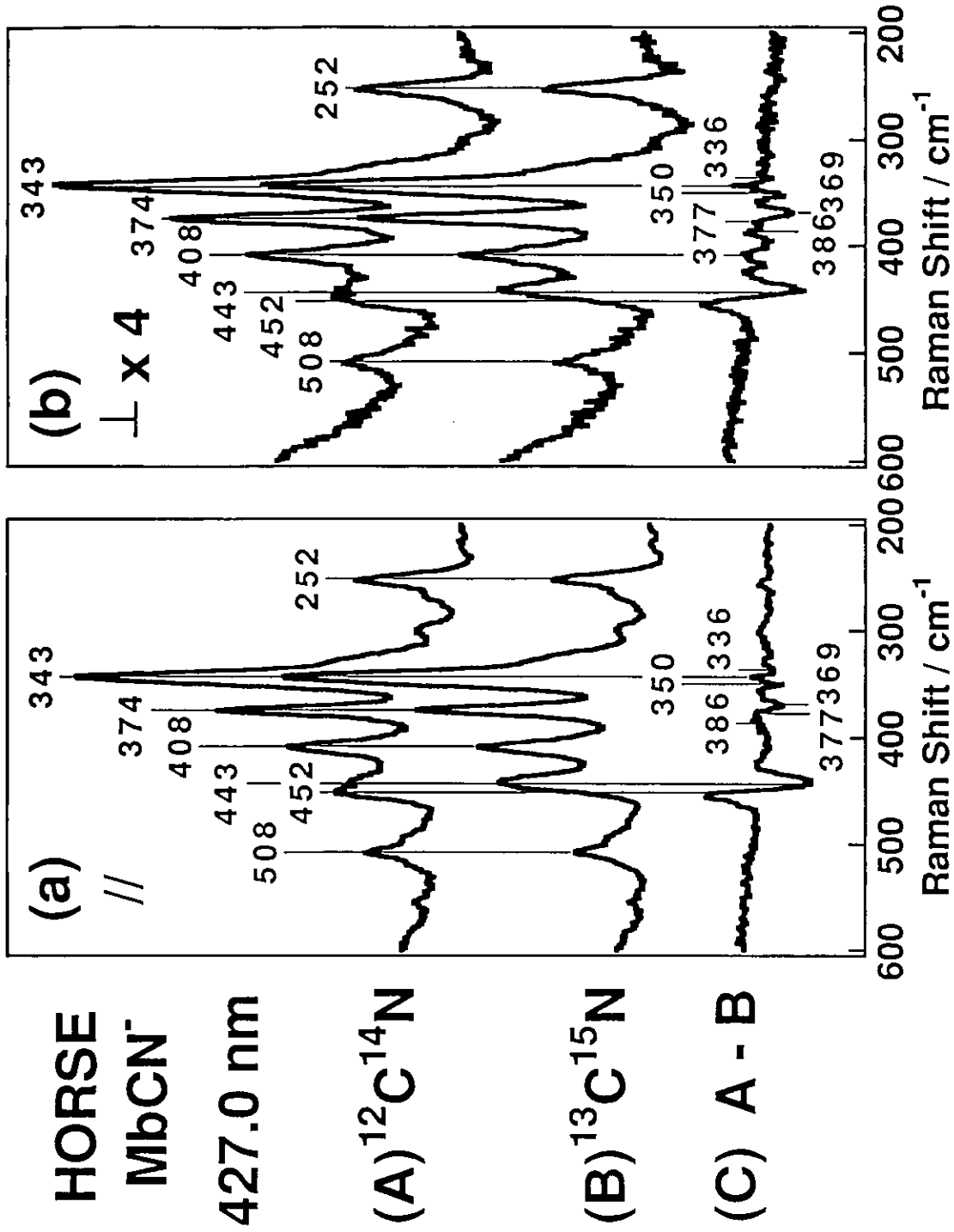


**Figure 6-5.** RR spectra in the region from 600 to 200 - $cm^{-1}$ of polarized components for $CN^-$ bound horse Mb. Traces A, B, and C represents the parallel (//,a) and perpendicular (⊥,b) polarized components of $Mb^{12}C^{14}N^-$ (A) and $Mb^{13}C^{15}N^-$ (B), and the difference spectrum (C), respectively. The intesities of the perpendicular spectra are multiplied by a factor of 0.25. Experimental conditions: excitation, 427.0 nm and 5 mW (at the sample); detector, diode array; grating, 900 - 1200 grooves/mm; sample, 50μM (heme) in 50 mM Tris-HCl buffer, pH8.0, with ~1 mM KCN.

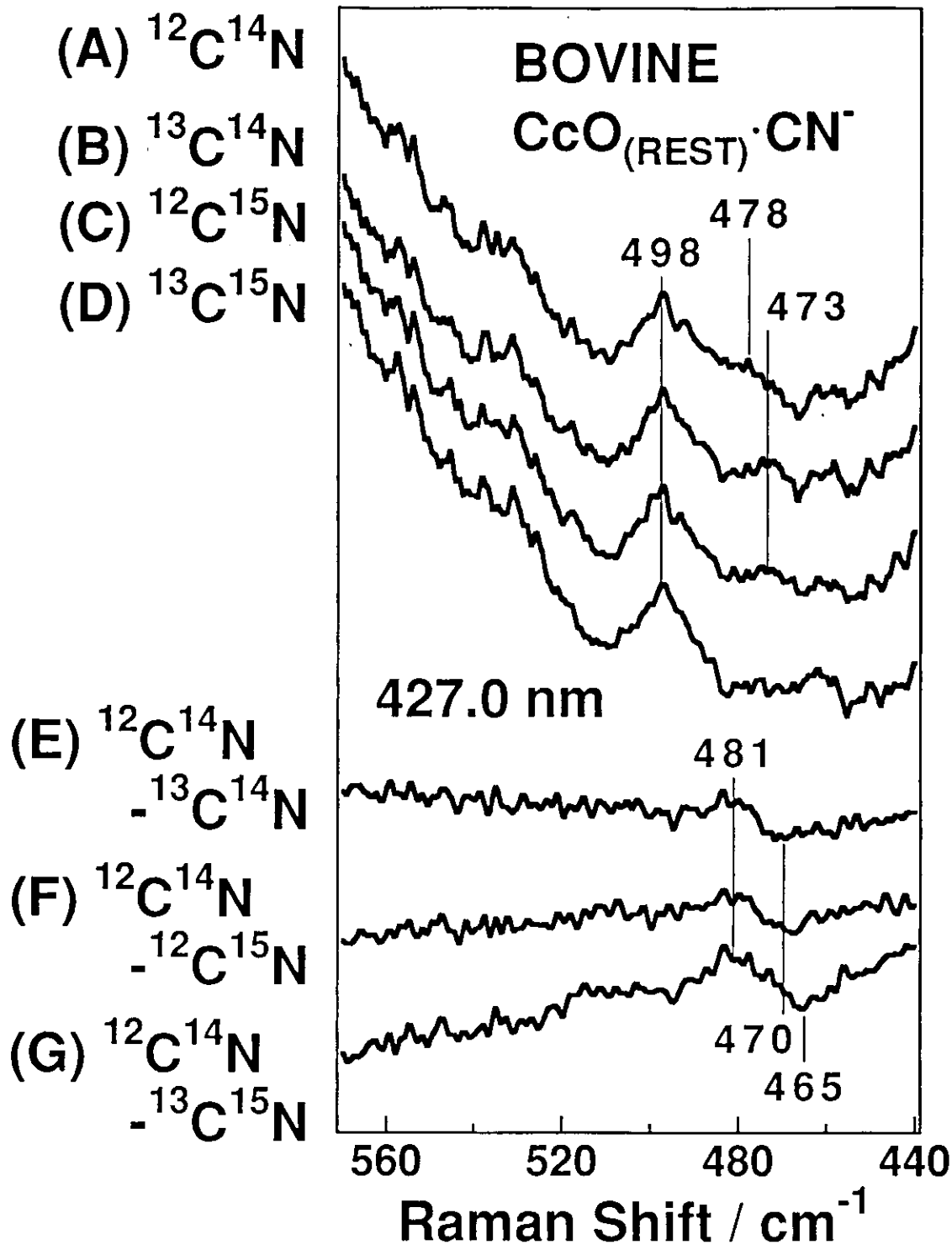


**Figure 6-6.** RR spectra in the 570 to 440 - $cm^{-1}$ region for $^{12}C^{14}N^-$ (A), $^{13}C^{14}N^-$ (B), $^{12}C^{15}N^-$ (C), and $^{13}C^{15}N^-$ (D) adducts of resting bovine CcO, and their difference spectra $Mb^{12}C^{14}N^-$ - $Mb^{13}C^{14}N^-$ (E), $Mb^{12}C^{14}N^-$ - $Mb^{12}C^{15}N^-$ (F), and $Mb^{12}C^{14}N^-$ - $Mb^{13}C^{15}N^-$ (G). The ordinate scales of the bands in A - D are normalized by the intensity of porphyrin bands. Experimental conditions: excitation, 427.0 nm and 1 mW (at the sample); grating, 900 nm - 1200 grooves/mm; sample, 50μM (heme) in 50 mM sodium phosphate buffer, pH7.2, with ~1 mM KCN.

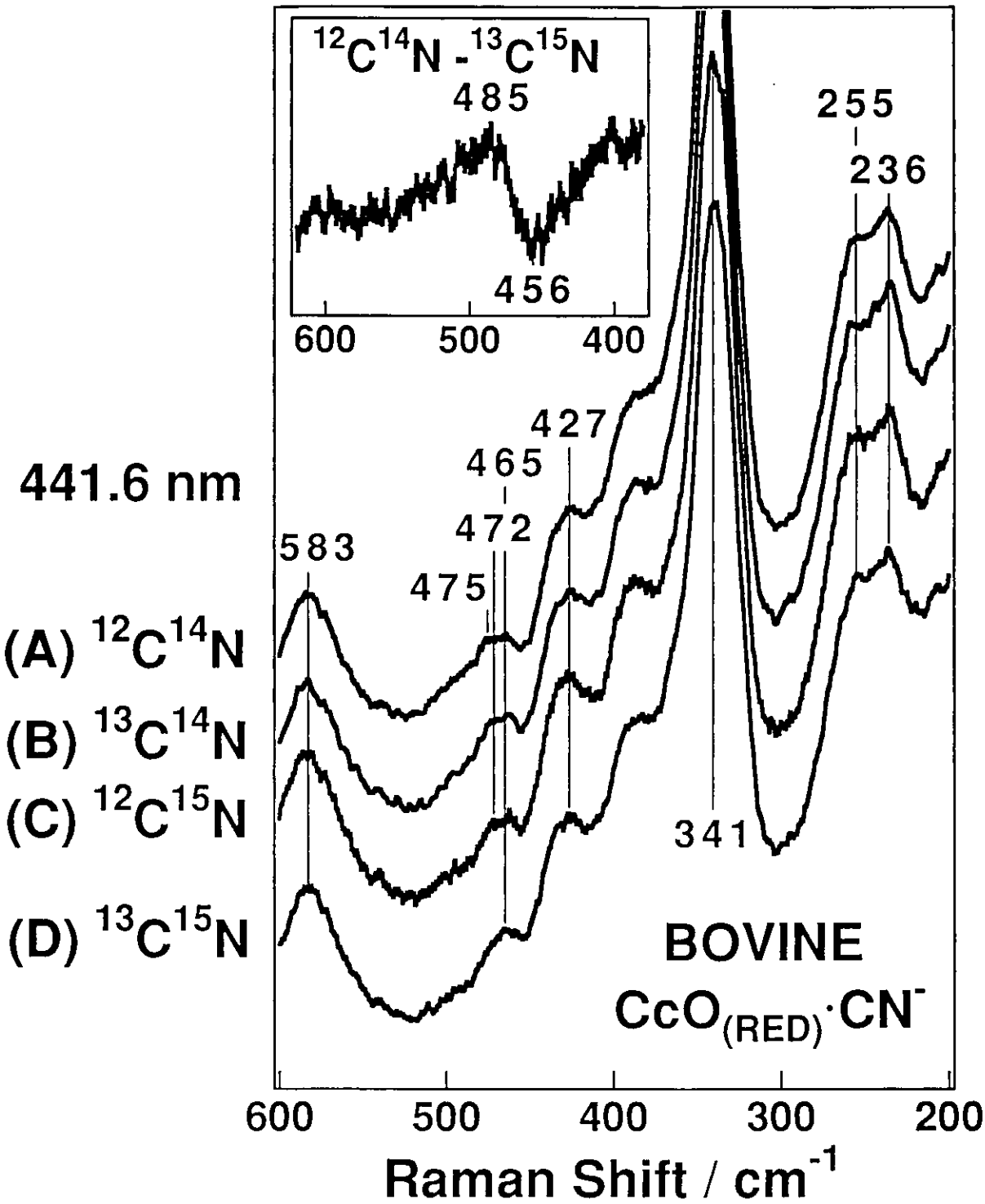


**Figure 6-7.** RR spectra in the 600 to 200 - $cm^{-1}$ region for $^{12}C^{14}N^-$ (A), $^{13}C^{14}N^-$ (B), $^{12}C^{15}N^-$ (C), and $^{13}C^{15}N^-$ (D) adducts of reduced bovine CcO. The difference spectrum $CcO_{red}$· $^{12}C^{14}N^-$ - $CcO_{red}$· $^{13}C^{15}N^-$ is shown in the inset. The ordinate scales of the bands in each spectrum are normalized by the intensity of porphyrin bands. Experimental conditions: excitation, 427.0 nm and 5 mW (at the sample); grating, 500 nm - 1200 grooves/mm; sample, 50μM (heme) in 50 mM sodium phosphate buffer, pH7.2, with ~10 mM KCN.

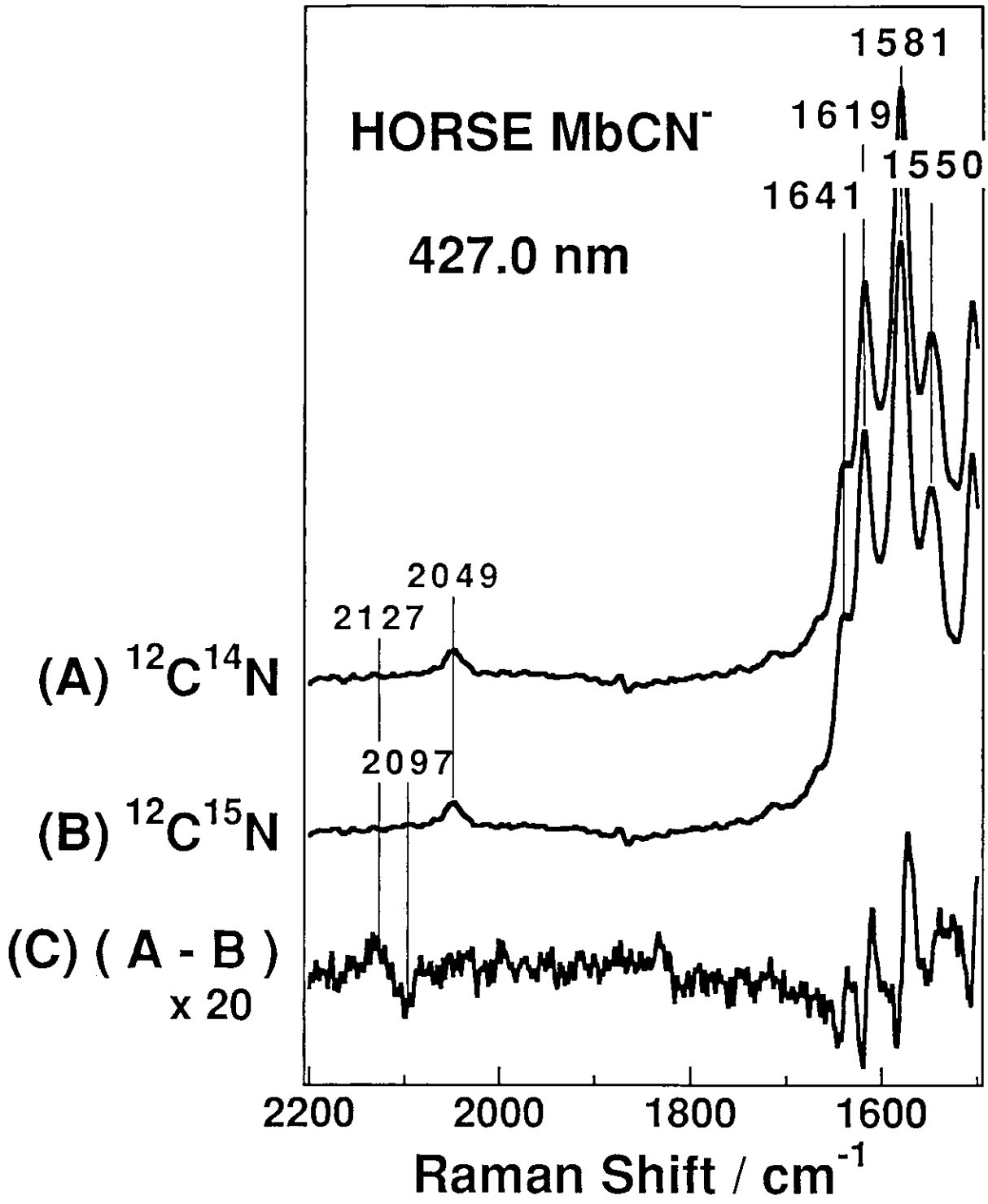


**Figure 6-8.** RR spectra in the 2200 to 1500 - $cm^{-1}$ region for $^{12}C^{14}N^-$ (A) and $^{12}C^{15}N^-$ (B), and $^{13}C^{15}N^-$ (D) adducts of horse Mb, and their difference spectrum (C). The ordinate scales of the bands in each spectrum are normalized by the intensity of porphyrin bands. Experimental conditions were the same as those for Figure 6-5 except for using a 500 nm - 1200 grooves/mm grating and a flow cell.

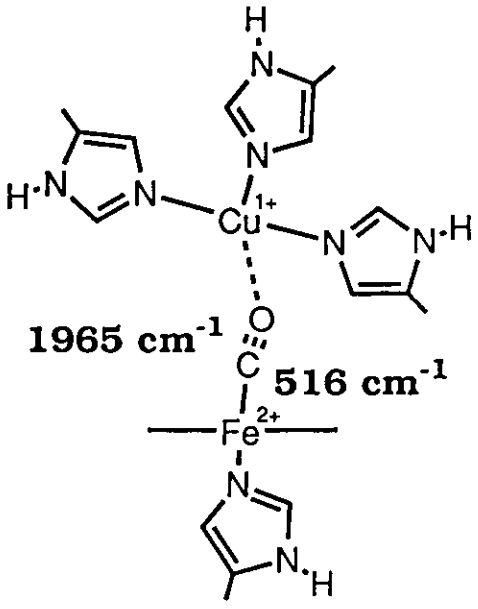


CcO·CO

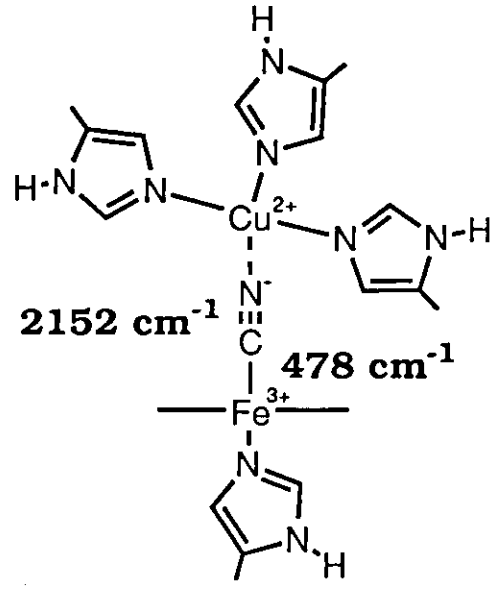


CcO·CN⁻

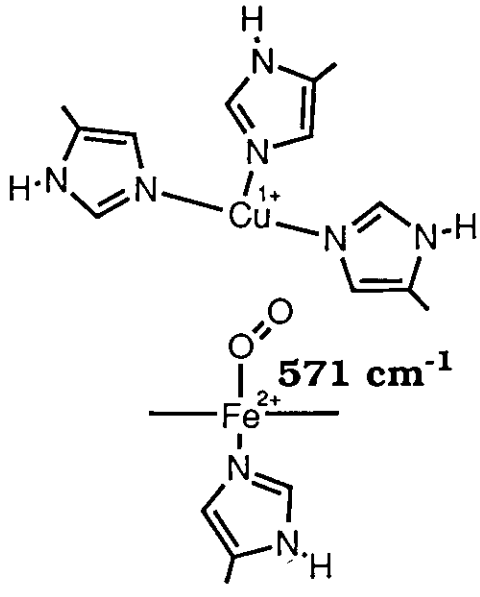


CcO·$O_2$

**Figure 6-9.** Models for ligand bound cytochrome *c* oxidase.

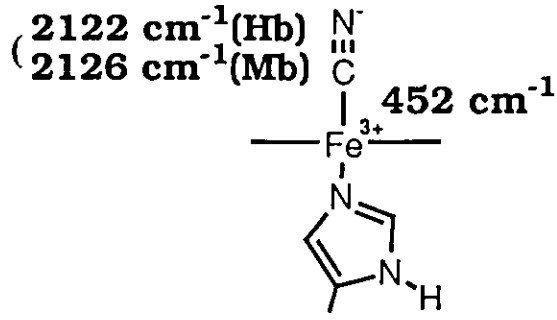


Hemoglobin
Myoglobin

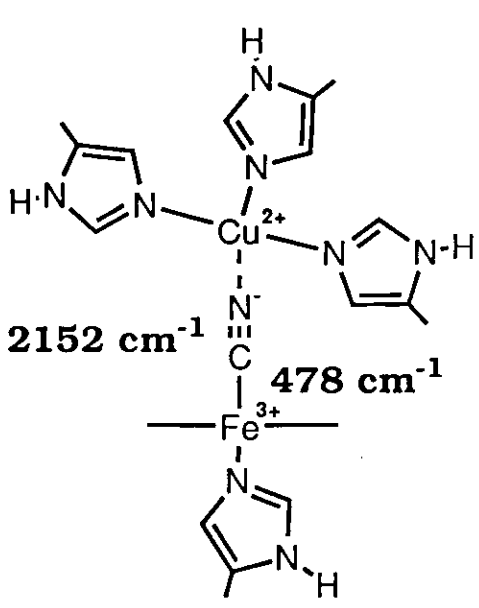


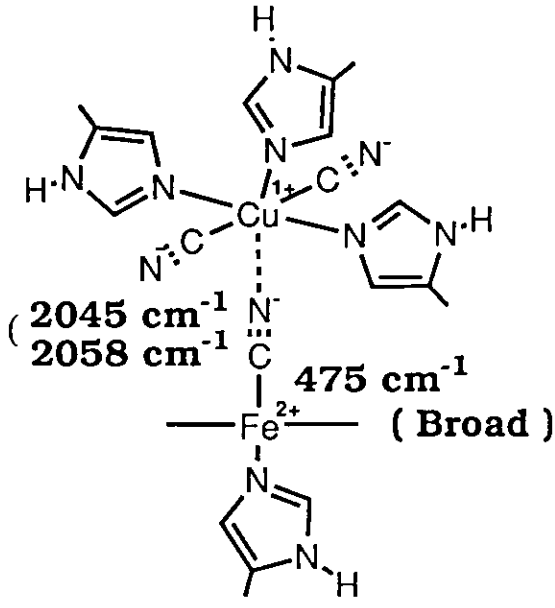


Cytochrome $aa_3$
Oxidized

Cytochrome $aa_3$
Reduced

**Figure 6-10.** Models for $CN^-$ bound heme proteins.

# Chapter I-7.

# Observation of a New Water-Isotope-Sensitive Raman Band for Oxidized Heme Proteins at Alkaline pH: Implication for the Fe-$OH^-$ Stretching Mode of Low-Spin Species

## Abstract

A new water-isotope-sensitive Raman band was found for hydroxy-myoglobin ($MbOH^-$) and hydroxy-hemoglobin ($HbOH^-$) and was assigned to the Fe-$OH^-$ stretching mode ($\nu_{Fe\text{-}OH^-}$) of low-spin species. The frequency of $\nu_{Fe\text{-}OH^-}$ was higher for low-spin species than for high-spin species, which was located at 486 ($Mb^{16}OH^-$), 473 ($Mb^{16}OD^-$), 465 ($Mb^{18}OH^-$), and 459 ($Mb^{18}OD^-$) $cm^{-1}$. $\nu_{Fe\text{-}OH^-}$ for low-spin species was located at 549 $cm^{-1}$ for $Mb^{16}OH^-$, and shifted to 538, 528, and 522 $cm^{-1}$ with $Mb^{16}OD^-$, $Mb^{18}OH^-$, and $Mb^{18}OD^-$, respectively. The corresponding band appeared at 552 $cm^{-1}$ for $Hb^{16}OH^-$, and shifted to 543 $cm^{-1}$ with $Hb^{16}OD^-$. When the temperature was decreased, the intensity of $\nu_{Fe\text{-}OH^-}$ for low-spin species against that of $\nu_{Fe\text{-}OH^-}$ for high-spin species decreased. The observed isotopic frequency shifts of the $\nu_{Fe\text{-}OH^-}$ for different water-isotopes were very similar for high- and low-spin species, indicating that the geometry of the $FeOH^-$ unit of hydroxy complexes are similar between the high- and low-spin states. Other water-isotope-sensitive bands were also observed around 340 - 390 $cm^{-1}$.

## 7.1 Introduction

Investigations on hydroxy complexes of heme proteins have been done extensively to deduce characters of heme environments around the ferric heme iron. Hydroxy complexes of metMb and metHb are in an equilibrium between the high- and low-spin states.[1] The population of high-spin species in hydroxy derivatives of metMb and metHb are quite different at room temperature; 70 % and 45 %, respectively.[2] Similar hydroxy complexes of heme proteins have been identified in the reaction of CcO with oxygen, and also in the reaction of reduced HRP with oxygen.

The Fe-$OH^-$ stretching ($\nu_{Fe\text{-}OH^-}$) band for hydroxy complexes of hydroxy-metMb and -Hb have been detected for only high-spin species at 490 and 495 $cm^{-1}$, as discussed in chapter I-1.[3] The $\nu_{Fe\text{-}OH^-}$ band for reaction intermediates of CcO and HRP are detected at 450 and 503 $cm^{-1}$, respectively.[4-8] The $\nu_{Fe\text{-}OH^-}$ band for methemerythrin has been detected at 565 $cm^{-1}$.[9]

The low-spin $\nu_{Fe\text{-}OH^-}$ band in heme proteins has not been identified yet, and the relationship between the structures of the $FeOH^-$ unit in low- and high-spin states has not been clarified. Therefore, we investigate the RR spectra of hydroxy complexes more carefully to obtain $\nu_{Fe\text{-}OH^-}$ of the low-spin species and to discuss the dependence of the characters of the Fe-$OH^-$ bond on the spin states.

## 7.2 Methods

Raman scattering was excited at 441.6 with a He-Cd laser (Kinmon Electronics, Model CD1805B) or at 413.1 nm with a $Kr^+$ ion laser (Spectra Physics, Model 2016), and was detected with a diode array (PAR 1421HQ) cooled to -20 °C and attached to a single polychromator (Ritsu Oyo Kogaku, DG-1000) using a 900-nm blaze, 1200 grooves/mm grating or a double monochromator (Spex, 1404). The slitwidth of 200 μm and slitheight of 1 cm were used. The laser power at the sample point was adjusted to 6 - 32 mW with a ND filter, and the width of the laser beam at the sample point was ca. 50 μm. A spinning cell (3500 rpm) was used for measurements carried out at room temperature. Low temperature Raman measurements were carried out by a cell spun at 1600 rpm in a cryostat that was cooled by flowing cold $N_2$ gas. Raman shifts were calibrated with ethanol and acetone. Uncertainties of the Raman bands and peaks for the

difference spectra were ±1 $cm^{-1}$ and ± 2 $cm^{-1}$, respectively, when measured with the single polychromator, and ±2 $cm^{-1}$ and ± 3 $cm^{-1}$ when measured with the double monochromator.

MetMb and MetHb obtained by diluting horse Mb (Sigma, type M-0630) and horse Hb (Sigma, type H-4632) were dissolved in 250 mM $Na_2CO_4$-$NaHCO_4$ buffer, pH 10.5, which contained little amount of potassium ferricyanide for complete oxidation of the sample. The ferricyanide was removed by gel filtration through Sephadex G25 column, and the eluted solution was concentrated by Amicon filtration first, and then diluted with $H_2O$, $D_2O$ (Showa-Electric, 99.5 atom% for D), $H_2{}^{18}O$ (ICON, 95 atom% for $^{18}O$), or $D_2{}^{18}O$ (ICON, 100 atom% for D and 98 atom% for $^{18}O$) to measuring concentrations.

### 7.3 Results

Figure 7-1 shows the RR spectra in the 600 to 300 $cm^{-1}$ region for $^{16}OH^-$ (A), $^{16}OD^-$ (B), $^{18}OH^-$ (C) and $^{18}OD^-$ (D) adducts of horse Mb excited at 441.6 nm. The Raman band at 486 $cm^{-1}$ of $Mb^{16}OH^-$ (A) shifted to 473 $cm^{-1}$ in $Mb^{16}OD^-$ (B), to 465 $cm^{-1}$ in $Mb^{18}OH^-$ (C), and to 459 $cm^{-1}$ in $Mb^{18}OD^-$ (D). This band showed a monotonous down shift in frequency upon the increase of the mass of $OH^-$, in agreement with the results reported so far for $\nu_{Fe\text{-}OH^-}$.[4,5] This band is assigned to the high-spin species from its excitation profile. The bandwidth of this band was broader compared to the porphyrin bands for all $OH^-$-isotope adducts. Apart from this difference, the relative intensity of the band at 547 $cm^{-1}$ seemed to be intense in $^{16}OH^-$ and $^{16}OD^-$ adducts compared with those in $^{18}OH^-$ and $^{18}OD^-$ adducts. To clarify this difference we calculated the difference spectra with regard to the $^{16}OH^-$ adduct Mb.

The calculated difference spectra between the four spectra in Figure 7-1 are shown in Figure 7-2. The difference pattern around 480 $cm^{-1}$ corresponds to $\nu_{Fe\text{-}OH^-}$ of high-spin species. What we want to stress is that a difference pattern exists around 550 $cm^{-1}$. This difference pattern corresponds to the $\nu_{Fe\text{-}OH^-}$ of low-spin species as discussed later. There also appeared difference peaks at 355 and 388 $cm^{-1}$ and trough at 339 and 379 $cm^{-1}$ when H of $OH^-$ was changed with D.

Figure 7-3 shows the RR spectra in the 600 to 300 $cm^{-1}$ region for $^{16}OH^-$ (A) and $^{18}OH^-$ (B) adducts of horse Mb excited at 406.7 nm and their

difference spectra (C). The difference peaks were clearly observed at 486/464 and 550/528 $cm^{-1}$. The intensity ratio of the difference peaks around 550 $cm^{-1}$ to those around 480 $cm^{-1}$ increased compared to the corresponding difference spectrum obtained by excitation at 441.6 nm (Figure 7-2B).

Figure 7-4 shows the RR spectra in the 600 to 300 $cm^{-1}$ region for $^{16}OH^-$ (A, C) $^{16}OD^-$ (B, D) adducts of horse Mb at 20 (A, B) and 5 °C (C, D), and their differences (E, F, G) excited at 406.7 nm. The difference pair is specified at the left for each difference spectrum. The ratio of the difference peaks around 550 $cm^{-1}$ against that around 480 $cm^{-1}$ also increased compared to the corresponding difference spectrum of $Mb^{16}OH^-$ - $Mb^{16}OD^-$ excited at 441.6 nm (Figure 7-2A). A peak at 372 $cm^{-1}$ existed in the difference spectra between 20 °C and 5 °C in both $OH^-$ (F) and $OD^-$ (G) adducts of Mb.

Figure 7-5 shows the RR spectra in the 600 to 300 $cm^{-1}$ region for $^{16}OH^-$ (A) and $^{16}OD^-$ (B) adducts of horse Hb excited at 406.7 nm and their difference spectra (C). Difference peaks appeared at 491/479 and 552/543 $cm^{-1}$ close to the frequency of the difference peaks obtained for $MbOH^-$ (Figure 7-2). The intensity ratio of the difference peaks around 550 $cm^{-1}$ to that around 480 $cm^{-1}$ increased compared to that for $MbOH^-$ excited at the same wavelength (Figure 7-4E).

Figure 7-6 shows the RR spectra in the 600 to 300 $cm^{-1}$ region for $^{16}OH^-$ adduct of horse Hb excited at 406.7 nm at different temperatures; (A) 5 °C, (B) -25 °C, (C) -55 °C, and (D) -85 °. The band at 484 $cm^{-1}$ arises from the solvent. The relative intensity of the band at 553 $cm^{-1}$ to that of the 491 $cm^{-1}$ band increased as the temperature decreased. This strongly suggests that the 553 $cm^{-1}$ band arises from the low-spin species, and is assignable to $\nu_{Fe\text{-}OH^-}$ of the low-spin species.

## 7.4 Discussions

### $\nu_{Fe\text{-}OH^-}$ for High Spin Species

The band at 486 $cm^{-1}$ was assigned to $\nu_{Fe\text{-}OH^-}$ on the basis of the excitation profile of this band having similar character to high-spin marker of porphyrin bands.[3] The intensity of the 486 $cm^{-1}$ band decreased upon lowering the temperature. Therefore it is reasonable to assign this band to $\nu_{Fe\text{-}OH^-}$ of the high-spin species ($\nu_{Fe\text{-}OH^-}$(hs)). The bandwidths of

this band for $^{16}OD^-$, $^{18}OH^-$ and $^{18}OD^-$ adducts were 20 ~ 21 $cm^{-1}$, while it was 26 $cm^{-1}$ for the $^{16}OH^-$ adduct, when they were estimated from Gaussian band fitting for the $\nu_{Fe\text{-}OH^-}$(hs) bands of Figure 7-1. The $\nu_{Fe\text{-}OH^-}$ (hs) bands were broader than the porphyrin bands and were fitted very well by symmetric Gaussian shapes. This suggest that $^{16}OH^-$ is bound in various conformations to the heme as seen in other ligand bound heme proteins.[10]

### $\nu_{Fe\text{-}OH^-}$ for Low Spin Species

The difference spectra for hydroxy complexes of metMb and metHb exhibited a shift pattern around 550 $cm^{-1}$ (Figures 7-2, 7-3, 7-4, 7-5). The intensities of the difference peaks around 540 $cm^{-1}$ relative to that around 480 $cm^{-1}$ was stronger for $HbOH^-$ than for $MbOH^-$ (Figures 7-4E, 7-5) when they are excited at the same wavelength. At room temperature, the population of low-spin species in $HbOH^-$ (55 %) is larger than that of $MbOH^-$ (30 %).[2] The intensity of the 550 $cm^{-1}$ band relative to the 490 $cm^{-1}$ band increased as the temperature was decreased to -85 °C. This strongly supports to assign this 550 $cm^{-1}$ band to the $\nu_{Fe\text{-}OH^-}$ mode of low-spin species ($\nu_{Fe\text{-}OH^-}$(ls)), in agreement with very recent reports.[11] The $\nu_{Fe\text{-}OH^-}$(ls) has higher frequencies by about 60 $cm^{-1}$ than those of $\nu_{Fe\text{-}OH^-}$(hs). This means that the Fe-$OH^-$ bond is stronger and shorter in low-spin species than in high-spin species. In ferric hydroxy model porphyrins, the $\nu_{Fe\text{-}OH^-}$(ls) frequency is reported to be higher by 50 $cm^{-1}$ than the $\nu_{Fe\text{-}OH^-}$(hs) frequency, and the results obtained here are consistent with it.[12]

### Fe-$OH^-$ Unit for High- and Low-Spin Species

The frequencies for the $\nu_{Fe\text{-}OH^-}$(hs) and $\nu_{Fe\text{-}OH^-}$(ls) bands are read from Figure 7-1 and Figures 7-1, 7-3, and 7-4, respectively, and are listed in TABLE 7-1 together with the frequency shifts. The frequency shifts of the bands were very similar between high- and low-spin species suggesting similar $OH^-$ conformation in the $FeOH^-$ unit for the high- and low-spin species. The frequency shifts of the $\nu_{Fe\text{-}OH^-}$ bands for high- and low-spin species upon substitution from $^{16}OH^-$ to $^{16}OD^-$ estimated from a simple diatomic oscillator are 11 and 13 $cm^{-1}$, respectively. These values are very close to the frequency shifts observed. If the $FeOH^-$ unit was bent significantly $\nu_{Fe\text{-}OH^-}$ would be less sensitive to the mass of the terminal H atom, and the frequency shift for $^{16}OD^-$ would be less. This suggests that

H of $OH^-$ moves together with the oxygen atom for $\nu_{Fe\text{-}OH^-}$ and the $FeOH^-$ unit in both high- and low-spin species have rather linear conformations. The difference between the spectra at 5 °C and 20°C for $MbOH^-$ indicates the presence of a difference at 372 $cm^{-1}$ (Figure 7-4). This band is assigned to the bending vibration of the propionic side chain.[13] Therefore, this difference may mean that the high-spin species has this mode at slightly lower frequency than the low-spin species with stronger intensity than the low-spin species.

**Water-Isotope Sensitive Band in the Low Frequency Heme Modes**

A shift pattern appeared in the difference spectra between $MbOH^-$ and $MbOD^-$ in the frequency region around 350 - 390 $cm^{-1}$ (Figure 7-2). This shift pattern was observed only when the mass of H differed. This shift was not clear in the spectra excited at 406.7 nm. A band at 377 $cm^{-1}$ observed at room temperature is assigned to the $\delta(C_\beta C_c C_d)$ propionate bending mode on the basis of the frequency shift upon propionate deuteration. The difference peak could be attributed to the changes in this band.[11] The propionic side chain is hydrogen bonded to water in the heme pocket. The $H_2O/D_2O$ exchange involves a change from hydrogen bond to deuterium bond. Presumably, the intensity of the RR band is decreased by a change from the hydrogen bond to the deuterium bond, and the difference peak appeared.[11]

## References


(1) (a) Beetlestone, J.; George, P. *Biochemistry* **1964**, *3*, 707-714. (b) Smith, D. W.; Williams, R. J. P. *Biochem. J.* **1968**, *110*, 297-301. (c) Beetlestone, J.; George, P. *Biochemistry* **1964**, *3*, 707-714.

(2) (a) George, P.; Beetlestone, J.; Griffith, J. S. *Rev. Mod. Phys.* **1964**, *36*, 441-463. (b) Yonetani, T.; Iizuka, T.; Waterman, M. R. *J. Biol. Chem.* **1971**, *24*, 7683-7689.

(3) (a) Asher, S. A.; Vickery, L. E.; Schuster, T. M. *Biochemistry* **1977**, *16*, 5849-5856. (b) Asher, S. A.; Schuster, T. M. *Biochemistry* **1979**, *18*, 5377-5387. (c) Asher, S. A. *Methods in Enzymology* **1981**, *76*, 312-413.

(4) Desbois, A.; Lutz, M.; Ramaprasad *Biochemisty* **1979**, *18*, 1510-1518.

(5) Ogura, T.; Takahashi, S.; Shinzawa-Itoh, K.; Yoshikawa, S.; Kitagawa, *T. Bull. Chem. Soc. Jpn.* **1991**, 64, 2901-2907.

(6) Han, S.; Ching, Y.-C.; Rousseau, D. L. *Nature* **1990**, *348*, 89-90.

(7) Han, S.; Ching, Y.-C.; Rousseau, D. L. *J. Biol. Chem.* **1989**, *264*, 6604-6607.

(8) Sitter, A. J.; Shifflett, J. R.; Terner, J. *J. Biol. Chem.* **1988**, *263*, 13032-13038.

(9) Shiemke, A. K.; Loehr, T. M.; Sanders-Loehr, J. *J. Am. Chem. Soc.* **1986**, *108*, 2437-2443.

(10) Hirota, S.; Ogura, T.; Appelman, E. V.; S.; Shinzawa-Itoh, K.; Yoshikawa, S.; Kitagawa, T. *J. Am. Soc. Chem.*, in press.

(11) Feis, A.; Marzocchi, M. P.; Paoli, M.; Smulevich, G. *Biochemistry* **1994**, *33*, 4577-4583.

(12) Rodgers, K. R.; Reed, R. A.; Spiro, T. G.; Su, Y. O. *New. J. Chem.* **1992**, *16*, 533-535.

(13) Hu, S.; Morris, I. K.; Singh, J. P.; Smith, K. M.; Spiro, T. G. *J. Am. Chem. Soc.* **1993**, *115*, 12446-12458.

**TABLE 7-1. $\nu_{Fe\text{-}OH^-}$ Frequencies and Frequency Shifts of $MbOH^-$[a]**

| | $^{16}OH^-$ | $^{16}OD^-$ | $^{18}OH^-$ | $^{18}OD^-$ |
|---|---|---|---|---|
| $\nu_{Fe\text{-}OH^-}$(hs) | 486 | 473 (13) | 465 (21) | 459 (27) |
| $\nu_{Fe\text{-}OH^-}$(ls) | 550 | 538 (12) | 528 (22) | 522 (28) |

[a] In $cm^{-1}$ unit.

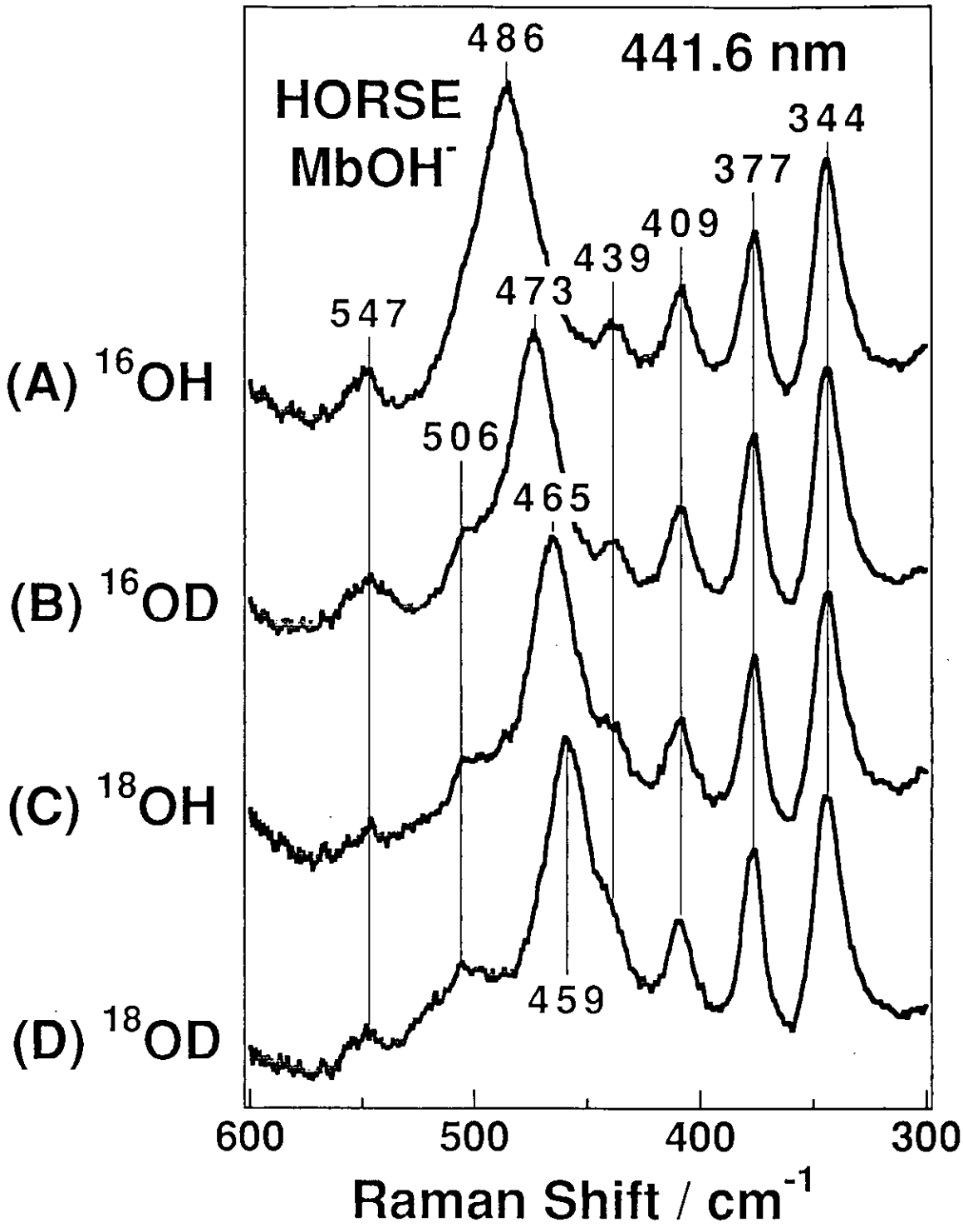


**Figure 7-1.** The RR spectra in the 600 to 300 $cm^{-1}$ region of the $^{16}OH^-$ (A), $^{16}OD^-$ (B), $^{18}OH^-$ (C), and $^{18}OD^-$ (D) adducts of horse Mb. The ordinate scales of spectra A - C are normalized by the intensity of the porphyrin bands. Experimental conditions: excitation, 441.6 nm, 32 mW at the sample; spectrometer, single polychromator; sample, 290 μM (heme) in 10 mM Tris-HCl buffer, pH 10.4.

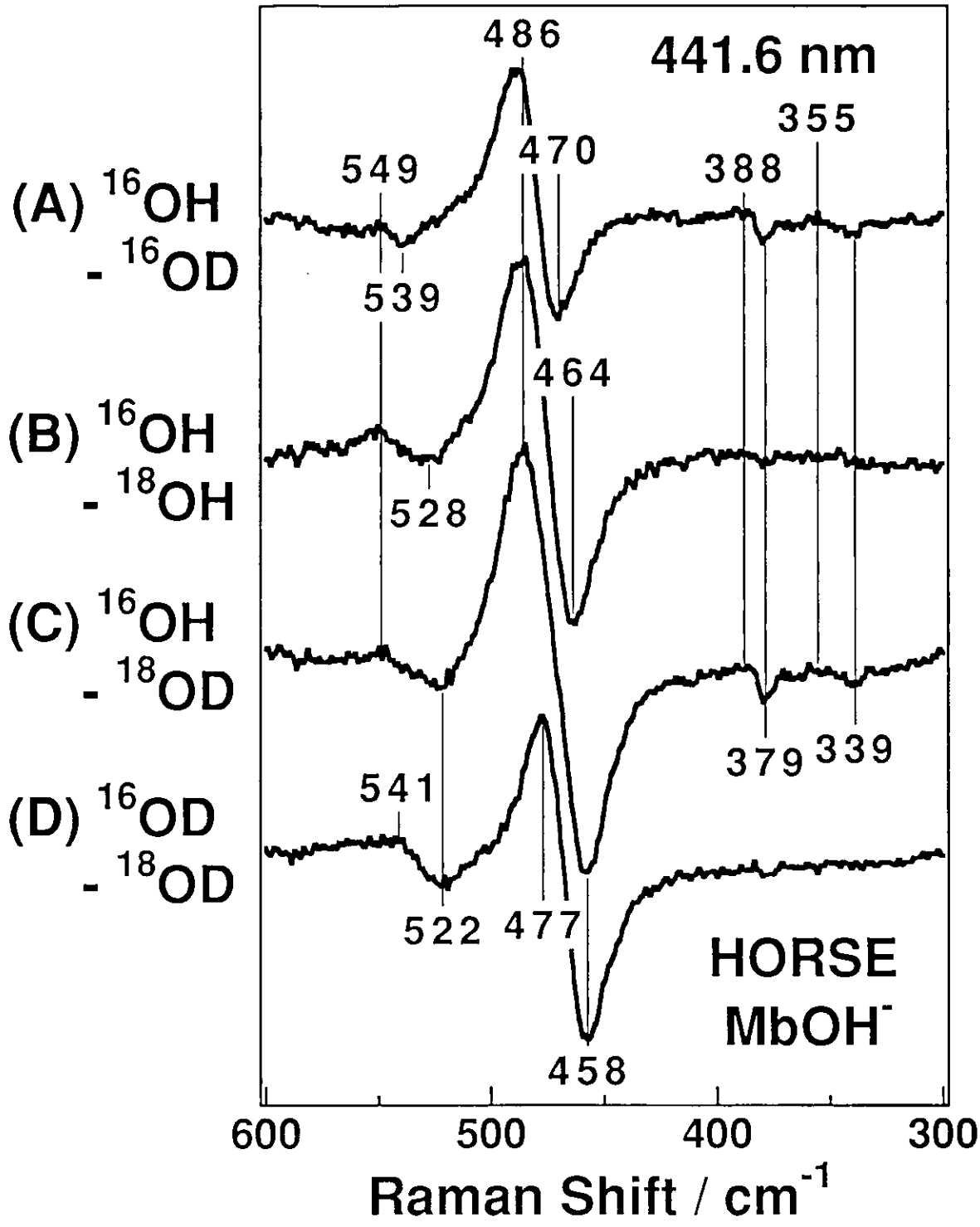


**Figure 7-2.** Differences between the RR spectra shown in Figure 7-1. The differences with regard to $Mb^{16}OH^-$ are displaced.

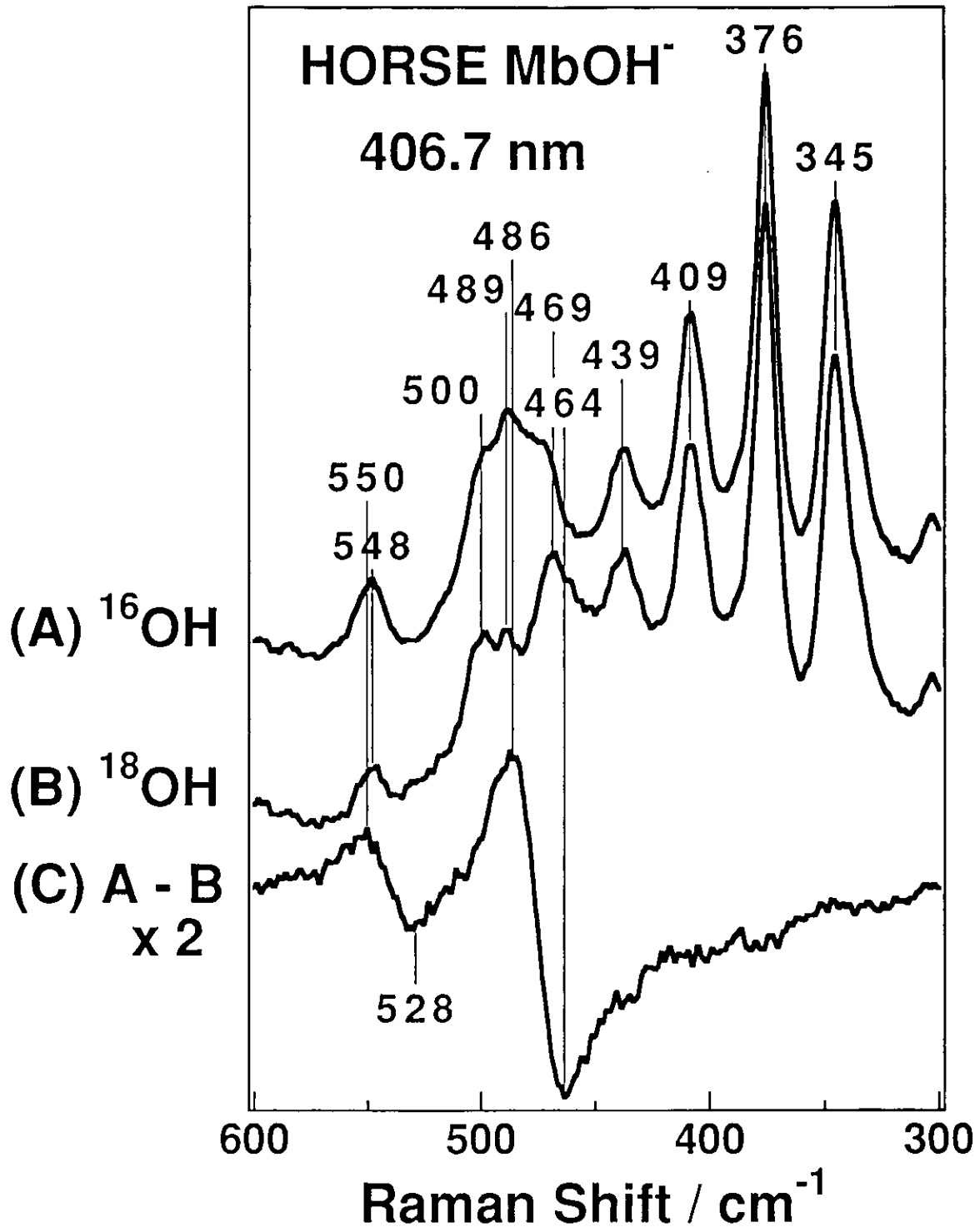


**Figure 7-3.** The RR spectra in the 600 to 300 $cm^{-1}$ region of the $^{16}OH^-$ (A), $^{18}OH^-$ (B) of horse Mb and their difference (C). The ordinate scales of spectra A and B are normalized by the intensity of the porphyrin bands. Experimental conditions are the same as those for Figure 7-1 except for the excitation was at 406.7 nm with 8 mW at the sample.

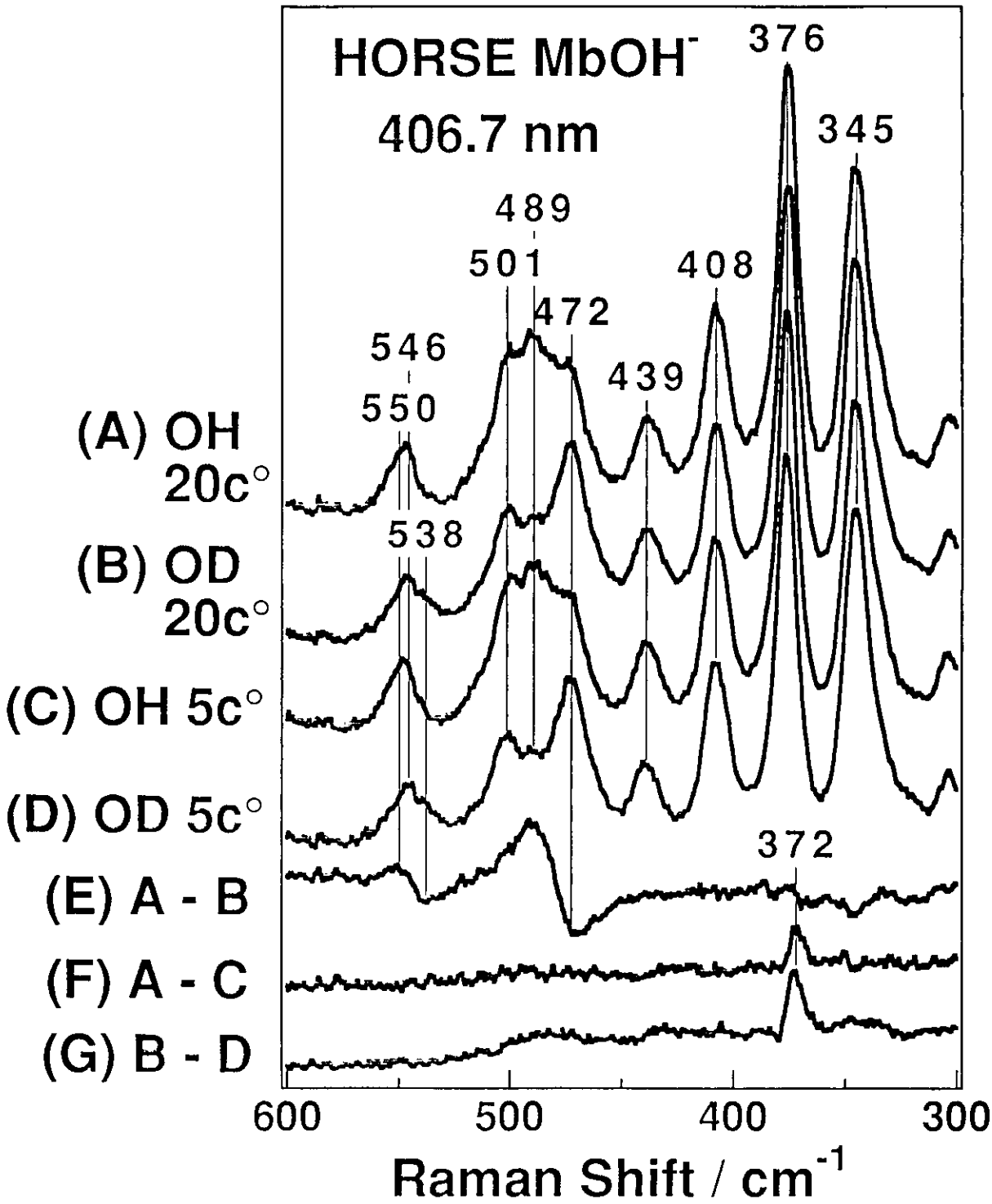


**Figure 7-4.** The RR spectra in the 600 to 300 $cm^{-1}$ region of the $OH^-$ and $OD^-$ adducts of horse Mb at 20 and 5 °C; (A) $OH^-$, 20 °C, (B) $OD^-$, 20 °C, (C) $OH^-$, 5 °C, (D) $OD^-$, 5 °C. Traces E, F and G represent the differences; spectrum E = (spectrum A - spectrum B), spectrum F = (spectrum A - spectrum C), and spectrum G = (spectrum B - spectrum D). Experimental conditions: excitation, 406.7 nm, 6 mW at the sample; spectrometer, single polychromator; sample, 90 μM (heme) in 50 mM Tris-HCl buffer, pH 10.5.

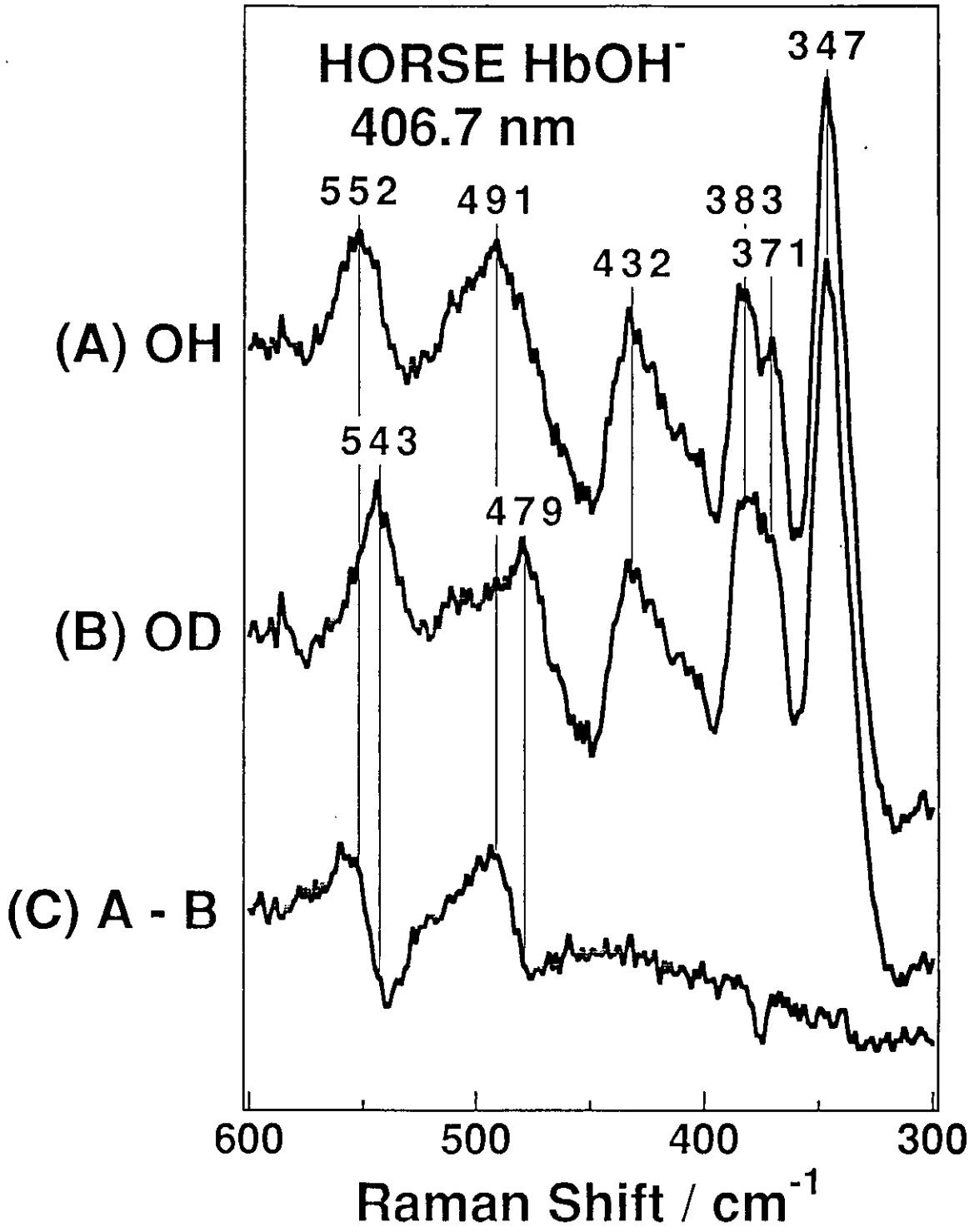


**Figure 7-5.** The RR spectra in the 600 to 300 $cm^{-1}$ region of the $^{16}OH^-$ (A), $^{16}OD^-$ (B) adducts of horse Hb and their difference (C). The ordinate scales of spectra A and B are normalized by the intensity of the porphyrin bands. Experimental conditions: excitation, 406.7 nm, 6 mW at the sample; spectrometer, single polychromator; sample, 20 μM (heme) in 10 mM Tris-HCl buffer, pH 10.5.

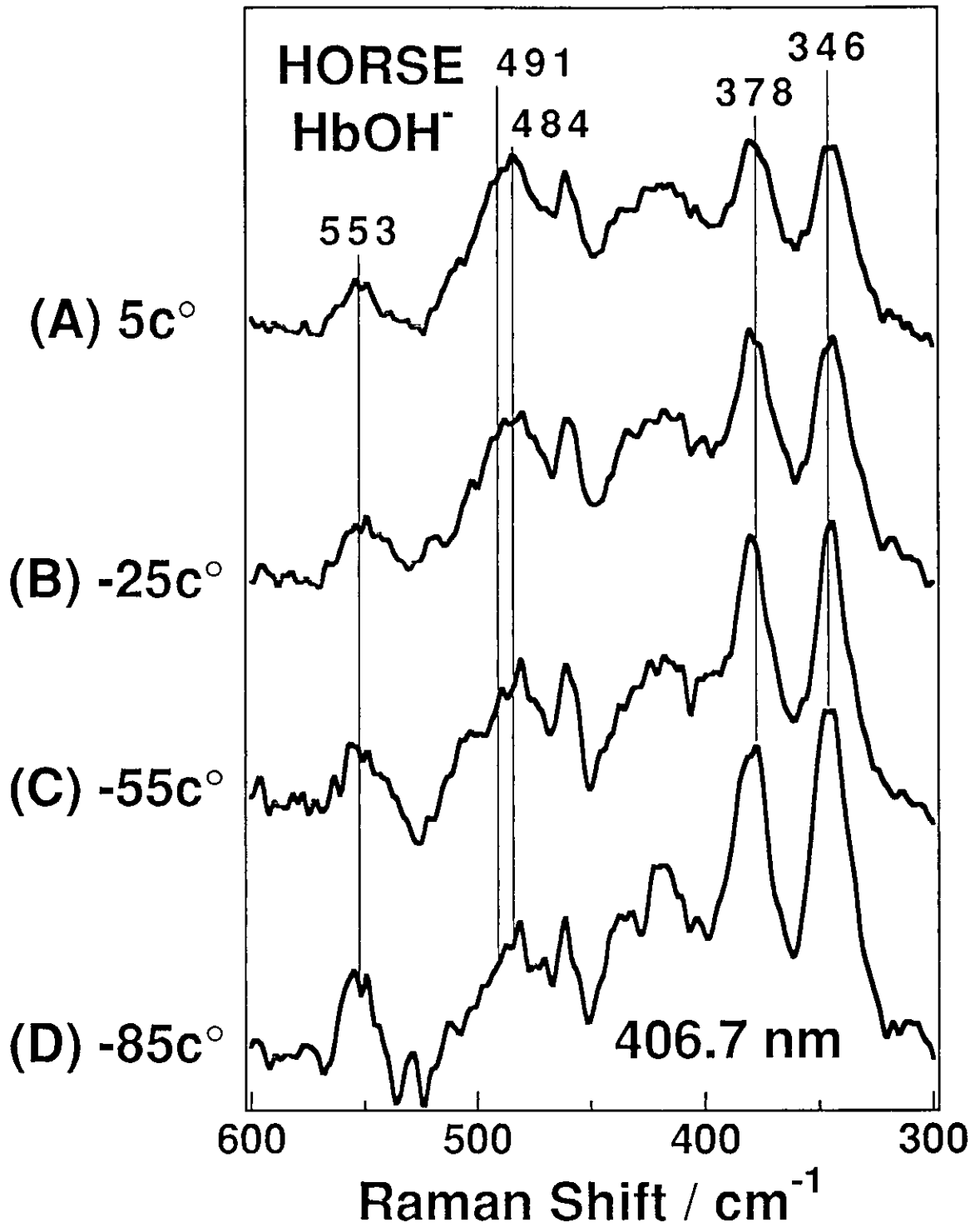


**Figure 7-6.** The RR spectra in the 600 to 300 $cm^{-1}$ region of the horse $Hb^{16}OH^-$ at 5 °C (A), -25 °C (B), -55 °C (C), and -85 °C (D). Experimental conditions: excitation, 406.7 nm, 5 mW at the sample; spectrometer, double monochromator; sample, 50 μM (heme) in 10 mM Tris-HCl buffer containing 67 % glycerol, pH 10.5.

# Chapter I-8.

# Conclusion

Assignments of the Fe-ligand stretching and bending vibrational modes of various ligand-bound heme proteins were studied throughout this part. $O_2$, CO, $CN^-$, and $OH^-$ ligand-bound forms of oxygen binding heme proteins were treated, and several new ligand stretching and bending vibrational modes were detected for the first time.

Chapter I-2 described the first observation of the $\delta_{FeOO}$ Raman band at 425 and 435 $cm^{-1}$ for $HbO_2$ and $CcO{\cdot}O_2$, respectively. The $\delta_{FeOO}$ frequencies for $HbO_2$ and $CcO{\cdot}O_2$ were very similar, suggesting that $HbO_2$ and $CcO{\cdot}O_2$ have similar Fe-O-O geometries, although their reactivities of the bound $O_2$ are quite different. The $\nu_{Fe\text{-}O_2}$ bandwidth of $CcO{\cdot}O_2$ was narrower than those of $HbO_2$ and $MbO_2$. This indicates that the Fe-O-O geometry is more fixed in $CcO{\cdot}O_2$ which might have a relation with its oxygen reactivity. $O_2$- and NO-bound heme proteins have very similar ligand-binding geometries, and thus $\nu_{Fe\text{-}O_2}$ and $\delta_{FeOO}$ frequencies of $O_2$-bound heme proteins have close similarity to $\nu_{Fe\text{-}NO}$ and $\delta_{FeNO}$ frequencies of NO-bound heme proteins. On the other hand, the $\delta_{FeOO}$ band was undetectable for $MbO_2$. There must be some structural origins that controls the intensity of the ligand bending mode in the heme pocket, although they are not known at the present stage.

Chapters I-3, I-4, and I-5 discussed the reassignment of the $\delta_{FeCO}$ RR band. The CO-isotope-sensitive band around 575 $cm^{-1}$ has been assigned heretofore to $\delta_{FeCO}$ for CO-bound heme proteins, but the frequency is higher than the $\nu_{Fe\text{-}CO}$ frequency. Chapter I-3 described the detection of a new CO-isotope-sensitive band around 365 $cm^{-1}$ for various CO-bound heme proteins. This band exhibited a zigzag pattern against the increase of CO similar to the 575 $cm^{-1}$ band. This CO-isotope-sensitive band at 365 $cm^{-1}$ was undetectable for MbCO, while it was detected for all other CO-bound heme proteins examined, including HbCO, its isolated chains, CcO·CO, and P-450·CO. In chapter I-4, the $^{54}Fe$ and $^{15}N$ isotope shifts of the new CO-isotope-sensitive band, the $\nu_{Fe\text{-}CO}$ band, and the 575 $cm^{-1}$ band were investigated with CO-bound cytochrome *bo* from *Escherichia coli* (*E. coli*). The $^{54}Fe$-isotope shifts of the 575 $cm^{-1}$ and $\nu_{Fe\text{-}CO}$ bands were 1.5 and 3.5 $cm^{-1}$, respectively. These isotope shifts were unable to be reproduced by normal coordinate calculation on the isolated FeCO unit if the 575 $cm^{-1}$ band was assigned to $\delta_{FeCO}$, but were well reproduced when the new CO-isotope-sensitive band around 365 $cm^{-1}$ was assigned to $\delta_{FeCO}$. The force constants for $\nu_{Fe\text{-}O_2}$ and $\nu_{Fe\text{-}CO}$ were very

similar, while the force constant of $\delta_{FeOO}$ was larger than that of $\delta_{FeCO}$. The $\delta_{FeCO}$ force constant might be lowered than expected, since the Fe-C-O unit at a non-equilibrium geometry in CO-bound heme proteins would have a reduced bond-strength and a flatter potential curve for the bending mode. The detection of nonfundamental Fe-$O_2$ and Fe-CO vibrations are discussed in chapter I-5. The overtone mode of $\nu_{Fe\text{-}O_2}$ and the combination mode of $\nu_{Fe\text{-}O_2}$ and $\delta_{FeOO}$ were observed for $HbO_2$ and $MbO_2$. The overtone mode of the 365 $cm^{-1}$ band and a combination mode of this band with $\nu_{Fe\text{-}CO}$ were detected for HbCO and MbCO, but the overtone mode of the 575 $cm^{-1}$ band was undetectable. These results support the assignment of the new CO-isotope sensitive band around 365 $cm^{-1}$ to a fundamental.

Chapter I-6 discussed the $\nu_{Fe\text{-}CN^-}$ and $\delta_{FeCN^-}$ frequencies of several $CN^-$-bound heme proteins systematically. The $CN^-$-isotope-sensitive band around 452 $cm^{-1}$ is assigned to $\nu_{Fe\text{-}CN^-}$. There were several peaks in a range from 340 to 440 $cm^{-1}$ of the $CN^-$-isotope difference spectra, and they are attributed to $\delta_{FeCN^-}$ coupled with porphyrin modes. As the ligand-binding geometries of $CN^-$- and CO-bound heme proteins are very similar and their electronic characters are also alike, their ligand vibrational frequencies should have similarities. As $\delta_{FeCN^-}$ appeared around 340-440 $cm^{-1}$, it is more reasonable to assign the CO-isotope-sensitive band around 365 $cm^{-1}$ to $\delta_{FeCO}$ rather than to assign the 575 $cm^{-1}$ band to it.

Chapter I-7 discussed the observation of the $\nu_{Fe\text{-}OH^-}$ bands for the low-spin species of hydroxy-Mb and -Hb at 549 and 552 $cm^{-1}$, respectively. The $\nu_{Fe\text{-}OH^-}$ frequencies of the high-spin species are reported to be lower by 60 $cm^{-1}$ than those of the low-spin species. This character was similar to that obtained with a hydroxy model compound, $Fe(TMPPyP)(OH)_{2(aq)}^{3+}$ {Fe(TMPPyP); [tetrakis-5,10,15,20-(2-N-methyl-pyridyl)porpyriato]iron(III) }, in which the $\nu_{Fe\text{-}OH^-}$ frequency of the high-spin species was lower by 50 $cm^{-1}$ than that of the low-spin species.

These newly detected ligand vibrational modes would not only make clear the Fe-ligand bond character of these ligand-bound heme proteins, but would also help investigations of other ligand-bound heme proteins. These stretching and bending modes, and their overtone and combination modes would also help as to characterize the character of the heme pocket. The results reported introduces a path to further investigations of these ligand-bound heme proteins.

# Part II.

# Structure-Function Relationship of Terminal Oxidases

# Chapter II-1.

# Introduction

## 1.1 Biological Energy[1]

In plants and some bacteria, the chemical energy is generated from electromagnetic radiation of the sun by trapping it with photoreceptor molecules, chloropylls. A charge separation is induced at the reaction center, and a concentration gradient of protons is built up over the membrane upon the transfer of separated electrons. The electrochemical energy generated is used for ATP (adenosine triphosphate) synthesis. In parallel to this reaction, an electron is transferred from water to $NADP^+$ (nicotinamide adenine dinucleotide phosphate) resulting in $O_2$ generation. In the carbon-fixation cycle, Calvin cycle, carbon dioxide ($CO_2$) is fixed into carbohydrates by sequential steps consuming the NADPH and ATP. The overall reaction of photosynthesis can be written as following:

$$6CO_2 + 6H_2O \xrightarrow{\text{light}} C_6H_{12}O_6 + 6O_2 .$$

Organisms which are unable to use the solar energy, utilize the energy of fuel molecules such as glucose and fatty acids. These fuel molecules are converted into pyruvate with concomitant production of ATP, and pyruvate is decarboxylated to form acetyl coenzyme A (acetyl CoA). This activated acetyl unit is oxidized to $CO_2$ though the citric acid cycle (Krebs cycle). Six electrons (three hydride ions) are transferred to three $NAD^+$ (nicotinamide adenine dinucleotide) molecules, and two electrons (two hydrogen atoms) are transferred to FAD (flavin adenine dinucleotide) in this cycle. Electrons of NADH and $FADH_2$ are transferred to $O_2$ by a series of electron transfer proteins, so-called the respiratory chain. The major part of ATP is synthesized during this electron transfer. The overall reaction of respiration is just the reverse reaction of photosynthesis.

## 1.2 Respiratory Chain[1]

The mitochondrial respiratory chain is illustrated in Figure 1-1. The mitochondrial respiratory chain consists of three enzyme complexes, NADH dehydrogenase (NADH-Q-Q reductase), $bc_1$ complex (cytochrome *c* reductase), and cytochrome *c* oxidase. All these complexes penetrate into the inner mitochondrial membrane, which are linked by two mobile electron carriers. One of the electron carriers is an ubiquinone, which

exists inside the inner mitochondrial membrane and transfers electrons from NADH dehydrogenase to the $bc_1$ complex. The other electron carrier is cytochrome *c*, a small heme protein located in the intermembrane space, which carriers electrons from the $bc_1$ complex to cytochrome *c* oxidase. The electron transfer through these respiratory enzymes is coupled with by generation of proton gradients across the inner mitochondrial membrane for ATP synthesis. This is known as the chemiosmotic theory.[2]

In aerobic prokaryotes, analogous systems and proteins are found in the cytoplasmic membrane. For example, the cytochrome *bo* complex in the aerobic respiratory chain of *Escherichia coli* (*E. coli*) catalyzes the reduction of $O_2$, but directly receives electrons from NADH dehydrogenases through ubiquinones, and does not possess the $bc_1$ complex. An electrochemical potential is created across the cytoplasmic membrane during the electron flow similar to the mitochondrial respiratory chain, and is utilized for ATP synthesis.

### 1.3 Terminal Oxidases[3,4]

Terminal oxidases are the last components in the respiratory chains, and about 90 % of the $O_2$ taken into our body are consumed by the enzyme. Figure 1-2 shows a model of the mitochondrial cytochrome *c* oxidase (CcO). The mitochondrial CcO with molecular weight of about 200 kD is composed of 13 subunits, while some bacterial oxidases consist of only three subunits. The three largest subunits are called subunits I, II, and III, and are coded by the mitochondrial DNA. These subunits are thought to be indispensable for their dioxygen and proton translocation activities. Other subunits, for example subunit IV, seem to be also indispensable for the proton translocation activity.

The respiratory enzyme was first discovered by O. Warburg 70 years ago.[5] In 1939, Keilin and Hartree pointed out that the enzyme is a cytochrome $aa_3$ complex, by finding unusual behaviors of respiratory inhibitors on the absorption spectrum which could not be interpreted as an effect of one cytochrome component.[6] Okunuki and Sekuzu showed a direct evidence for the formation of an oxygenated cytochrome complex.[7] On the other hand, various interesting techniques have been developed to investigate this enzyme. For example, Gibson and Greenwood developed

the flow-flash method to study the reaction with dioxygen in 1963.[8] In this method, CO-bound enzyme starts its reaction with dioxygen as soon as CO is photodissociated. This method utilizes the character of CcO that the on-rate of $O_2$ is 1400 times faster than that of CO. In 1975, Chance et al. trapped intermediates by developing the low-temperature triple-trapping method and observed the absorption spectra of intermediates, which were named as Compounds A and B.[9] In 1977, Wikström showed that the free energy released in the reduction of dioxygen is used to pump protons from the matrix to the intermembrane space to create a proton-gradient between the mitochondrial membrane.[10]

It is has been demonstrated by recent development in molecular biology that most of the terminal oxidases are defined as a member of the heme-copper oxidase superfamily, which are common in the following two points:[11]

(1) High conservation in the amino acid sequences in the largest subunit, subunit I.

(2) Possession of an unique heme-copper binuclear site at the active center.

Besides the heme-copper binuclear site where dioxygen molecules bind, oxidases have an electron accepting site which varies among different oxidases.

### 1.4 Structure of Oxidases[4]

**Oxygen Reduction Site**

The heme-copper binuclear site functions as the oxygen reduction site. For CcO, the binuclear center consists of a five coordinated high-spin heme called heme $a_3$ and an EPR invisible Cu ion called $Cu_B$. Heme $a_3$ has a long isoprenoid chain called farnesylhydroxyethyl group at position 2 and a formyl group at position 8 of the porphyrin ring. The heme iron-Cu distance is reported to be 3.75 Å by EXAFS studies.[12] It has been demonstrated from EPR studies that heme $a_3$ and $Cu_B$ are antiferromagnetically coupled *via* a bridging ligand.[13] According to recent site-directed mutagenesis studies of bacterial CcO, the axial ligand of heme $a_3$ is a histidine residue, the axial ligands for heme $a$ are both histidine residues, and three histidines are ligated to $Cu_B$.[11b]

Subunit I of the *E. coli bo*-type quinol oxidase contains a *hexa*-coordinated low-spin heme B, a *penta*-coordinated high-spin heme O and one copper ion ($Cu_B$).[14,15] Heme O is biosynthetically converted from heme B by addition of a farnesyl goup.[15] The high-spin heme O and $Cu_B$ are also antiferromagnetically coupled, forming an Fe-$Cu_B$ binuclear center where dioxygen reduction takes place. For *E. coli bd*-type quinol oxidase, there seems to be a heme-heme binuclear site instead of the heme-$Cu_B$ binuclear site to which $O_2$ binds.[16]

**Electron Accepting Site**

An interesting character of CcO is that it has a $Cu_A$ center for accepting electrons. $Cu_A$ is located at the water soluble part of subunit II near the intermembrane space, so as to accept electrons from cytochrome *c*. Very recently, many evidences have been collected to show that the $Cu_A$ site has a Cu-Cu binuclear character. $Cu_A$ of CcO has been isolated and the mass of this copper-containing $Cu_A$ domain was reported to be 126-129 Da higher than that of the apoprotein.[17-19] This indicates that two copper atoms are bound in the $Cu_A$ domain. Chemical copper measurements also proved that Cu/monomer ratio was 1.9 for the isolated domain of *Paracoccus* enzyme. Approximately one half of copper ions in this domain was EPR-visible, and was in agreement with the binuclear $Cu_A$ center model.[18] Also the $Cu_A$ site of the *caa3*-type oxidase of *Bacillus subtilis* is reported to consist of one $Cu^{2+}$ and one $Cu^{1+}$.[19] Recently, X-ray absorption spectrum of the $Cu_A$-binding domain of Bacillus *subtilis* cytochrome *c* oxidase was compared with that of a structurally characterized Cu(1.5)-Cu(1.5) inorganic complex with the direct bonding of two Cu ions, and it was suggested that the Cu-Cu interaction in the $Cu_A$ domain is 2.5 ± 0.1Å and a short Cu-S interaction (2.2 Å) possibly exists.[20] In order to identify the $Cu_A$ ligands, all putative and conserved copper-binding residues have been point-mutated in isolated *Paracoccus* $Cu_A$ domain.[17,21] Optical spectroscopy and quantitative Cu/protein measurements showed that two histidines, two cysteins, and a methionine are important for $Cu_A$. The replacement of the conserved methionine caused changes in the protein folding, and it was suggested that this methionine residue is important for the folding of the protein around the $Cu_A$ center.[21]

On the other hand, *E. coli* cytochrome *bo* does not contain the $Cu_A$ center, but provides an oxidation site which is dissolved in the membrane lipid for a lipophilic two-electron donor, ubiquinol-8.[22]

### 1.5 Functions of Oxidases

#### Oxygen Reduction Mechanism

Terminal oxidases catalyze the $O_2$ reduction as follows:

$$O_2 + 4H^+ + 4e^- \rightarrow 2H_2O$$

A proposed mechanism for dioxygen reduction in CcO at the binuclear site is shown in Figure 1-3. Dioxygen binds to the heme iron and forms an oxy-complex. According to flow-flash experiments in the reaction of CcO with $O_2$ (CcO:$O_2$=3:1000 concentration) at 25 °C, this oxy intermediate is formed within 10 μs.[23] The FeOO geometry of this intermediate is very similar to those of oxyHb and oxyMb (see chapter I-2 of this thesis).

The electron transfer to the oxy-complex generates the next reaction intermediate. This intermediate is at the peroxy electronic level. The intermediate has been detected in the reaction of reverse electron transport and was found to give rise to a difference absorption maximum at 607 nm with regard to the oxidized enzyme,[24] although this intermediate is converted into the next intermediate (ferryl intermediate) without manifesting a transient appearance in the transient absorption spectra in the reaction of reduced CcO with dioxygen.[25] In the reaction of fully reduced CcO with dioxygen, the second electron comes from cytochrome *a*,[26] and the oxidized cytochrome *a* is partially re-reduced by $Cu_A$ forming a rapid reduction equilibrium between cytochrome *a* and $Cu_A$. The structural character of this intermediate had not been known well, but recent RR studies of this intermediate suggested that this intermediate has a Fe=O bond character.[27]

The next electron input to the binuclear center produces the ferryl intermediate. According to flow-flash experiments on the reaction of the reduced CcO with dioxygen, this electron seems to come from $Cu_B$. From recent RR studies, the transition rate from the peroxy level intermediate to this ferryl intermediate is about an order slower in $D_2O$ than in $H_2O$.[28]

The fourth electron generates the hydroxy form, and the enzyme becomes completely oxidized. The Fe-OH stretching frequency of this intermediate is lower by 40 $cm^{-1}$ than those of hydroxyMb and

hydroxyHb,[29,30] and therefore it is thought that the Fe-OH bond of hydroxyCcO is weaker than those of hydroxyMb and hydroxyHb.[30]

**Proton Translocation**

The knowledge of the proton translocation is now of extensive concern. The proton pumping action of the protein was identified only in two steps in the oxygen reduction sequences, i.e., electron transfer from the peroxy level to ferryl intermediates, and from the ferryl to hydroxy intermediates.[31] Each step translocate two protons for one electron transfer.[31] However, the reduction of dioxygen might be directly linked with the proton uptake and release.

Later, proton slip phenomenon was found in several cases.[32-34] In the reaction starting with the fully reduced enzyme reconstructed in vesicles, proton release to the outside has been observed in the step from the ferryl state to the oxidized enzyme, but not in the peroxy level state to the ferryl intermediate.[32] Lack of proton pumping in cytochrome *bo* at high pH has also been reported.[33] Recent site-directed mutagenesis studies of cytochrome *bo* showed that substitution of aspartate located in the intracellular loop to asparagine resulted in a dramatic decrease in proton pumping, while about 40 % of the activity was retained.[34] It was suggested that this residue might serve as a gate to open a proton-conducting channel specific to pumped protons.[34] However, the proton pump mechanism is known little, and this will be a future subject.

## References


(1) See for example, (a) Stryer, L. In *Biochemistry,* 3rd Ed.; Freeman: New York, 1988. (b) Albets, B.; Bray, D.; Lewis, J.; Raff, M.; Roberts, K.; Watson, J. D. In *Molecular Biology of the Cell*; Garland: New York, 1983, Chap 9.

(2) Mitchell, P. *Nature* **1961**, *191*, 144-148.

(3) Wikström, M.; Krab, K.; Saraste, M. In *Cytochrome Oxidase-A synthesis*; Academic Press: London, 1981.

(4) Babcock, G. T.; Wikström, M. *Nature* **1992**, *356*, 301-309.

(5) Warburg, O.; Negelein, E. *Biochem. Z.* **1928** *193*, 339.

(6) Keilin, D.; Hartree, E. F. *Proc. Roy. Soc. London* **1939**, *B127*, 167-191.

(7) (a) Okunuki, K; Sekuzu, I. *Seitai no Kagaku* **1954** *5*, 265-272. (b) Sekuzu, I.; Takemori, S.; Yonetani T.; Okunuki, K. *J. Biolchem.* **1959**, *46*, 43-49.

(8) Gibson, Q. H.; Greeenwood, C. *Biochem. J.* **1963**, *86*, 541-555.

(9) Chance, B.; Saronio, C.; Leich Jr., J. S. *J. Biol. Chem.* **1975**, *250*, 9226-9237.

(10) Wikström, M. *Nature* **1977**, *266*, 271-273.

(11) (a) Calhoun, M. W.; Thomas, J. W.; Gennis, R. B. *TIBS* **1994**, *19*, 325-330. (b) Hosler, J. P.; Ferguson-Miller, S.; Calhoun, M. W.; Thomas, J. W.; Hill, J.; Lemieux, L.; Ma, J.; Georgiou, C.; Fetter, J.; Shapleigh, J.; Tecklenburg, M. M. J.; Babcock, G. T.; Gennis, R. B. *J. Bioeng. Biomembr.* **1993**, *25*, 121-136.

(12) Powers, L.; Chance, B.; Ching, Y.; Angiolillo, P. *Biophys. J.* **1981**, *34*, 465-498.

(13) (a) Palmer, G.; Babcock, G. T.; Vickery, L. E. *Proc. Natl. Acad. Sci. U.S.A.* **1976**, *73*, 2206-2210. (b) Tweedle, M. F.; Wilson, L. J.; García-Iniguez, L.; Babcock, G. T.; Palmer, G. *J. Biol. Chem.* **1978**, *22*, 8065-8071.

(14) Mogi, T.; Nakamura, H.; Anraku, Y. *J. Biochem.* **1994**, *116*, 471-477.

(15) Mogi, T.; Saiki, K.; Anraku, Y. *Mol. Microbiol.* **1994**, *14*, 391-398.

(16) Hill, J. J.; Alben, J. O.; Gennis, R. B. *Proc. Natl. Acad. Sci. U.S.A.* **1993**, *90*, 5863-5867.

(17) Kelly, M.; Lappalainen, P.; Talbo, G.; Haltia, T.; Oost, J. v. d.; Saraste, M. *J. Biol. Chem.* **1993**, *268*, 16781-16787.

(18) Lappalainen, P.; Aasa, R.; Malmström, B. G.; Saraste, M. *J. Biol. Chem.* **1993**, *268*, 26416-26421.
(19) von Wachenfeldt, C.; de Vries, S.; van der Oost, J. *FEBS Lett.* **1994**, *340*, 109-113.
(20) Blackburn, N. J.; Barr, M. E.; Woodruff, W. H.; van der Oost, J.; Vries, S. *Biochemistry* **1994**, *33*, 10401-10407.
(21) Lappalainen, P.; Saraste, M. *Biochim. Biophys. Acta* **1994**, *1187*, 222-225.
(22) Welter, R.; Gu, L.-Q.; Yu, C.-A.; Rumbley, J.; Gennis, R. B. *Biophys. J.* **1994**, *66*, A367.
(23) Oliveberg, M.; Brzezinski, P.; Malmström, B. G. *Biochim. Biophys. Acta* **1989**, *977*, 322-328.
(24) Wikström, M.; Morgan, J. E. *J. Biol. Chem.* **1992**, *267*, 10266-10273.
(25) Orii, Y. *Ann. N. Y. Acad. Sci* **1988**, *550*, 105-117.
(26) Han, S.; Ching, Y.-C.; Rousseau, D. L. *Proc. Natl. Acad. Sci. USA* **1990**, *87*, 8408-8412.
(27) Proshlyakov, D. A.; Ogura, T.; Shinzawa-Itoh, K.; Yoshikawa, S.; Appelman, E. H.; Kitagawa, T. *J. Biol. Chem.* **1994**, *269*, 29385-29388.
(28) Ogura, T.; Hirota, S.; Shinzawa-Itoh, K.; Yoshikawa, S.; Kitagawa, T., to be submitted.
(29) (a) Asher, S. A.; Vickery, L. E.; Schuster, T. M. *Biochemistry* **1977**, *16*, 5849-5856. (b) Asher, S. A.; Schuster, T. M. *Biochemistry* **1979**, *18*, 5377-5387. (c) Asher, S. A. *Methods in Enzymology* **1981**, *76*, 312-413.
(30) (a) Ogura, T.; Takahashi, S.; Shinzawa-Itoh, K.; Yoshikawa, S.; Kitagawa, T. *Bull. Chem. Soc. Jpn.* **1991**, 64, 2901-2907. (b) Han, S.; Ching, Y.-C.; Rousseau, D. L. *Nature* **1990**, *348*, 89-90.
(31) (a) Wikström, M. *FEBS Lett.* **1988**, *231*, 247-252. (b) Wikström, M. *Nature* **1989**, *338*, 776-778.
(32) Nilsson, T.; Hallen, S.; Oliveberg, M. *FEBS Lett.* **1990**, *260*, 45-47.
(33) Verkhovskaya, M.; Verkhovsky, M.; Wikström, M. *J. Biol. Chem.* **1992**, *267*, 14559-14562.
(34) Thomas, J. W.; Puustinen, A.; Alben, J. O.; Gennis, R. B.; Wikström, M. *Biochemistry* **1993**, *32*, 10923-10928.

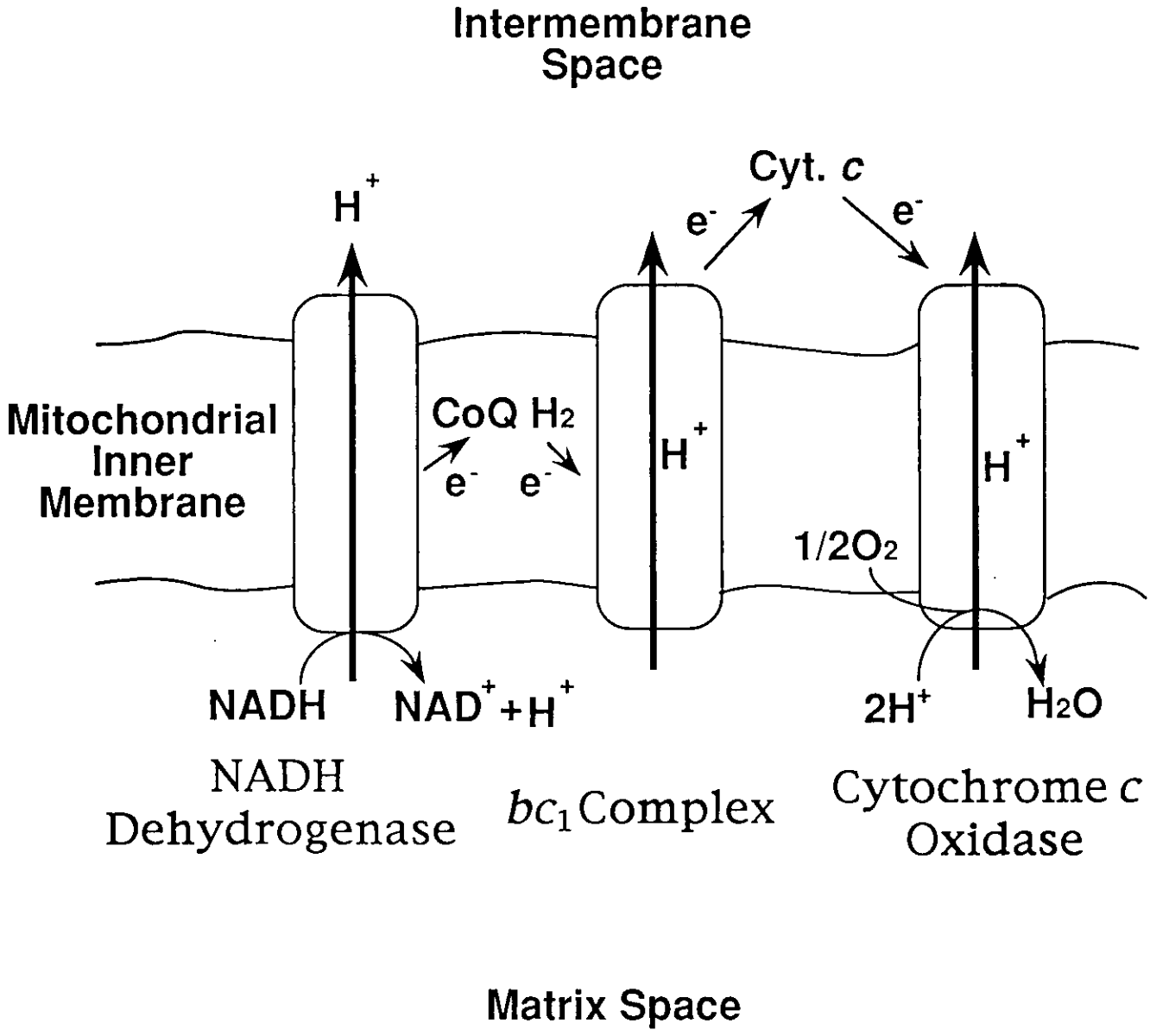


**Figure 1-1.** Schematic view of the electron transfer pathways of the mitochondrial respiratory chain.

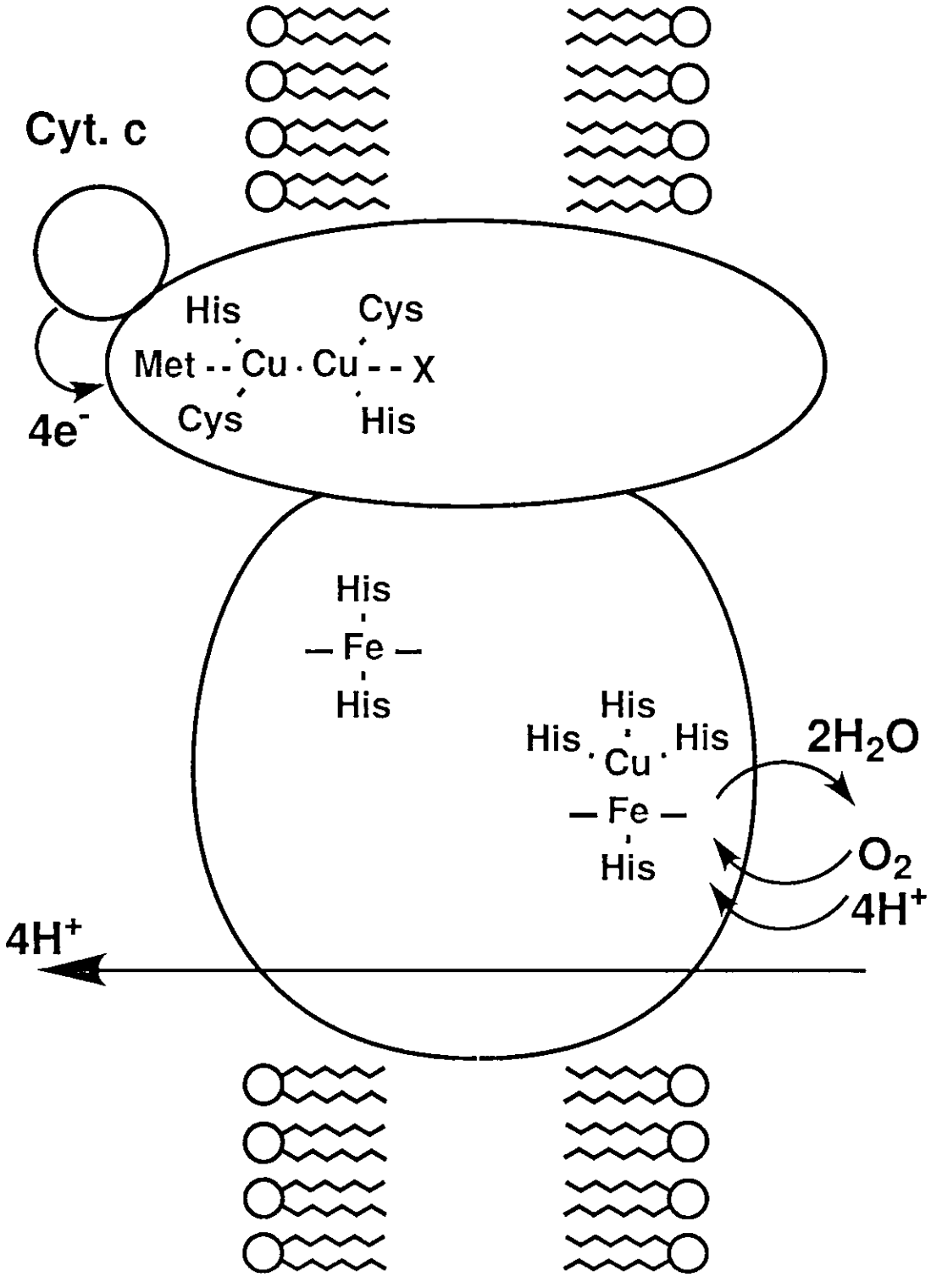


**Figure 1-2.** Model of cytochrome *c* oxidase. Structures of the heme-$Cu_B$ binuclear center and the $Cu_A$ binuclear center are taken from references 11b and 21, respectively.

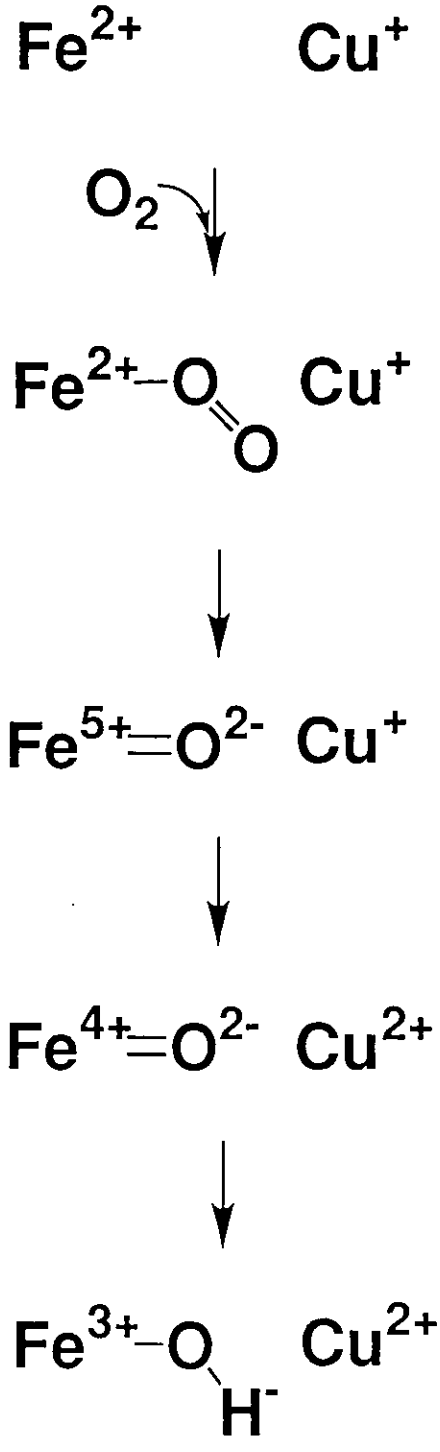


**Figure 1-3.** Proposed sequence for the reaction between the fully reduced cytochrome *c* oxidase and dioxygen.

# Chapter II-2.

# Resonance Raman Studies on CO-Bound Bovine $aa_3$-Type Cytochrome *c* Oxidase

## Abstract

The $\nu_{CO}$ band of CO-bound cytochrome *c* oxidase (CcO·CO) and the $\nu_{Fe\text{-}CO}$ band in the recombination process of CO-photodissociated CcO·CO were observed by resonance Raman (RR) spectroscopy. The observed $\nu_{CO}$ RR frequency was the same as that obtained by infrared (IR) spectroscopy. The RR bandwidths of $\nu_{Fe\text{-}CO}$ and $\nu_{CO}$ of CcO·CO were narrower than those of CO-bound myoglobin (MbCO). This character is also seen for the bandwidths of the $\nu_{Fe\text{-}CO}$ RR band and the $\nu_{CO}$ IR band of CO-bound cytochrome *bo* which are sharper than those of other CO-bound heme proteins, respectively. This suggests that CO takes a more fixed CO conformation in the heme pocket in CcO·CO than in other CO-bound heme proteins. The CO recombination rate was well fitted with a single exponential curve with a lifetime of 30 ms. This lifetime was very long compared with those of MbCO and HbCO which are of ms order. No intermediate $\nu_{Fe\text{-}CO}$ frequency was observed during the CO recombination. This suggests that the bound CO immediately relaxes to its equilibrium conformation as soon as CO binds to the heme, although the CO binding rate is an order slower than those of MbCO and HbCO.

## 2.1 Introduction

Cytochrome *c* oxidase (cytochrome *c*; oxygen oxidoreductase, EC 1.9.3.1) is the terminal enzyme of the mitochondrial respiratory chain.[1,2] This enzyme contains two heme A groups (cytochrome *a* and cytochrome $a_3$), and exists on the mitochondria membrane. Cytochrome *c* oxidase (CcO) receives electrons from cytochrome *c* at subunit I which has a copper binuclear center ($Cu_A$). Electrons are transported to the cytochrome $a_3$ site, and dioxygen is reduced to water at this site consuming protons of the matrix space. Transportation of protons through the membrane is coupled with this catalytic reaction.[3] To understand the molecular mechanism of this enzyme many physicochemical studies have been made with visible absorption,[4-7] EPR,[6-8] time-resolved infrared (IR),[9] and resonance Raman (RR) spectroscopy.[6,10-12] Especially RR spectroscopy is powerful to obtain information on the bond characters. RR studies on the ligand-bound enzymes are useful to investigate the character of the heme pocket, since they give information not only on the Fe-ligand bonds but also on the internal states of the ligands.[13-16] One of the most exciting results obtained by RR spectroscopy is the detection of the iron-ligand frequencies of CcO-dioxygen reaction intermediates, with which the oxy,[17-19] hydroperoxy[20,21] ferryloxo,[22-24] and hydroxy intermediates have been established.[21,23] Since dioxygen and CcO reacts relatively fast, studies of other stable ligand-bound forms are easier to investigate the properties of the heme pocket. Accordingly, we investigated the CO-bound CcO (CcO·CO) by RR spectroscopy.

There is a relationship between the iron-carbon stretching ($\nu_{Fe\text{-}CO}$) frequencies and the $\nu_{CO}$ frequencies for various CO-bound heme proteins.[13] It is reported that CO-bound myoglobin (MbCO) has four bands for the carbon-oxygen stretching mode ($\nu_{CO}$),[25] and other CO-bound heme proteins including CcO·CO also have several bands for $\nu_{CO}$.[26] It is suggested that the existence of several $\nu_{CO}$ bands in CO-bound heme proteins is due to several stable CO conformations in these complexes. However, each component of the $\nu_{CO}$ band of CcO·CO shows a narrower bandwidth than that of other CO-bound heme proteins in IR spectra.[26,27] On the other hand, $\nu_{Fe\text{-}CO}$ of CcO has been assigned by RR spectroscopy using CO-isotopes.[28] $\nu_{CO}$ of CcO·CO has only been observed by IR spectroscopy[29] and had not been observed by the RR spectroscopy yet. This

was due to the insufficient resonance condition of the excitation light. So far for the measurement of the $\nu_{Fe\text{-}CO}$ RR band, the excitation light at 413nm was used for its convenience, but by using the excitation wavelengths closer to the Soret peak than the wavelengths used before we succeeded in detecting the $\nu_{CO}$ RR band for the first time. Using these wavelengths, we also obtained a stronger intensity for the $\nu_{Fe\text{-}CO}$ band of CcO·CO than before, and this enabled us to discuss the bandwidth of $\nu_{Fe\text{-}CO}$. We compared the bandwidths of $\nu_{Fe\text{-}CO}$ and $\nu_{CO}$ of CcO·CO with those of MbCO. Finally we investigated the CO-recombination after CO-photodissociation of CcO·CO by time-resolved RR spectroscopy. We will discuss the character of the heme pocket of CcO.

## 2.2 Materials and Methods

The Raman scattering was excited at 422.5, 423.0, and 430.0 nm obtained from an $Ar^+$ ion laser (Spectra Physics, 2045)-pumped dye laser (Spectra Physics, 375B) with stilbene-420, and was detected with a CCD (Astromed, CCD 3200) or a cooled (-20 °C) diode array (PAR, 1421HQ) attached to a polychromator (Ritsu Oyo Kogaku, DG-1000). The slit-width and slit-height were 200 μm and 10 mm, respectively, for all measurements. The beamwidth was about 50 μm at the sample point. The laser power at the sample was adjusted with a ND filter to be about 5 mW. For the measurements of steady state CcO·CO, a spinning cell (3000 rpm) was used to avoid the dissociation of CO. The measurements were carried out at room temperature. Raman shifts were calibrated with $CCl_4$, $CH_3CN$, and indene. The accuracy of the peak positions of the Raman bands were $\pm 1 cm^{-1}$.

CcO was isolated from bovine heart according to the methods described elsewhere.[30] About 750 μl of 50 μM CcO solution dissolved in 50mM sodium phosphate buffer, pH 7.2, was transferred to an airtight spinning cell for the measurements of the steady state. The fully reduced form ($a^{2+}a_3{}^{2+}$) of CcO was obtained by adding small amount of $N_2$-saturated dithionite solution, so that the final concentration of dithionite was 10mM. The CcO·CO was obtained as the same way as that described in chapter I-3. Myoglobin (Mb) (Sigma, type M630) was dissolved in 50 mM tris buffer, pH 8.5. metMb was reduced by adding sodium dithionite, and the sample was subjected to gel filtration though Sephadex G-25 to

remove dithionite. The CO adduct was formed as the same way as described for CcO.

Time-resolved RR spectra was observed by the pump-probe method using a flow cell (quartz, cross section, 2 x 2 $mm^3$) (Figure 2-1). The sample solution containing 50 μM of CcO, 16.6 μM of cytochrome *c* (Sigma, Type IV) and 50 mM of sodium ascorbate (Wako Chemical) in 50 mM sodium phosphate buffer, pH 7.2, was circulated under CO atmosphere. CO was photodissociated by a 590 nm-pump beam obtained from an $Ar^+$ ion laser (Spectra Physics, 164)-pumped dye laser (Spectra Physics, 375) with Rhodamine 6G. The intensity of the pump beam was fixed to about 200 mW. RR scattering was excited at 423.0 nm. The flow speed of the sample solution was 40 ml/min, and the delay time was adjusted by changing the distance of the two beams as shown in Figure 2-1. The temperature was kept at room temperature during the measurement. Raman shifts were calibrated with acetone. Band fitting were carried out with the dumped least square method by assuming Gaussian shapes for the bands.

**2.3 Results**

Figure 2-2 shows the RR spectra in the 2200 to 1500 $cm^{-1}$ region of fully reduced (A), $^{12}C^{16}O$ (B), $^{13}C^{16}O$ (C), $^{12}C^{18}O$ (D), and $^{13}C^{18}O$ (E) adducts of CcO excited at 430.0 nm. The band at 1965 $cm^{-1}$ for $^{12}C^{16}O$-bound CcO (CcO·$^{12}C^{16}O$) was absent in the spectrum of the fully reduced CcO (A), and was shifted to 1921 $cm^{-1}$ ($^{13}C^{16}O$), 1921 $cm^{-1}$ ($^{12}C^{18}O$), and 1875 $cm^{-1}$ ($^{13}C^{18}O$) upon isotope substitution of CO. It is clear that this CO related band corresponds to the bound carbon-oxygen stretching mode ($\nu_{CO}$). These results were in good agreement with the results obtained in IR studies by Volpe et al.[29] This $\nu_{CO}$ band was shifted to lower frequencies by 44 $cm^{-1}$ for $^{13}C$ and $^{18}O$, and 90 $cm^{-1}$ for $^{13}C^{18}O$. The magnitudes of the isotope shifts are very close to those observed for MbCO and HbCO.[15]

Figure 2-3 presents the same RR spectra of MbCO and deoxyMb for the same region as for Figure 2-2. The band at 1945 $cm^{-1}$ in Mb$^{12}C^{16}O$ shifted to lower frequencies to 1902 $cm^{-1}$ with $^{13}C^{16}O$, to 1901 $cm^{-1}$ with $^{12}C^{18}O$, and to 1855 $cm^{-1}$ with $^{13}C^{18}O$. These frequencies are in agreement with the $\nu_{CO}$ frequencies obtained by IR spectroscopy.[28] We can see that

there are no bands at these frequencies in the deoxyMb spectrum (A). Therefore, this band is assigned to $\nu_{CO}$.

Next we measured the $^{12}C^{16}O$- and $^{13}C^{18}O$-bound CcO and Mb at same conditions, just replacing the sample one after another in the spinning cell. The RR spectra of these complexes are shown in Figure 2-4. The Raman bands at 516 and 574 $cm^{-1}$ of $CcO{\cdot}^{12}C^{16}O$ were shifted to 503 and 556 $cm^{-1}$, respectively, with $CcO{\cdot}^{13}C^{18}O$. Their difference spectrum C ($CcO{\cdot}^{12}C^{16}O$ - $CcO{\cdot}^{13}C^{18}O$) clearly demonstrating these shifts. The difference spectrum C showed additional difference peaks around 350 $cm^{-1}$. These difference peaks could be attributed to the iron-carbon-oxygen bending mode ($\delta_{FeCO}$) as discussed in chapter I-3.

The same measurements were carried out with MbCO, and the results are shown in Figure 2-5. In contrast with CcO·CO, the difference peaks around 350 $cm^{-1}$ did not appear in the difference spectrum between $^{12}C^{16}O$-bound Mb ($Mb^{12}C^{16}O$) and $^{13}C^{18}O$-bound Mb ($Mb^{13}C^{18}O$).

The RR spectra of CO-bound horse Mb shows the $\nu_{Fe\text{-}CO}$ band at 509 $cm^{-1}$ and another CO-isotope-sensitive band at 575-583 $cm^{-1}$, respectively (Figure 2-5). The peaks at 509 and 575-583 $cm^{-1}$ were shifted to 494 and 558 $cm^{-1}$, respectively, but there existed a shoulder peak at 509 $cm^{-1}$ for $Mb^{13}C^{18}O$. There must be no contamination of the $Mb^{12}C^{16}O$ in the preparation of $Mb^{13}C^{18}O$, as the band at 575-583 $cm^{-1}$ disappeared completely in spectrum B. A porphyrin band was observed around 509 $cm^{-1}$ for deoxyMb and cyanometMb (chapter I-7). The 509 $cm^{-1}$ band in the $Mb^{13}C^{18}O$ spectrum must be a porphyrin band. This porphyrin band around 509 $cm^{-1}$ was also observed for CO-bound sperm whale Mb.[15] The CO-isotope-sensitive band around 580 $cm^{-1}$ of $Mb^{12}C^{16}O$ showed 2 peaks, while that of $Mb^{13}C^{18}O$ showed only one peak. This feature was also the seen in CO-bound sperm whale Mb.[16] The splitting of this band in $Mb^{12}C^{16}O$ must be caused by a porphyrin band at 585 $cm^{-1}$ which couples with the CO-isotope-sensitive band of $Mb^{12}C^{16}O$, but not with that of $Mb^{13}C^{18}O$.

Figure 2-6 shows the time-resolved RR spectra for CO-recombination following CO-photodissociation of CcO·CO. The delay time ($\Delta t$) of -12 ms represents the spectrum for CcO·CO before CO-photodissociation which shows the $\nu_{Fe\text{-}CO}$ RR band at 516 $cm^{-1}$. In the spectrum for $\Delta t$=0.6 ms, this band disappeared and accordingly we can see that CO is dissociated completely. The $\nu_{Fe\text{-}CO}$ band increases its

intensity as the delay time increases. The center of the $\nu_{Fe\text{-}CO}$ band did not shift from the beginning of its appearance and the bandwidth of it did not change at all.

## 2.4 Discussion

### $\nu_{Fe\text{-}CO}$

The $\nu_{Fe\text{-}CO}$ band at 516 $cm^{-1}$ for $^{12}C^{16}O$-bound CcO was shifted to a lower frequency by 13 $cm^{-1}$ to 503 $cm^{-1}$ with $^{13}C^{18}O$-bound CcO. The corresponding shift for MbCO and HbCO are about 12 $cm^{-1}$.[15] On the other hand, the $\nu_{Fe\text{-}CO}$ band of CcO·$^{12}C^{16}O$ was down shifted by 4 $cm^{-1}$ with CcO·$^{13}C^{18}O$ (Figure 3-6 in Part I). $\nu_{Fe\text{-}CO}$ of Mb$^{12}C^{16}O$ is also down shifted by 4 $cm^{-1}$ to 503 $cm^{-1}$ with Mb$^{13}C^{18}O$, and that of HbCO is down shifted by 4 $cm^{-1}$ with same CO-isotopes (Figure 3-3 in Part I).[15] As mentioned in part I, this $^{13}C$-isotope shift of $\nu_{Fe\text{-}CO}$ is sensitive to the Fe-C-O angle. MbCO and HbCO are both supposed to have a tilt or bent structure, where the Fe-C-O angle is around 140°-165°.[31,32] Therefore CcO·CO seems to have a conformation similar to those in MbCO and HbCO, taking a bent or tilt form.

Figure 2-7 shows the results of the fitting of the $\nu_{Fe\text{-}CO}$ bands of $^{12}C^{16}O$- and $^{13}C^{18}O$-bound CcO and Mb. The $\nu_{Fe\text{-}CO}$ band of Mb$^{13}C^{18}O$ was fitted first with two Gaussian functions, one band at 509 $cm^{-1}$ corresponding to a porphyrin band and another band at 494 $cm^{-1}$ corresponding to the $\nu_{Fe\text{-}CO}$ band. We subtracted this smaller 509 $cm^{-1}$ band from the RR spectrum of Mb$^{12}C^{16}O$, and fitted the remaining part of $\nu_{Fe\text{-}CO}$ band with a single Gaussian function. The $\nu_{Fe\text{-}CO}$ bands of $^{12}C^{16}O$- and $^{13}C^{18}O$-bound CcO were fitted with a single Gaussian function. The fitted curves and residues are shown in Figures 2-7. The bandwidths of these bands were obtained from the fitted bands, and the results are listed in TABLE 2-1. The $\nu_{Fe\text{-}CO}$ bandwidths of CcO·CO are narrower than those of MbCO. The $\nu_{CO}$ bandwidths of CcO·CO and MbCO are listed in TABLE 2-2, which were obtained from Figures 2-2 and 2-4, respectively. We can see from this table that the $\nu_{CO}$ bandwidths of CcO·CO are also narrower than those of MbCO. These results are consistent with the results obtained from the IR spectra.[27]

The $\nu_{CO}$ IR bandwidth is expected to be narrower for a more fixed conformation. Although there are other factors which determine the

bandwidths of RR bands, the bandwidth of $\nu_{Fe\text{-}CO}$ of CcO·CO was narrower than that of MbCO. This could be caused by the fact that the conformation around heme pocket has a less flexible conformation for CO in CcO·CO compared with that in MbCO. The more fixed conformation in the heme pocket of CcO is deduced form the sharpness in the $\nu_{CO}$ IR band of CcO·CO,[27] and also from the similarity in the $\nu_{CO}$ bandwidth between CcO·CO in a solution and in the crystal state.[35] It is recently reported that the $\nu_{Fe\text{-}CO}$ RR band and $\nu_{CO}$ IR band of CO-bound cytochrome *bo* are narrower than those of other CO-bound heme proteins.[36] The narrowness of the $\nu_{Fe\text{-}CO}$ RR band and $\nu_{CO}$ IR band in CO-bound complexes seem to be characteristic of oxidases. This might be caused by the presence of a copper ion ($Cu_B$) close to the heme iron, in the distance of 3.75 Å,[37] whereas there is no copper ion in MbCO. Both the $\nu_{Fe\text{-}CO}$ and $\nu_{CO}$ bands of CO-bound $Cu_B$-deleted cytochrome *bo* prepared by mutagenesis have been recently observed and it exhibited broader bandwidths than those of CO-bound wild-type cytochrome *bo*.[36b]

**Correlation between $\nu_{Fe\text{-}CO}$ and $\nu_{CO}$**

The $\nu_{Fe\text{-}CO}$ frequencies are plotted against the $\nu_{CO}$ frequencies for various CO-bound model compounds and heme proteins in Figure 2-8 (Ref.38 and references sited therein). This is a method to examine the properties of heme proteins introduced by Tsubaki and Ichikawa first.[39] The heme proteins which fall on the upper line in the figure, have a histidine residue as the proximal ligand like Mb and Hb. The heme proteins which fall on the lower line include P-450 proteins which have a cystein residue as the fifth ligand. This line lays lower than the former line because of a stronger ligand field made by the thiolate ligation of cystein.[40] If the $\pi$ back-bonding between the $\pi^*$ orbital of CO and the $\pi$ orbital of iron Fe increases, the $\nu_{Fe\text{-}CO}$ increases while the $\nu_{CO}$ decreases, and therefore the $\nu_{Fe\text{-}CO}$ and $\nu_{CO}$ have a linear relationship.[13] The $\nu_{Fe\text{-}CO}$ and $\nu_{CO}$ frequencies of CcO·CO obtained from Figures 2-2 and 2-4, respectively are off the upper line, even though CcO has a histidine residue as a proximal ligand. So far, the $\nu_{Fe\text{-}CO}$ and $\nu_{CO}$ frequencies were obtained by different methods, that is, the $\nu_{Fe\text{-}CO}$ frequency by RR spectroscopy and the $\nu_{CO}$ frequency by IR spectroscopy, but it is the first time to observe $\nu_{Fe\text{-}CO}$ and $\nu_{CO}$ frequencies for a same sample with a same method. Therefore, the deviation from the line is not due to differences in

samples of methods. The relationship between the $\nu_{Fe\text{-}CO}$ and $\nu_{CO}$ frequencies of CO-bound cytochrome *bo* is also above the line of the histidine-ligand group. This character seems to be common for all oxidases.

The iron-histidine vibrational frequencies ($\nu_{Fe\text{-}His}$) are 214 $cm^{-1}$ and 215 $cm^{-1}$ for the fully reduced CcO and the T type Hb, respectively.[41,42] The $\nu_{Fe\text{-}His}$ frequency of the transient species following CO-photodissociation of CcO·CO is 222 $cm^{-1}$,[43] while the $\nu_{Fe\text{-}His}$ frequency of the R type Hb is 221$cm^{-1}$.[42] From these results we can say that the proximal histidine site have similar properties in these heme proteins. Therefore $Cu_B$ is more likely to cause the $\nu_{Fe\text{-}CO}$ and $\nu_{CO}$ frequencies to be characteristic of CcO·CO. The main difference of this site of CcO from Mb and other heme proteins is the existence of the $Cu_B$ site.[37] The $\nu_{Fe\text{-}CO}$ and $\nu_{CO}$ frequencies of the $Cu_B$-deleted cytochrome *bo* were recently observed at 498 and 1970 $cm^{-1}$, which are lower than those of the CO-bound wild-type cytochrome *bo* by 25 $cm^{-1}$ and 10 $cm^{-1}$, respectively. The electric charge of $Cu_B$ may cause these frequency to shifts.

**CO Recombination Rate**

In the time-resolved RR measurement of CO-recombined CcO, the center and bandwidth of the $\nu_{Fe\text{-}CO}$ band were unaltered for all times during the recombination. This indicates that the structure of CO reaches its equilibrium as soon as CO rebinds. The area intensity of the $\nu_{Fe\text{-}CO}$ band for various times relative to that of -12 ms shown in Figure 2-6 are plotted against the delay time in Figure 2-9. Unity means the magnitude when CO is completely rebound. The fitted curve in the figure is a single exponential curve with lifetime of 30 ms. The lifetime is very long compared with the CO-recombination rates of photodissociated MbCO and HbCO which occur in the ms order.[43,44] The result obtained here is consistent with the results obtained from flash photolysis.[44]

## References


(1) Wikström, M.; Krab, K.; Saraste, M. In *Cytochrome Oxidase-A Synthesis*; Academic Press: London, 1981.

(2) Babcock, G. T.; Wikström, M. *Nature* **1992**, *356*, 301-309.

(3) Wikström, M. *Nature* **1977**, *266*, 271-273.

(4) Chance, B.; Saronio, C.; Leich Jr., J. S. *J. Biol. Chem.* **1975**, *250*, 9226-9237.

(5) Clore, G. M.; Andreasson, L.-E.; Karlsson, B.; Aasa, R.; Malmström, B. G. *Biochem. J.* **1980**, *185*, 139-154.

(6) Orii, Y. *Ann. N. Y. Acad. Sci.* **1988**, *550*, 105-117.

(7) Surerus, K. K.; Ortling, W. A.; Fan, C.; Gurbiel, R. J.; Einarsdottir, O.; Antholine, W. E.; Dyer, R. B.; Hoffman, B. M.; Woodruff, W. H.; Fee, J. A. *Proc. Natl. Acad. Sci. U.S.A.* **1992**, *89*, 3195-3199.

(8) Witt, S. N.; Chan, S. I. *J. Biol. Chem.* **1987**, *262*, 1446-1448.

(9) Woodruff, W. H.; Einarsdottir, O.; Dyer, R. B.; Bagley, K. A.; Palmer, G.; Atherton, S. J.; Goldbeck, R. A.; Dawes, T. D.; Kliger, D. S. *Proc. Natl. Acad. U.S.A.* **1991**, *88*, 2588-2592.

(10) Ogura, T.; Yoshikawa, S.; Kitagawa, T. *Biochemistry* **1985**, *24*, 7746-7752.

(11) Babcock, G. T.; Callahan, P. M.; Ondrias, M. R.; Salmeen, I. *Biochemistry* **1981**, *20*, 959-966.

(12) Choi, S.; Lee, J. J.; Wei, Y. H. ; Spiro, T. G. *J. Am. Chem. Soc.* **1983**, *105*, 3692-3707.

(13) (a) Yu, N. T.; Kerr, E. In *Biological Application of Raman Spectroscopy*; Spiro, T. G., Ed.; Wiley-Interscience: New York, 1988; Vol. 3, pp. 39-95. (b) Yu, N. T. *Methods Enzymol.* **1986**, *130*, 350-409.

(14) Yu, N.-T.; Kerr, E. A.; Ward, B.; Chang, C. K. *Biochemistry* **1983**, *22*, 4534-4540.

(15) Tsubaki, M.; Srivastava, R. B.; Yu,N.-T. *Biochemistry* **1982**, *21*, 1132-1140.

(16) Li, X.-Y.; Spiro, T. G. *J. Am. Chem. Soc.* **1988**, *110*, 6024-6033.

(17) Ogura, T.; Takahashi, S.; Shinzawa-Itoh, K.; Yoshikawa, S.; Kitagawa, T. *J. Am. Chem. Soc.* **1990**, *112*, 5630-5631.

(18) Han, S.; Ching, Y.-C.; Roussian, D. L. *Proc. Natl. Acad. Sci. U.S.A.* **1990**, *87*, 2491-2495.

(19) (a) Varotsis, C.; Woodruff, W. H.; Babcock, G. T. *J. Am. Chem. Soc.* **1989**, *111*, 6439-6440. (b) Varotsis, C.; Woodruff, W. H.; Babcock, G. T. *J. Am. Chem. Soc.* **1989**, *112*, 1297.

(20) Ogura, T.; Takahashi, S.; Shinzawa-Itoh, K.; Yoshikawa, S.; Kitagawa, T. *Bull. Chem. Soc. Jpn.* **1991**, *64*, 2901-2907.

(21) Varotsis, C.; Zhang, Y.; Appelman, E. H.; Babcock, G. T. *Proc. Natl. Acad. Sci. U.S.A.* **1993**, *90*, 237-241.

(22) Ogura, T.; Takahashi, S.; Shinzawa-Itoh, K.; Yoshikawa, S.; Kitagawa, T. *J. Biol. Chem.* **1990**, *265*, 14721-14723.

(23) Han, S.; Ching, Y.-C.; Roussean, D. L. *Nature* **1990**, *348*, 89-90.

(24) Varotsis, C.; Babcock, G. T. *Biochemistry* **1990**, *29*, 7357-7362.

(25) Caughey, W. S.; Shimada, H.; Choc, M. G.; Trucker, M. P. *Proc. Natl. Acad. Sci. U.S.A.* **1981**, *76*, 2903-2907.

(26) Yoshikawa, S.; Caughey, W. S. *J. Biol. Chem.* **1982**, *257*, 412-420.

(27) Einarsdottir, O.; Choc, M. G.; Weldon, S.; Caughey, W. S. *J. Biol. Chem.* **1988**, *263*, 13641-13654.

(28) (a) Argade, P. V.; Ching, Y.; Rousseau, D. L. *Nature* **1984**, *225*, 329-331. (b) Hirota, S.; Ogura, T.; Shinzawa-Itoh, K.; Yoshikawa, S.; Nagai, M.; Kitagawa, T. *J. Phys. Chem.* **1994**, *26*, 6652-6660.

(29) Volpe, J. A.; O'Toole, M. C.; Caughey, W. S. *Biochem. Biophys. Res. Commun.* **1975**, *62*, 48-53.

(30) Yoshikawa, S.; Choc, M. G.; O'Toole, M. C.; Caughey, W. S. *J. Biol. Chem.* **1977**, *252*, 5498-5508.

(31) Kuriyan, J.; Wilz, S.; Karplus, M.; Petsko, G. A., *J. Mol. Biol.* **1986**, *192*, 133-154.

(32) (a) Cheng, X.; Schoenborn, B. P., *J. Mol. Biol.* **1991**, *220*, 381-399. (b) Cheng, X.; Schoenborn, B. P. *Acta Cryst.* **1990**, *B46*, 195-208. (c) Hanson, J. C.; Schoenborn, B. P. *J. Mol. Biol.* **1981**, *153*, 117-146.

(33) (a) Collman, J. P.; Brauman, J. I.; Iverson, B. L.; Sessler, J. L.; Morris, R. M.; Gibson, Q. H. *J. Am. Chem. Soc.* **1983**, *105*, 3052-3064. (b) Collman, J. P.; Brauman, J. I.; Collins, T. J.; Iverson, B. L.; Lang, G.; Pettman, R. B.; Sessler, J. L.; Walters, M. A. *J. Am. Chem. Soc.* **1983**, *105*, 3038-3052.

(34) (a) Moore, J. N.; Hansen, P. A.; Hochstrasser, R. M.; *Proc. Natl. Acad. Sci. U.S.A.* **1988**, *85*, 5062-5066. (b) Locke, B.; Diller, R.; Hochstrasser, R. M. In *Advances in Spectroscopy*, Clark, R. J. H.; Hester, R. E. Eds.; Wiley & Sons: New York, 1993; Vol. 21B, pp 1-47.

(35) Tsubaki, M.; Shinzawa, K.; Yoshikawa, S. *Biophys. J.* **1992**, *63*, 1564-1571.
(36) (a) Tsubaki, M.; Mogi, T.; Anraku, Y.; Hori, H. *Biochemistry* **1993**, *32*, 6065-6072. (b) Uno, T.; Mogi, T.; Tsubaki, M.; Nishimura, Y.; Anraku, Y. *J. Biol. Chem.* **1994**, *269*, 11912-11920.
(37) Powers, L.; Chance, B.; Ching, Y.; Angiolillo, P. *Biophys. J.* **1981**, *34*, 465-498.
(38) Nagai, M.; Yoneyame, Y.; Kitagawa, T. *Biochemistry* **1991**, *30*, 6495-6503.
(39) Tsubaki, M.; Ichikawa, Y. *Biochim. Biophys. Acta.* **1984**, *827*, 268-274.
(40) Han, S.; Madden, J. F.; Siegel, L. M.; Spiro, T. G. *Biochemistry* **1989**, *28*, 5477-5485.
(41) Ogura, T.; Hon-nami, K.; Oshima, T.; Yoshikawa, S.; Kitagawa, T. *J. Am. Chem. Soc.* **1983**, *105*, 7781-7783.
(42) Nagai, K.; Kitagawa, T.; Morimoto, H. *J. Mol. Biol.* **1980**, *136*, 271-289.
(43) Findsen, E. W.; Centeno, J.; Babcock, G. T.; Ondrias, M. R. *J. Am. Chem. Soc.* **1987**, *109*, 5367-5372.
(44) Mims, M. P.; Porras, A. G.; Olson, J. S.; Noble, R. W.; Peterson, J. A. *J. Biol. Chem.* **1983**, *258*, 14219-14232.
(45) (a) Sakan, Y.; Ogura, T.; Kitagawa, T. *Chem. Phys. Lett.* **1992**, *196*, 150-154. (b) Sakan, Y.; Ogura, T.; Kitagawa, T.; Fraunfelter, F. A.; Mattera, R.; Ikeda-Saito, M. *Biochemisty* **1993**, *32*, 5815-5824.

**TABLE 2-1. Bandwidths of $\nu_{Fe\text{-}C}$ for CO-Bound CcO and Mb[a]**

| | | $\nu_{CO}$ | $\Delta_{1/2}$ / $cm^{-1}$ |
|---|---|---|---|
| CcO | $^{12}C^{16}O$ | 516 | 11.0 |
| | $^{13}C^{18}O$ | 503 | 12.8 |
| Mb | $^{12}C^{16}O$ | 509 | 21.5 |
| | $^{13}C^{18}O$ | 494 | 19.8 |

[a] In $cm^{-1}$ unit.

**TABLE 2-2. Bandwidths of $\nu_{CO}$ of CO-Bound CcO and Mb[a]**

| | | $\nu_{CO}$ | $\Delta_{1/2}$ / $cm^{-1}$ |
|---|---|---|---|
| CcO | $^{12}C^{16}O$ | 1965 | 9.8 |
| | $^{13}C^{18}O$ | 1921 | 9.2 |
| | $^{12}C^{16}O$ | 1921 | 8.5 |
| | $^{13}C^{18}O$ | 1875 | 8.5 |
| Mb | $^{12}C^{16}O$ | 1945 | 16 |
| | $^{13}C^{18}O$ | 1902 | 11 |
| | $^{12}C^{16}O$ | 1901 | 13 |
| | $^{13}C^{18}O$ | 1855 | 14 |

[a] In $cm^{-1}$ unit.

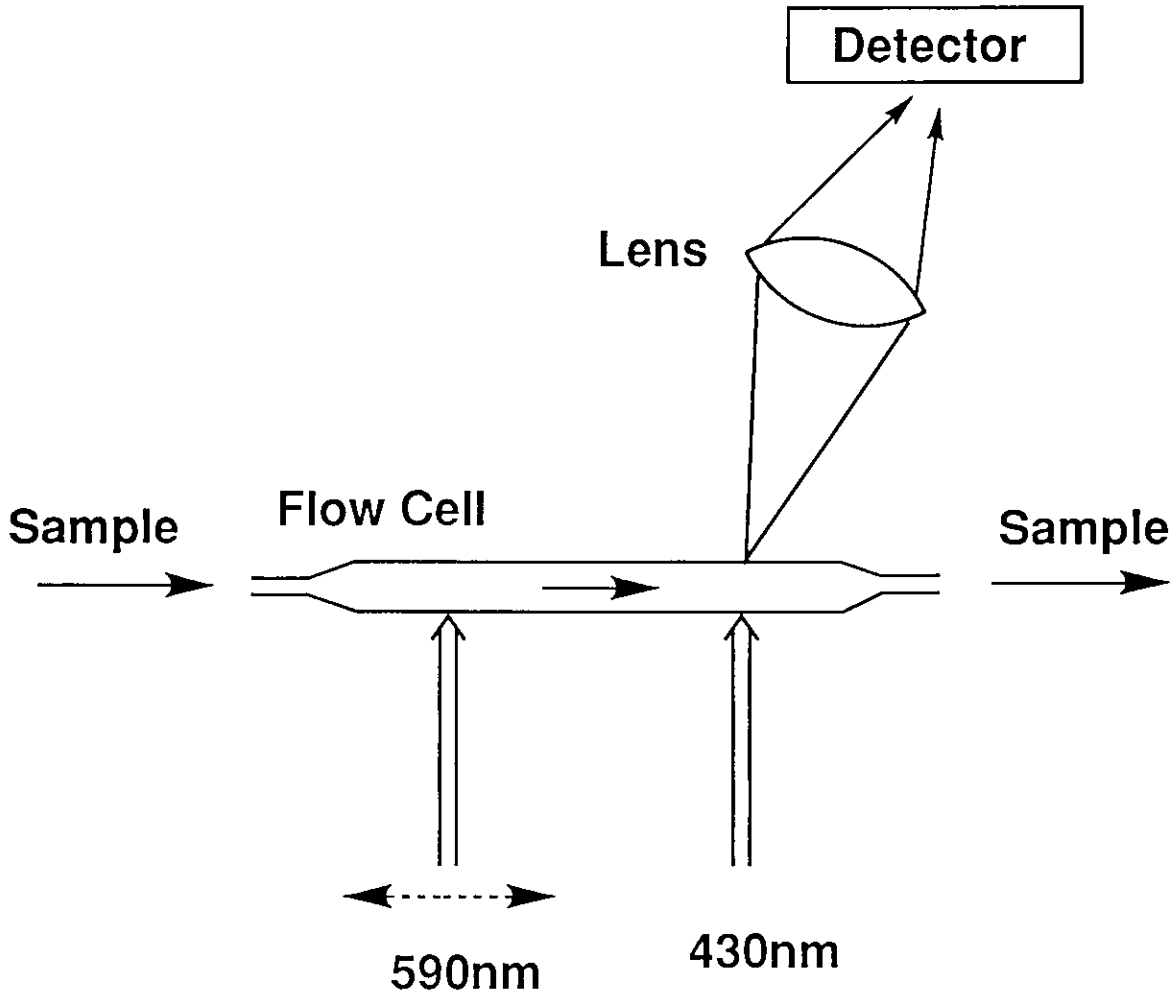


**Figure 2-1.** Schematic view for the flow system.

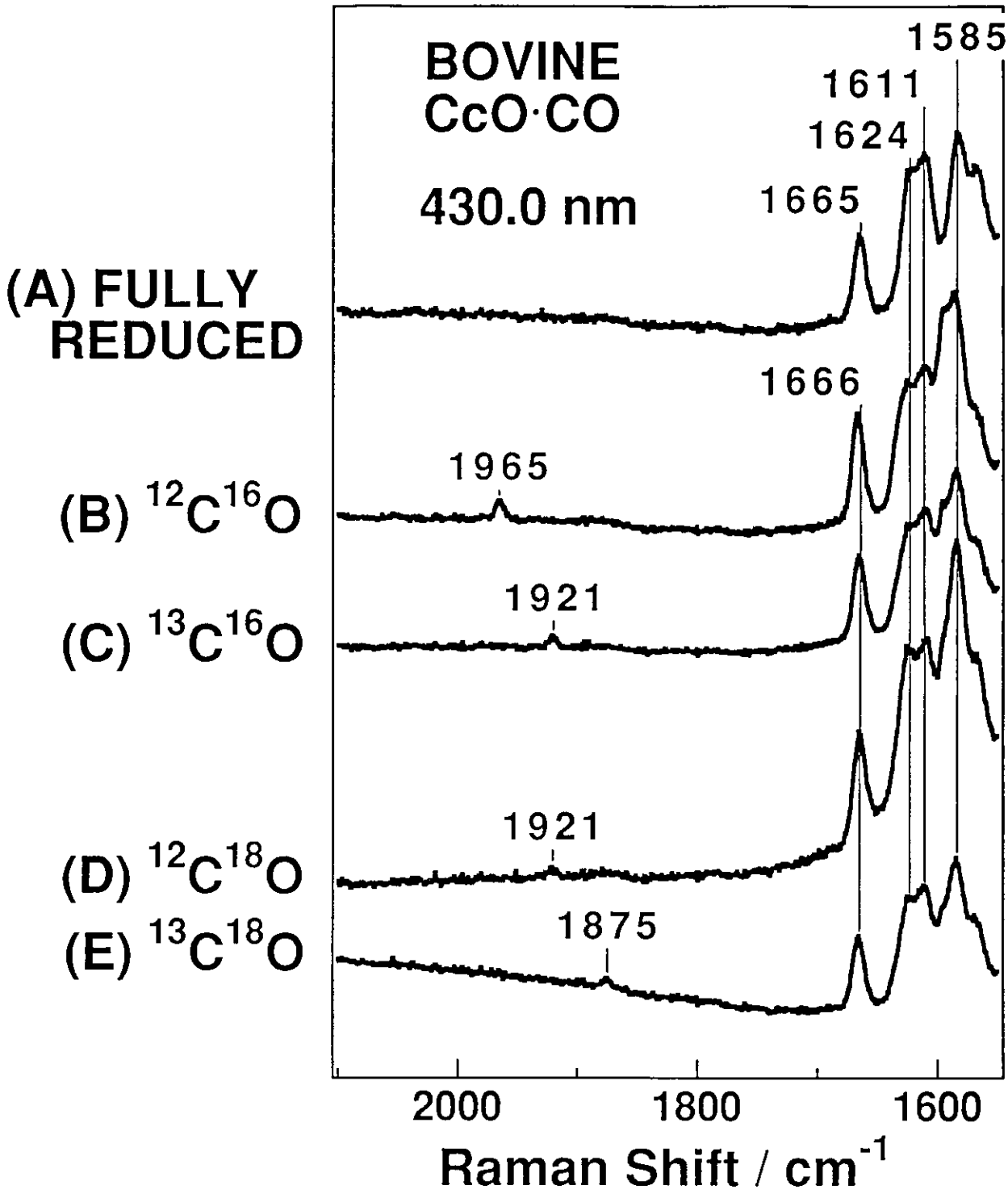


**Figure 2-2.** RR spectra in the 2200 to 1500 $cm^{-1}$ region of fully reduced (A) and $^{12}C^{16}O$ (B), $^{13}C^{16}O$ (C), $^{12}C^{18}O$ (D), and $^{13}C^{18}O$ (E) adducts of bovine CcO. The ordinate scales in spectra B - E are normalized with the intensity of porphyrin bands. Experimental conditions; excitation: 430.0 nm, 5 mW at the sample; detector, CCD; sample, 50 μM (heme) in 50 mM sodium phosphate buffer, pH 7.2.

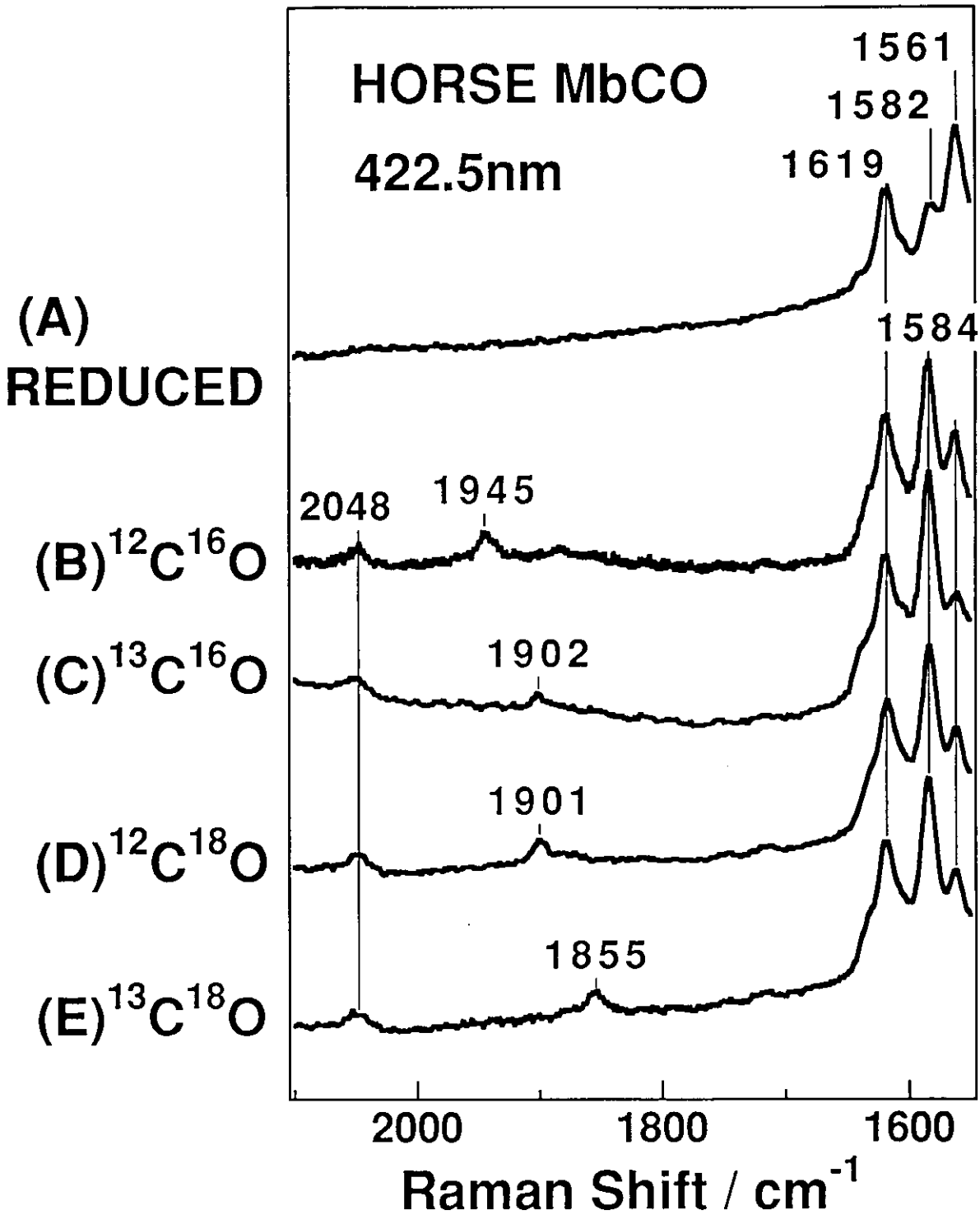


**Figure 2-3.** RR spectra in the 2200 to 1500 $cm^{-1}$ region of fully reduced (A) and $^{12}C^{16}O$ (B), $^{13}C^{16}O$ (C), $^{12}C^{18}O$ (D), and $^{13}C^{18}O$ (E) adducts of horse Mb. The ordinate scales are treated in the same way as that in Figure 2-2. Experimental conditions are the same as those for Figure 2-2.

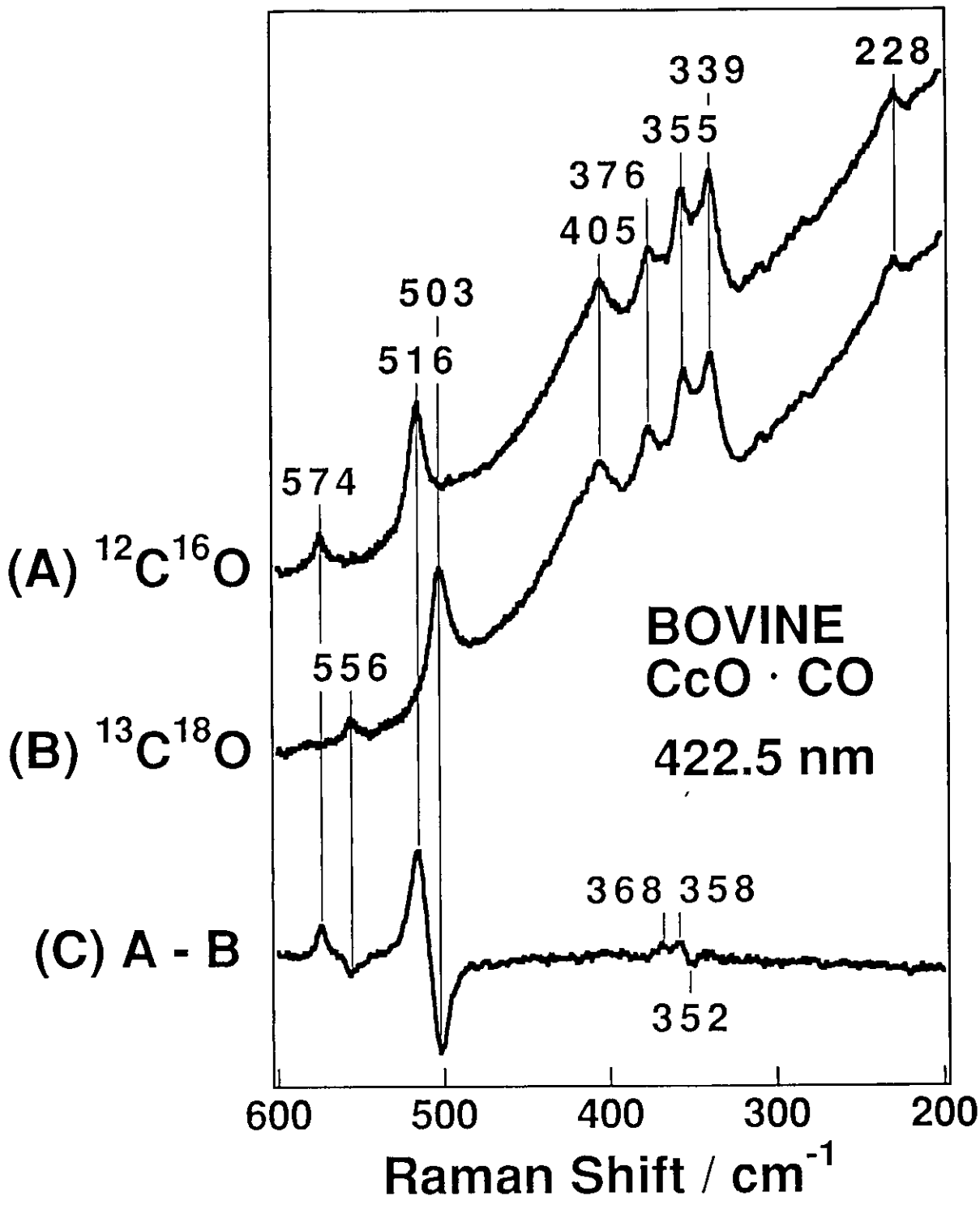


**Figure 2-4.** RR spectra in the 600 to 200 $cm^{-1}$ region of $^{12}C^{16}O$ (A) and $^{13}C^{18}O$ (B) adducts of bovine CcO and their difference (C). The ordinate scales in spectra A and B are normalized with the intensity of porphyrin bands. Experimental conditions are the same as those for Figure 2-2, except for using a diode array detector.

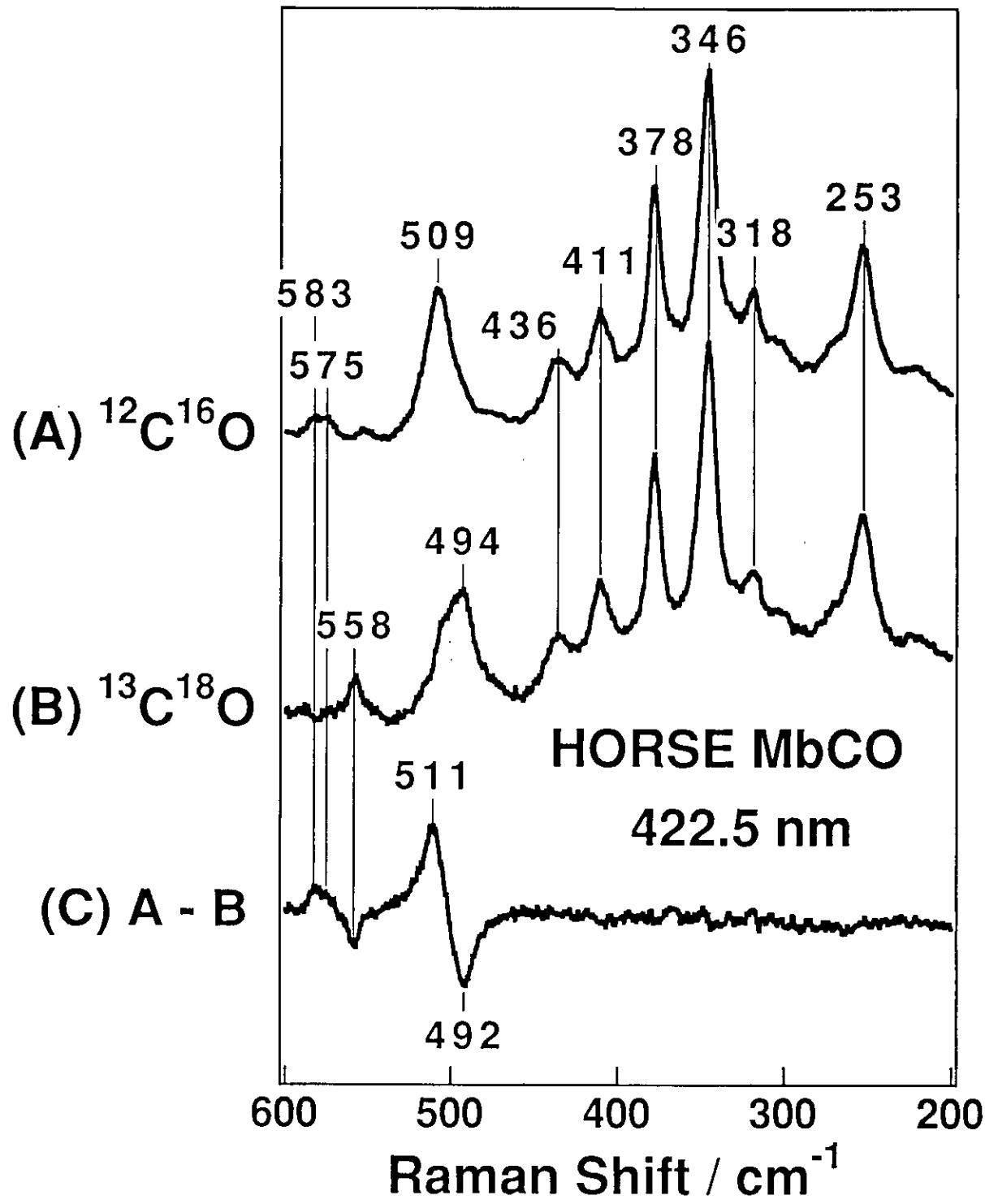


**Figure 2-5.** RR spectra in the 600 to 200 $cm^{-1}$ region of $^{12}C^{16}O$ (A) and $^{13}C^{18}O$ (B) adducts of horse Mb and their difference (C). The ordinate scales in spectra A and B are normalized with the intensity of porphyrin bands. Experimental conditions are the same as those for Figure 2-4.

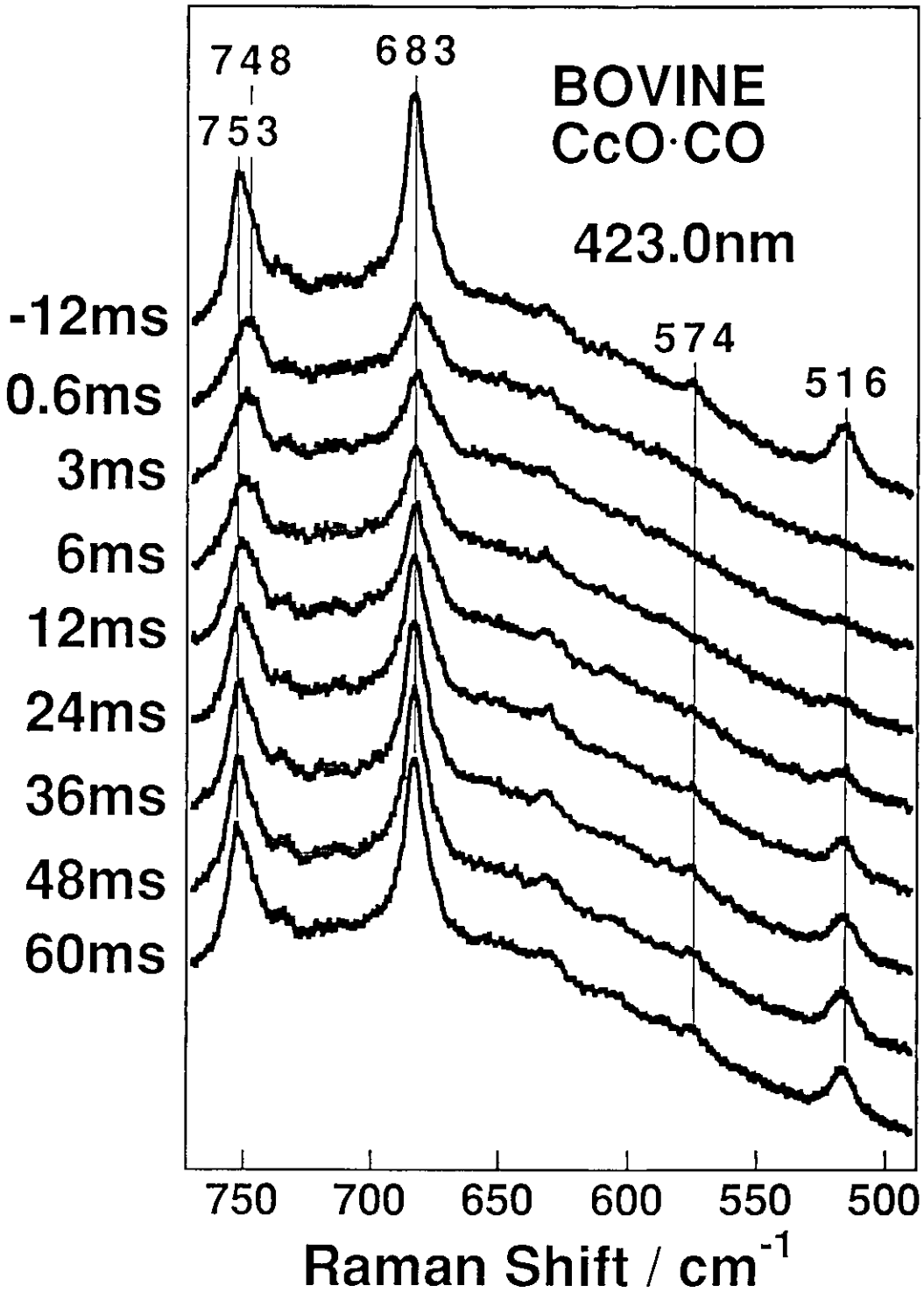


**Figure 2-6.** Time-resolved RR spectra in the 770 to 490 $cm^{-1}$ region for CO-recombination of CO-photodissociated bovine CcO·CO. Experimental conditions; excitation: 430.0 nm, 5 mW at the sample;pump beam, 590.0 nm 200 mW; sample, 50 μM (heme) in 50 mM sodium phosphate buffer, pH 7.2.

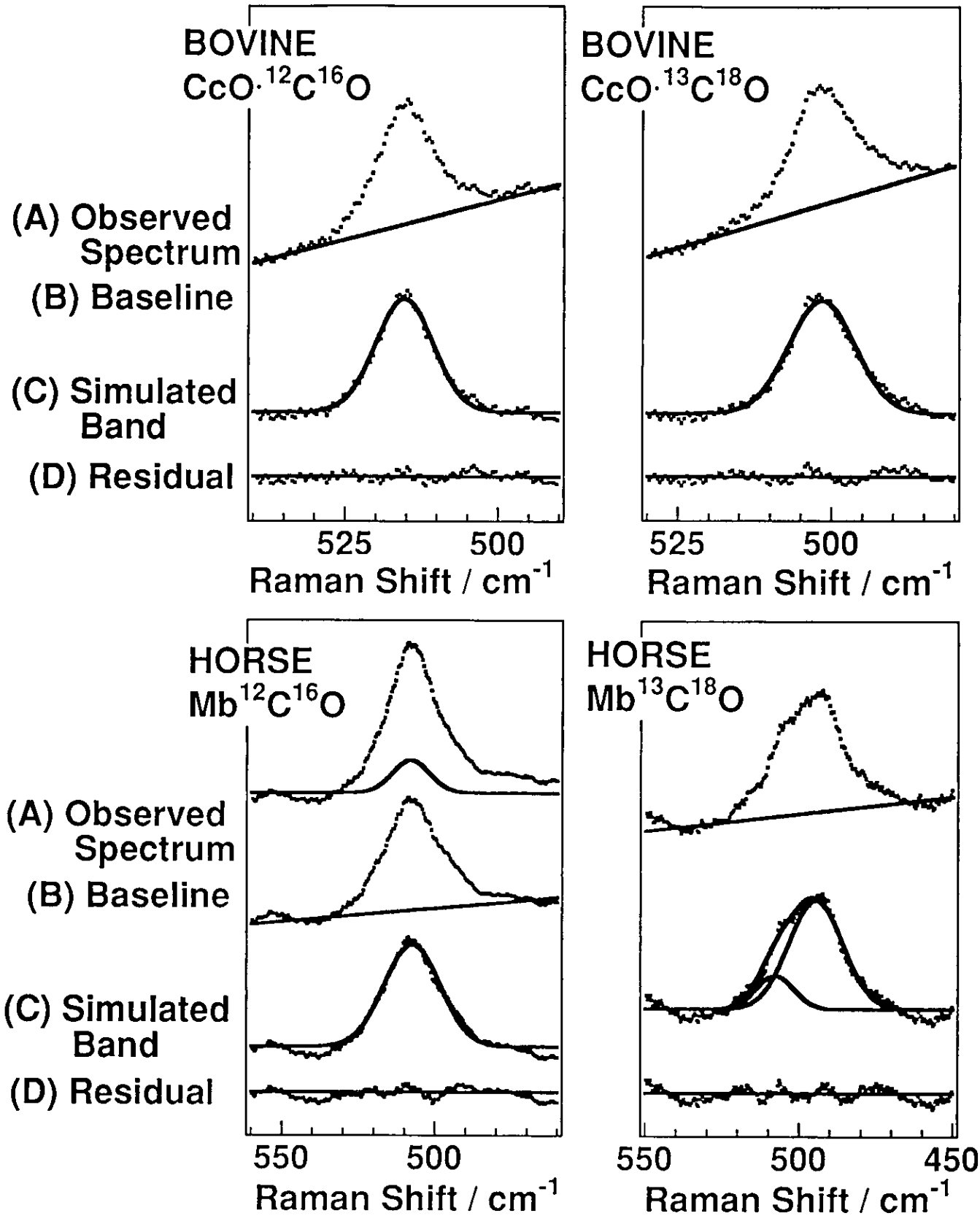


**Figure 2-7.** Simulation for the $\nu_{Fe\text{-}CO}$ bands of CcO·CO and MbCO: (A) observed spectra, (B) baseline, (C) simulated bands (Gaussian shape), and (D) residuals.

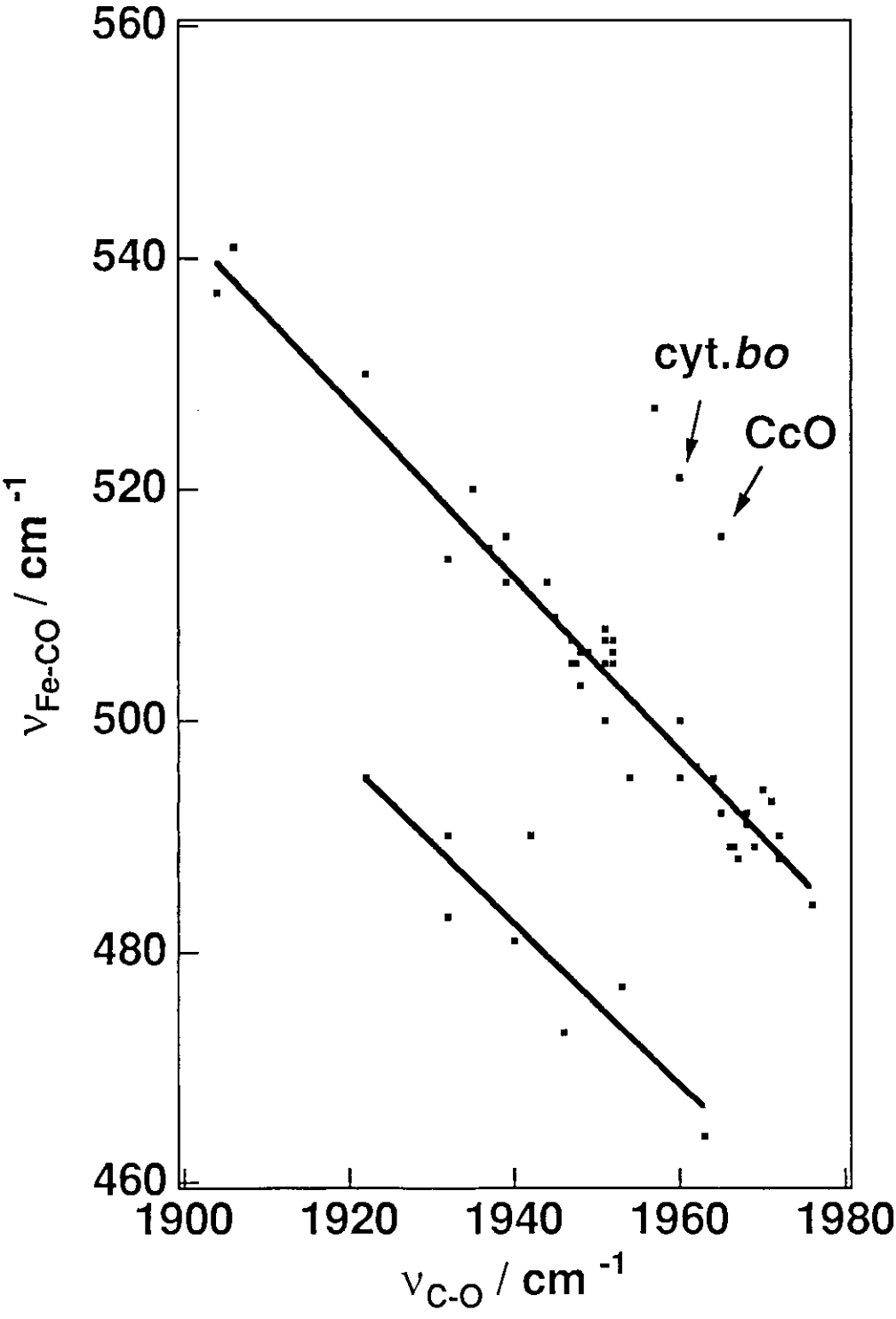


**Figure 2-8.** Correlation between the $\nu_{Fe-CO}$ and $\nu_{CO}$ frequencies.

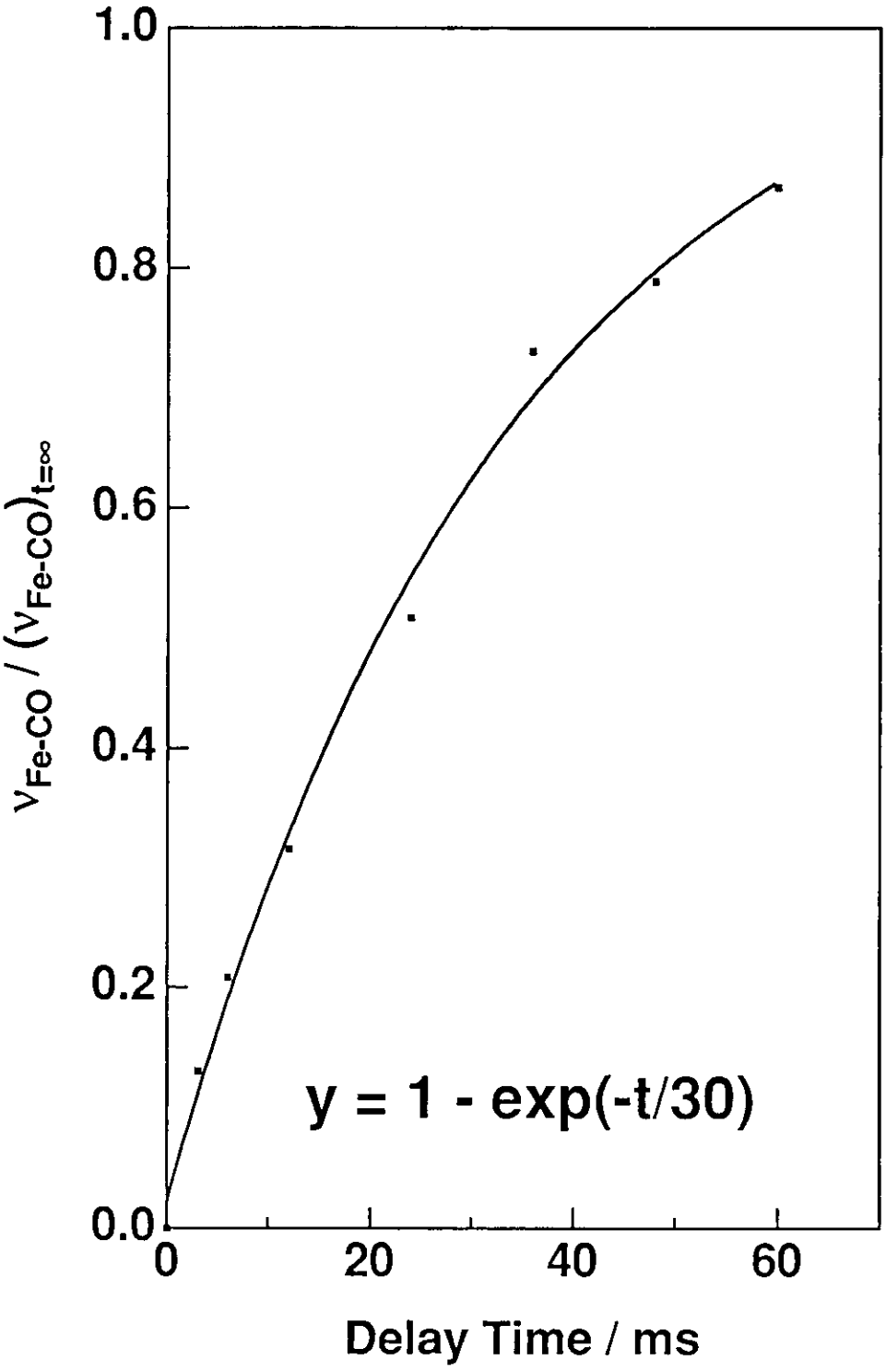


**Figure 2-9.** Recovery of CO for CO-photodissociated CcO·CO calculated form the Fe-CO stretching bands in Figure 2-6.

# Chapter II-3.

# Observation of the Fe-$O_2$ and $Fe^{IV}$=O Stretching Raman Bands for Dioxygen Reduction Intermediates of Cytochrome *bo* Isolated from *Escherichia coli*

## Abstract

Reaction intermediates in dioxygen reduction by the *E. coli* cytochrome *bo*-type ubiquinol oxidase were studied by time-resolved resonance Raman spectroscopy using the artificial cardiovascular system. At 0~20 μs following photolysis of the enzyme-CO adduct in the presence of $O_2$, we observed the Fe-$O_2$ stretching Raman band at 568 $cm^{-1}$ which shifted to 535 $cm^{-1}$ with the $^{18}O_2$ derivative. These frequencies are remarkably close to those of other oxyhemoproteins including dioxygen-bound hemoglobin and $aa_3$-type cytochrome *c* oxidase. In the later time range (20~40μs), other oxygen-isotope-sensitive Raman bands were observed at 788 and 361 $cm^{-1}$. Since the 781 $cm^{-1}$ band exhibited a downshift by 37 $cm^{-1}$ upon $^{18}O_2$ substitution, we assigned it to the $Fe^{IV}$=O stretching mode. This band is considered to arise from the ferryl intermediate, but its appearance was much earlier than the corresponding intermediate of bovine cytochrome *c* oxidase (>100 μs). The 361 $cm^{-1}$ band showed the $^{16}O/^{18}O$ isotopic frequency shift of 14 $cm^{-1}$ similar to the case of bovine cytochrome *c* oxidase reaction.

### 3.1 Introduction

As described in chapter II-1, cytochrome *bo*-type ubiquinol oxidase is a terminal oxidase of the aerobic respiratory chain of *Escherichia coli* (*E. coli*) and is predominantly expressed under highly-aerated growth conditions (see 1 for a review). It catalyzes the four-electron reduction of molecular oxygen at the cytoplasmic side of membranes, which is coupled with the two-electron oxidation of two ubiquinol-8 molecules at the periplasmic side. Redox reactions at different surfaces of the membrane can create a difference in electrochemical potential across the cytoplasmic membrane. In addition to the protolytic scalar reactions, this enzyme is known to function as an electron transfer-linked proton-pump[2] like bovine $aa_3$-type cytochrome *c* oxidase. Recent molecular biological[3-7] and physicochemical[8-10] studies demonstrated that the *bo*-type quinol oxidase belongs to the heme-copper oxidase superfamily and shares a common molecular mechanism for the redox-coupled proton pumping.[11]

Subunit I of the *E. coli bo*-type quinol oxidase contains a *hexa*-coordinated low-spin heme B, a *penta*-coordinated high-spin heme O and one copper ion ($Cu_B$) (see 3,12 for recent reviews). The high-spin heme and $Cu_B$ are antiferromagnetically coupled, forming an Fe-$Cu_B$ binuclear center where dioxygen reduction takes place. Subunit II provides the oxidation site for a lipophilic two-electron donor, ubiquinol-8,[13] but does not contain the $Cu_A$ center which accepts electrons from ferrous cytochrome *c* for mammalian cytochrome *c* oxidases. Thus, electrons are transferred from the quinol bound to subunit II to the binuclear center of subunit I *via* the low-spin heme.

Resonance Raman (RR) spectroscopy can bring about structural information on hemes and their vicinities,[14,15] and is especially powerful for studies of reaction intermediates. In fact, for the reaction of reduced bovine cytochrome *c* oxidase with dioxygen, the oxy,[16-18] ferryl,[19-21] and hydroxy[20,22] intermediates have been identified by this technique. It is extremely interesting to examine similar intermediates for the reaction of cytochrome *bo* with $O_2$, although there are large differences between *bo*-type quinol oxidase and $aa_3$-type cytochrome *c* oxidase, regarding electron donors, presence or absence of the $Cu_A$ center, and heme species at the dioxygen reduction site. Therefore, we applied time-resolved RR spectroscopy using the artificial cardiovascular system[23,24] successfully to characterize intermediates involved in dioxygen reduction by *bo*-type

quinol oxidase. We detected the Fe-$O_2$ and $Fe^{IV}$=O stretching modes at 568 and 788 $cm^{-1}$, respectively, for the first time, suggesting that the dioxygen reduction mechanism of quinol oxidases is similar to that of $aa_3$-type cytochrome *c* oxidases.

### 3.2 Materials and Methods

Cytochrome *bo*-type quinol oxidase was purified from the cytochrome *bd*-deficient strain GO103 (Δ*cyd*::$Km^r$)[25] harboring pHN3795-1 (H. Nakamura, unpublished results), as described previously.[8] pHN3795-1 is a derivative of pBR322 which carries the cytochrome *bo* operon (*cyoABCDE*$^+$) and was obtained from pHN3795 as a clone that can support the aerobic growth of the Δ*cyo* Δ*cyd* strain on nonfermentable carbon source.[26]

The enzyme was dissolved in 100 mM Tris-HCl buffer (pH 7.4) containing 1.0% sucrose monolaurate SM-1200 (Mitsubishi-Kasei Food Co. Ltd., Tokyo), 200 mM ubiquinone-1 (a kind gift from Dr. S. Ohsono, Eisai Co. Ltd., Tsukuba) and 100 mM sodium ascorbate (pH 7.4). About 75 ml of the 50 μM enzyme solution in the fully-reduced CO-bound form was circulated at 5 °C at a flow rate of 20 or 40 ml/min and brought under oxygen concentration of 150 μM using the artificial cardiovascular system. Details of this system are described in chapter I-2.[23,24] Raman scattering was excited at 406.7 nm by a $Kr^+$ ion laser (Spectra Physics, Model 2016), and detected with a cooled (-20 °C) diode array (PAR 1421HQ) attached to a single polychromator (Ritsu Oyo Kogaku, DG-1000), for which the slit width of 200 mm and slit height of 10 mm were used. A single laser beam with a power of ~5 mW was focused to 40 mm on a flow cell with a cross section of 0.6 x 0.6 $mm^2$ and was used to photolyze CO for initiation of the reaction and also to excite RR scattering. The transit time of a given molecule across the laser beam was 40 or 20 μs according to the flow rate used. Raman shifts were calibrated with ethanol as a standard under the same illumination geometry.

### 3.3 Results and Discussion

Figure 3-1 shows time-resolved RR spectra in the 1000 to 300 $cm^{-1}$ region for reaction intermediates of the *bo*-type quinol oxidase with $^{16}O_2$ (A

and C) and $^{18}O_2$ (B and D). Spectra A and B represent the raw spectra of intermediates generated in the time range of 0 ~ 20 μs following photolysis, while spectra C and D display those around 0~ 40 μs following photolysis. Spectra E and F illustrate the differences between spectra A and B, and between spectra C and D, respectively, in which an intense porphyrin band at 678 $cm^{-1}$ was used as a marker for subtraction.

A differential pattern exhibiting a peak at 568 $cm^{-1}$ and a trough at 535 $cm^{-1}$ appeared in difference spectra E and F. The frequencies 568 $cm^{-1}$ for $^{16}O_2$ and 535 $cm^{-1}$ for $^{18}O_2$ are in reasonable agreement with the Fe-$O_2$ stretching frequencies reported for oxyhemoglobin,[27,28] oxymyoglobin,[29,30] and dioxygen-bound bovine cytochrome *c* oxidase.[16-18,24] Cryogenic flash/trap absorption experiments on the CO adduct of this enzyme in the presence of oxygen suggested the formation of an oxygenated heme at low temperatures.[31] Therefore we assign this band to the Fe-$O_2$ stretching mode ($\nu_{Fe\text{-}O_2}$) of the dioxygen adduct. Note that the $\nu_{Fe\text{-}O_2}$ frequencies of the *bo*-type oxy-quinol oxidase (568/535 $cm^{-1}$ for $^{16}O_2/^{18}O_2$) and *aa3*-type oxy-cytochrome *c* oxidase (571/545 $cm^{-1}$) are alike, suggesting similarity in their Fe-O-O geometry.

Spectrum F shows the presence of other oxygen-isotope-sensitive bands around 785 and 361 $cm^{-1}$ which must be arising from the species generated around 20~40 μs following the start of the reaction. The 785 $cm^{-1}$ band is shifted to 751 $cm^{-1}$ with the $^{18}O_2$ derivative. The frequency and its $^{18}O/^{16}O$-isotopic shift (37 $cm^{-1}$) are close to those observed for the $Fe^{IV}$=O stretching mode ($\nu_{Fe^{IV}=O}$) of the oxoferryl intermediate for the bovine cytochrome *c* oxidase,[19-21] of horseradish peroxidase compound II,[32-35] and of other oxoferryl hemeprotein species.[36-39] Therefore we assign this band to the $\nu_{Fe^{IV}=O}$ mode of the oxoferryl intermediate. In the case of bovine cytochrome *c* oxidase, there are two oxygen-isotope-sensitive bands in this frequency region (786 and 804 $cm^{-1}$),[22,24] but it is not clear from this experiment whether the 785 $cm^{-1}$ feature in Figure 3-1 is a single band or not. It should be noted that the rise time (ca. 20~40 μs at 5 °C) of the oxoferryl intermediate of the *bo*-type quinol oxidase is significantly faster than that of bovine cytochrome *c* oxidase, in which the $\nu_{Fe^{IV}=O}$ band was undetectable before 100 μs under similar experimental conditions except for removal of detergents for bovine cytochrome *c* oxidase.[24] Recently, we found that the *E. coli bo*-type quinol oxidase contains a tightly-bound ubiquinone-8 ($Q_H$) which exists in the proximity

of both the quinol oxidation site ($Q_L$) and the low-spin heme and may serve as a pathway for an electron transfer between these two centers.[40] The faster decay of the oxy intermediate to the oxoferryl intermediate in the *bo*-type quinol oxidase may be due to the unique electron transfer pathway. The other oxygen-isotope-sensitive band at 361 $cm^{-1}$ showed an $^{16}O/^{18}O$ isotopic shift of 14 $cm^{-1}$. A similar band is also reported for an intermediate in dioxygen reduction by bovine cytochrome *c* oxidase,[21,24,41] although the nature of the species giving this band has not been characterized yet.

In conclusion, we observed oxygen-isotope-sensitive Raman bands at 568 and 788 $cm^{-1}$ during turnovers of the *E. coli bo*-type quinol oxidase for the first time, and assigned them to the $\nu_{Fe\text{-}O_2}$ and $\nu_{Fe^{IV}=O}$ of its oxy- and ferryl intermediates, respectively. These frequencies and their $^{16}O/^{18}O$ isotopic shifts suggest that structures of these intermediates at the catalytic site are similar to the corresponding intermediates of $aa_3$-type cytochrome *c* oxidases. However, the occurrence of the ferryl intermediate was evidently faster in the *bo*-type quinol oxidase than in the $aa_3$-type cytochrome *c* oxidase.

## References


(1) Anraku, Y; Gennis, R. B. *Trends Biochem. Sci.* **1987**, *12*, 262-266.

(2) Puustinen, A.; Finel, M.; Virkki, M. and Wikström, M. *FEBS Lett.* **1989**, *249*, 163-167.

(3) Mogi, T.; Nakamura, H.; Anraku, Y. *J. Biochem.* **1994**, *116*, 471-477.

(4) Chepuri, V.; Lemieux, L.; Au, D. C.-T.; Gennis, R. B. *J. Biol. Chem.* **1990**, *265*, 11185-11192.

(5) Minagawa, J.; Mogi, T.; Gennis, R. B.; Anraku, Y. *J. Biol. Chem.* **1992**, 267, 2096-2104.

(6) Lemieux, L. J.; Calhoun, M. W.; Thomas, J. W.; Ingledew, W. J.; Gennis, R. B. *J. Biol. Chem.* **1992**, *267*, 2105-2113.

(7) Shapleigh, J. P.; Hosler, J. P.; Tecklenburg, M. M. J.; Kim, Y.; Babcock, G. T.; Gennis, R. B.; Ferguson-Miller, S. *Proc. Natl. Acad. Sci. U.S.A.* **1992**, *89*, 4786-4790.

(8) Tsubaki, M.; Mogi, T.; Anraku, Y.; Hori, H. *Biochemistry* **1993**, *32*, 6065-6072.

(9) Salerno, J. C.; Bolgiano, B.; Poole, R. K.; Gennis, R. B.; Ingledew, W. J. *J. Biol. Chem.* **1990**, *265*, 4364-4368.

(10) Uno, T.; Mogi, T.; Tsubaki, M.; Nishimura, Y.; Anraku, Y. *J. Biol. Chem.* **1994**, *269*, 11912-11920.

(11) Babcock, G. T.; Wikström, M. *Nature* **1992**, *356*, 301-309.

(12) Mogi, T.; Saiki, K.; Anraku, Y. *Mol. Microbiol.* **1994**, *14*, 391-398.

(13) Welter, R.; Gu, L.-Q.; Yu, C.-A.; Rumbley, J.; Gennis, R. B. *Biophys. J.* **1994**, *66*, A367.

(14) Yu, N.-T. *Methods Enzymol.* **1986**, *130*, 350-409.

(15) Yu, N. T.; Kerr, E. In *Biological Application of Raman Spectroscopy*; Spiro, T. G., Ed.; Wiley-Interscience: New York, 1988; Vol. 3, pp. 39-95.

(16) Ogura, T.; Takahashi, S.; Shinzawa-Itoh, K.; Yoshikawa, S.; Kitagawa, T. *J. Am. Chem. Soc.* **1990**, *112*, 5630-5631.

(17) Han, S.; Ching, Y.-C.; Rousseau, D. L. *Proc. Natl. Acad. Sci. U.S.A.* **1990**, *87*, 2491-2495.

(18) (a) Varotsis, C.; Woodruff, W. H.; Babcock, G. T. *J. Am. Chem. Soc.* **1989**, *111*, 6439-6440. (b) Varotsis, C.; Woodruff, W. H.; Babcock, G. T. J. *Am. Chem. Soc.* **1989**, *J. Am. Chem. Soc. 112*, 1297.

(19) Ogura, T.; Takahashi, S.; Shinzawa-Itoh, K.; Yoshikawa, S.; Kitagawa, T. *J. Biol. Chem.* **1990**, *265*, 14721-14723.
(20) Han, S.; Ching, Y.-C.; Rousseau, D. L. *Nature* **1990**, *348*, 89-90.
(21) Varotsis, C.; Babcock, G. T. *Biochemistry* **1990**, *29*, 7357-7362.
(22) Ogura, T.; Takahashi, S.; Shinzawa-Itoh, K.; Yoshikawa, S.; Kitagawa, T. *Bull. Chem. Soc. Jpn.* **1991**, *64*, 2901-2907.
(23) Ogura, T.; Yoshikawa, S.; Kitagawa, T. *Biochemistry* **1989**, *28*, 8022-8027.
(24) Ogura, T.; Takahashi, S.; Hirota, S.; Shinzawa-Itoh, K.; Yoshikawa, S.; Appelman, E. H.; Kitagawa, T. *J. Am. Chem. Soc.* **1993**, *115*, 8527-8536.
(25) Oden, K. L.; DeVeaux, L. C.; Vibat, C. R. T.; Cronan, J. E., Jr.; Gennis, R. B. *Gene* **1990**, *96*, 29-36.
(26) Nakamura, H.; Yamato, I.; Anraku, Y.; Lemieux, L.; Gennis, R. B. *J. Biol. Chem.* **1990**, *265*, 11193-11197.
(27) Brunner, H. *Naturwissenschaften* **1974**, *61*, 129.
(28) Nagai, K.; Kitagawa, T.; Morimoto, H. *J. Mol. Biol.* **1980**, *136*, 271-289.
(29) Kerr, E. A.; Yu, N.-T.; Bartnicki, D. E.; Mizukami, H. *J. Biol. Chem.* **1985**, *260*, 8360-8365.
(30) Hirota, S.; Ogura, T.; Appelman, E. H.; Shinzawa-Itoh, K.; Yoshikawa, S.; Kitagawa, T. *J. Am. Chem. Soc.* **1994**, *116*, 10564-10570.
(31) (a) Poole, R. K.; Waring, A. J.; Chance, B. *FEBS Lett.* **1979**, *101*, 56-58. (b) Svensson, M.; Nilsson, T. *Biochemistry* **1993**, *32*, 5442-5447. (c) Poole, R. K.; Salmon, I.; Chance, B. *Microbiology* **1994**, *140*, 1027-1034. (d) Orii, Y.; Mogi, T.; Kawasaki, M.; Anraku, Y. *FEBS Lett.* **1994**, *352*, 151-154.
(32) Sitter, A. J.; Reczek, C. M.; Terner, J. *J. Biol. Chem.* **1985**, *260*, 7515-7522.
(33) Terner, J.; Sitter, A. J.; Reczek, C. M. *Biochim. Biophys. Acta* **1985**, *828*, 73-80.
(34) Hashimoto, S.; Tatsuno, Y.; Kitagawa, T. *Proc. Natl. Acad. Sci. U.S.A.* **1986**, *83*, 2417-2421.
(35) Hashimoto, S.; Tatsuno, Y.; Kitagawa, T. *Proc. Japan Acad. Ser. B. Phys. Biol. Sci.* **1984**, *60*, 345-348.
(36) Sitter, A. J.; Reczek, C. M.; Terner, J. *Biochim. Biophys. Acta* **1985**, *828*, 229-235.

(37) Hashimoto, S.; Teraoka, J.; Inubushi, T.; Yonetani, T.; Kitagawa, T. *J. Biol. Chem.* **1986**, 261, 11110-11118.
(38) Oertling, W. A.; Hoogland, H.; Babcock, G. T.; Wever, R. *Biochemistry* **1988**, *27*, 5395-5400.
(39) Egawa, T.; Miki, H.; Ogura, T.; Makino, R.; Ishimura, Y.; Kitagawa, T. *FEBS Lett.* **1992**, *305*, 206-208.
(40) Sato-Watanabe, M.; Mogi, T.; Ogura, T.; Kitagawa, T.; Miyoshi, H.; Iwamura, H.; Anraku, Y. *J. Biol. Chem.* **1994**, *269*, 28908-28912.
(41) Varotsis, C.; Zhang, Y.; Appelman, E. H.; Babcock, G. T. *Proc. Natl. Acad. Sci. U.S.A.* **1993**, *90*, 237-241.

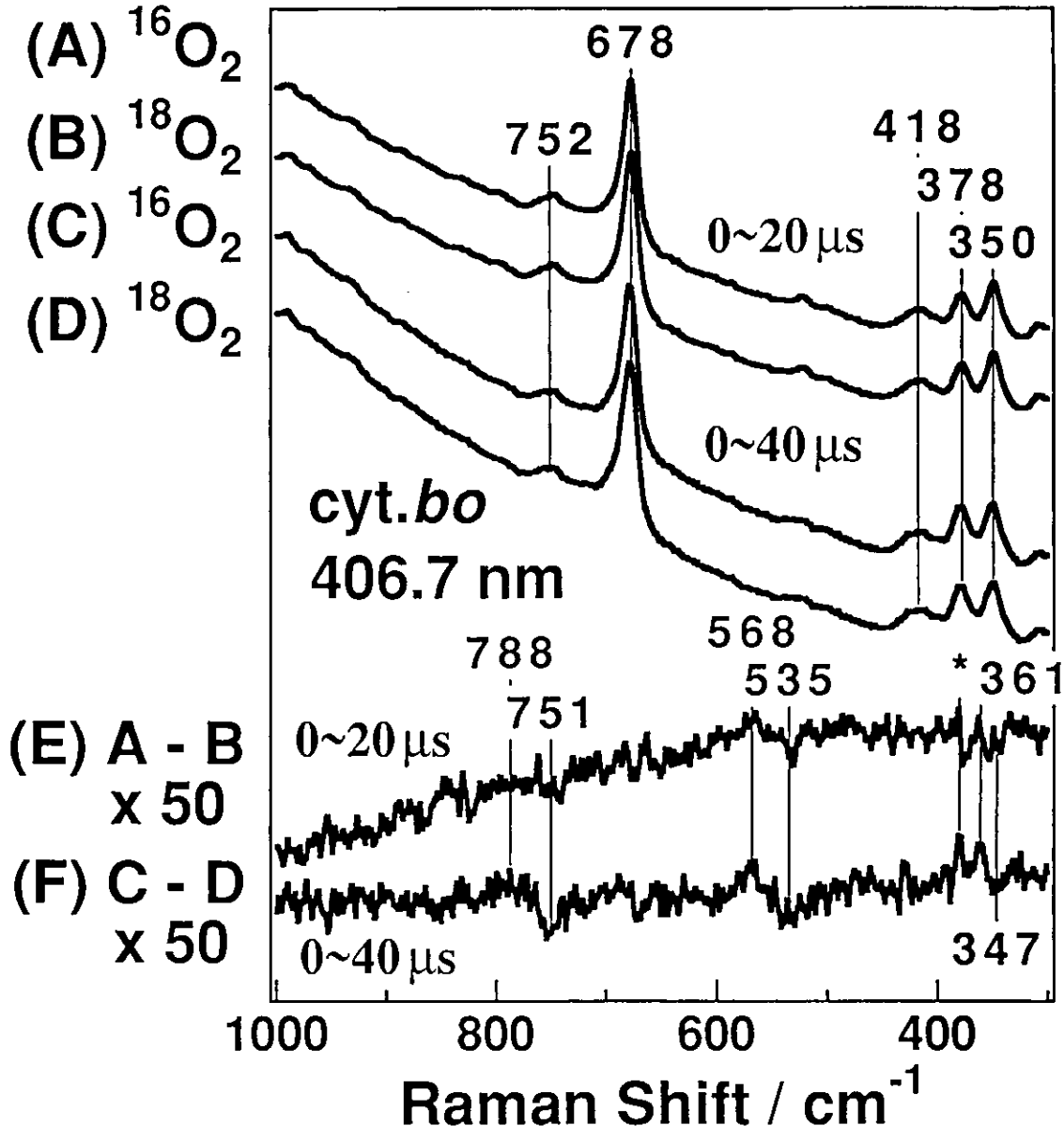


**Figure 3-1.** Time-resolved RR spectra of the *E. coli bo*-type quinol oxidase in the 1000 to 300 $cm^{-1}$ region for $^{16}O_2$ (A, C) and $^{18}O_2$ (B, D) derivatives and their difference spectra (E, F). The ordinate scales of spectra A, B, C and D are normalized by the intensity of porphyrin bands. Traces E and F represent the differences; spectrum E = (spectrum A - spectrum B) x 50 and spectrum F = (spectrum C - spectrum D) x 50. The band marked with an asterisk denote a plasma line from a $Kr^+$ ion laser. Transit time of a given molecule across the laser beam is 0-20 μs for spectra A, B, and E and 0-40 μs for spectra C, D, and F. Experimental conditions: excitation, 406.7 nm, 5 mW (at the sample) for spectra A and B, and 6 mW (at the sample) for spectra C and D; accumulation time, 3840s for spectra A and B, and 6080s for spectra C and D.

# Chapter II-4.

# Axial Ligands of Heme Irons in Cytochrome *bd* Isolated from *Escherichia coli*

**Abstract**

To characterize the axial ligands of the 5-coordinated cytochromes in cytochrome *bd*-type ubiquinol oxidase, resonance Raman (RR) spectra of the $^{54}Fe$- and $^{56}Fe$-labeled enzymes were measured with 441.6 and 424.0 nm excitations for the reduced state and with 647.1 nm excitation for the oxidized state, and those of the $^{12}C^{16}O$- and $^{13}C^{18}O$-bound enzymes were measured with 406.7 nm excitation. For the reduced enzyme excited at 441.6 nm, a band at 250 $cm^{-1}$ for the $^{56}Fe$-labeled enzyme was shifted to 252 $cm^{-1}$ with the $^{54}Fe$-labeled enzyme. This frequency is close to the $Fe^{2+}$-His stretching frequency for reduced peroxidases. The intensity of the 250 $cm^{-1}$ band retained its intensity more than 80 % upon exposure to CO. When the RR scattering was excited at 424.0 nm for the reduced enzyme, a band at 397 $cm^{-1}$ for $^{56}Fe$-labeled enzyme shifted to 400 $cm^{-1}$ with the $^{54}Fe$-labeled enzyme. For the oxidized enzyme, a band at 432 $cm^{-1}$ for the $^{56}Fe$-labeled enzyme shifted to 434 $cm^{-1}$ with the $^{54}Fe$-labeled enzyme when excited at 647.1 nm near the absorption of cytochrome *d*. For the CO-bound enzyme, bands at 477 and 571 $cm^{-1}$ for the $^{12}C^{16}O$-bound enzyme shifted to 466 and 552 $cm^{-1}$ with the $^{13}C^{18}O$-bound enzyme, respectively. The 477 $cm^{-1}$ band is assignable to the Fe-CO stretching vibration, and has a lower frequency than those of other CO-bound heme proteins which have a histidine residue as an axial ligand. The frequency for the CO-isotope-sensitive band at 571 $cm^{-1}$ was close to that of bovine cytochrome *c* oxidase (574 $cm^{-1}$). The frequency of the $\nu_4$ band for the reduced enzyme was around 1355 to 1360 $cm^{-1}$ for all the RR spectra excited at 406.7, 424.0, and 441.6 nm. These results suggest that the axial ligand for the 5-coordinated cytochrome *b* is a histidine residue and that for the 5-coordinated cytochrome *d* seems to be neither a histidine nor a cystein residue.

## 4.1 Introduction

Cytochrome *bd*-type ubiquinol oxidase is a terminal oxidase of the aerobic respiratory chain of *Escherichia coli* (*E. coli*) and is predominantly expressed under poorly-aerated growth conditions, while cytochrome *bo*-type ubiquinol oxidase is expressed under highly-aerated conditions (see 1 for a review). Similar to cytochrome *bo*-type ubiquinol oxidase, cytochrome *bd*-type ubiquinol oxidase catalyzes the four-electron reduction of molecular oxygen by using ubiquinol-8 as an electron donor,[1,2] but it does not function as a proton pump in contrast with cytochrome *bo*-type ubiquinol oxidase.[3] Cytochrome *bd*-type ubiquinol oxidase has a higher affinity than cytochrome *bo*-type ubiquinol oxidase for molecular oxygen and other respiratory inhibitors such as $CN^-$ and $N_3$.[2]

Based on optical studies, it is thought that cytochrome *bd*-type ubiquinol oxidase contains three cytochrome species; two *b* hemes and one iron-chlorin (heme *d*).[4] One of the heme *b* is called cytochrome $b_{558}$ which functions as the ubiquinol-8 oxidation site located at subunit II.[5] Its reduced form shows absorption peaks at 562 and 532 nm as the α and β bands, respectively.[6] The other heme *b* is called cytochrome $b_{595}$, an unusual *b*-type cytochrome exhibiting α and β peaks at 595 and 562 nm, respectively, in the reduced *minus* oxidized spectra.[5] Heme *d* has a typical absorption band at 628 nm in the reduced state.[7] It functions primarily as the binding site for an exogenous ligand, and molecular oxygen binds to this site in the reduced state.[8] Recently, FT-IR study indicated that CO-photodissociation from CO-cytochrome *d* adduct at low temperature (e.g., 20 K) results in the formation of a kinetically trapped CO-cytochrome $b_{595}$ adduct, suggesting that cytochrome $b_{595}$ and cytochrome *d* form a binuclear site.[9]

Resonance Raman (RR) spectroscopy can bring about structural information on hemes and their vicinities.[10] One of its most efficient use is to detect bands due to iron-ligand stretching modes as demonstrated in chapter II-3. For the reaction intermediates of cytochrome *bd*-type ubiquinol oxidase, the Fe-$O_2$ and $Fe^{IV}$=O stretching modes have been detected at 568 and 815 $cm^{-1}$, respectively.[11,12] The Fe-$O_2$ stretching frequency has similar values to those of other oxy heme proteins,[11] while the $Fe^{IV}$=O stretching frequency ($\nu_{Fe^{IV}=O}$) is higher by 10 $cm^{-1}$ than those of other oxoferryl heme proteins.[12] RR spectroscopy is also very useful to

characterize native axial ligands of the heme iron in proteins. The iron-histidine stretching ($\nu_{Fe\text{-}His}$) RR bands have been detected in many 5-coordinated heme proteins around 210-240 $cm^{-1}$ for the reduced state.[13-16] The iron-cystein stretching ($\nu_{Fe\text{-}Cys}$) RR band has also been detected for oxidized P-450 at 351 $cm^{-1}$.[17]

It is interesting to investigate what the axial residues of the 5-coordinated cytochromes in cytochrome *bd*-type ubiquinol oxidase are and to know what kind of relationship there is between the axial ligands of the cytochromes and the functions of oxidases. Recent RR and FT-IR studies[18] pointed out that the axial ligand of cytochrome *d* is likely to be a histidine residue with an anomalous condition or to be a residue other than a histidine residue. To make further characterization of the axial ligands of cytochromes of cytochrome *bd*-type ubiquinol oxidase, we measured the RR spectra for the oxidized and reduced states of the $^{54}Fe$- and $^{56}Fe$-labeled enzymes.

### 4.2 Materials and Methods

Raman scattering was excited at 441.6 nm with a He/Cd laser (Kinmon Electrics, Model CD1805B), at 406.7 and 647.1 nm with a $Kr^+$ ion laser (Spectra Physics, Model 2016), and at 424.0 nm with the laser system using a $KNbO_3$ crystal described in chapter I-2. The scattering was detected with a cooled (-20 °C) diode array (PAR, 1421HQ) attached to a 1m-single polychromator (Ritsu Oyo Kogaku, DG-1000) for 406.7, 424.0, and 441.6 nm excitation, and with a CCD (PAR, 1530-CUV) attached to a 25cm-single polychromator (CHROMEX, 250IS) for 647.1 nm excitation. The slit width of 200 mm and slit height of 10 mm were used for all measurements. The excitation laser beam was focused to the sample to about 50 μm, and the laser power was adjusted to 4 to 170 mW (at the sample). All measurements were carried out at room temperature with a spinning cell (3500 rpm). Raman shifts were calibrated with $CCl_4$ and accuracy of the peak positions of the Raman bands were ±1 $cm^{-1}$.

The enzyme was a kind gift from Dr. Mogi and Prof. Anraku of Tokyo University. The stored enzyme was dissolved in 50 mM Tris-HCl buffer (pH 7.2) containing 0.1% sucrose monolaurate SM-1200 (Mitsubishi-Kasei Food Co. Ltd., Tokyo). For reduction of the enzyme, a small amount of $N_2$-saturated dithionite solution was added (final concentration 10 mM).

### 4.3 Results

Figure 4-1 shows the RR spectra in the 450 to 200 $cm^{-1}$ region for the $^{54}Fe$-labeled (A) and $^{56}Fe$-labeled (B) reduced cytochrome *bd*-type ubiquinol oxidases excited at 441.6 nm and their difference spectrum (C). The Raman bands of the $^{54}Fe$-labeled enzyme (A) at 252 $cm^{-1}$ was shifted to 250 $cm^{-1}$ with the $^{56}Fe$-labeled enzyme (B), and their difference spectrum C clearly demonstrates this. This frequencies were close to the iron-histidine stretching ($\nu_{Fe\text{-}His}$) frequencies of other reduced heme proteins.[13-16] The 250 $cm^{-1}$ band retained its intensity for more than 80% upon exposure to CO. The frequency of the 227 cm-1 band also seems to be altered by iron isotopes, but the frequency shift was very little.

Figure 4-2 shows the RR spectra in the 600 to 200 $cm^{-1}$ region for the same sample which were excited at 424.0 nm. This excitation wavelength is close to the absorption maximum of reduced cytochrome *b* (~427 nm). The Raman band of the $^{54}Fe$-labeled enzyme (A) at 400 $cm^{-1}$ was shifted to 397 $cm^{-1}$ with the $^{56}Fe$-labeled enzyme (B). The difference spectrum C clearly demonstrate this Fe-isotope shift, in which the intensities of the strong porphyrin bands at 339 and 420 $cm^{-1}$ were canceled completely.

Figure 4-3 displays the RR spectra in the 600 to 200 $cm^{-1}$ region for the $^{54}Fe$-labeled (A) and $^{56}Fe$-labeled (B) oxidized cytochrome *bd*-type ubiquinol oxidases excited at 647.1 nm and their difference spectrum (C). This wavelength is close to the absorption maximum of oxidized cytochrome *d*. The strong band at 432 $cm^{-1}$ in spectrum A was shifted to 434 $cm^{-1}$ in spectrum B. Cytochrome *d* adopts a dioxygen bound form at the oxidized state, and the 568 $cm^{-1}$ band is assigned to the $Fe\text{-}O_2$ stretching vibration mode.[11]

Figure 4-4 displays the RR spectra in the 600 to 200 $cm^{-1}$ region for the $^{12}C^{16}O$-bound (A) and $^{13}C^{18}O$-bound (B) reduced cytochrome *bd*-type ubiquinol oxidases excited at 406.7 nm and their difference spectrum (C). Bands at 477 and 571 $cm^{-1}$ for the $^{12}C^{16}O$-bound enzyme shifted to 466 and 552 $cm^{-1}$ with the $^{13}C^{18}O$-bound enzyme, respectively, and the 477 $cm^{-1}$ band is assignable to the Fe-CO stretching vibration.[18]

## 4.4 Discussion

### Axial Ligand of Cytochrome *b*

A Band at 250 $cm^{-1}$ for the $^{56}Fe$-labeled reduced enzyme was shifted to 252 $cm^{-1}$ with the $^{54}Fe$-labeled reduced enzyme, when excited at 441.6 nm (Figure 4-1). The $\nu_{Fe\text{-}His}$ RR bands are observed for many 5-coordinated heme proteins with an axial histidine ligand. The $\nu_{Fe\text{-}His}$ frequencies are observed at 220 $cm^{-1}$ for deoxy myoglobin (Mb),[14] at 216 and 221 $cm^{-1}$ for T and R state deoxy human hemoglobin A (Hb A), respectively,[15] and at 244 $cm^{-1}$ for reduced horseradish peroxidase (HRP).[16] The intensity of the 250 $cm^{-1}$ band observed for the reduced state did not differ when the pH value was raised from 7.2 to 8.5. The $\nu_{Fe\text{-}His}$ frequency of reduced HRP is higher than those of deoxy Mb and deoxy Hb. This is explained as a deprotonation effect of the histidine proton. The deprotonation effects of the axial imidazole for $Fe^{2+}$(PP)(2MeIm) (PP; protoporphyrin IX, 2MeIm; 2-methylimidazole) on the $\nu_{Fe\text{-}2MeIm}$ mode has been investigated as a model of the Fe-His system.[16] It was deduced from it that the removal of the proton or the formation of a strong hydrogen bond to neighboring amino acid residues would cause an upshift of the $\nu_{Fe\text{-}His}$ frequency from 208 to 233 $cm^{-1}$.[16] The $\nu_{Fe\text{-}His}$ band generally disappears when CO is bound to the heme iron, but the iron-isotope-sensitive band at 250 $cm^{-1}$ in the RR spectra for the reduced enzyme excited at 441.6 nm in Figure 4-1 did not reduce its intensity upon exposure to CO so much. Thus the 250 $cm^{-1}$ band could represent the $\nu_{Fe\text{-}His}$ mode of the heme at which CO does not bind, and thus the axial ligand for the 5-coordinated cytochrome *b* is likely to be a histidine residue. This $\nu_{Fe\text{-}His}$ frequency is close to that of reduced HRP. Therefore, the strength of the iron-histidine bond of the 5-coordinated cytochrome *b* seems to be similar to HRP and the proximal histidine could be deprotonated or strongly hydrogen bonded.

Using an excitation wavelength of 424.0 nm which is close to the absorption maximum of the reduced cytochromes *b*, the band of the $^{56}Fe$-labeled reduced enzyme at 397 $cm^{-1}$ was shifted to 400 $cm^{-1}$ with the $^{54}Fe$-labeled reduced enzyme (Figure 4-2). This band was also seen with 427 nm excitation. This band did not change its intensity upon exposure to CO, and thus must be related to one of the cytochrome *b*. Further experiments is needed to characterize this mode. Recently, it is found that cytochrome *bd*-type ubiquinol oxidase contains 2.2 times of iron

atoms compared to the amount of heme irons in the enzyme. The iron atoms other than the heme iron could also cause this band. Further investigation is needed to clarify the axial ligand of cytochrome *b*.

**Axial Ligand of Cytochrome *d***

The frequency for the CO-isotope-sensitive band at 571 $cm^{-1}$ in the RR spectra of the CO-bound enzyme excited at 406.7 nm (Figure 4-4) was close to that of bovine cytochrome *c* oxidase (574 $cm^{-1}$). This band was also detected in the spectra excited at 427 nm, but with lower S/N ratio because of its lower intensity. P-450 has a cystein residue as an axial ligand, and CO-isotope-sensitive band has been detected at around 560 $cm^{-1}$ for the CO-bound form, whose frequency is lower than those of heme proteins having a histidine residue as an axial ligand.[19] The frequency of the $\nu_4$ band for the reduced enzyme was around 1355 to 1360 $cm^{-1}$ for all the RR spectra excited at 406.7, 424.0, and 441.6 nm (data not shown). The frequency of this band for reduced P-450 is around 1345 $cm^{-1}$ and is lower than those of heme proteins which have a histidine residue as an axial ligand.[20] The 477 $cm^{-1}$ band in the CO-bound enzyme is assignable to the Fe-CO stretching vibration, and it has a lower frequency than those of other CO-bound heme proteins which have a histidine residue as an axial ligand. Also no $\nu_{Fe\text{-}His}$ band which disappeared upon exposure to CO was observed at the reduced state. These results suggest that neither a cystein nor a histidine residue is the axial ligand of cytochrome *d* at which CO binds.

For the oxidized enzyme, a band at 432 $cm^{-1}$ for the $^{56}Fe$-labeled enzyme was shifted to 434 $cm^{-1}$ with the $^{54}Fe$-labeled enzyme when RR scattering was excited at 406.7 nm (Figure 4-3). This mode was not affected by addition of $CN^-$. This iron-isotope-sensitive band might be a Fe-ligand vibrational mode, although further studies are needed to specify the mode.

## References


(1) (a) Anraku, Y; Gennis, R. B. *Trends Biochem. Sci.* **1987**, 12, 262-266. (b) Anraku, Y. *Annu. Rev. Biochem.* **1988**, *57*, 101-132.

(2) Poole, R. G. *Biochim. Biochem. Acta* **1983**, *726*, 205-243.

(3) Puustinen, A.; Finel, M.; Haltia, T.; Gennis, R. B.; Wikström, M. *Biochemistry* **1991**, *30*, 3936-3942.

(4) (a) Koland, J. G.; Miller, M. J.; Gennis, R. B. *Biochemistry.* **1984**, *23*, 1051-1056. (b) Lorence, R. M.; Koland, J. G.; Gennis, R. B. *Biochemistry* **1986**, *25*, 2314-2321.

(5) Yang, F.-D.; Yu, L.; Yu, C.-A.; Lorence, R. M.; Gennis, R. B. *J. Biol. Chem.* **1986**, *261*, 14987-14990.

(6) Green, G. N.; Kranz, R. G.; Lorence, R. M.; Gennis, R. B. *J. Biol. Chem.* **1984**, *259*, 7994-7997.

(7) Miller, M. J.; Gennis, R. B. *J. Biol. Chem.* **1983**, *258*, 9159-9165.

(8) (a) Hata, A.; Kirino, Y.; Matsuura, K.; Itoh, S.; Hiyama, T.; Konishi, K.; Kita, K.; Anraku, Y. *Biochim. Biophys. Acta* **1985**, *810*, 62-72. (b) Kahlow, M. A.; Loehr, T. M.; Zuberi, T. M.; Gennis, R. B. *J. Am. Chem. Soc.* **1993**, *115*, 5845-5846.

(9) Hill, J. J.; Alben, J. O.; Gennis, R. B. *Proc. Natl. Acad. Sci. U.S.A.* **1993**, *90*, 5863-5867.

(10) (a) Yu, N.-T. *Methods Enzymol.* **1986**, *130*, 350-409. (b) Yu, N. T.; Kerr, E. In *Biological Application of Raman Spectroscopy*; Spiro, T. G., Ed.; Wiley-Interscience: New York, 1988; Vol. 3, pp. 39-95.

(11) Kahlow, M. A.; Loehr, T. M.; Zuberi, T. M.; Gennis, R. B. *J. Am. Chem. Soc.* **1993**, *115*, 5845-5846.

(12) Kahlow, M. A.; Zuberi, T. M.; Gennis, R. B.; Leohr, T. M. *Biochemistry* **1991**, *30*, 11485-11489.

(13) Kitagawa, T. In *Biological Application of Raman Spectroscopy*; Spiro, T. G., Ed.; Wiley-Interscience: New York, 1988; Vol. 3, pp. 97-131.

(14) Kitagawa, T.; Nagai, K.; Tsubaki, M. *FEBS Lett.* **1979**, *104*, 376-378.

(15) Nagai, K.; Kitagawa, T.; Morimoto, H. *J. Mol. Biol.* **1980**, *136*, 271-289.

(16) Teraoka, J.; Kitagawa, T. *J. Biol. Chem.* **1981**, *256*, 3969-3977.

(17) Champion, P. M.; Stallard, B. R.; Wangner, G. C.; Gunsalus, L. C. *J. Am. Chem. Soc.* **1982**, *104*, 5469-5472.

(18) Tsubaki, M.; Uno, T.; Hori, H.; Mogi, T.; Nishimura, Y.; Anraku, Y. *FEBS Lett.* **1993**, *335*, 13-17.
(19) Uno, T.; Nishimura, Y.; Makino, R.; Iizuka, T.; Ishimura, Y.; Tsuboi, M. *J. Biol. Chem.* **1985**, *4*, 2023-2026.
(20) (a) Shimizu, Y.; Kitagawa, T.; Mitani, F.; Iizuka, T.;Ishimura, Y. *Biochim. Biophys. Acta* **1981**, *670*, 236-242. (b) Ozaki, Y.; Kitagawa, T.; Kyogoku, Y.; Shimada, H.; Iizuka, T.; Ishimura, Y. *J. Biochem (Tokyo)* **1976**, *80*, 1447-1451. (c) Ozaki, Y.; Kitagawa, T.; Kyogoku, Y.; Imai, Y.; Hashimato-Yutsudo, C.; Sato, R. *Biochemistry* **1978**, *17*, 5826-5831.

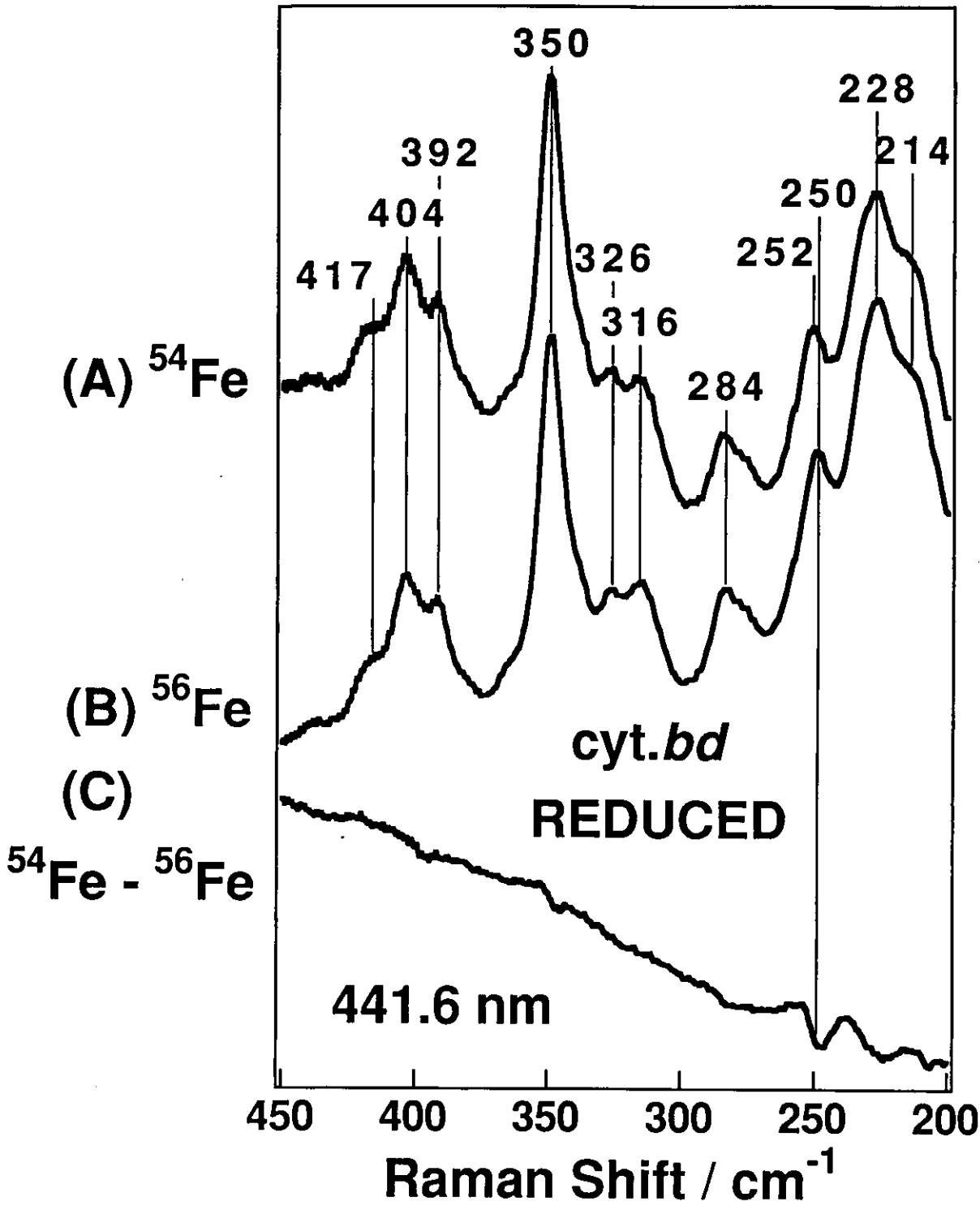


**Figure 4-1.** The RR spectra in the 450 to 200 $cm^{-1}$ region of the $^{54}Fe$-labeled (A) and $^{56}Fe$-labeled (B) reduced *E. coli bd*-type quinol oxidases, and their difference spectrum (C). The ordinate scales of spectra A and B are normalized by the intensity of the porphyrin bands. Experimental conditions: excitation, 441.6 nm, 35 mW at the sample; sample, 50 μM (heme) in 50 mM Tris-HCl buffer, pH 7.2, containing 0.1 % sucrose monolaurate.

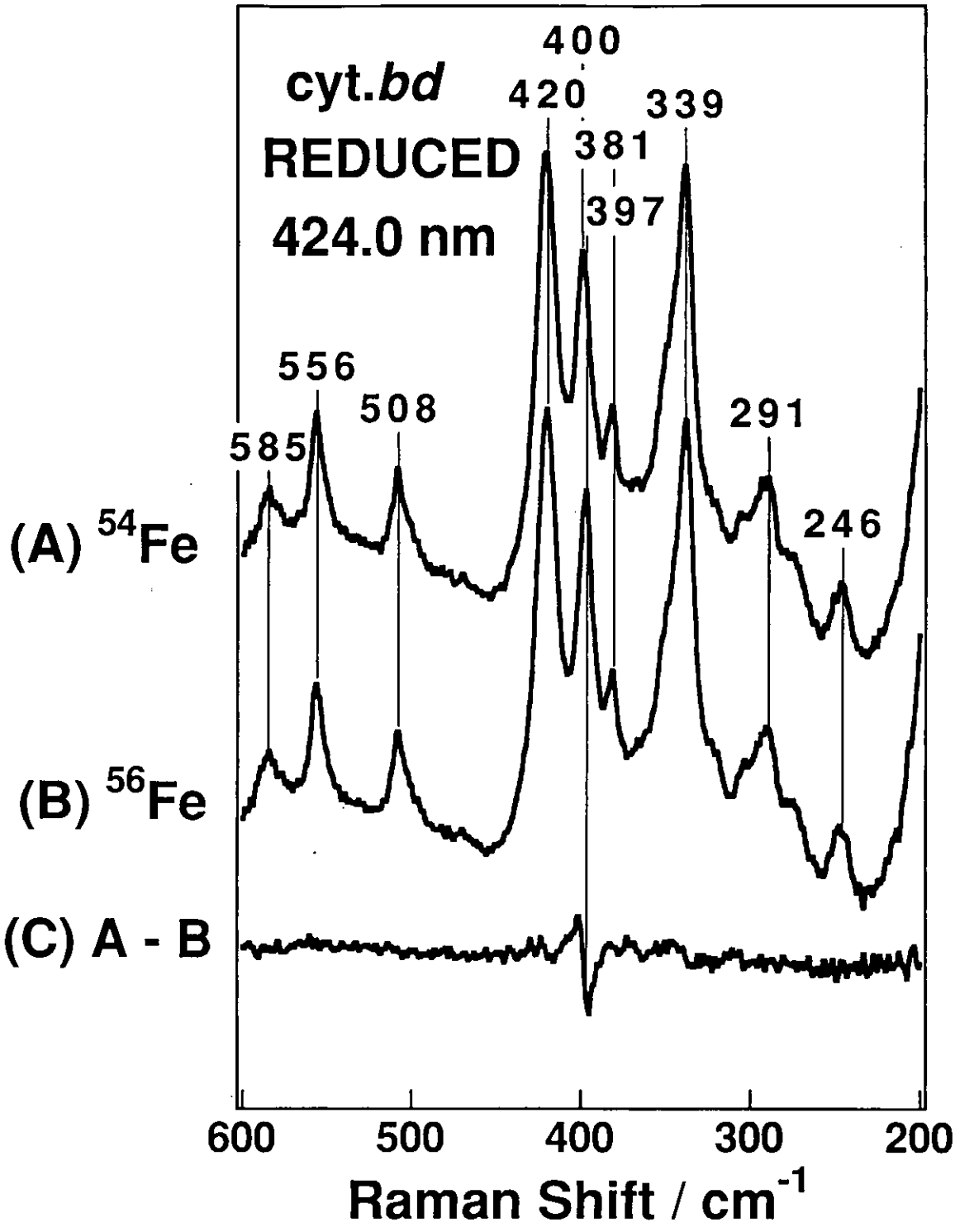


**Figure 4-2.** The RR spectra in the 600 to 200 $cm^{-1}$ region of the $^{54}Fe$-labeled (A) and $^{56}Fe$-labeled (B) reduced *E. coli bd*-type quinol oxidases, and their difference spectrum (C). The ordinate scales of spectra A and B are normalized by the intensity of the porphyrin bands. Experimental conditions are the same as those in Figure 4-1 except for the excitation at 424.0 nm with 4 mW at the sample.

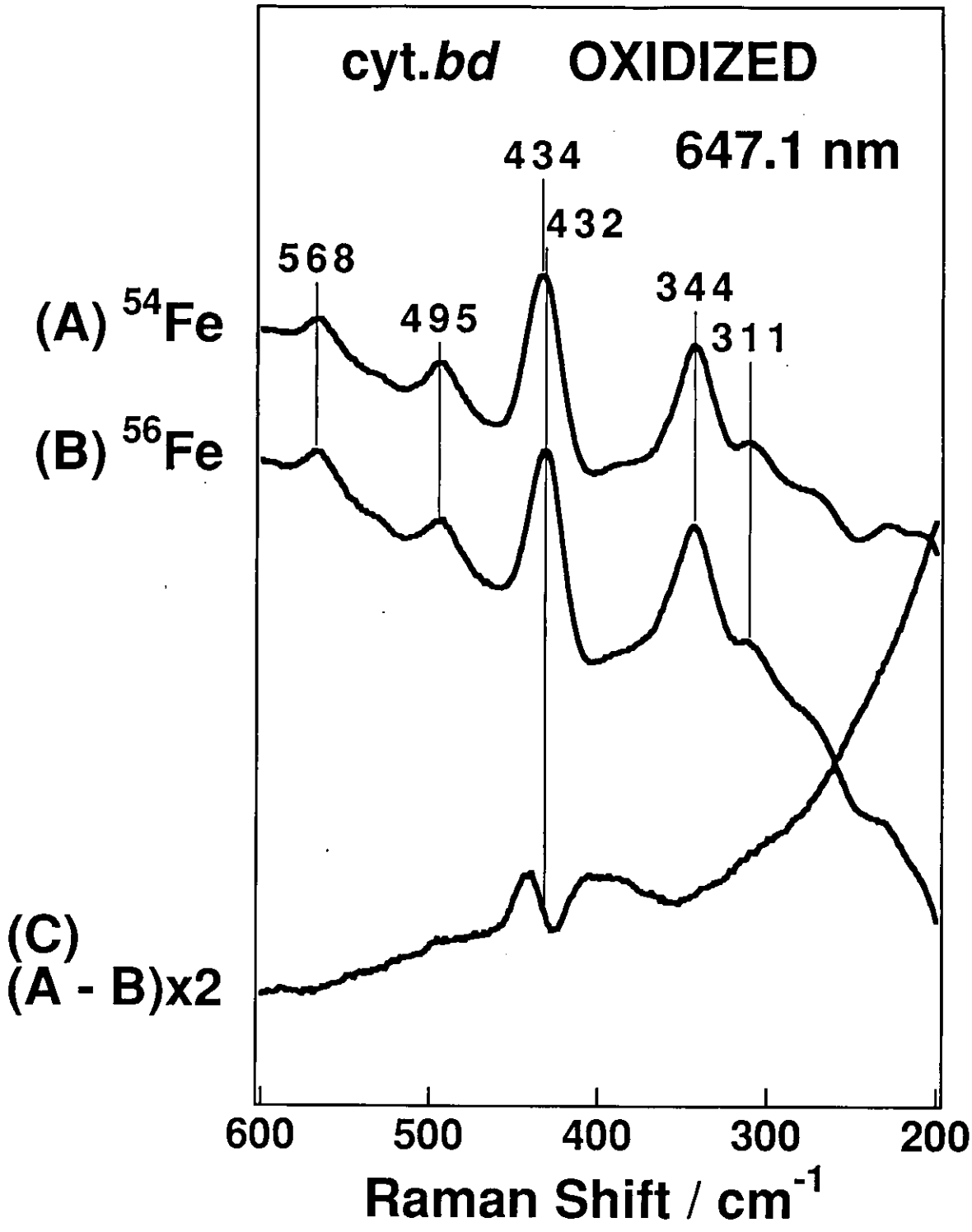


**Figure 4-3.** The RR spectra in the 600 to 200 $cm^{-1}$ region of the $^{54}Fe$-labeled (A) and $^{56}Fe$-labeled (B) oxidized *E. coli bd*-type quinol oxidases, and their difference spectrum (C). The ordinate scales of spectra A and B are normalized by the intensity of the porphyrin bands. Experimental conditions are the same as those in Figure 4-1 except for the excitation at 647.1 nm with 170 mW at the sample and the sample concentration of 100 μM (heme).

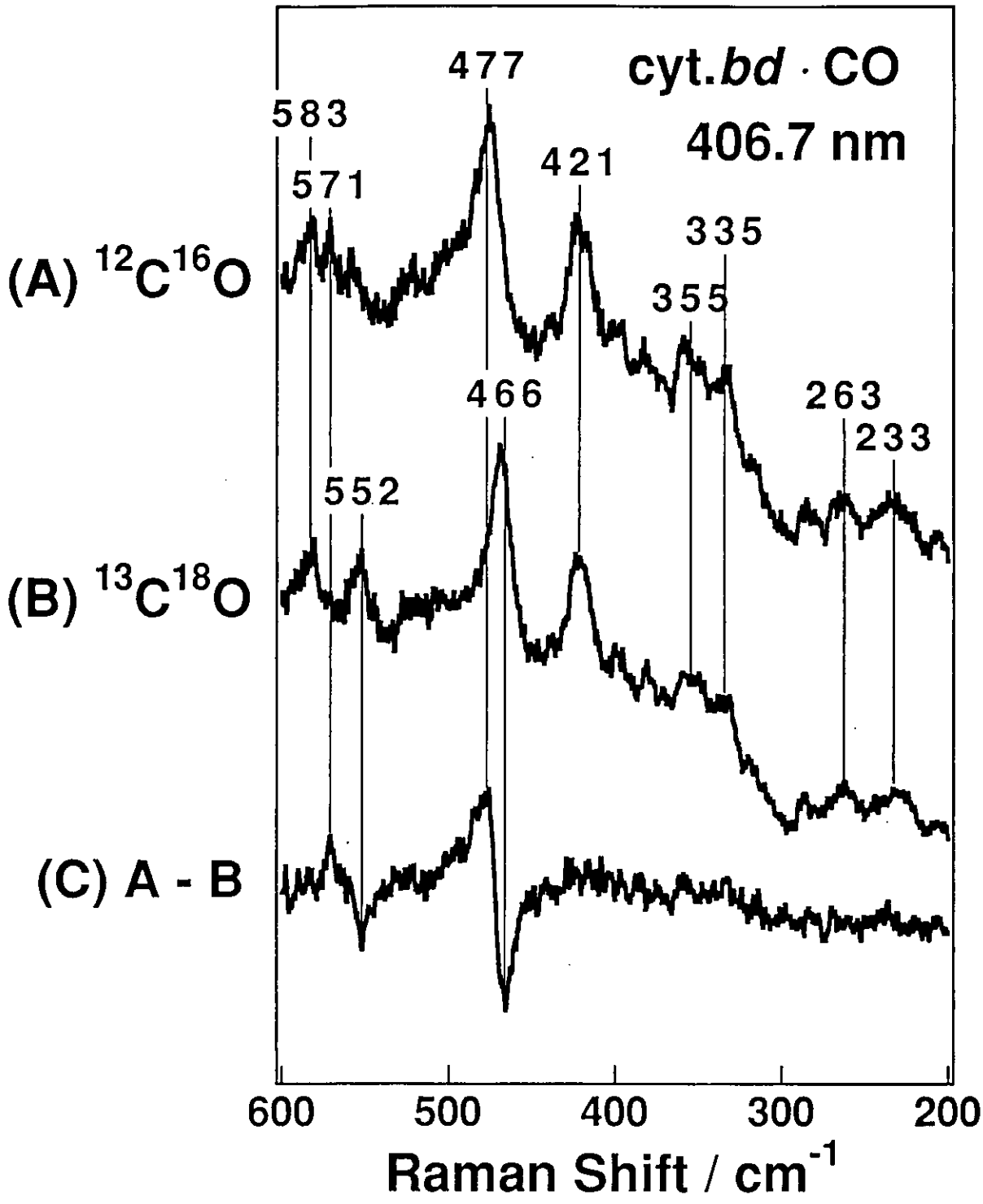


**Figure 4-4.** The RR spectra in the 600 to 200 cm$^{-1}$ region of the $^{12}C^{16}O$-bound (A) and $^{13}C^{18}O$-bound (B) *E. coli bd*-type quinol oxidases, and their difference spectrum (C). The ordinate scales of spectra A and B are normalized by the intensity of the porphyrin bands. Experimental conditions are the same as those in Figure 4-1 except for the excitation at 406.7 nm with 4 mW at the sample.

# Chapter II-5.

# Conclusion

Some similarities and differences in the physicochemical properties of three kinds of terminal oxidases were investigated in this part. The steady state and kinetic characters among different oxidases were compared to know the structure-function relationship of terminal oxidases. Chapters II-2, II-3, and II-4 presented RR spectra of $aa_3$-type cytochrome *c* oxidase, *bo*-type ubiquinol oxidase, and *bd*-type ubiquinol oxidase, respectively.

Chapter II-2 discussed the static RR band of $\nu_{CO}$ for CO-bound $aa_3$-type cytochrome *c* oxidase (CcO·CO) obtained from bovine heart, and also transient bands for CO-recombination of CO-photodissociated CcO·CO by using time-resolved RR spectroscopy. The bandwidths of the $\nu_{Fe\text{-}CO}$ and $\nu_{CO}$ RR bands of CcO·CO were narrower than that of CO-bound myoglobin (MbCO). This character was the same as those seen for the $\nu_{Fe\text{-}CO}$ and $\nu_{CO}$ bands of CO-bound *E. coli* cytochrome *bo*-type ubiquinol oxidase, suggesting that CO takes a more fixed CO conformation in the heme pocket for CO-bound terminal oxidases than for MbCO. The CO-recombination rate was well fitted with a single exponential curve, and the lifetime of the photodissociated species was 30 ms. This lifetime was longer by a factor of ten compared with those of MbCO and HbCO. No new $\nu_{Fe\text{-}CO}$ RR band was observed during the CO-recombination. This suggests that CO relaxes to its equilibrium form as soon as CO binds to the heme.

Chapter II-3 described the observation of the reaction intermediates in dioxygen reduction by the *E. coli* cytochrome *bo*-type ubiquinol oxidase. Experiments were carried out with the technique of time-resolved RR spectroscopy using the artificial cardiovascular system, and the results are compared with those obtained from the bovine cytochrome *c* oxidase. At 0~20 μs following photolysis of the enzyme-CO adduct in the presence of $O_2$, the Fe-$O_2$ stretching Raman band was observed at 568 $cm^{-1}$ which was shifted to 535 $cm^{-1}$ with $^{18}O_2$. These frequencies are remarkably close to those of other oxyhemoproteins, including $O_2$-bound hemoglobin and $aa_3$-type cytochrome *c* oxidase. In the later time range (20~40μs), other $O_2$-isotope-sensitive Raman bands were observed at 788 and 361 $cm^{-1}$. The 781 $cm^{-1}$ band was assigned to the $Fe^{IV}$=O stretching mode, since it exhibited a downshift by 37 $cm^{-1}$ upon $^{18}O_2$ substitution. Its appearance was much earlier than the corresponding intermediate of bovine cytochrome *c* oxidase (>100 μs), although their frequencies were similar.

The 361 $cm^{-1}$ band showed the $^{16}O/^{18}O$ isotopic frequency shift of 14 $cm^{-1}$ similar to the case of bovine cytochrome *c* oxidase. The detection of the intermediates for *E. coli* cytochrome *bo*-type ubiquinol oxidase has importance since it enables us to extend the time-resolved investigation of the reaction to enzymes obtained by site-directed mutagenesis. This will be a future subject.

Chapter II-4 described the RR spectra of the $^{54}Fe$- and $^{56}Fe$-labeled *E. coli* cytochrome *bd*-type ubiquinol oxidase in the reduced and oxidized states. For the reduced enzyme, iron-isotope-sensitive bands were detected at 250 $cm^{-1}$ upon excitation at 441.6 nm and at 397 $cm^{-1}$ upon excitation at 424.0 nm. For the oxidized enzyme, an iron-isotope-sensitive band was observed at 432 $cm^{-1}$ upon excitation at 647.1 nm. The band at 250 $cm^{-1}$ of the reduced enzyme excited at 441.6 nm is assignable to the $Fe^{2+}$–His stretching vibration. Judging from the intensity change of this 250 $cm^{-1}$ band upon exposure to CO, the axial ligand of heme *b* must be a histidine residue. The axial ligand of heme *d* seems to be neither a histidine nor a cystein residue .

The physicochemical properties of terminal oxidases seem to be similar between different kinds of terminal oxidases, which are different from Mb and Hb. These properties must be indispensable for the oxygen-reducing function of terminal oxidases.